Dissertation zur Erlangung des Doktorgrades

der Fakultät für Chemie und Pharmazie

der Ludwig-Maximilians-Universität München

Precise biodegradable carriers for nucleic acid delivery

Sören Reinhard

aus Annweiler am Trifels, Deutschland

2018

Erklärung

Diese Dissertation wurde im Sinne von § 7 der Promotionsordnung vom 28. November 2011 von Herrn Prof. Dr. Ernst Wagner betreut.

Eidesstattliche Versicherung

Diese Dissertation wurde eigenständig und ohne unerlaubte Hilfe erarbeitet.

München, 12.02.2019

.....

Sören Reinhard

Dissertation eingereicht am: 13.12.2018

1. Gutachter: Prof. Dr. Ernst Wagner

2. Gutachter: Prof. Dr. Wolfgang Frieß

Mündliche Prüfung am: 07.02.2019

Table of Contents

1 Introduction

This chapter provides a brief introduction into the research field of siRNA delivery with sequence-defined oligoamino amides. It was adapted from:

S. Reinhard, E. Wagner, How to Tackle the Challenge of siRNA Delivery with Sequence-Defined Oligoamino Amides, Macromol. Biosci. 17(1) (2017)

1.1 The Requirements for Efficient Nucleic Acid Delivery

The transcription of genes in RNA and the subsequent translation into proteins is described by the central dogma of molecular biology.[1, 2] Beyond that, the discovery of RNA interference (RNAi) in 1998 as a pathway of gene regulation provides exciting opportunities for medical applications.[3] Noncoding double-stranded small interfering RNA (siRNA) was found to modulate the knockdown of complementary mRNA sequences catalytically, thus preventing protein translation. One of the two 21-23 bases long strands, the guide-strand, is complexed in phosphorylated form with argonaute (Ago) protein, forming an RNA-induced silencing complex (RISC). This mechanism has to be triggered by delivery of synthetic siRNA into the cytosol of the targeted cells since it is not naturally occurring in mammals.[4-6] As gene overexpression and dysregulation is involved in several human diseases including cancer, the development of siRNA therapeutics is a major interest in research and has resulted in first preclinical and clinical trials.[7-9] However, free siRNA is far larger than conventional drugs, negatively charged, and rapidly cleared or degraded in the host. To enhance the consequential inefficient uptake, siRNA has to be formulated with suitable carriers.

Critical issues of nucleic acid delivery via synthetic vehicles are (i) extracellular stability by stable polyplex formation and shielding to avoid rapid decay, clearance and unspecific interactions (ii) specific target cell binding and uptake through receptor-mediated endocytosis, (iii) efficient endosomal escape and (iv) release of the cargo in the cytosol (**Fig. 1**).[10]

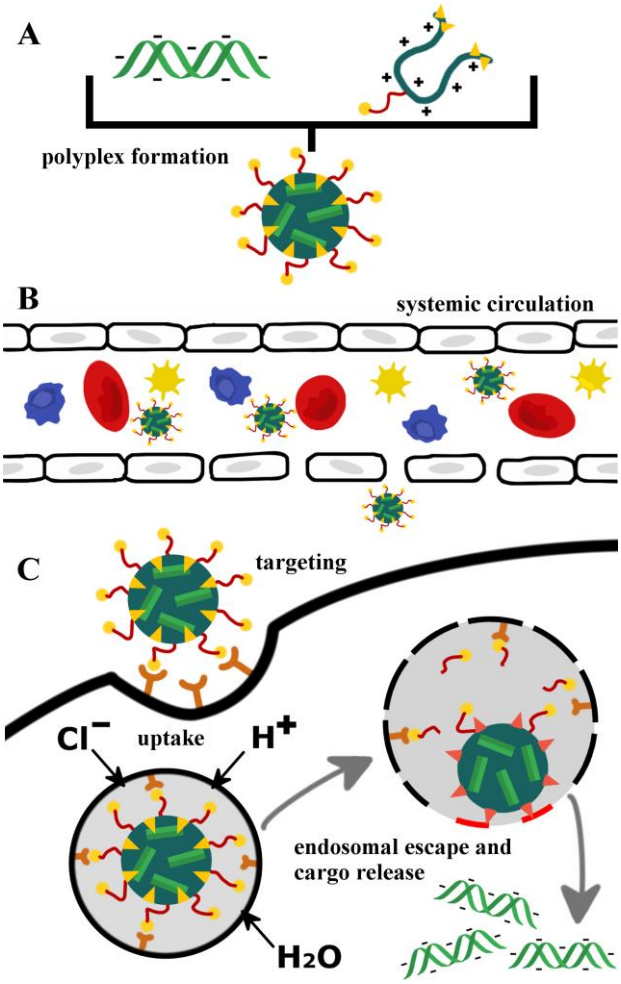

Fig. 1 Barriers in the nucleic acid delivery pathway of polyplexes. A) Formation of stable polyplexes, B) avoidance of rapid clearance and unspecific interactions with blood components, and C) receptor targeting, endocytosis, endosomal escape and cytosolic cargo release.

Viruses are natural masterpieces in respect of nucleic acid delivery and can be transformed into therapeutic vectors by replacing parts of their genome with the desired oligonucleotides and further genetic and chemical modifications.[11, 12] However, viral vectors are limited to natural nucleic acids as payload, their production and analytics are sophisticated, and they may trigger immune responses caused by recognition of viral antigens and nucleic acids. Synthetic carriers may resolve these issues and are the only option for the delivery of chemically modified nucleic acids.[13, 14] Chemical modification of siRNA has proven successful as one possible way to circumvent the immunogenic potential of the nucleic acid itself.[15-19] Viruses, as they are dynamic and bioresponsive within the delivery process, are used as models for the development of synthetic carriers.[20, 21] A broad range of non-viral gene delivery systems has been developed over the past decades, including physical methods, inorganic nanoparticles,

lipid-based or polymeric transfection agents[22-24] and siRNA- or siRNNs- (short interfering ribonucleic neutrals) conjugates.[25-30] The development of polyplexes, formed by electrostatic interaction of negatively charged nucleic acids with cationic polymers, started in 1965 with the transfection of phenol-extracted purified poliovirus RNA with cationic diethylaminoethyl (DEAE) dextran[31] and already comprises five decades of research.[32] Cationic polymers like polylysine (pLys), polyethylenimine (PEI), chitosan and others have been widely investigated as carriers for nucleic acids.[33-36] Such polymers, however, are facing issues regarding toxicity, heterogeneity, and polydispersity which might be critical for clinical studies, reproducible manufacturing and polyplex formation and the establishment of clear structure-activity relationships. For low-molecular weight transfection carriers, such as cationic lipids, small changes in chemistry may result in big differences.[37, 38] Similarly, different molecular weights and topologies may change properties of carriers.[39-41] The drawbacks of rather inhomogeneous polymeric carriers can be overcome by solid-phase assisted precise synthesis of sequence-defined cationic oligomers. Oligomers can be modified and tailored in multiple ways to meet specific requirements of nucleic acid binding, size, shielding and targeting of the polyplexes and intracellular release of the cargo. In this way, sequence-defined cationic oligomers can mimic the dynamic and bioresponsive behavior of viruses and present a group of highly versatile nucleic acid carriers.[42-44]

1.2 Nucleic Acid Binding – The Polyplex Formation Process

1.2.1 Different requirements of nucleic acid cargos

Condensation of nucleic acids by polycations are important and well-known processes in all kinds of organisms.[45] Although the packaging is necessary to reduce the size, prevent degradation and neutralize negative charges of the nucleic acids, it has to be reversible at a particular time point when the cargo has to be accessible for subsequent biological processes such as replication or transcription. The compaction is particularly relevant for large plasmid DNA (pDNA), where approximately 10,000 negative charges are condensed in 20 - >100 nm nanoparticles by polymers.[45-50] The reduction in size is not required in case of the much smaller double-stranded siRNA molecule with a dimension of ~ 2.3 x 6 nm (for a 21mer A-form siRNA duplex plus single-stranded overhangs, 0.24 nm/base). In a properly shielded form, polyplexes with single siRNA

molecules as small as 5.8 nm in average dynamic diameter by fluorescence correlation spectroscopy have been reported, which is only 1.6 nm larger than the diameter of 4.2 nm measured for a free fluorescently labeled 21mer siRNA duplex.[51] To avoid rapid renal clearance of such small polyplexes, the co-packaging of multiple siRNA molecules in larger nanoparticles might be beneficial. siRNA with only 42 - 46 negative charges, however, suffers from less entropic gain of electrostatic polyplex formation[47] compared to the much larger pDNA. Extracellular stability of polyplexes however is a critical issue of the delivery process because interaction with electrolytes, proteins, or cellular surfaces can cause partial or complete polyplex dissociation which would result in rapid clearance or degradation of the nucleic acid.[52] Altogether, this demonstrates the necessity to optimize the carrier system towards the requirements of the cargo.[53, 54]

1.2.2 Modification of polycationic carriers

Common strategies to stabilize siRNA polyplexes include bioreducible crosslinking[43, 55, 56] and hydrophobic stabilization[43, 57-60] of the polycations or covalent attachment of the siRNA to the carrier.[61-63] In our previous work, we investigated the influence of cysteines for bioreducible disulfide-linkage and hydrophobic domains such as tyrosine trimers and fatty acids on the properties of polyplexes formed with siRNA and sequence-defined cationic oligoaminoamide oligomers.[44, 64] The aminoethylene motif contained in these oligomers is a well-known structure element from the cationic polymer PEI and mediates both nucleic acid binding and endosomal buffer capacity.[33, 65] To insert the aminoethylene motif in a precise sequence-defined way, these units were incorporated in synthetic amino acid-like building blocks such as succinoyl-tetraethylene-pentamine (Stp) or succinoyl-pentaethylene-hexamine (Sph). In properly protected form, they are compatible with solid-phase supported synthesis[42] (**Fig. 2A**) and can be assembled into precise peptide-like oligoamides. Because of their medium molecular weight between ~ 1,500 – 11,000 Da they are well biocompatible at the standard transfection conditions.[40] Polyplexes assemble upon mixing cationic oligomers with nucleic acids. This assembly is far less precise and less controllable than the SPS synthesis of the oligomers. Reproducibility can be improved by automated mixing[66, 67] and defined storage conditions such as lyophilization.[67] The actually formed polyplex nanostructures can be assessed indirectly for example by determination of physicochemical properties[68] or biological activity.

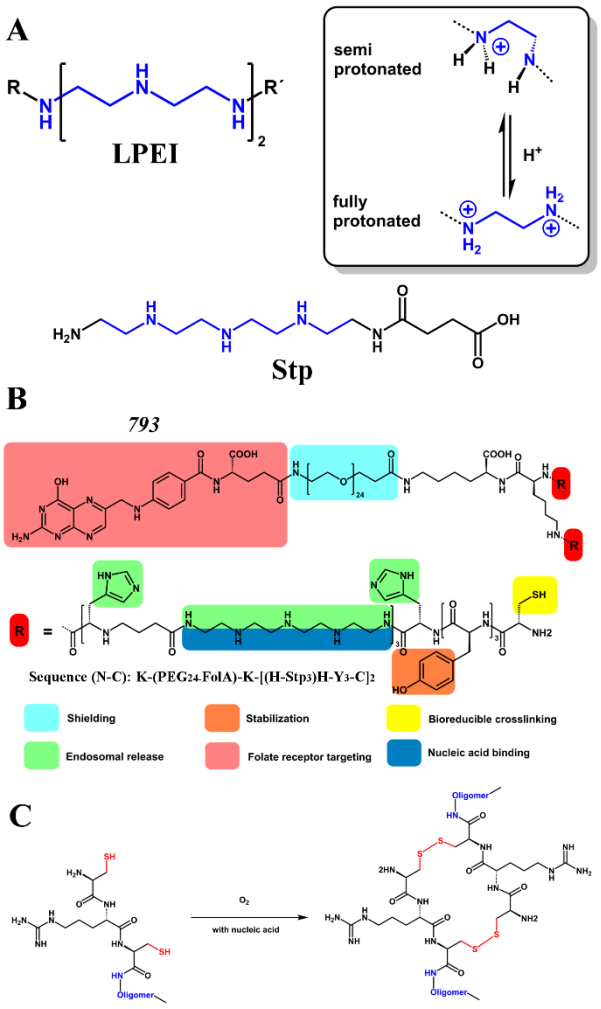

Fig. 2 A) Polycationic transfection agent linear polyethylenimine (LPEI) presented with different degrees of protonation and the synthetic amino acid Stp (succinimidyl tetraethylene pentamine), containing the aminoethylene motif B) Sequence-defined oligomer 793 containing the ligand folic acid, shielding agent PEG_{24}, lysine for branching, histidine for endosomal buffering, the synthetic amino acid Stp and tyrosine trimers and cysteines as stabilizing motifs C) Polyplex stabilization via twin-disulfide formation of CRC structures

To name a few, reduction of size and zeta-potential compared to unshielded polyplexes indicate the exposure of shielding domains on the surface. Receptor specificity of targeted polyplexes allows conclusions to the accessibility of targeting ligands. The evaluation of polyplex stability in agarose gel shift assays, which can also be performed under osmotic stressing, reducing conditions or serum exposure, provides information about the siRNA binding capacity of the oligocationic part and successful interaction of stabilizing motifs. Based on formerly established structure-activity relationships, we recently evaluated a library of 42 sequence-defined oligo(ethanamino)amides generated by solid-phase assisted syntheses on their

suitability as carriers for pDNA and siRNA.[69] The oligomers are assembled in 2-arm and 4-arm structures and consist of variations of Stp and Sph for nucleic acid binding and endosomal buffering, lysines as branching units, tyrosines for hydrophobic stabilization, cysteines for bioreducible crosslinking and histidines to further enhance the endosomal buffer capacity. To shield the polyplexes against aggregation and interaction with serum-containing media, all oligomers contained monodisperse, discrete polyethylene glycol (dPEG). Additionally, folic acid (FolA) for folic acid receptor targeting or glutamic acid as non-targeted control was used.

The combined integration of histidines and tyrosine trimers into two-arm structures (for example in oligomer ***793***) turned out to be the most efficient combination for siRNA mediated gene silencing (**Fig. 2B**). In agreement with their reduced stability and compaction compared to their pDNA counterparts, siRNA polyplexes showed less receptor specificity. Interestingly the same structure elements turned out to be most effective for pDNA and siRNA transfections, although both nucleic acids have different demands during their delivery process. It seems that shared critical steps of the nucleic acid delivery, including polyplex stabilization, endocytosis, and endosomal release dominated the selection of functional domains for this library of 42 oligomers.[69]

Polyplex stabilization via disulfide bond formation between cysteines can be reversed in the bioreductive environment of the cytosol with approximately 100−1,000-fold higher intracellular glutathione (GSH) levels.[70, 71] To further evaluate the influence of crosslinking by bioreducible disulfide bridges, several structures including 2-arm, 3-arm, and t-shaped oligomers were synthesized containing a twin disulfide-forming cysteine–arginine–cysteine (CRC) motif.[72] The CXC (cysteine–any amino acid–cysteine) motif was previously found to selectively form stable twin disulfide dimers with other CXC peptides. This process was particularly enhanced when the central amino acid is arginine (**Fig. 2C**).[73] When incorporated into sequence-defined oligo(ethanamino)amides, the CRC motif improves the stability of both pDNA and siRNA polyplexes in the presence of serum and also under short term reducing conditions (2 h incubation at 37 °C at 0.1 – 10 mM concentration of glutathione). Low surface exposure of the disulfides through PEG-shielding and the higher overall amount of disulfides in CRC-containing polyplexes compared to single cysteine structures may promote this probably kinetic effect. It is important to note that an increased stability did not necessarily result in better transfection efficacy. This might

be explained by an insufficient intracellular release or reduced accessibility of the nucleic acid cargo at the delivery site due to strong binding to the carrier.

Therefore, the influence of the CRC motif on siRNA transfection efficacies ranged from total abolishment (for already quite stable polyplexes) to significant increase (for less stable ones). PEGylated oligomers, usually lacking stability when formed into siRNA polyplexes, profit from the additional stabilization of twin disulfide motifs. Besides, the CRC motif could be used to tailor the size of polyplexes. Cationic oligomers with cysteines and tyrosine trimers decreased in size by incorporation of CRC motifs while polyplexes formed with oleic acid or PEG-containing oligomers increased in size. Altogether the CRC motif could be a useful tool for the optimization of polyplex stability and size depending on the delivery task.[72] In general, sizes of polyplexes formed with sequence-defined oligo(ethanamino)amides depend on the functional domains of the oligomer and the type of nucleic acid. Polyplexes formed with siRNA usually range from below 10 nm (when formed with PEGylated oligomers)[51] up to several hundred nanometers when multiple siRNA molecules are aggregated into one particle for example upon formulation with lipo-oligomers.[44, 64] Polyplexes formed with the much larger pDNA are less influenced by functional domains of the carrier and usually range above 100 nm.[40, 41, 69]

1.2.3 Modification of siRNA

Another strategy to stabilize siRNA polyplexes is the conversion of single siRNA molecules into larger polyanions by hybridization[74], chemical ligation[75], click-chemistry[76], and coformulation with pDNA[77] or other polyanions. Our group recently used DNA oligomers as adaptors to increase the size and charge of siRNA to form more stable polyplexes and thus boost transfection efficacies.[78] Several DNA/siRNA nanostructures ranging from DNA extension of one siRNA up to structures with two to ten siRNA units were merged, and polyplexes were formed with a 3-arm sequence-defined oligomer. Both polyplex stability and transfection efficacy could be improved with the extended structures. Interestingly, the larger constructs containing multiple siRNAs were less potent than the simple ones with one or two siRNA units. This observation might be explained by disturbed RISC loading or passenger strand removal due to steric hindrance of larger constructs. A step-by-step extension of a single siRNA revealed that a prolongation of up to 181 DNA nucleotides results in a significant improvement of transfection efficacy (**Fig. 3A**).

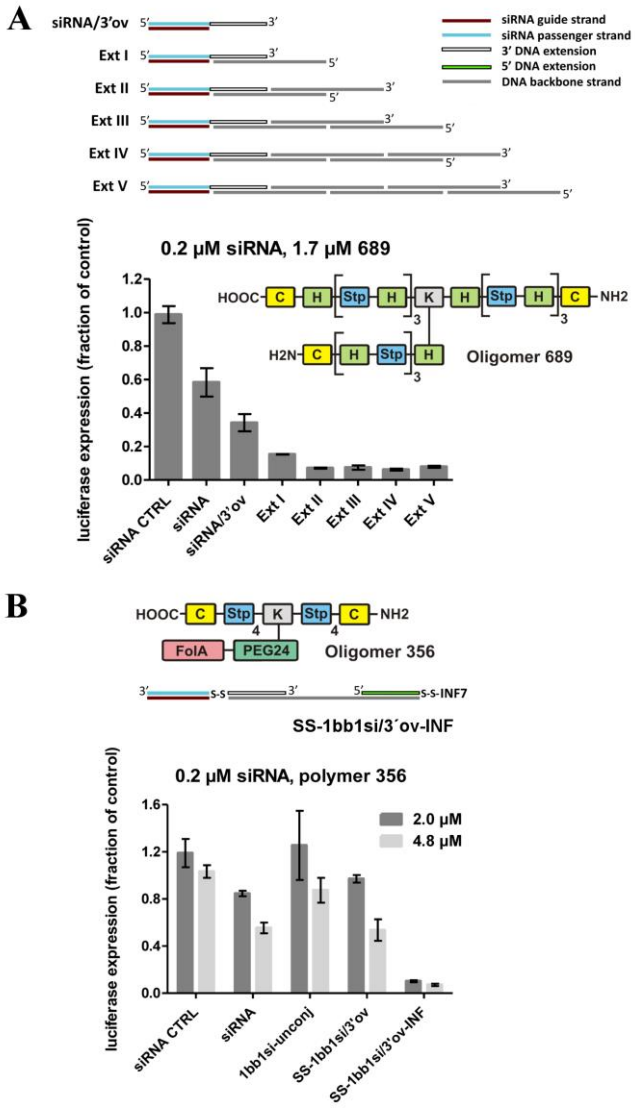

Fig. 3 A) Schematic representation of the stepwise DNA extension of siRNA and gene silencing of polyplexes formed with oligomer 689 and control siRNA, eGFP-targeted siRNA (siGFP) and all extensions in Neuro2A-eGFPLuc cells B) Gene silencing of folic acid targeted polymer 356 with bioreducibly extended siRNA and bioreducibly attached lytic peptide INF7.

This could also be confirmed when using the cationic polymer linear PEI as transfection agent[78], which is in good agreement with previous findings showing enhanced activity of linear PEI when using sticky siRNA.[74] The stabilizing effect of the siRNA modification ideally lasts throughout the delivery process where polyplex stability is critical but should not hinder the cytosolic release of the cargo. To avoid possible steric hindrance of the interaction of siRNA with the RISC, a bioreducible disulfide linker between the siRNA passenger strand and the DNA extension was introduced. In this way, the siRNA is liberated from the DNA adaptor in the cytosol (**Fig. 3B**).[78]

Altogether, several strategies can be applied to stabilize polyplexes with siRNA and sequence-defined cationic oligomers. Stabilization however is only one requirement for successful nucleic acid delivery. Extracellular shielding, receptor targeting for improved and specific intracellular uptake[79] and transport across the endolysosomal barrier[80, 81] are additional critical steps that have to be addressed.

1.3 Shielding and Targeting – The Polyplex as Trojan Horse

Nucleic acid formulations can be applied systemically by intravenous injection or locally for example by direct injection into the skin, retina, central nervous system or tumors. Depending on the delivery route, different extracellular tasks have to be considered. Intravenous administration of free siRNA would lead to rapid clearance and degradation by nucleases in the blood. The stable packaging of nucleic acids into polyplexes by oligocations is a way to prevent a loss of delivery efficacy. Complexation however may cause binding of positively charged polyplexes to serum proteins, activation of the innate immune system[82, 83], self-aggregation into larger microstructures or aggregation of erythrocytes and other blood cells[84] thus resulting in life-threatening conditions.[32] Shielding of positive charges by hydrophilic polymers such as polyethylene glycol (PEG)[49, 62, 79, 85-87], N-(2-hydroxypropyl) methacrylamide (pHPMA)[88-90], hydroxyethyl starch (HES)[91], hyaluronic acid[92], poly(2-oxazoline)[93] or polysarcosine[94] are well-established approaches to circumvent unspecific interactions of drug delivery systems. Hydrophilic shielding of polyplexes can significantly improve biocompatibility and blood circulation time.[95, 96] Long-term plasma circulation is a critical requirement for cancer therapy to take advantage of the “enhanced permeability and retention” (EPR) effect. By this mechanism of passive tumor targeting, circulating nanoparticles can extravasate and passively accumulate at tumor sites due to the leakiness of tumor vessels and ineffective lymphatic efflux.[97] Optimum polyplex shielding, however, may result in a loss of transfection efficacy due to reduced intracellular interaction with endolysosomal membranes thus preventing the endosomal escape of the cargo (“PEG dilemma”). PEGylation of PEI sharply reduced the transfection activity of the polyplexes. The linkage of PEG via acid-labile pyridylhydrazone bonds could recover the transfection efficacy by pH-triggered deshielding in the acidic endosomal environment.[21, 98]

To achieve specific receptor-mediated uptake, a broad range of ligands from small chemical compounds such as vitamins and drugs[51, 99-101], carbohydrates[61] to peptides[102], proteins[50, 87, 103-105], antibodies[106, 107] and aptamers[108] can be presented on the polyplex surface. In a dual targeting approach, pDNA polyplexes with PEI and sequence-defined oligoamino amides containing two different peptidic ligands showed a synergistic targeting effect. RGD, a peptide for integrin targeting, dominated in cell surface binding while peptide B6 for transferrin receptor-targeting contributed to intracellular uptake.[109, 110]

Solid-phase assisted synthesis enables the direct attachment of shielding and targeting domains to the oligocation in a sequence-defined manner. PEG and targeting moieties depending on their biophysical characteristics, however, can alter the polyplex formation process.[111] This might, on the one hand, result in self-aggregation of polyplexes leading to unspecific cellular uptake *in vitro* and clogging of blood vessels when applied intravenously. On the other hand, siRNA polyplexes with sequence-defined cationic FolA-PEG-oligomers with sizes below 10 nm have been reported. Such small structures undergo rapid renal clearance *in vivo*.[51, 79, 112] Considering the effect of shielding and targeting moieties on the polyplex formation, post-modification strategies present a promising alternative. Our group recently reported post-modified transferrin receptor (TfR) targeted siRNA polyplexes based on the sequence-defined cationic lipo-oligomer ***454***.[113] Polyplexes are pre-formed with the cysteine containing ***454*** without any shielding or targeting moieties. In a second step, PEG-Transferrin (Tf) or PEG-TfR-targeting-antibody (TfRab) are attached to the polyplex surface by bioreducible disulfide-linkage (**Fig. 4**). This approach both excludes the influence of PEG or ligands during the polyplex formation process and enables bioresponsive deshielding in reducing environments. The bulky negatively charged protein ligand Tf contributes with an additional shielding effect, leading to entirely shielded particles with sizes around 200 nm, nearly neutral zeta potential and low polydispersity by the addition of only 5 mol% PEG-Tf to the pre-formed polyplexes. Highly specific TfR-dependent cellular uptake and efficient target gene silencing could be demonstrated in several cell systems leading to potent tumor cell killing *in vitro*.

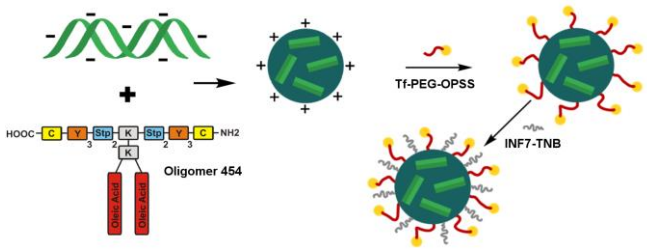

Fig. 4 Schematic illustration of Tf and INF7 post-modified siRNA polyplexes pre-formed with lipo-oligomer ***454***. Both Tf-PEG-OPSS and INF7-TNB contain reactive groups able to bond with cysteine thiol groups of oligomer

1.4 Endosomal Escape – The Major Bottleneck for Delivery?

The endosomal escape is considered as a major bottleneck for successful nucleic acid delivery.[80] When polyplexes are entrapped in vesicles after endocytosis, degradation by lysosomal enzymes under acidic conditions present a dead end for a significant amount of nucleic acids. Rapid endosomal escape is particularly required for the delivery of nuclease-sensitive siRNA. The disintegration or destruction of endosomal membranes should be triggered after the endocytosis for example by the acidification within the vesicles to avoid toxicity of nucleic acid formulations in the extracellular environment. Viruses developed efficient cytosolic delivery pathways. Endocytosed enveloped viruses such as influenza virus expose fusion peptides that are part of viral glycoproteins and trigger fusion of the viral with the endosomal membrane. Non-enveloped viruses such as rhinovirus or adenovirus present lytic domains which directly disrupt the endosomal membrane after endocytosis.[10] Synthetic virus-derived or artificial lytic peptides have been incorporated into polyplexes to enhance the endosomal escape.[13, 80, 114, 115] The synthetic peptide Inf7, a glutamic acid-enriched analog derived from the influenza hemagglutinin membrane protein HA2, triggers membrane disruption specifically at endosomal pH around 5 to 6, thus strongly increasing transfection efficiency of pDNA polyplexes after incorporation in a covalent or non-covalent manner.[116] The Inf7 peptide can be attached directly to the nucleic acid to improve the delivery of siRNA. Both the bioreversible attachment of Inf7 to the 5´-end of siRNA with a C6-ss-C6 spacer[51] and linkage to the 5′ DNA adaptor of DNA-extended siRNA[78] (**Fig. 3B**) lead to significantly enhanced gene knockdown of PEGylated FolA-targeted polyplexes. Inf7 was also an indispensable element of post-modified TfR targeted siRNA polyplexes.[113] However, unfavorable interaction of the

hydrophobic Inf7 peptide with fatty acids of lipid-containing oligomers was encountered when Inf7 was attached directly to the siRNA. To circumvent this issue, Inf7 was attached to the polyplex surface in a post-modification approach via a bioreducible disulfide linkage (**Fig. 4**).[113]

The antimalaria drug and hydrophobic weak base chloroquine accumulates in acidic endolysosomal vesicles and was found to enhance the endosomal escape of DEAE-dextran and polylysine polyplexes significantly.[117] Chloroquine-triggered vesicle swelling and subsequent generation of osmotic pressure, the inhibition of endolysosomal maturation due to pH buffering and a direct effect on nucleic acids by intercalation are the hypothesized mechanisms.[118, 119] The beneficial effect of endosomal buffering and osmotic swelling on endosomal escape was further investigated by the screening of polycations with “proton sponge” characteristics, which provide buffer capacity between physiological neutral and endolysosomal acidic pH.[120] Polyethylenimine (PEI) with repeating units of the aminoethylene motif was found to be a very potent transfection polymer.[33] In contrast to polymers such as polylysine that are fully protonated at neutral pH, proton sponge structures are only partly protonated at neutral pH and reach a higher degree of protonation throughout the endosomal acidification. It has been demonstrated that the increasing protonation leads to an influx of chloride and water; it has been hypothesized that the resulting osmotic pressure on the membrane triggers endosomal escape.[121, 122] Endosomal escape of polyplexes, however, is not always enhanced by endosomal buffer capacity of the polymers.[123, 124] Even for PEI polyplexes, PEGylation strongly reduced the endosomal escape.[21] Apparently, in addition to endosomal buffering and osmotic pressurizing, a direct exposure of the pH-induced cationic charge residues of the protonated polymer to the lipid membrane is needed for destabilization and subsequent endosomal burst.[10, 36] In our view, cooperation of osmotic pressuring (such as by chloroquine or PEI) with direct target lipid membrane disruption activity (such as by cationic interaction with phospholipids, lytic or fusogenic peptides or lipids) is required, similarly as a moderately pressured gas balloon will pop only upon the stitch by a needle.

The diaminoethylene motif of PEI has been incorporated in synthetic building blocks such as succinoyl-tetraethylene-pentamine (Stp) to synthesize sequence-defined oligocations with proton sponge activity.[42] The incorporation of the basic amino acid

histidine can provide additional pH-buffering via the protonation of imidazole groups, thus facilitating endosomal escape.[69, 125, 126] Histidinylated pLys or pLys/His copolymers also present proton sponges and, in contrast to unmodified pLys, mediate efficient pDNA and siRNA delivery.[127, 128] As an alternative or in addition to the proton sponge effect, endosomal pH-specific membrane destabilization can be mediated by hydrophobic polymer or lipid domains.[43, 129-131] Sequence-defined lipo-oligoamino amides such as oligomer ***454*** combine both proton sponge activity and pH-triggered lytic activity of hydrophobic domains to achieve enhanced endosomal escape.[64] Oligomer ***454*** was used for surface coating of siRNA-loaded mesoporous silica nanoparticles (MSN) thus leading to efficient release from the endosome and subsequent high transfection efficacy of this delivery system.[132] MSN have been recognized as powerful tools for packaging of fragile or toxic pharmaceuticals. By tuning of the internal surface charge of the pores as well as the pore size and morphology in the MSN, very high siRNA loadings of up to 380 µg per mg MSN with desorption rates of up to 80 % after 24 h could be achieved. The external exposure of mercapto groups allowed for interactions with the cysteine containing ***454*** to neutralize negative surface charges of the MSN for better cell binding and enhanced endosomal escape. In several examples siRNA knockdown efficacies of 80 % and more could be achieved with a very low exposure of the cells to mesoporous silica.[132]

1.5 Polyplexes *in vivo*

Efficient and targeted gene knockdown *in vivo* without off-target side effects is the ultimate goal of siRNA delivery. The genetic evolution of viruses resulted in natural masterpieces of nucleic acid delivery and can partly be mimicked by the chemical evolution of synthetic carrier systems. The solid-phase assisted synthesis of sequence-defined oligomers is an elegant approach to shuffle functional domains and draw structure-activity relationships.[43, 69, 126] Michael addition chemistry has been applied for semi-automated synthesis of thousands of polymers to evaluate combinations of amines and hydrophobic (di)acrylates with high-throughput transfection screenings, resulting in libraries of poly(β-aminoesters) for pDNA delivery and lipophilic modified oligoamines (lipidoids) for siRNA delivery.[57, 133-135] Packaging of cargo nucleic acids in stable, well-sized and monodisperse polyplexes, shielding against cargo degradation and undesired cross-reactions during blood circulation,

efficient cell binding and uptake, and sufficient endosomal release of the nucleic acid in bioactive form are prerequisites of successful *in vivo* delivery. Several *in vitro* screening methods can be utilized to examine each critical step of the delivery process. Still such *in vitro* assays are only partly predictive of the performance in whole organisms. Therefore, not least because of animal welfare considerations, to keep numbers of experimental animals as low as possible, identification of most relevant selection criteria for *in vivo* efficacy and design of corresponding robust screening assays has critical importance.[136] A recent noteworthy example in this direction is the identification of four necessary structural and pKa criteria for the prediction of *in vivo* performance of siRNA lipidoid nanoparticles.[137] Extracellular stability of polyplexes has recently been confirmed as a critical hurdle for the *in vivo* delivery of oligonucleotides.[60, 113] A nanomicelle-based platform prepared from mRNA and (PEG)-polycation block copolymers showed significantly enhanced *in vivo* stability and mRNA translation when a stabilizing cholesterol (Chol) moiety was attached.[41] In sharp contrast, when evaluating mRNA degradation after serum incubation, nanomicelles with and without Chol showed comparable nuclease resistance. Destabilization of nanomicelles in the blood but not in serum in the presence of anionic macromolecules with high charge densities on cell surfaces, such as proteoglycans was formulated as a potentially important factor for extracellular stability. Indeed, in the presence of anionic macromolecules, which exist in the blood but not in serum, Chol-containing nanomicelles showed enhanced stability compared to mRNA nanomicelles without Chol.[60] These findings emphasize the need to develop assays that closely mimic *in vivo* conditions for best possible predictive value. Another critical parameter for polyplex biodistribution and intra-tissue delivery is the optimal nanoparticle size. Too large nanoparticles may be restricted in intra-tissue diffusion.[138] Very small siRNA nanoparticles of < 10 nm have been shown to be stable in the blood upon systemic intravenous injections but are rapidly eliminated via the kidneys in approximately four hours, with recovery of intact polyplexes from the urine.[51] Such small nanoparticles, however, can be utilized for local intratumoral administration. Series of sequence-defined oligomers, which include a cationic (oligoethanamino)amide core, cysteines and PEG coupled to the antifolate drug methotrexate (MTX) as terminal targeting ligand were synthesized recently (**Fig. 5A**).[139]

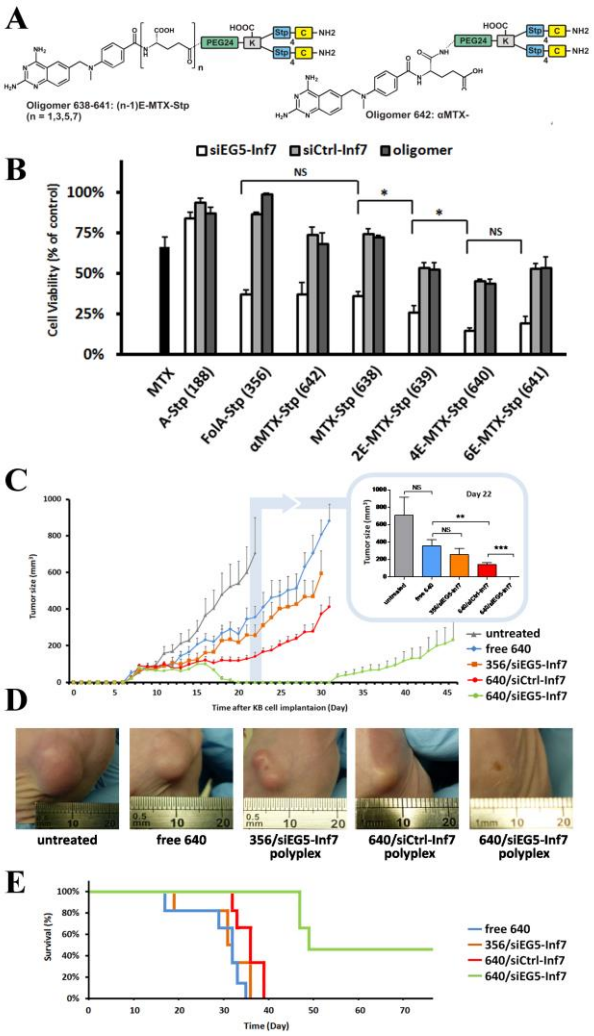

Fig. 5 A) Overview of the oligomers with MTX polyglutamates B) Cell viability of KB cells after transfection with Inf7 peptide-modified EG5-targeted siRNA (siEG5-Inf7) or control siRNA (siCtrl-Inf7) polyplexes. Cells were transfected with MTX conjugates (***638***-***642***), alanine conjugate (***188***) or folate conjugate (***356***). Free MTX was applied in concentrations corresponding to that of siRNA polyplexes C) Therapeutic efficacy of MTX-conjugated ***640*** polyplexes (with siEG5-Inf7 or siCtrl-Inf7), free oligomer ***640*** (without siRNA), or folate-conjugated ***356***/siEG5-Inf7 polyplexes in KB xenograft (n = 6 per group). The insert shows a comparison of the tumor volume in different groups 5 days after the last treatment (day 22). D) Representative KB tumor lesions from the cohorts in C) on day 25. E) The Kaplane-Maier survival curve of the animals treated with the indicated formulations. In the animals receiving 640/siEG5-Inf7 polyplexes, tumors largely disappeared by day 22, and in 3 mice no recurrence was observed until the end of the study (day 70).

These oligomers form homogeneous spherical siRNA polyplexes with hydrodynamic average diameter of approximately 6 nm and were therefore applied intratumorally *in vivo*. The endosomolytic peptide Inf7 was coupled via bioreducible linkage to the 5´ end of the siRNA to enhance endosomal escape of the polyplexes. MTX is a well-

established chemotherapeutic agent and serves as both targeting ligand and anticancer agent. In combination with toxic eglin5 (EG5) siRNA potent dual treatment of KB cancer cells could be achieved (**Fig. 5B**). MTX-conjugated polyplexes bind and enter KB cells via FolA receptors. Attachment of MTX significantly increased the intratumoral retention (168 h) of the siRNA, as compared to alanine-substituted non-targeted control polyplexes (48 h). The combination of MTX-conjugated polyplexes and EG5 siRNA provided enhanced antitumoral potency with 50 % of recurrence-free survival of KB tumor-bearing mice (**Fig. 5C-E**). Polyglutamylation of the MTX at its γ-carboxylic acid was introduced to increase the potency of MTX-targeted polyplexes.[139] Glutamic acid residues are attached to MTX by the folylpolyglutamyl synthetase (FPGS) after cell entering, producing MTX polyglutamates that are retained in the cytosol and represent the more pharmacologically active form.[140] Polyglutamylated MTX inhibits dihydrofolate reductase (DHFR), resulting in blockage of de novo synthesis of thymidylates and purines and consequently of DNA and RNA.[141] Polyplexes formed with polyglutamylated MTX oligomers were found to be more cytotoxic than free MTX presumably because the degree of glutamylation of MTX conjugates correlates to DHFR inhibition potency.[139] Polyplex size and sophisticated targeting strategies are particularly important for the delivery of nucleic acids into the brain. The therapy of central nervous system (CNS) and brain pathologies, including Parkinson's disease, Alzheimer's disease, and glioma, are inadequate because of the limited ability to deliver drugs across the blood-brain barrier (BBB).[142] The BBB separates circulating blood from the brain extracellular fluid (BECF) in the CNS and protects the brain from various circulating substances.[143, 144] Barbiturate coated gold nanoparticles (GNPs) with sizes ranging from 20 to 110 nm have been evaluated regarding their ability to penetrate the BBB. GNPs of 70 nm size showed the highest uptake with maximum amounts of gold within the brain cells.[145] The BBB is especially restrictive in normal healthy brain, but also a barrier in diseased brain such as glioma. In order to generate stable polyplexes in a size range suitable for glioma-targeted siRNA delivery across the BBB, a solid-phase synthesized lipo-oligomer (***49***) containing two central oleic acids, 4 Stp units and two terminal cysteines has been combined with a lipoprotein receptor-related protein LRP-targeting oligomer containing a precise sequence of Angiopep-2 peptide linked with PEG, 8 Stp units and two terminal cysteines (***727***) (**Fig. 6A**).[146]

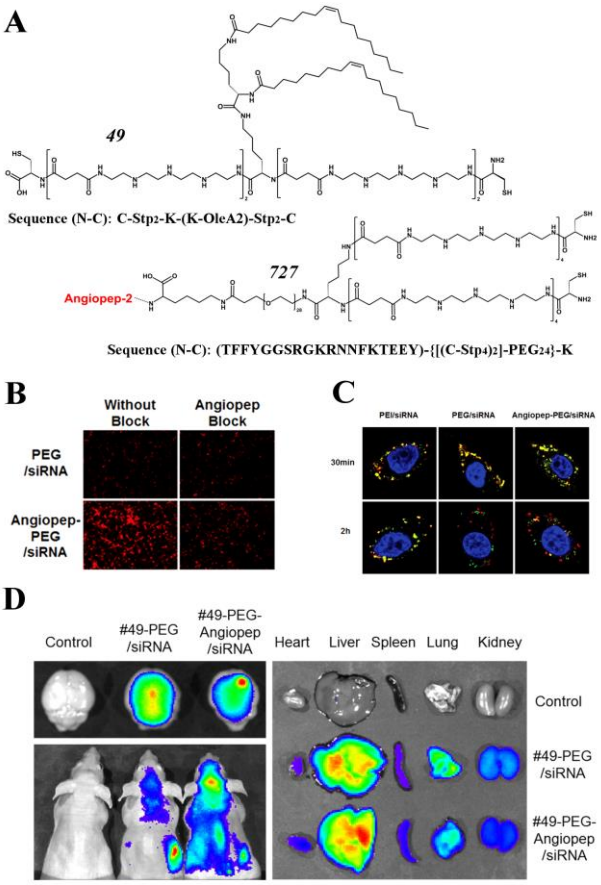

Fig. 6 A) Sequence and chemical structure of untargeted lipo-oligomer 49 and Angiopep-2-targeted shielded 2-arm polymer 727 B) Cellular uptake of cy3-labeled siRNA polyplexes PEG/siRNA and Angiopep-PEG/siRNA with and without Angiopep pretreatment (block) in U87/Luc cells C) Cellular uptake and release of polymer/siRNA complexes in U87/Luc cells with time. PEI/siRNA complex was exploited as control. Red: Cy3-siRNA; Green: BODIPY-labeled polymer Blue: Hoechst D) Distribution of polymer/siRNA complexes *in vivo*. Real-time fluorescence images of glioma model nude mice injected with saline, PEG/siRNA complex, and Angiopep-PEG/siRNA complex after 24 h. Fluorescence images of excised brain (upper left) and peripheric organs (right).

siRNA-polyplexes around 100 nm in size with low polydispersity and nearly neutral zeta potential could be generated. This emphasizes the possibility to tailor polyplex characteristics by mixing oligomers with different functional subdomains in precise ratios. The addition of the non-targeted lipo-oligomer increases the polyplex size to avoid rapid renal clearance and facilitates the endosomal escape of the polyplexes. High cellular uptake of Angiopep-2 targeted polyplexes into U87 glioma cells could be detected and was reversible upon ligand competition by pretreatment of the cells with free Angiopep-2 (**Fig. 6B**). Endosomal escape efficacy and the cytosolic reversibility of the extracellular polyplex stabilization via disulfide bond formation between

cysteines was shown by fluorescent microscopy (**Fig. 6C**). The separation behavior of fluorescently labeled carrier and siRNA was detected 30 min and 2 hours after polyplex endocytosis into U87 glioma cells. Colocalization of BODIPY labeled carrier oligomer and Cy3-labeled siRNA was detected 30 min after internalization. After 2 hours, initially complexed carrier and Cy3-siRNA began to separate in the cytosol, allowing the siRNA cargo to be incorporated into the RISC for efficient gene downregulation. BODIPY labeled branched polyethylenimine (bPEI) was selected as a non-reducible control to prepare Cy3-siRNA polyplexes. As expected, bPEI/siRNA polyplexes remained a tight binding between carrier and siRNA after 2 hours. These observations confirm endosomal escape of both formulations and GSH-triggered reductive disassembly of polyplexes only in case of the sequence-defined oligomers. The Angiopep-2-targeted siRNA polyplexes exhibited effective siRNA delivery, resulting in significant gene downregulation both in glioma cells and upon intravenous delivery in glioma model nude mice without significant biotoxicity. High amounts of fluorescently labeled siRNA could be detected in the brain when targeted polyplexes where applied (Figure 6d). BAG3 siRNA was chosen as therapeutic cargo.[147] BAG3 is a member of the BAG family of HSC/HSP70 co-chaperones, which plays a critical role in tumor cell survival.[147] BAG3 downregulation has been reported to sensitize cells to tumor necrosis factor-related apoptosis inducing ligand (TRAIL)-dependent apoptosis.[148] Almost 70 % of BAG3 expression (determined at mRNA and protein level) was inhibited in U87 glioma cells after intravenous administration of Angiopep-2-targeted polyplexes compared to the saline treated control group, which should induce effective TRAIL-dependent apoptosis of the tumor cells.[146]

1.6 Aim of the Thesis

Sequence-defined cationic oligoaminoamide oligomers can mimic the dynamic and bioresponsive behavior of viruses and present a group of highly versatile nucleic acid carriers. Solid-phase assisted precise synthesis and establishment of structure–activity relationships enables optimization of this nucleic acid carrier class. In properly protected form, all natural amino acids, synthetic building blocks and other compounds such as fatty acids, dyes or sugars can be incorporated into customized oligomers.

In this thesis, the main focus was the optimization of the synthesis of oleic acid containing structures and the biodegradability of oligocationic carriers.

As a first aim of the thesis, the synthesis of cationic oligomers containing oleic acid had to be optimized to minimize side products. Oleic acid is a substantial part of several nucleic acid carriers as it provides polyplex stabilization via hydrophobic interactions and enhanced endosomolytic activity by lipid membrane interaction. TFA-mediated cleavage of acid-labile protecting groups and the oligomer from the resin leads to side products via protonation of the double bond, subsequent nucleophilic addition of the trifluoroacetate anion and TFA ester hydrolysis in neutral or basic aqueous solution during storage or polyplex formation. Biophysical properties and biological performance of siRNA polyplexes of structures containing intact oleic acid were to be investigated in comparison to analogs with chemically stable stearic acid or 8-nonanamidooctanoic acid moieties and an analog containing only the hydroxylated side product. The main focus was to be put on the effect of intact oleic acid on the endosomolytic activity profile, transfection efficiency and cytotoxicity.

The second aim was the design, synthesis and evaluation of the bioactivity of biodegradable lipo-oligomers. Biodegradability was to be introduced by two different strategies, first via a bioreducible disulfide building block and second by introducing cleavage sites for enzymatic lysosomal degradation.

Bioreducible lipo-oligomers should be synthesized by solid-phase assisted synthesis by precise incorporation of the disulfide building block Fmoc-succinoyl-cystamine between a lipophilic diacyl (bis-myristyl, bis-stearyl or bis-cholestanyl) domain and an ionizable oligocationic siRNA binding unit. Cytosolic glutathione-mediated disassembly of the polyplexes should improve the release of siRNA and RNA-induced silencing

complex formation. Especially the effect on transfection efficiency and toxicity had to be analyzed.

Enzymatic degradability should be tailored by precise integration of cleavage sites such as L-Arg dipeptides. Degradation of a surplus of carrier molecules by lysosomal enzymes such as cathepsin B targets the majority of transfection material which is known to initially accumulate in the lysosomal compartment. Most importantly, the influence of improved biodegradability on cell tolerability was to be studied.

The last aim was the modification of siRNA lipo-polyplexes and proteins with shielding and targeting domains to enhance the uptake in glioma and brain endothelial cells. Polyplexes were to be modified with various peptide ligands using click chemistry by incorporating azide functions in the lipo-oligomers and DBCO moieties in the shielding and targeting agents. Protein uptake in glioma cells was to be improved by modification with apelin-derived peptides via targeting of the apelin receptor APLNR.

2 Materials and Methods

2.1 Materials

The solvents, reagents and buffers used for the experiments are presented in **Table 1**, **Table 2** and **Table 3**.

Table 1 Solvents used for experimental procedures

Solvent	CAS-No.	Supplier
Acetonitrile [1]	75-05-8	VWR Int. (Darmstadt, Germany)
Chloroform [2]	67-66-3	VWR Int. (Darmstadt, Germany)
Chloroform-d [3]	865-49-6	Euriso-Top (Saint-Aubin Cedex, France)
Deuterium oxide [3]	7789-20-0	Euriso-Top (Saint-Aubin Cedex, France)
Dichloromethane [4]	75-09-2	Bernd Kraft (Duisburg, Germany)
*N,N-D*imethylformamide [5]	68-12-2	Iris Biotech (Marktredewitz, Germany)
Dimethyl sulfoxide [6]	67-68-5	Sigma-Aldrich (Munich, Germany)
Ethanol absolute [4]	64-17-5	VWR Int. (Darmstadt, Germany)
Ethyl acetate [7]	141-78-6	Staub & Co. (Nürnberg, Germany)
n-Heptane [8]	142-82-5	Grüssing (Filsum, Germany)
n-Hexane [8]	110-54-3	Brenntag (Mülheim/Ruhr, Germany)
Methanol [4]	67-56-1	Fisher Scientific (Schwerte, Germany)
Methanol-d4 [3]	811-98-3	Euriso-Top (Saint-Aubin Cedex, France)
Methyl-*tert*-butyl ether [9]	1634-04-4	Brenntag (Mülheim/Ruhr, Germany)
N-Methyl-2-pyrrolidone [5]	872-50-4	Iris Biotech (Marktredewitz, Germany)
Tetrahydrofuran [4]	109-99-9	Fisher Scientific (Schwerte, Germany)
Water [10]	7732-18-5	In-house purification

[1] HPLC grade; [2] DAB grade; [3] NMR grade (> 99.9 %); [4] analytical grade; [5] peptide grade; [6] BioReagent grade (> 99.9 %); [7] purum, distilled before use; [8] purissimum; [9] synthesis grade; [10] purified, deionized;

Table 2 Reagents used for experimental procedures

Reagent	CAS-No.	Supplier
1-Hydroxybenzotriazole hydrate	123333-53-9	Sigma-Aldrich (Munich, Germany)
2-Chlorotritylchloride resin	42074-68-0	Iris Biotech (Marktredewitz, Germany)
5,5′-Dithiobis(2-nitrobenzoic acid)	69-78-3	Sigma-Aldrich (Munich, Germany)
5β-Cholanic acid	546-18-9	Sigma-Aldrich (Munich, Germany)
Acetic acid	64-19-7	Sigma-Aldrich (Munich, Germany)
Acetic anhydride	108-24-7	Sigma-Aldrich (Munich, Germany)
Agarose NEEO Ultra	9012-36-6	Carl Roth (Karlsruhe, Germany)
Boc-L-Cys(Trt)-OH	21947-98-8	Iris Biotech (Marktredewitz, Germany)
Bromophenol blue	115-39-9	Sigma-Aldrich (Munich, Germany)
cis-2-Hexene	7688-21-3	Sigma-Aldrich (Munich, Germany)
Cyclohexene	110-83-8	Sigma-Aldrich (Munich, Germany)
Cystamine · 2HCl	56-17-7	Sigma-Aldrich (Munich, Germany)
D-(+)-Glucose monohydrate	14431-43-7	Merck Millipore (Darmstadt, Germany)
DBU	6674-22-2	Sigma-Aldrich (Munich, Germany)
Dde-L-Lys(Fmoc)-OH	156648-40-7	Iris Biotech (Marktredewitz, Germany)

Dibenzocyclooctyne-acid	1353016-70-2	Sigma-Aldrich (Munich, Germany)
Diisopropylcarbodiimid (DIC)	693-13-0	Sigma-Aldrich (Munich, Germany)
EDTA disodium salt dihydrate	6381-92-6	Sigma-Aldrich (Munich, Germany)
Fmoc-8-aminooctanoic acid	126631-93-4	Iris Biotech (Marktredewitz, Germany)
Fmoc-L-Arg(Pbf)-OH	154445-77-9	Iris Biotech (Marktredewitz, Germany)
Fmoc-D-Arg(Pbf)-OH	187618-60-6	Iris Biotech (Marktredewitz, Germany)
Fmoc-L-Glu-O*t*Bu	84793-07-7	Merck Millipore (Darmstadt, Germany)
Fmoc-L-Gly-OH	29022-11-5	Iris Biotech (Marktredewitz, Germany)
Fmoc-L-His(Trt)-OH	109425-51-6	Iris Biotech (Marktredewitz, Germany)
Fmoc-L-Leu-OH	35661-60-0	Iris Biotech (Marktredewitz, Germany)
Fmoc-L-Lys(Boc)-OH	71989-26-9	Iris Biotech (Marktredewitz, Germany)
Fmoc-L-Lys(Fmoc)-OH	78081-87-5	Iris Biotech (Marktredewitz, Germany)
Fmoc-L-Lys(ivDde)-OH	204777-78-6	Iris Biotech (Marktredewitz, Germany)
Fmoc-L-Lys(N_3)-OH	159610-89-6	Iris Biotech (Marktredewitz, Germany)
Fmoc-L-Trp(Boc)-OH	43824-78-6	Iris Biotech (Marktredewitz, Germany)
Fmoc-L-Tyr(*t*Bu)-OH	71989-38-3	Iris Biotech (Marktredewitz, Germany)
Fmoc-L-Val-OH	68858-20-8	Iris Biotech (Marktredewitz, Germany)
Fmoc-*N*-amido-dPEG$_{24}$-acid	756526-01-9	Quanta Biodesign (Powell, OH, USA)
Fmoc-OSu	82911-69-1	Iris Biotech (Marktredewitz, Germany)
Fmoc-Stp(Boc_3)-OH	-	In-house synthesis [13]
GelRed	-	Biotium Inc. (Hayward, CA, USA)
Glutathione reduced	70-18-8	Sigma-Aldrich (Munich, Germany)
HBTU	94790-37-1	Multisyntech (Witten, Germany)
Heparin sodium 5000 I.E/mL	9041-08-1	ratiopharm GmbH (Ulm,.Germany)
HEPES	7365-45-9	Biomol (Hamburg, Germany)
Hydrazine monohydrate	7803-57-8	Sigma-Aldrich (Munich, Germany)
Hydrochloric acid solution	7647-01-0	Sigma-Aldrich (Munich, Germany)
MTT	298-93-1	Sigma-Aldrich (Munich, Germany)
Myristic acid	544-63-8	Sigma-Aldrich (Munich, Germany)
N,N-Diisopropylethylamine	7087-68-5	Iris Biotech (Marktredewitz, Germany)
N-Hydroxysuccinimide (NHS)	6066-82-6	Sigma-Aldrich (Munich, Germany)
Ninhydrin	485-47-2	Sigma-Aldrich (Munich, Germany)
Nonanoic acid	112-05-0	Sigma-Aldrich (Munich, Germany)
Oleic acid	112-80-1	Sigma-Aldrich (Munich, Germany)
Phenol	108-95-2	Sigma-Aldrich (Munich, Germany)
Piperidine	110-89-4	Iris Biotech (Marktredewitz, Germany)
Potassium cyanide	151-50-8	Sigma-Aldrich (Munich, Germany)
Pybop®	128625-52-5	Multisyntech GmbH (Witten, Germany)
Sephadex® G-10	9050-68-4	GE Healthcare (Freiburg, Germany)
Sodium hydroxide (anhydrous)	1310-73-2	Sigma-Aldrich (Munich, Germany)
Sodium hydroxide solution	1310-73-2	Sigma-Aldrich (Munich, Germany)
SPDP	68181-17-9	Thermo Scientific (Waltham, USA)
Stearic acid	57-11-4	Sigma-Aldrich (Munich, Germany)
STOTDA	172089-14-4	Sigma-Aldrich (Munich, Germany)
Succinic anhydride	108-30-5	Sigma-Aldrich (Munich, Germany)
Suc-PEI 10 %	-	In-house synthesis[149]
TCEP	51805-45-9	Sigma-Aldrich (Munich, Germany)
Tetraethylene pentamine·5HCl	4961-41-5	Sigma-Aldrich (Munich, Germany)
Triethylamine	121-44-8	Sigma-Aldrich (Munich, Germany)
Trifluoroacetic acid	76-05-1	Iris Biotech (Marktredewitz, Germany)
Triisopropylsilane	6485-79-6	Sigma-Aldrich (Munich, Germany)
Triton™ X-100	9002-93-1	Sigma-Aldrich (Munich, Germany)
Trizma® base	77-86-1	Sigma-Aldrich (Munich, Germany)

Table 3 Buffers used for experimental procedures

Buffer	Composition
10 mM HCl SEC solvent	693 mL water, 300 mL acetonitrile, 7 mL 1M HCl solution
Electrophoresis loading buffer	6 mL glycerine, 1.2 mL 0.5 M EDTA solution (pH 8.0), 2.8 mL H_2O, 20 mg bromophenol blue
Ellman buffer	0.1 M sodium phosphate buffer (pH 8.0), 1 mM EDTA
HBG	20 mM HEPES, 5 % glucose, pH 7.4
TBE buffer	89 mM Trizma® base, 89 mM boric acid, 2 mM EDTA-Na_2

Citrate-buffered human blood for erythrocyte leakage assays was kindly supplied by Klinikum der Universität München (Munich, Germany). Recombinant nlsEGFP was produced as previously reported.[150] g7 (H_2N-Gly-L-Phe-D-Thr-Gly-L-Phe-L-Leu-L-Ser(O-β-D-Glucose)-$CONH_2$) and scrg7 (H_2N-Gly-Leu-Phe-Phe-Gly-Ser(O-β-D-Glucose)-D-Thr-$CONH_2$) were provided by Novo Nordisk (Bagsværd, Dänemark) within the COMPACT (Collaboration on the Optimization of Macromolecular Pharmaceutical Access to Cellular Targets) consortium.

2.1.1 Equipment for solid-phase synthesis

Automated parallel synthesis or synthesis with microwave irradiation was carried out using a Biotage Syro Wave (Biotage AB, Uppsala, Sweden) peptide synthesizer. Disposable polypropylene (PP) syringe microreactors with the volume sizes 2 mL, 5 mL, and 10 mL were purchased from Multisyntech (Witten, Germany). It was conducted with polytetrafluoroethylene (PTFE) filters. The recommended size of the reactors was chosen according to the resin amount. For manual solid-phase synthesis microreactors with polyethylene filters were used. Reactors were mixed with an overhead shaker during reactions.

2.1.2 siRNA

All siRNAs and modified siRNA compounds used are presented in **Table 4**. They were synthesized by Roche Kulmbach GmbH (now Axolabs GmbH, Kulmbach, Germany).

Table 4 siRNA strands

siRNA	Target	Sequence
siCtrl	-	5'-AuGuAuuGGccuGuAuuAGdTsdT-3' (sense) 5'-CuAAuAcAGGCcAAuAcAUdTsdT-3' (antisense)
siGFP	eGFP-Luc	5'-AuAucAuGGccGAcAAGcAdTsdT-3' (sense) 5'-UGCUUGUCGGCcAUGAuAUdTsdT-3' (antisense)

Small letters: 2'-methoxy-RNA, s: phosphorothioate. All nucleic acids were synthesized by the Roche Kulmbach GmbH (now Axolabs GmbH, Kulmbach, Germany).

2.1.3 Cell culture

Cell culture work was carried out by Dr. Wei Zhang, Dr. Katharina Müller, Dr. Dian-Jang Lee, Jasmin Kuhn and Dr. Yanfang Wang (Pharmaceutical Biotechnology, LMU) and by Dr. Giorgia Mastrella (Department of Neurosurgery, Klinikum LMU). All cell culture media, antibiotics and fetal bovine serum (FBS) were purchased from Invitrogen (Karlsruhe, Germany). The individual media used for the different cell cultures are summarized in **Table 5**. All media were supplemented with 10 % FBS, 4 mM stable glutamine, 100 U/mL penicillin and 100 µg/mL streptomycin. Exponentially growing cells were detached from the culture flasks using trypsin-EDTA solution (Invitrogen, Karlsruhe, Germany) and cell suspensions were seeded at the desired density for each experiment. Luciferase cell culture lysis buffer and D-luciferin sodium salt were purchased from Promega (Mannheim, Germany).

Table 5 Overview of the used cell lines and culture media

Cell line	Description	Medium
bEnd.3 [1]	Mouse brain endothelioma cells	DMEM (5 % glucose)
DU145/eGFPLuc[44]	Human prostate cancer cells expressing the eGFP-Luciferase fusion gene	RPMI-1640
Huh7/eGFPLuc[151]	Human hepatoma cells	DMEM and Ham's F12 medium (50:50)
KB/eGFPLuc[51]	Human cervix carcinoma cells expressing the eGFP-Luciferase fusion gene	RPMI-1640, folate-free
Neuro2A	Mouse neuroblastoma cells	DMEM
Neuro2A/eGFPLuc[44]	Mouse neuroblastoma cells expressing the eGFP-Luciferase fusion gene	DMEM

[1] bEnd.3 cells were provided by GSK (Brentford, UK) within the COMPACT consortium.

2.2 Methods

2.2.1 Synthesis of disulfide-linker building block (ssbb):

Fmoc-succinoyl-cystamine

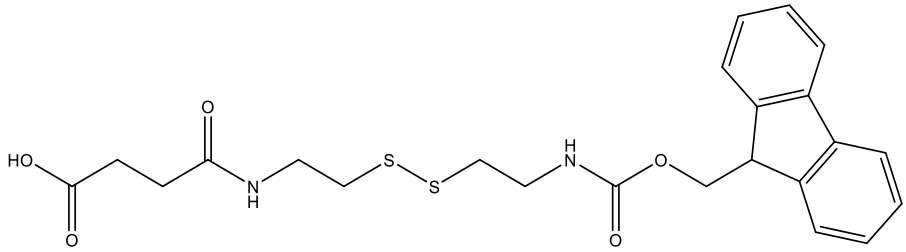

15.0 g of cystamine dihydrochloride (66.6 mmol, 1 eq.) were suspended in 150 mL of THF with 23.2 mL of DIPEA (133.2 mmol, 2 eq.) and cooled down to -80 °C. 18.0 g (53.3 mmol, 0.8 eq.) of Fmoc-OSu were dissolved in 200 mL of THF and added dropwise over the course of 3 h. The reaction was stirred for additional 1 h at -80 °C and then for 1 h at room temperature (RT). DIPEA (23.2 mL, 133.2 mmol, 2 eq.) was added and the reaction mixture was cooled to 0 °C. Succinic anhydride (12.0 g, 119.9 mmol, 1.8 eq.) was dissolved in 150 mL of THF. This solution was added dropwise to the reaction mixture at 0 °C and stirred over-night. The reaction mixture was concentrated to approximately 200 mL, mixed with 200 mL of DCM and was washed 5 × with 0.1 M sodium citrate buffer (pH 5.2). The organic phase was dried over sodium bicarbonate, concentrated and purified by dry column vacuum chromatography (DCVC) using a n-heptane/EtOAc gradient (starting from 1:1) to elute Fmoc-byproducts, followed by a EtOAc/MeOH gradient to isolate the product. The solvent was removed under reduced pressure to give 6.2 g of a white solid (13.1 mmol, 24.5 %).

2.2.2 Loading of a 2-chlorotrityl chloride resin with an Fmoc protected amino acid

(T-shape: 0.75 eq. Fmoc-Tyr(*t*Bu)-OH or Fmoc-Cys(Trt)-OH; i-shape: 0.75 eq. Fmoc-Stp(Boc_3)-OH; U-shape: 0.75 eq. Fmoc-Lys(Fmoc)-OH; $DBCO_2$-PEG_{24}-g7 agents: 0.75 eq. Fmoc-N-amido-$dPEG_{24}$-acid; Apelin-derived peptides: 0.75 eq. Fmoc-Phe-OH (Apelin-13), Fmoc-Ala-OH (Apelin-F13A), Fmoc-Lys(Boc)-OH (Apelin-13scr)

After swelling of 750 mg of 2-chlorotrityl chloride resin (1.2 mmol chloride) in water-free DCM for 10 min, the first Fmoc protected amino acid and DIPEA (1.5 eq.) were added to the resin for 1 h. The reaction solvent was drained and a mixture of DCM/MeOH/DIPEA (80:15:5) was incubated twice for 10 min. After removal of the reaction mixture, the resin was washed 5 times with DCM.

About 30 mg of the resin were collected and dried to determine the loading of the resin. For this purpose, an exact amount of resin was treated with 1 mL deprotection solution (20 % piperidine in DMF) for 1 h. The solution was diluted and absorption was measured at 301 nm. The loading was then calculated according to the equation: resin load [mmol g^{-1}] = (A•1000)•(m[mg]•7800•df)$^{-1}$ with df as dilution factor.

The resin was treated twice with 20 % piperidine in DMF and twice with 20 % piperidine DMF with 2 % DBU to remove the Fmoc protection group. The resin was washed with DMF, DCM and n-hexane and dried in vacuo.

2.2.3 Oligomer and targeting and shielding agent synthesis

Oligomers were synthesized using a 2-chlorotrityl resin preloaded with the first C-terminal amino acid of the respective topology (see **2.2.2**) as solid support. All sequences and topologies of oligomers can be found in **Table 19**, all sequences of targeting and shielding agents can be found in **Table 20**. Unless otherwise stated, coupling steps were carried out using 4 eq. Fmoc-amino acid, 4 eq. HOBt, 4 eq. PyBOP or HBTU and 8 eq. DIPEA (10 mL g^{-1} resin) for 90 min. General steps of a manual and automated synthesis are shown in **Table 6** and **Table 7**.

Table 6 General steps of a manual synthesis cycle

Step	Description	Solvent	Volume	Time
1	Coupling	DCM/DMF 50/50	5 mL g^{-1} resin	90 min
2	Wash	DMF, DCM	10 mL g^{-1} resin	3 x 1 min DMF 3 x 1 min DCM
3	Kaiser test	-	-	-
4	Fmoc deprotection	20 % piperidine/DMF	10 mL g^{-1} resin	4 x 10 min
5	Wash	DMF, DCM	10 mL g^{-1} resin	3 x 1 min DMF 3 x 1 min DCM
6	Kaiser test	-	-	-

Table 7 General steps of an automatic synthesis cycle

Step	Description	Solvent	Volume	Time
1	Coupling	NMP/DMF	5 mL g^{-1} resin	90 min
2	Double-coupling	NMP/DMF	5 mL g^{-1} resin	90 min
3	Wash	DMF	8 mL g^{-1} resin	5 x 1 min
4	Fmoc deprotection	20 % piperidine/DMF	7 mL g^{-1} resin	4 x 10 min
5	Wash	DMF	8 mL g^{-1} resin	5 x 1 min

2.2.3.1 Synthesis of T-shapes

After swelling of the preloaded resin, backbones were synthesized with an automated synthesizer as described in **Table 7**. Before deprotection of the central Dde group with 2 % hydrazine solution, the N-terminal NH_2-group was protected with 10 eq Boc anhydride and 10 eq DIPEA in DCM/DMF. In case of an N-terminal cysteine, Boc-Cys(Trt)-OH was used. Dde-deprotection was performed 30 times with a Syro Wave™ synthesizer (Biotage, Uppsala, Sweden). Hydrazine–DMF solution 1 : 50 was added and vortexed for 2 min. The reaction solvent was drained and fresh solution was added again. Afterwards, the resin was washed with 5 × 1 min DMF 5 × 1 min 10 % DIPEA/DMF and 3 × 1 min DCM (10 mL g^{-1} resin). The following coupling steps were carried out using the manual protocol in **Table 6**. In case of a positive result of the Kaiser test after coupling, the last coupling step was repeated. In case of a negative result after deprotection, the last deprotection step was repeated (optionally with 2 % DBU added to 20 % piperidine solution). In case of coupling Fmoc-succinoyl-cystamine, no HOBt was used and only DMF was used as solvent. All couplings after Fmoc-succinoyl-cystamine were carried out without HOBt. Symmetrical branching points were introduced using Fmoc-Lys(Fmoc)-OH, asymmetric branching in T-shape structures was introduced using Fmoc-Lys(Dde)-OH.

2.2.3.2 Synthesis of OH-SteA-t

The precipitated ***OleA-t*** used for ***OH-SteA-t*** synthesis was dissolved in TFA/DCM 95:5 and stirred for 12 h at RT to generate ***TFA-SteA-t***. ***TFA-SteA-t*** was precipitated in 40 mL of pre-cooled MTBE/n-hexane 1:1. The identity of ***TFA-SteA-t*** was validated by mass spectrometry. The product was re-dissolved in 20 mM HEPES and incubated for 12 h at room temperature to generate ***OH-SteA-t***. 10-fold molar excess of TCEP was added and stirred at room temperature for 30 min. The oligomer was purified by HPLC and a white powder was obtained.

2.2.3.3 Synthesis of i-shapes

After swelling of the preloaded resin, the structures were synthesized manually as described in **Table 6**. Symmetrical branching points were introduced using Fmoc-Lys(Fmoc)-OH. In case of coupling Fmoc-succinoyl-cystamine, no HOBt was used and only DMF was used as the solvent (Kaiser tests are not always correct after the deprotection). All couplings after Fmoc-succinoyl-cystamine were carried out without HOBt.

2.2.3.4 Synthesis of U-shapes

After swelling of the preloaded resin, the structures were synthesized manually as described in **Table 6**. Symmetrical branching points were introduced using Fmoc-Lys(Fmoc)-OH. In case of coupling Fmoc-succinoyl-cystamine, no HOBt was used and only DMF was used as solvent (Kaiser tests are not always correct after the deprotection). All couplings after Fmoc-succinoyl-cystamine were carried out without HOBt.

2.2.3.5 Synthesis of apelin-derived PEGylated agents and GFP-conjugates

After swelling of the preloaded resin, apelin-13 (H-QRPRLSHKGPMPF-OH), apelin-F13A (H-QRPRLSHKGPMPA-OH) and apelin-13scr (H-HGFPRPQMPRLSK-OH) peptides were synthesized with an automated synthesizer as described in **Table 7**. The coupling of Fmoc-N-amido-dPEG$_{24}$-acid and cysteine was carried out using the manual protocol in **Table 6**. Coupling of peptides or cationic lipo-oligomer ***728*** (GFP-control) to GFP was performed analogous as described before.[152]

2.2.3.6 Synthesis of DBCO$_2$-PEG$_{24}$-g7 agents

After swelling of the preloaded resin, Fmoc-Lys(Fmoc)-OH, STOTDA and DBCO-acid were coupled using the manual protocol in **Table 6**. After cleavage using the conditions in section **2.2.5.4**, (DBCO-STOTDA)$_2$-K-PEG$_{24}$-COOH was dissolved in DCM and each 1.5 eq. of N,N′-Diisopropylcarbodiimide (DIC) and N-Hydroxysuccinimide (NHS) were added in DCM. After 2 h incubation at RT, (DBCO-STOTDA)$_2$-K-PEG$_{24}$-NHS was precipitated in 40 mL of pre-cooled MTBE–n-hexane (1:4) and dried in vacuo. (DBCO-STOTDA)$_2$-K-PEG$_{24}$-NHS was dissolved in DMF and 1.1 eq. of g7 or scrg7 were added in PBS 7.4. After 2 h of incubation at RT, the product was purified by HPLC and lyophilized.

2.2.4 Kaiser test

Free amines of deprotected amino acids on the resin were determined qualitatively by the Kaiser test.[153] A small sample of DCM washed resin was transferred into an Eppendorf reaction tube. One drop of each 80 % phenol in EtOH (w/v), 5 % ninhydrin in EtOH (w/v) and 20 µM potassium cyanide (KCN) in pyridine (mixture of 1 mL aqueous 0.001 M KCN solution and 49 mL pyridine) were added. The tube was incubated at 99 °C for 4 min under shaking. The presence of free amines was indicated by blue color.

2.2.5 Cleavage conditions

2.2.5.1 General cleavage conditions

All oligomers containing neither oleic acid nor DBCO were cleaved off the resin by incubation with TFA–TIS–H_2O (95:2.5:2.5) (10 mL g^{-1} resin) for 90 min. The cleavage solution was concentrated in a stream of nitrogen and oligomers were precipitated in 40 mL of pre-cooled MTBE–n-hexane (1:1). All oligomers were purified either by size exclusion chromatography using an Äkta purifier system (GE Healthcare Bio-Sciences AB, Uppsala, Sweden), a Sephadex G-10 column and 10 mM hydrochloric acid solution–acetonitrile (7:3) as solvent or HPLC. All oligomers were lyophilized.

2.2.5.2 Cleavage of test structures containing oleic acid for kinetic studies

All oligomers were cleaved off the resin by incubation with TFA-EDT-H_2O-TIS 94:2.5:2.5:1 (10 mL g^{-1} resin, 5 mmol each) for certain times either at 20 °C, +4 °C or +22 °C. The cleavage solution and the resins were cooled to 4 °C before addition if not stated otherwise. The oligomers were immediately precipitated in 40 mL of pre-cooled MTBE/n-hexane 1:1. All oligomers were analyzed by HPLC-DAD at 280 nm.

2.2.5.3 Cleavage of oligomers containing oleic acid

The cleavage of oleic acid-containing structures was performed according to an optimized protocol by incubation with TFA-TIS-H_2O 95:2.5:2.5 (10 mL g^{-1} resin cooled to 4 °C prior to addition) for 20 min followed by immediate precipitation in 40 mL of pre-cooled MTBE–n-hexane (1:1). The oleic acid containing oligomers were then purified either by size exclusion chromatography using an Äkta purifier system (GE Healthcare Bio-Sciences AB, Uppsala, Sweden), a Sephadex G-10 column and 10 mM

hydrochloric acid solution–acetonitrile (7:3) as solvent or by HPLC. The oligomers were lyophilized.

2.2.5.4 Cleavage of oligomers containing DBCO

The cleavage of DBCO-containing structures was performed with DCM-TFA-TIS 92.5:5:2.5 (10 mL g^{-1} resin) for 60 min followed by immediate precipitation in 40 mL of pre-cooled MTBE–n-hexane (1:4). The DBCO-containing oligomers were then purified by size exclusion chromatography using an Äkta purifier system (GE Healthcare Bio-Sciences AB, Uppsala, Sweden), a Sephadex G-10 column and 10 mM hydrochloric acid solution–acetonitrile (7:3) as solvent and lyophilized.

2.2.6 siRNA polyplex formation

Nucleic acid and oligomers at indicated nitrogen/phosphate (N/P) ratios were diluted in 20 mM HEPES buffered 5 % glucose pH 7.4 (HBG) in separate tubes of equal volumes. 500 ng siRNA were dissolved in 10 µL HBG. Only protonatable nitrogens were considered in the N/P calculations (see **Table 19**). The siRNA solution was added into the lipo-oligomer solution, mixed by 5 × rapid pipetting and incubated for 40 min at RT.

2.2.7 Polyplex modification with DBCO agents

After polyplex formation, 1 eq. (representing the molar ratio of DBCO agents to oligomers in the polyplex solution) was added to the polyplex solution. The reaction time was 4 h.

2.2.8 siRNA binding assays

An agarose gel was prepared by boiling of 1 % agarose in TBE buffer (10.8 g of trizma base, 5.5 g of boric acid, 0.75 g of disodium EDTA, and 1 L of water). After cooling down to about 50 °C, GelRed™ was added. Polyplexes in 20 µL volume were pipetted into the sample pockets after 4 µL of loading buffer (prepared from 6 mL of glycerol, 1.2 mL of 0.5 M EDTA, 2.8 mL of H_2O, 0.02 g of bromophenol blue) was added. Electrophoresis was performed at 100 V for 40 min in TBE buffer.

2.2.9 siRNA polyplexes under reducing conditions

Polyplexes were formed at N/P ratio 20 with 500 ng siRNA in 20 µL. After polyplex incubation, 5 µL of a GSH solution were added to 20 µL of the polyplex solution. The

GSH stock solution had a concentration of 50 mM and pH was adjusted to 7.4. It was diluted to concentrations of 5 mM and 0.5 mM. Consequently, the resulting solutions had the final concentrations 0.1 mM, 1 mM and 10 mM, respectively. HBG was used as negative control (0 mM GSH). The solutions were incubated at 37 °C for 90 min. 5 µL loading buffer was added and a siRNA binding assay was performed.

2.2.10 siRNA polyplex stability in 90 % serum

Polyplexes were formed using 2.5 µg siRNA in 6.25 µL HBG mixed with the lipo-oligomer at N/P 12 resulting in a total volume of 12.5 µL. After incubation for 40 min, 112.5 µL fetal calf serum (FCS) was added to the samples. All samples had a final concentration of 90 % FCS. The samples were incubated at 37 °C for the indicated time. 20 µL of the samples were put into the sample pockets after 4 µL of loading buffer was added. Electrophoresis was performed at 100 V for 40 min as described above.

2.2.11 Particle size and zeta potential

For dynamic light scattering (DLS) measurements the polyplex solution was measured in a folded capillary cell (DTS 1070) using a Zetasizer Nano ZS with backscatter detection (Malvern Instruments, Worcestershire, UK). Polyplexes were prepared at the indicated N/P in a total volume of 100 µL. For size (z-average) and polydispersity index (PDI) measurements, the equilibration time was 0 min, the temperature was 25 °C and an automatic attenuator was used. The refractive index of the solvent was 1.330 and the viscosity was 0.8872 mPa•s. Each sample was measured 3 times. For zeta potential measurements, the sample was diluted with 700 µL 10 mM NaCl (pH 7.4). Zeta potentials were calculated by the Smoluchowski equation. Ten to fifteen sub runs lasting 10 s each at 25 °C (n = 3) were measured.

2.2.12 Ellman´s assay

Oligomers containing the ssbb or cysteines were diluted to a concentration of 1.67 mg mL^{-1}. 30 µL of the solution was mixed with 170 µL working solution (2.44 mL Ellman´s buffer (0.2 M Na_2HPO_4, 1 mM EDTA, pH 8.0) and 60 µL DTNB solution in methanol (c = 4 mg mL^{-1})). After 15 min incubation at 37 °C absorption was measured at 412 nm using a GENESYS™ UV-VIS spectrophotometer (Thermo Scientific). The percentage of free mercapto groups is based on the theoretical amount (100 %) of thiols in case of complete cleavage.

2.2.13 Oligomer digestion with cathepsin B

A cathepsin B solution (0.379 mg mL^{-1}, 331 U mg^{-1}) was added to an acetate-incubation buffer (sodium acetate 0.1 M, EDTA 1 mM and DTT 1 mM, pH 5.5) and activated for 5 min at 22 °C under constant shaking. The activated enzyme was added to the oligomer or polyplex sample to reach a final concentration of 0.25 µM cathepsin B. Test structures were incubated for 2 h at 37 °C at a final concentration of 0.5 mM. Lipo-oligomers were incubated for 24 h at 37 °C at a final concentration of 0.125 mM. Polyplexes formed with lipo-oligomers and siRNA at indicated N/P ratios were incubated for 24 h at 37 °C at a final concentration of 500 ng siRNA in 50 µL reaction mixture. For MALDI mass spectrometry, 1 µL of the reaction mixture was pipetted on top of a MF-Millipore membrane filter placed in 2 L deionized water and microdialyzed for 60 min.

2.2.14 Erythrocyte leakage assay

Fresh, citrate-buffered human blood was washed with phosphate-buffered saline (PBS). The washed human erythrocyte suspension was centrifuged and the pellet was diluted to 5×10^7 erythrocytes per mL with PBS (pH 7.4, 6.5 and 5.5). In case of GSH treatment, oligomers were incubated in 10 mM GSH in HEPES (pH adjusted to 7.4) at a concentration of 1 mg mL^{-1} at 37 °C for 90 min. To determine the lytic activity at the endolysosomal pH 5.5 before and after digestion with cathepsin B, the oligomer solution was either incubated with incubation buffer only or incubation buffer with cathespin B before dilution with PBS at pH 5.5. A volume of 75 µL of erythrocyte suspension and 75 µL of oligomer solution (previously diluted with PBS of the respective pH to the indicated concentration) were added to each well of a V-bottom 96-well plate (NUNC, Denmark). The plates were incubated at 37 °C under constant shaking for 1 h. After centrifugation, 100 µL of the supernatant was analyzed for hemoglobin release at 405 nm wavelength using a microplate reader (Spectrafluor Plus, Tecan Austria GmbH, Grödig, Austria).

2.2.15 Gene silencing with siRNA

Gene silencing experiments were performed in Neuro2A/eGFPLuc, KB/eGFPLuc, Huh7/eGFPLuc or DU145/eGFPLuc cells. The siRNA against eGFP (siGFP) for silencing the eGFPLuc gene or its control sequence (siCtrl) was used. Silencing experiments were performed in triplicates in 96-well plates with 5000 cells for

Neuro2A/eGFPLuc, Huh7/eGFPLuc and DU145/eGFPLuc cell line or 4000 cells for KB/eGFPLuc cell line and 500 ng siRNA per well. Cells were seeded 24 h prior to transfection and then medium was replaced with 80 µL fresh growth medium containing 10 % FBS. Transfection complexes for siRNA delivery (20 µL in HBG, prepared as described above) at different N/P ratios were added to each well and incubated at 37 °C. Medium was replaced with 100 µL fresh medium after 45 min in case of targeted polyplexes and after 4 h in case of lipo-oligomers with enzymatic cleavage sites. Luciferase activity in the cell lysate was measured 48 h after initial transfection using a luciferase assay kit (Promega, Mannheim, Germany) and a Centro LB 960 plate reader luminometer (Berthold Technologies, Bad Wildbad, Germany). The experiments were performed in triplicates, and the relative light units (RLU) were presented as percentage of the luciferase gene expression obtained with HBG-treated control cells.

2.2.16 Cell viability assay (MTT)

MTT assays were performed using Huh7/eGFPLuc or DU145/eGFPLuc cells. 5×10^3 cells per well were seeded onto 96-well plates, and medium was replaced with 80 µL fresh growth medium after 24 h. Polyplex or oligomer solutions were added to each well in 20 µL volume and incubated for 4 h at 37 °C. The medium was replaced with 100 µL fresh growth medium and the cells were incubated for additional 44 h at 37 °C. MTT assay (Life Technologies, Darmstadt, Germany) was performed and measured using a SpectraFluor Plus microplate reader to evaluate the cytotoxicity. The experiments were performed in triplicates and the cell viability was calculated as percentage compared to untreated control cells.

2.2.17 Cell viability assay (CellTiter-Glo® assay)

CellTiter-Glo® assays were performed using Neuro2A/eGFPLuc or DU145/eGFPLuc cells. 5000 cells per well were seeded on 96-well plates, and medium was replaced with 80 µL fresh growth medium after 24 h. Polyplexes in 20 µL volume at indicated N/P ratios was added to each well and incubated for 48 h at 37 °C. Cell viability was measured using CellTiter-Glo® (Promega, Dübendorf, Switzerland) and a Centro LB 960 plate reader luminometer (Berthold Technologies, Bad Wildbad, Germany).

2.2.18 Identification of degradation products from cell lysates

Human hepatoma Huh7-eGFPLuc cells were transfected with polyplexes at N/P 20 as described in the reporter gene silencing section. A protocol for the identification of mammalian cell lines using MALDI-TOF mass spectrometry[154] was adapted as follows: After transfection, medium was removed and the cells were resuspended in 100 µL of a 10 mg mL^{-1} solution of sDHB in acetonitrile/water (3:7) with 0.1 % (v/v) TFA. The cell suspension was stored at -80 °C for 1 h. Then the cell lysate was sonicated for 5 min at 22 °C. One µL of the sample solution was added on a dried sDHB matrix spot and MALDI mass spectrometry was performed.

2.2.19 Specific GFP-apelin internalization

The internalization assay was performed on GBM14 GSCs. The cells were plated at a density of 10.000 cells/well on a glass coverslip previously coated with poly-D-lysin 50 µg mL^{-1} followed by laminin 50 µg mL^{-1}. The day after, the medium was replaced with 200 µL of fresh medium and the N-terminally GFP-conjugated apelin-13, apelin-F13A, apelin-13scr (containing the scrambled amino acid sequence of apelin-13) or GFP-linked cationic lipo-oligomer ***728***[152, 155] were added to the cells for 120 min at 37 °C. For the competition experiment, unlabelled apelin-13 or apelin-F13A was added to the GBM14 cells 30 min prior to the addition 200 nM GFP-apelin-13 or GFP-apelin-F13A, respectively. After that, cells were fixed for 30 min with 4 % PFA and incubated for 10 min at room temperature with WGA-594 1:200 and DAPI 1:1000 diluted in 1 × PBS washed and mounted on a glass slide with Dako Fluorescent Mounting Medium. The pictures were taken at the Leica SP8X WLL upright confocal microscope or at the Leica SP5 inverted confocal microscope, with the LAS X software, and analysed with ImageJ. For the quantification of the GFP-positive cells, 6 pictures per condition were used, and for each picture the data were measured as number of GFP-positive cells on the total number of cells.

2.2.20 HPLC analysis

For kinetic studies of test structures containing oleic acid, samples were dissolved in H_2O containing 0.1 % formic acid (HCOOH). Column: YMC-UltraHT Hydrosphere C18, 150 x 4.6 mm,5 µm, 12 nm. Conditions: A: 0.1 % HCOOH in H_2O; B: 0.1 % HCOOH in ACN; 5 % B for 5 min, 5-45 % B in 15 min, 45 % B for 10 min; 1.00 mL min^{-1}, 35 °C, 280 nm.

For purification of lipo-oligomers, samples were dissolved in H_2O/MeOH 60:40 containing 0.1 % TFA. Column: YMC-Pack C4, 250 x 10 mm, 5 µm, 12 nm. Conditions: A: 0.1 % TFA in H_2O/MeOH 60:40; B: 0.1 % TFA in ACN; 0 % B for 10 min, 0-90 % B in 40 min, 90 % B for 10 min; 2.00 mL min^{-1}, 35 °C, 280 nm.

To analyze the cathepsin B-triggered cleavage of the test structures, samples were dissolved in H_2O containing 0.1 % TFA either before or after digestion. Column: YMC-UltraHT Hydrosphere C18, 150 x 4.6 mm, 5 µm, 12 nm. Conditions: A: 0.1 % TFA in H_2O; B: 0.1 % TFA in ACN; 5 % B for 5 min, 5-90 % B in 10 min, 90 % B for 5 min; 1.00 mL min^{-1}, 30 °C, λ = 280 and 370 nm. Chromatograms were recorded using a Chromaster HPLC-DAD system by VWR Hitachi and analyzed using Chromaster System Manager (Ver. 1.1 by Hitachi).

The redox-sensitivity of oligomer ***740*** was analyzed by RP-HPLC using a Waters HPLC system equipped with a Waters 600E multisolvent delivery system and a Waters 996 PDA detector. The compounds were analyzed using a Xbridge C18 column (5 µm, 4.6 x 150 mm) and a water/acetonitrile gradient (95:5 – 0:100) containing 0.1 % TFA. For detection, the extinction at 280 nm was monitored.

2.2.21 Proton ^{1}H NMR spectroscopy

^{1}H NMR spectra were recorded using an AVANCE III HD 500 (500 MHz) by Bruker with a 5 mm CPPBBO probe. All spectra were recorded without TMS as internal standard and therefore all signals were calibrated to the residual proton signal of the deuterium oxide (D_2O) solvent. Chemical shifts are reported in ppm and refer to the solvent as internal standard (D_2O at 4.79). Integration was performed manually. The spectra were analyzed using MestreNova (Ver. 9.0 by MestReLab Research).

2.2.22 MALDI mass spectrometry

A drop of 1 µL matrix solution, consisting of 10 mg mL^{-1} sDHB (sum of 2,5-dihydroxybenzoic acid and 2-hydroxy-5-methoxybenzoic acid) in acetonitrile/water (3:7) with 0.1 % (v/v) TFA, was spotted on a MTP AnchorChip (Bruker Daltonics, Bremen, Germany). After the sDHB matrix crystallized, 1 µL of the sample solution was added on the matrix spot. Samples were analyzed in positive ion mode using an Autoflex II mass spectrometer (Bruker Daltonics, Bremen, Germany).

2.2.23 Statistical analysis

The results are presented as mean values of experiments performed in at least triplicates. Unless otherwise stated, error bars show standard deviation (SD). Significance was evaluated by unpaired t test: *p < 0.05; **p < 0.01; ***p < 0.001. Two-tailed Student's t-test, calculations and graphical presentation were performed with Prism 6.01 (GraphPad Software Inc.).

3 Results

3.1 Optimized Solid-Phase-Assisted Synthesis of Oleic Acid Containing siRNA Nanocarriers

This chapter has been adapted from:

S. Reinhard, W. Zhang, E. Wagner, Optimized Solid-Phase-Assisted Synthesis of Oleic Acid Containing siRNA Nanocarriers, ChemMedChem 12(17) (2017) 1464-1470.

Lipo-polyplexes assemble upon mixing of cationic lipids or lipo-oligomers with nucleic acids and association is driven by intermolecular hydrophobic and electrostatic interactions. Such carriers provide high plasmid DNA (pDNA) or siRNA polyplex stability and transfection efficacy.[37, 57, 156-158] Minor variations in the different subunits (polar head group, hydrophobic tails, linkages) have significant influence on the bioactivity of cationic lipids.[38, 159] Well known cationic lipids like DOPE, DOTMA and DOSMA contain the cis-unsaturated fatty acid (FA) oleic acid and were first used to efficiently delivery DNA and mRNA in 1987 and 1989 respectively.[160-163] Cationic lipids containing cis-unsaturated FAs can promote membrane lipid disorders by interacting with anionic phospholipids.[164] The fusion between two lipid membranes is mediated by a lamellar-to-hexagonal inverted phase transition.[165-168] This process is promoted by cone-shaped cationic lipids, where the cross-sectional area of the hydrophilic head groups is smaller than that of the hydrophobic tails.[37, 169-172] Double bonds or other modifications of hydrocarbon moieties can lead to broader conical shapes by increasing its steric demands and fluidity, thereby elevating the tendency to form the hexagonal phase during membrane fusion events.[159, 172] Cationic carriers with unsaturated fatty acids and amino acids can be produced by solid-phase-assisted synthesis or in solution.[43, 44, 64, 129, 172-175] However, the trifluoroacetic acid (TFA)-mediated cleavage of acid-labile protecting groups and the oligomer from the resin (in case of SPS) is accompanied by side reactions as TFA adds to double bonds of alkenes.[176-184] The resulting TFA esters are readily hydrolyzed in neutral or basic aqueous solution, generating hydroxylated hydrocarbons. Such side products can drastically lower the yield of the synthesis or, if not purified properly, might affect the properties of the nucleic acid carrier. In this chapter, we investigated the reaction kinetics of the addition of TFA to the mono-unsaturated oleic acid (C18:1) during TFA-

mediated cleavage. The cleavage protocol was optimized in terms of temperature and time to minimize side products caused by TFA addition to oleic acid, while ensuring complete cleavage of the oligomer from the resin and of acid-labile protecting groups. The optimized protocol was used to obtain a purified oleic acid containing T-shape lipo-oligomer (***OleA-t***) in high yields. The same oligomer was modified by long-time treatment with TFA followed by TFA-ester hydrolysis, generating a mono-hydroxylated hydrocarbon chain (***OH-SteA-t***) to investigate how this reaction might affect the nucleic acid carrier. A lipo-oligomer with 8-nonanamidooctanoic acid moieties (***NonOcA-t***) was synthesized as an alternative analog including a polar amide bond. Together with a lipo-oligomer containing the unsaturated C18 FA stearic acid (***SteA-t***), all carriers were evaluated regarding their nucleic acid delivery characteristics such as siRNA binding and lytic potential of oligomers, gene silencing efficacy and cytotoxicity of lipo-polyplexes.

3.1.1 Synthesis of test structures and reaction kinetics of addition of TFA to oleic acid

Functional groups of amino acid side chains in standard Fmoc-based solid-phase assisted synthesis need to be protected orthogonally to the base-labile Fmoc protecting. Acid-labile protecting groups like O*t*Bu for carboxylic acids (Glu, Asp), *t*Bu for thiols and hydroxyl groups (Cys, Ser, Thr, Tyr), Trt for thiols, carboxamides and imidazoles (Cys, Asn, Gln, His) and Boc for amino groups, imidazoles and indols (Lys, His, Trp) are common choices which, according to literature, should be cleaved with at least 50 % TFA (Trt on His) and up to 90 % TFA (Boc, O*t*Bu, *t*Bu, Trt on Cys) for 30 min at room temperature.[185] Commonly used linker resins for SPS like Wang, Rink acid and -amide and chlorotrityl resins also require TFA treatment for peptide cleavage.[185] Such TFA-mediated cleavage of protecting groups and product from the resin can corrupt the double bonds of unsaturated fatty acids. TFA can protonate alkene groups which enables nucleophilic addition of a trifluoroacetate anion. As trifluoroacetate is a weak nucleophile, the addition is the rate-limiting step of the reaction.[177] The addition results in four mono-TFA esters as major side products (R and S configuration for each hydrocarbon group) in case of linear hydrocarbon chains with a central double bond like in oleic acid (**Fig. 7A** and **7B**).

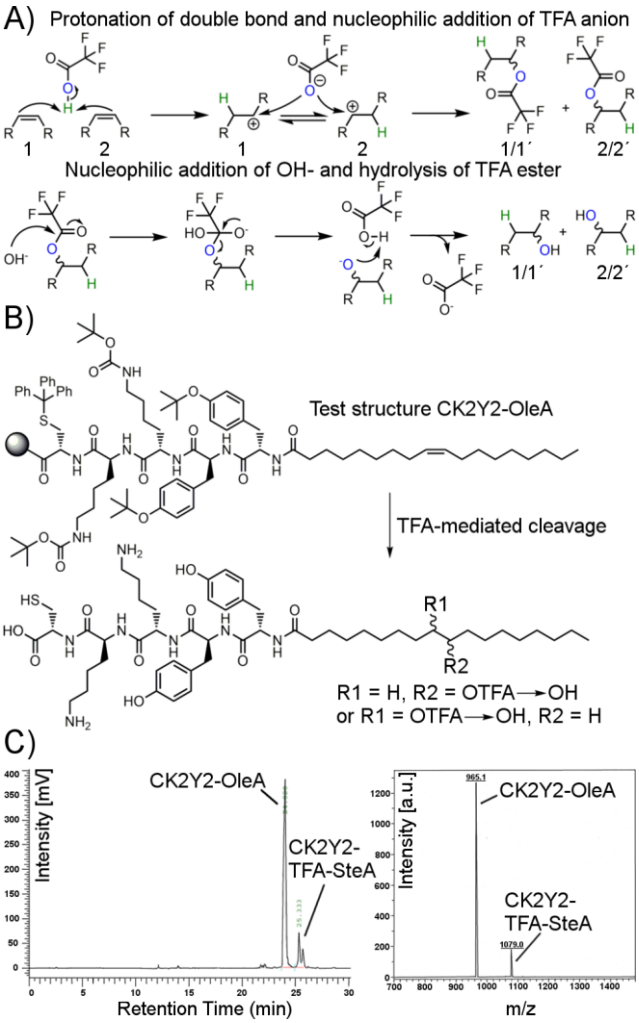

Fig. 7 A) Reaction mechanism of TFA addition to double bonds and subsequent TFA ester hydrolyzation. B) Test structure CK_2Y_2-OleA and the four major side products after TFA-mediated cleavage. C) HPLC chromatogram of CK_2Y_2-OleA after 30 min cleavage at 22 °C and MALDI spectrum.

However, carbocation rearrangement might occur after electrophilic protonation in absence of a good nucleophile, leading to minor amounts of further side products.[176] Complete cleavage of acid-labile protecting groups has to be ensured when an optimized cleavage protocol with low amounts of TFA adducts is established. Three test structures with common protecting groups (Trt, Boc, *t*Bu and O*t*Bu) were synthesized and cleaved at different temperatures (**Table 8**).

Table 8 Evaluation of cleavage time and temperature for sufficient cleavage of acid-labile protecting groups

		Sufficient cleavage time at indicated temperature [min][a]		
Test structure	**Protecting groups**	**-20 °C**	**4 °C**	**22 °C**
Stp-W-OleA	Boc (Stp, W)	x[b]	120	15
CKEHEK-OleA	Trt (C, H); Boc (K); O*t*Bu (E)	x[b]	120	20
CK_2Y_2-OleA	Trt (C); Boc (K); *t*Bu (Y)	not tested	120	15

[a] Cleavage solution (TFA/H_2O/EDT/TIS 94:2.5:2.5:1, 1 mL) was precooled to 4 °C before addition to the resin (5 µmol oligomer). Detection of uncleaved protecting groups by MALDI mass spectrometry [b] Not determined because of very low yields and high amounts of uncleaved protecting groups after 360 min cleavage time.

The temperature strongly influenced the cleavage of acid-labile protecting groups. While 15-20 min at 22 °C were sufficient for complete cleavage, side products with remaining protecting groups could be observed at 4 °C when the cleavage time was less than 120 min. The sufficient time for cleavage at -20 °C was not determined, as both yield and cleavage efficacy were poor after 360 min. The test structure CK_2Y_2-OleA, containing Trt-, Boc- and *t*Bu-protected amino acids and the unsaturated oleic acid, was used to determine the reaction kinetics of the TFA addition at 4 °C and 22 °C. TFA adducts could be observed both in MALDI spectra and HPLC chromatograms (**Fig. 7C**). In accordance with literature, first-order rate behavior was observed and the rate constant was evaluated from a first-order plot of the HPLC quantification (**Table 9**).[176, 177, 184]

Table 9 Reaction kinetics of addition of TFA to CK_2Y_2-OleA at different cleavage temperatures[a]

Temperature [°C]	k x 10^4 [sec^{-1}][b]	$T_{1/2}$ [min]	TFA adducts after complete cleavage [%][c]
22	0.802	104	7.4
4	0.197	423	15.2

[a] Cleavage solution (TFA/H_2O/EDT/TIS 94:2.5:2.5:1, 1 mL) precooled to 4 °C before addition to resin (5 µmol oligomer). [b] Rate constant from a first-order plot of HPLC quantification. [c] TFA adducts after sufficient cleavage time (120 min at 4 °C and 20 min at 22 °C) of protecting groups and product from resin as determined by HPLC quantification.

The rate constant at 22 °C is almost five times higher than at 4 °C and the half-life time of the unsaturated oleic acid is accordingly reduced. However, the sufficient cleavage of acid-labile protecting groups has to be considered for an optimized cleavage protocol. 20 min was determined as sufficient cleavage time at 22 °C for all three test structures. After that time, 7.4 % TFA adducts were measured by HPLC quantification. At 4 °C, at least 120 min were necessary for sufficient cleavage of protecting groups, after which 15.2 % of TFA adducts were quantified. Although lowering the temperature slows down the TFA adduct formation, the cleavage of acid-labile protecting groups seems to be reduced even more. All cleavage solutions were adjusted to 4 °C before addition to the resins.

The precooling of the cleavage solution is important, as exothermic cleavage of protecting groups and the product from the resin increases the temperature of the cleavage solution after addition. Significantly higher amounts of TFA adducts were detected when the cleavage solution was added at room temperature (**Table 10**).

Table 10 Influence of oligomer sequence and temperature of the cleavage solution before addition to the resin[a]

Test structure	Temperature of cleavage solution [°C]	Amount of TFA adducts [%]	Alkene scavenger
CK_2Y_2-OleA	**4**	11.6	x
CK_2Y_2-OleA	**4**	11.8	cis-2-Hexene
CK_2Y_2-OleA	**4**	12.6	Cyclohexene
CK_2Y_2-OleA	**22**	20.0	x
Stp-W-OleA	**4**	11.7	x

[a] Cleavage time 30 min at 22 °C. Cleavage solution (TFA/H_2O/EDT/TIS 94:2.5:2.5:1 or TFA/Alkene/H_2O/EDT/TIS 90:4:2.5:2.5:1, 1 mL) was precooled to 4 °C or kept at 22 °C before addition to the resin (5 µmol oligomer). Quantification by HPLC-DAD at 280 nm

Quantification of TFA adducts on a Stp-W-OleA test structure confirmed that the sequence of the oligomer does not influence the amount of adducts (**Table 10**). Adding a >100-fold molar excess of cyclohexene or cis-2-hexene to the cleavage solution did not reduce the percentage of TFA adduct formation (**Table 10**). SPS products are

usually precipitated in cold ether and/or hexane after TFA-mediated cleavage. To enhance the yield, the precipitation is often done after evaporation of TFA and volatile scavengers.[185] This step should obviously be avoided when the structures contain unsaturated FAs.

3.1.2 T-shape lipo-oligomers containing oleic acid and analogs with saturated or modified hydrophobic moieties

The optimized cleavage protocol, including precooling of the cleavage solution to 4 °C before adding to the resin, 20 min cleavage time at 22 °C followed by immediate precipitation in cold t-butyl methyl ether/n-hexane was used to obtain an oleic acid containing T-shape lipo-oligomer ***OleA-t*** (**Fig. 8**) in good yield (overall 65 %).

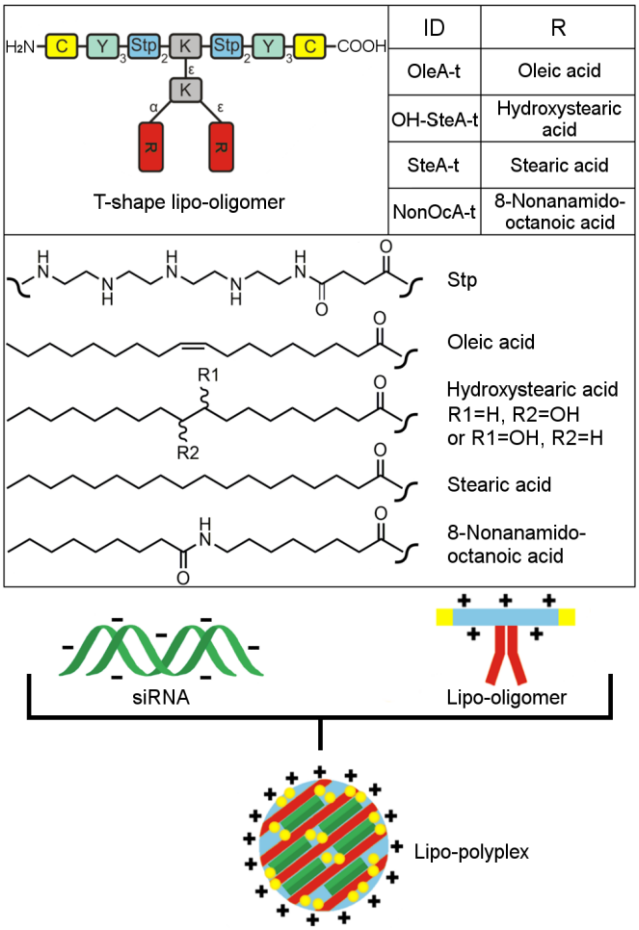

Fig. 8 Sequence-defined lipo-oligomers with T-shape topology. Top: schematic overview of the structures with different modifications (C: cysteine, Y: tyrosine, K: lysine, Stp: succinoyl-tetraethylene-pentamine. The broken lines represent amide linkages. Bottom: lipo-polyplex assembly upon mixing of lipo-oligomers with siRNA

In a separate approach, the resin was treated for 12 hours with TFA to ensure complete modification of the double bonds, followed by TFA ester hydrolysis at pH 7.4 for 12 hours, generating a mono-hydroxylated hydrocarbon chain (***OH-SteA-t***). This structure represents the major side product of the ***OleA-t*** synthesis and can be used to study the influence of the TFA-induced hydrocarbon chain modification. As additional structure with polar modification, a lipo-oligomer with 8-nonanamidooctanoic acid moieties (***NonOcA-t***) was synthesized. Amide bonds are chemically far more stable than double bonds and could present an alternative to unsaturated fatty acids with regard to perturbation of the aliphatic chain. Last not least, stearic acid as saturated C18 FA (***SteA-t***) was incorporated in another reference structure to further evaluate the influence of the hydrocarbon chain modifications. By this approach, any differences between the lipo-oligomers can be attributed to the hydrocarbon moieties, as the rest of the structures was retained unchanged. The oligocation part of the structures contains several Stp units as artificial oligoamino acids for nucleic acid binding and endosomal protonation,[42] and α,ε-modified lysines (K) as branching units. The cationic part was further equipped with tyrosine trimers (Y_3)[64] for additional hydrophobic polyplex stabilization and cysteines (C) for stabilizing disulfide crosslinking during polyplex formation by air oxygen.[43, 173] The lipo-oligomers were purified by HPLC. The presence of the free thiol groups was confirmed by Ellman´s assay (**Table 11**).

Table 11 Determination of free thiols in oligomers via Ellman´s assay

Oligomer	Free thiols [% of calculated][a]
OleA-t	87
OH-SteA-t	84
SteA-t	80
OcNonA-t	87

[a] Determined as percentage of calculated thiols based on weighted samples. Deviation from 100 % might be due to residual water or salt and premature oxidation of thiols.

All carriers form lipo-polyplexes upon mixing with siRNA and were evaluated regarding their analytical, biophysical (**Fig. 9**) and biological (**Fig. 10**) characteristics. Analytical characterization by MALDI mass spectrometry showed high purity without side products (**Fig. 9A**).

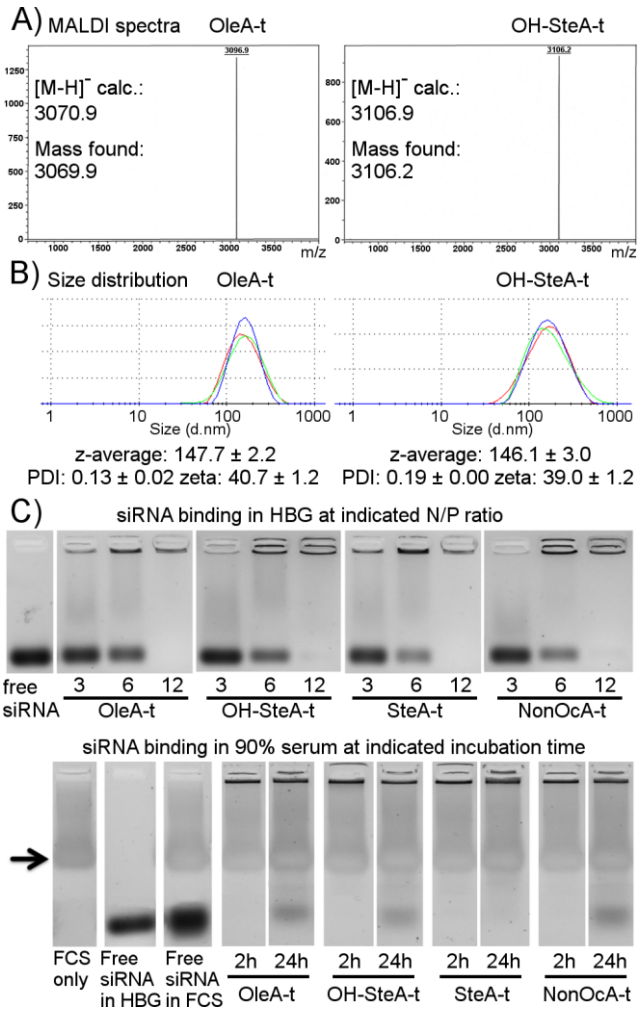

Fig. 9 A) Analytical characterization of the T-shape lipo-oligomers ***OleA-t*** and ***OH-SteA-t*** by MALDI mass spectrometry. B) Biophysical characterizations of lipo-polyplexes formed with oligomers and siRNA at N/P 12 by DLS. B) Agarose gel shift assays. Top: siRNA binding at different N/P ratios. Bottom: Lipo-polyplexes formed at N/P 12 and subsequent treatment at 37 °C with 90 % serum (FCS). The black arrow points at a band that is caused by serum (see serum blank in band one)

The particle sizes of formed siRNA lipo-polyplexes were measured by dynamic light scattering (DLS). All formulations showed uniform sizes just below 150 nm z-average. (**Fig. 9B**, **Table 12**). Positive zeta potentials, ranging from +39 to +46 mV, were detected due to the cationizable properties of the oligomers (**Table 12**).

Table 12 Particle size (z-average), polydispersity index (PDI) and zeta potential of siRNA lipo-polyplexes determined with a DLS zetasizer

Oligomer	N/P	z-average [nm]	Mean PDI	Mean zeta potential [mV]
OleA-t	12	147.7 ± 2.2	0.13 ± 0.02	40.7 ± 1.2
OH-SteA-t	12	146.1 ± 3.0	0.19 ± 0.00	39.0 ± 1.2
SteA-t	12	145.9 ± 2.0	0.15 ± 0.02	45.7 ± 0.6
NonOcA-t	12	149.3 ± 2.5	0.14 ± 0.01	47.5 ± 1.2

The uniform size distribution with low polydispersities and similar z-averages and zeta potentials render T-shape oligomers well-suited for the evaluation of structure-activity relationships. siRNA binding ability of the lipo-oligomers was determined by measuring the electrophoretic mobility of siRNA in a 2.5 % agarose gel. The N/P values depict the ratio of protonatable amines (N) of the oligomer to phosphates (P) of the siRNA. As the diaminoethylene motif of Stp is pH-responsive, not all protonatable amines are protonated at neutral pH, which is why the N/P ratio does not present charge ratios during polyplex formation. All lipo-oligomers showed similar siRNA binding abilities with sufficient binding at N/P ≥ 12 (**Fig. 9C** top). Polyplexes were exposed to 90 % full serum at 37 °C for two and 24 hours (**Fig. 9C** bottom). This assay can be indicative for extracellular stability, as the incubation with full serum at body temperature partly resembles the blood stream. None of the lipo-polyplexes released siRNA after two hours of incubation. After 24 hours, small amounts of siRNA were released from polyplexes with unsaturated or modified hydrocarbon chains (***OleA-t***, ***OH-SteA-t*** and ***NonOcA-t***). The lipo-polyplexes formed with the saturated structure SteA-t did not release siRNA after 24 hours, indicating a slight benefit in long-term extracellular stability of this formulation. This is in accordance with the concept of higher steric requirement of the unsaturated or modified hydrocarbon chains, resulting in less hydrophobic polyplex stabilization compared to the saturated counterpart. Altogether, no significant differences in size, zeta potential, siRNA binding and lipo-polyplex stability could be observed comparing the unsaturated oleic acid containing lipo-oligomer ***OleA-t*** to the ***OH-SteA-t*** and ***NonOcA-t*** structures.

3.1.3 Lytic activity, cell tolerability and transfection efficiency of T-shape lipo-oligomers

Changes in the hydrocarbon chain might alter the interaction of the lipo-oligomers with the membrane lipids, resulting in different membranolytic potentials. This was assessed in an erythrocyte leakage assay comparing the lysis of erythrocyte membranes at different concentrations and pH values. (**Fig. 10A**)

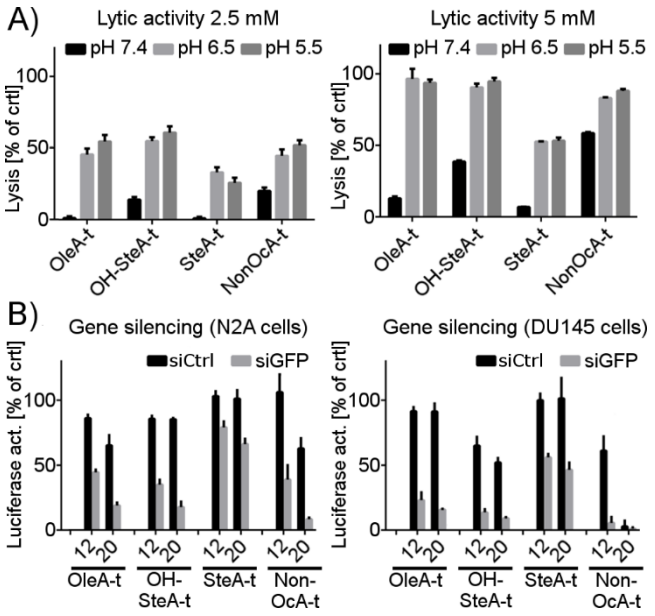

Fig. 10 A) Erythrocyte leakage triggered by lipo-oligomers at different concentrations and pH values. Negative control (hemoglobin release from PBS-treated erythrocytes) was set to 0 %. Triton X treatment served as positive control and was set to 100 %. Data are presented as mean value (± SD) out of quadruplicates. B) Gene silencing by siRNA lipo-polyplexes in neuroblastoma cells (left) and human prostate cancer cells (right). Lipo-polyplexes with 500 ng (37 pmol) eGFP-targeted siRNA (siGFP) per well respectively control siRNA (siCtrl) at N/P 12 and 20 were tested for eGFPLuc gene silencing in Neuro2A-eGFPLuc and DU145-eGFPLuc cells. The luciferase activity of siRNA treated cells is presented related to buffer treated cells. HBG-treated cells were set to 100 %. Data are presented as mean value (±SD) out of triplicates. Transfections were performed by Dr. Wei Zhang (Pharmaceutical Biotechnology, LMU).

All four lipo-oligomers showed the desirable increase in lytic activity at slightly acidic pH as occurring after cellular endocytosis. This is in accordance with the progressive protonation of the Stp-units, increasing the cationic character beneficial for lipid membrane binding. The structures with unsaturated or modified hydrocarbon chains displayed significantly higher lytic activity than the saturated ***SteA-t*** oligomer. The steric requirement of the OleA-, OH-SteA- and NonOcA-moieties presumably results

in a broader conical shape of the lipo-oligomers, increasing their lytic potential as expected. Interestingly, both ***OH-SteA-t*** and ***NonOcA-t*** showed significantly higher erythrocyte lysis at pH 7.4 with 3-fold and 4.5-fold increase compared to ***OleA-t***. This might result in increased cellular internalization on the one hand, but in undesired cytotoxicity on the other hand, as cell membrane lysis might occur prematurely at the cell surface or may affect intracellular membranes after endosomal release of lipo-oligomers into the cytosol. ***OleA-t*** showed particularly favorable pH dependency of membranolytic activity with low lysis at pH 7.4, while having similar lytic activity as ***OH-OleA-t*** and ***NonOcA-t*** at lower pH values. Gene silencing experiments were performed in Neuro2A neuroblastoma cells and DU145 human prostate cancer cells stably expressing an eGFP-Luciferase fusion protein. Thus, silencing by siGFP (light bars) can be quantified by a standard luciferase assay (resulting in luciferase activity decrease); treatment with analogous control siCtrl (black bars) should maintain luciferase activity close to 100 % unless unspecific effects take place (**Fig. 10B**). In Neuro2A cells, similar gene silencing efficacy was observed for both ***OleA-t*** and ***OH-SteA-t***. This is presumably due to the tolerance of N2A cells towards the elevated lytic activity of ***OH-SteA-t*** at neutral pH. If unspecific toxicity is not an issue, the transfection efficacy *in vitro* is mainly driven by the endosomolytic potential of the carrier. In DU145 cells, lipo-polyplexes formulated with ***OH-SteA-t*** and control siRNA showed reduced luciferase activity, indicating unspecific toxicity of the formulations, while ***OleA-t*** formulations displayed high cell tolerability and high gene silencing efficacy. ***SteA-t*** showed low gene silencing activity in both cell lines, in accordance with the low lytic activity of the lipo-oligomer. Reduced luciferase levels were observed for ***NonOcA-t*** lipo-polyplexes formulated with control siRNA at the higher N/P 20 in N2A cells, and for both N/P ratios in DU145 cells. This can be explained by unspecific cytotoxicity, as confirmed by measuring metabolic cell activities compared to untreated cells via a CellTiter-Glo® assay as an indicator for cell viability (**Fig. 11**). High metabolic activities of cells treated with ***OleA-t*** and ***SteA-t*** polyplexes, on the other hand, reaffirmed their high cellular compatibility. Apparently, alterations of the unsaturated fatty acids by TFA mediated cleavage after SPS, leading to TFA esters and subsequently mono-hydroxylated hydrocarbon chains, have the potential to enhance the lytic activity at physiological pH and therefore can increase the cytotoxicity of lipo-oligomers. Introducing an amide bond as an alternative to unsaturated FAs even enhanced this

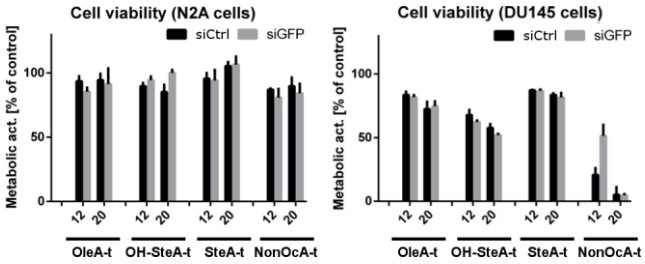

Fig. 11 Cell viability of murine neuroblastoma cells (left) and human prostate cancer cells (right) determined by CellTiter-Glo®. Lipo-polyplexes with 500 ng (37 pmol) eGFP-targeted siRNA (siGFP) per well respectively control siRNA (siCtrl) at N/P 12 and 20 were tested for cytotoxicity in Neuro2A-eGFPLuc and DU145-eGFPLuc cells. The metabolic activity of cells incubated with siRNA complexes for 48 h at 37 °C is presented related to buffer treated cells. HBG-treated cells were set to 100 %. Data are presented as mean value (±SD) out of triplicates. Gene silencing as shown in main Figure 4 B was performed under same conditions. Cell viability assays were performed by Dr. Wei Zhang (Pharmaceutical Biotechnology, LMU).

effect. DU145 cells seemed to be more sensitive to changes in lytic potential as cytotoxic effects were predominantly observed in this cell line. The comparison with the chemically stable saturated FA stearic acid, however, confirmed that steric modification of the hydrophobic domain (such as by cis- double bonds in oleic acid or linoleic acid) is needed for enhanced lipid membrane interaction and to achieve efficient gene silencing efficacy mediated by high lytic potential throughout the endosomal acidification. Analogous studies with a linoleic acid containing lipo-oligomer confirm both the possibility of TFA adduct formation and the measures to avoid them (**Fig. 12** and Analytical Data in section **6.4**)

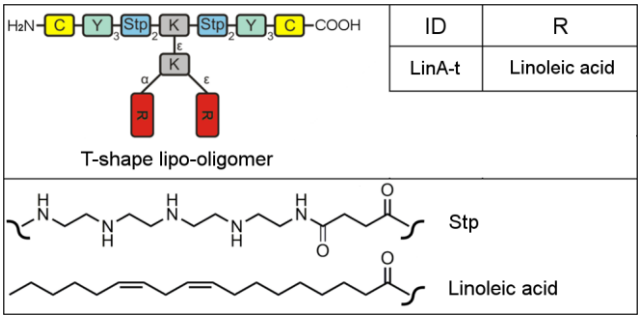

Fig. 12 Schematic overview of the structure LinA-t with linoleic acid and different modifications (C: cysteine, Y: tyrosine, K: lysine, Stp: succinoyl-tetraethylene-pentamine. The broken lines represent amide linkages. Analytical data of the purified LinA-t, as well as of the side product OH-(C18:1)-t resulting from TFA-addition and subsequent TFA ester hydrolization, can be found in the analytical section.

3.2 Precise Redox-Sensitive Cleavage Sites for Improved Bioactivity of siRNA Lipopolyplexes

This chapter has been adapted from:

P.M. Klein*, S. Reinhard*, D.-J. Lee, K. Müller, D. Ponader, L. Hartmann, E. Wagner, Precise redox-sensitive cleavage sites for improved bioactivity of siRNA lipopolyplexes, Nanoscale 8(42) (2016) 18098-18104.

* Authors contributed equally

Our previous work demonstrated the beneficial effect of hydrophobic elements and disulfide-forming cysteines on siRNA polyplex stabilization.[44, 64, 72] Maximum stabilization, however, was not advantageous for gene silencing; the incorporation of disulfide bonds should facilitate disassembly of polyplexes in the intracellular reductive milieu caused by increased cytosolic glutathione (GSH) concentrations.[71, 186-188]

Cysteine-based disulfide formation during polyplex formation by air oxygen is a poorly controllable, incomplete process.[43, 173] Alternatively, integration of bioreducible bonds into carriers can be achieved before nanoparticle formation by polymerization reactions with disulfide-bearing compounds.[186-188] Disulfide bonds can be accurately integrated during SPS of polymers, as already demonstrated by Hartmann et al.[189] Cleavable cationic domains, as well as disassembly of stabilizing domains, have been demonstrated to improve delivery systems.[71]

In this chapter, we designed novel bioreducible cationic lipo-oligomers. By precisely positioning the disulfide bond between the fatty acid and polycationic domain (and not into the polycationic domain) via a Fmoc-succinoyl-cystamine building block, we intended to obtain a most drastic molecular change upon bioreduction. The amphiphilic, detergent-like character, which is considered favorable for endosomolysis but might also be associated with cytotoxicity, should be abolished upon entry into the reductive cytosol by the split into separate pure lipidic and cationic fragments; the latter have insufficient ability to bind siRNA.

We evaluate three lipo-oligomer topologies (T-shape, i-shape and U-shape) and different representatives of fatty acids as variables, which previously were found[44] to affect polyplex characteristics such as siRNA binding and lytic potential of oligomers,

gene silencing efficacy and toxicity of polyplexes. Compared with their nonreducible lipo-oligomer analogs, the favorable polyplex characteristics should remain indifferent until intracellular release into the cytosol, where improved siRNA release and biocompatibility would be expected.

3.2.1 Synthesis of the bioreducible Fmoc-succinoyl-cystamine building block and evaluation of its sensitivity towards reducing conditions

A building block applicable for standard Fmoc solid-phase peptide synthesis requires a protected amino group and a free carboxylic acid function. The synthesis of the disulfide building block (ssbb) was carried out starting from cystamine by selective protection of one terminal amine with Fmoc in the first step avoiding change of protecting groups as was previously presented.[190] To achieve reaction selectivity towards mono-functionalization, 0.8 eq. Fmoc-succinimide (Fmoc-OSu) was added dropwise to a cooled solution (-80 °C) of cystamine dihydrochloride in THF with DIPEA as a base. The carboxylic acid function was introduced in the second step by addition of 1.8 eq. succinic anhydride (Succ anhydride) solved in THF with DIPEA (**Fig. 13A**). The ssbb structure was purified via column chromatography and the identity confirmed by ^{1}H-NMR. A test structure (***740***) was synthesized on solid phase to prove the applicability for SPS. Here the ssbb connects a lipophilic peptide sequence containing three leucines (L_3) to a hydrophilic sequence with two succinoyl-tetraethylene pentamine (Stp) units (**Fig. 13B**). Tryptophane (W) was incorporated into both parts to facilitate photometric analysis. The product structure was confirmed by mass spectrometry and ^{1}H-NMR. The product was incubated with increasing concentrations of the physiological antioxidant glutathione (GSH) at 37 °C to simulate the behavior of the ssbb at different extra- and intracellular milieus. A GSH concentration of 0.1 mM mimics the barely reducing extracellular environment. As expected, the test oligomer mostly retained its structural integrity. Increasing the GSH concentration to 10 mM resembling the cytosolic reducing conditions resulted in cleavage of the test structure without detectable fractions of the intact oligomer (**Fig. 13C**).

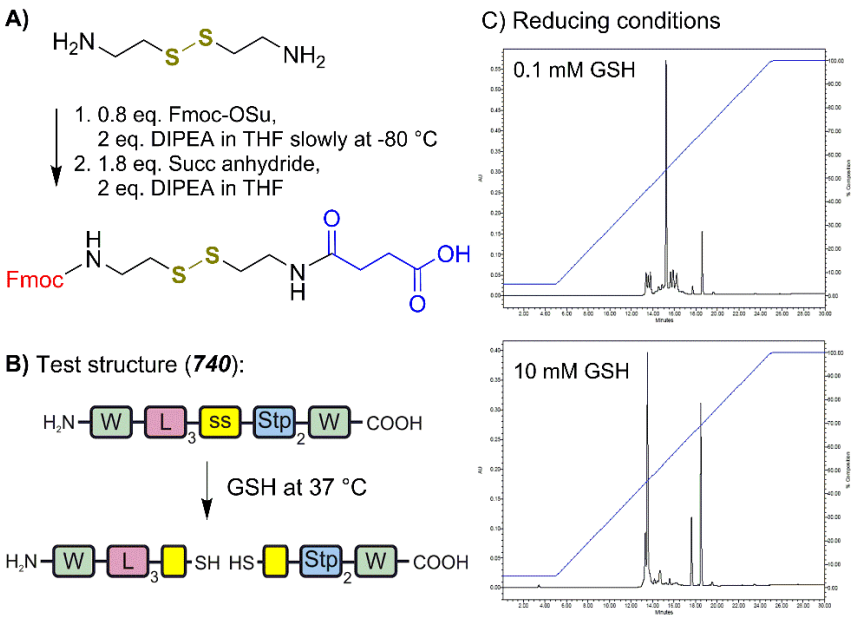

Fig. 13 A) Synthesis of the disulfide building block Fmoc-succinoyl-cystamine (Fmoc-ssbb). B) Glutathione (GSH) triggered cleavage of the test structure (***740***) with a hydrophilic (Stp_2) and a hydrophobic (L_3) part connected by ssbb. C) Test structure monitored by HPLC (280 nm wavelength) after incubation for 90 min at 37 °C in 0.1 mM GSH- (top) and 10 mM GSH- (bottom) containing HEPES buffer pH 7.4. Synthesis of Fmoc-ssbb, test structure ***740***, cleavage experiments and HPLC analysis were performed by Dr. Philipp Klein (Pharmaceutical Biotechnology, LMU).

3.2.2 Design and synthesis of cationic lipo-oligomers to form siRNA polyplexes

The ssbb unit was applied in SPS of lipo-oligomers supposed to form siRNA polyplexes that are stable in the extracellular and labile in the intracellular environment. Lipo-oligomers with three different topologies, T-shape, i-shape, and U-shape, were synthesized (**Fig. 14** top and **Fig. 15**). As shown in our previous work, topologies, as well as specific moieties of structures, may influence the biophysical and biological properties of the resulting polyplexes.[32, 43, 44, 64] For bioreducible crosslinking between oligocations, previous oligomers were designed with cysteines terminating the cationic backbone.[43, 44, 64] Differently, in the current work, the ssbb unit was positioned between the ionizable oligocationic part of the molecule and a bis (fatty acid) unit.

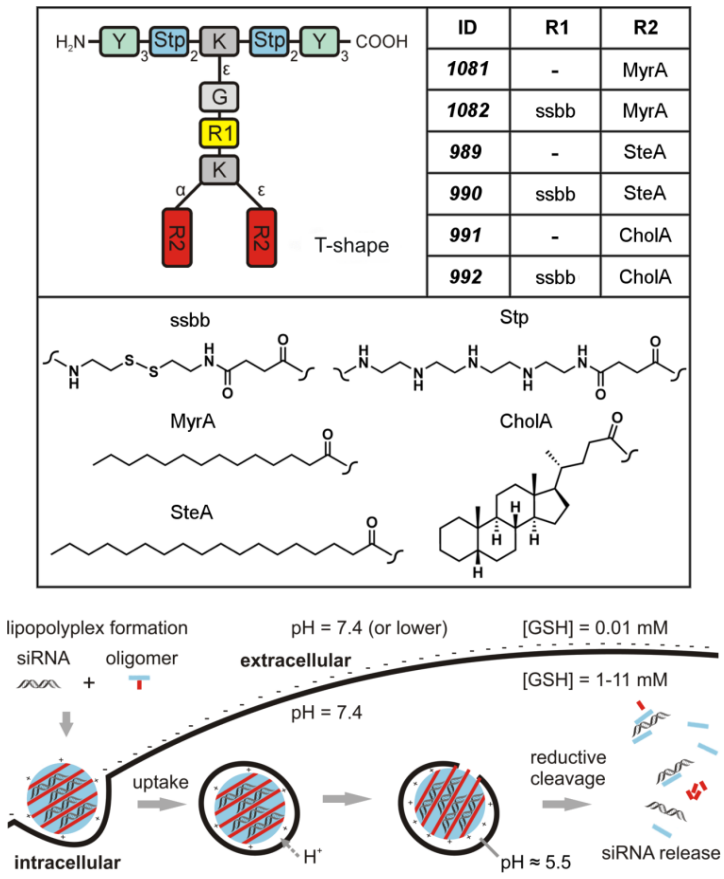

ID	R1	R2
1081	-	MyrA
1082	ssbb	MyrA
989	-	SteA
990	ssbb	SteA
991	-	CholA
992	ssbb	CholA

Fig. 14 Sequence-defined oligomers with T-shape topology. Top: schematic overview of the structures with different modifications (Y: tyrosine, K: lysine, G: glycine, Stp: succinoyl-tetraethylene-pentamine, ssbb: succinoyl-cystamine, MyrA: myristic acid, SteA: stearic acid, CholA: 5β-Cholanic acid). The broken lines represent amide linkages. IDs are unique database identification numbers. Bottom: cellular uptake, acidic pH-triggered endosomal escape, and GSH triggered cytosolic disassembly of siRNA polyplexes. Structures ***991*** and ***992*** were synthesized by Dr. Philipp Klein (Pharmaceutical Biotechnology, LMU).

Structures	ID	R1
CholA, CholA, K, R1, H, Stp, COOH — i-shape	***871***	-
	969	ssbb
CholA R1 Stp, CholA R1 Stp, K, K, COOH, NH2 — U-shape	***783***	-
	782	ssbb

Fig. 15 Sequence-defined oligomers with i-shape and U-shape topology. Schematic overview of the structures with different modifications (K: lysine, H: histidine, Stp: succinoyl-tetraethylene-pentamine, ssbb: succinoyl-cystamine, CholA: 5β-Cholanic acid). IDs are unique database identification numbers. U-shape structures were synthesized by Dr. Philipp Klein (Pharmaceutical Biotechnology, LMU).

Thus, upon reductive cleavage maximum destabilization of the polyplex on the one hand, and abolition of the membrane-active amphiphilic character on the other hand, should be achieved. The oligocationic part contains several Stp units as artificial oligoamino acids for nucleic acid binding and endosomal protonation[42], and lysines (K) as branching units. Additionally, the cationic part was equipped with tyrosine trimers (Y_3)[64] for further hydrophobic stabilization of the T-shape oligomers (**Fig. 14**), and with histidine blocks (H_6) for increased endosomal buffering of the i-shape oligomers. The saturated C14 short chain myristic acid (MyrA), the stearic acid (SteA) with the longer C18 chain, and the bulky cholanic acid (CholA) were incorporated as fatty acids for hydrophobic polyplex stabilization. For all oligomers, the corresponding non-reducible control structures lacking ssbb were synthesized. The ssbb was incorporated into various different structures to proof the concept independently of shape and other functional domains and to put this work into a broader context. The structures were analyzed with mass spectrometry and ^{1}H-NMR. To exclude that lipo-oligomers contain significant amounts of reduced fragments, Ellman´s assay was performed to detect free thiols (**Table 13**). Lack of free thiols (< 3 %) indicate high integrity of the ssbb linkage.

Table 13 Determination of free thiols in reducible T-shape, i-shape and U-shape structures via Ellman´s assay. Ellman´s assay was performed by Dr. Philipp Klein (Pharmaceutical Biotechnology, LMU).

Oligomer	Ratio of free thiols (in %)
1082 **(MyrA-ss-t)**	2.0
990 **(SteA-ss-t)**	2.3
992 **(CholA-ss-t)**	2.7
969 **(CholA-ss-i)**	1.2
782 **(CholA-ss-u)**	0.6

3.2.3 Formulation of siRNA polyplexes and biophysical characterization

Polyplexes were formed by mixing the cationic oligomers with siRNA, followed by 40 minutes incubation and biophysical characterization (**Fig. 16** shows a summary for stable and reducible CholA T-shapes ***991*** and ***992***). The siRNA binding ability of oligomers was determined by measuring the electrophoretic mobility of siRNA in a 2.5 % agarose gel. Different N/P values depict the ratio of protonatable amines (N) of the oligomer to phosphates (P) of the siRNA.

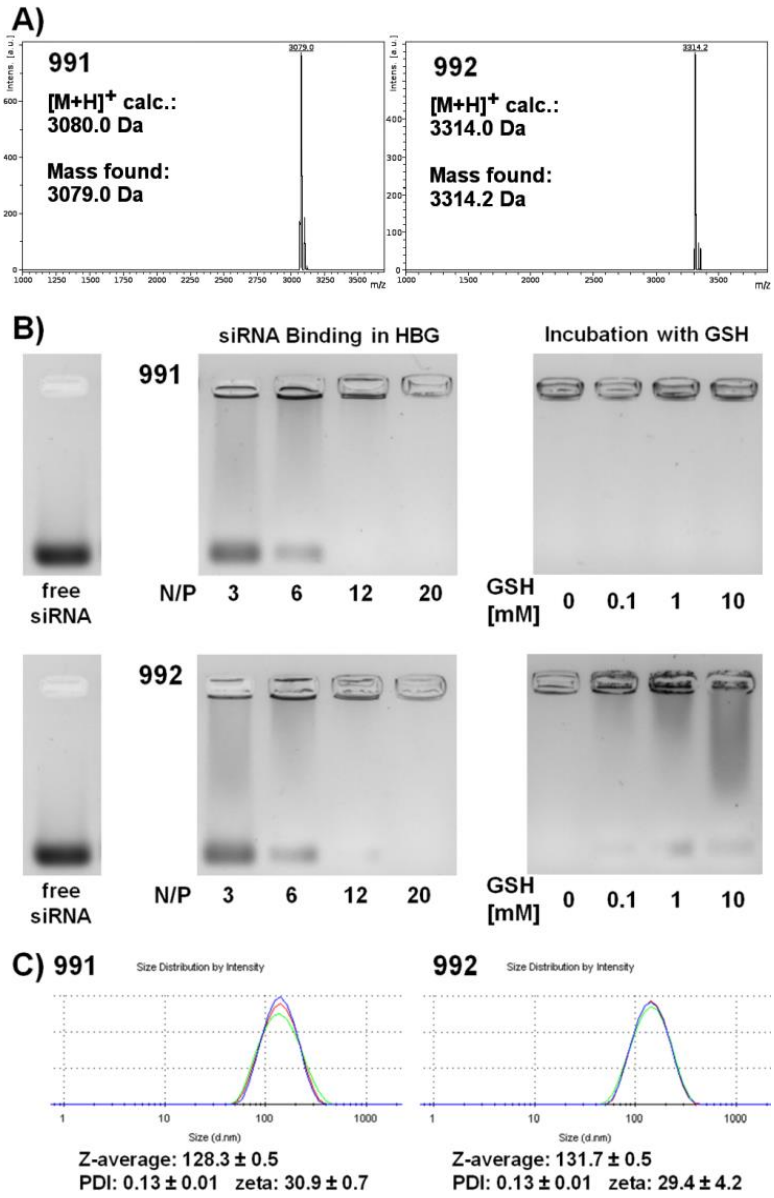

Fig. 16 A) Analytical characterization of stable oligomer ***991*** and bioreducible oligomer ***992*** by mass spectrometry. B) Agarose gel shift assays. Left: siRNA binding at different N/P ratios. Right: Lipopolyplexes formed at N/P 20 and subsequent 90 min treatment at 37 °C with different concentrations of GSH in HEPES buffer pH 7.4. C) Biophysical characterizations of lipopolyplexes formed with oligomers and siRNA at N/P 12 by DLS. DLS measurements were performed by Dr. Philipp Klein (Pharmaceutical Biotechnology, LMU).

This does not present charge ratios, as only a fraction of the protonatable amines are protonated at physiological pH. All T-shape, i-shape and U-shape structures showed sufficient binding at N/P ≥ 12 (**Fig. 17**, **Fig. 18**).

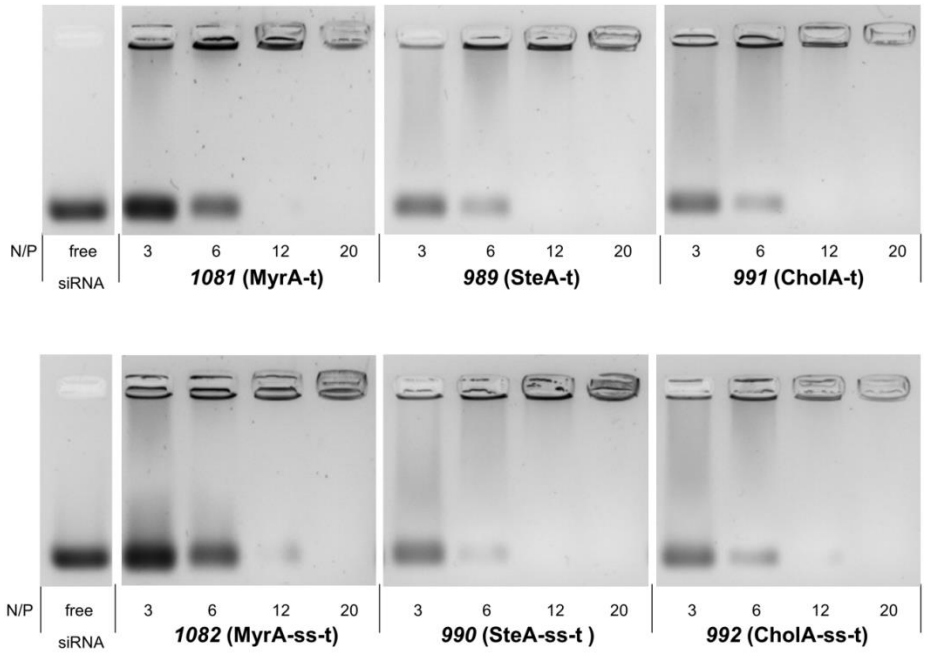

Fig. 17 siRNA binding ability of T-shape structures analyzed with an agarose gel shift assay. The left lane shows the running distance of free siRNA in HBG that is not complexed by lipo-oligomers. Polyplexes were tested for siRNA binding ability at different N/P ratios. Top: stable structures, bottom: reducible structures.

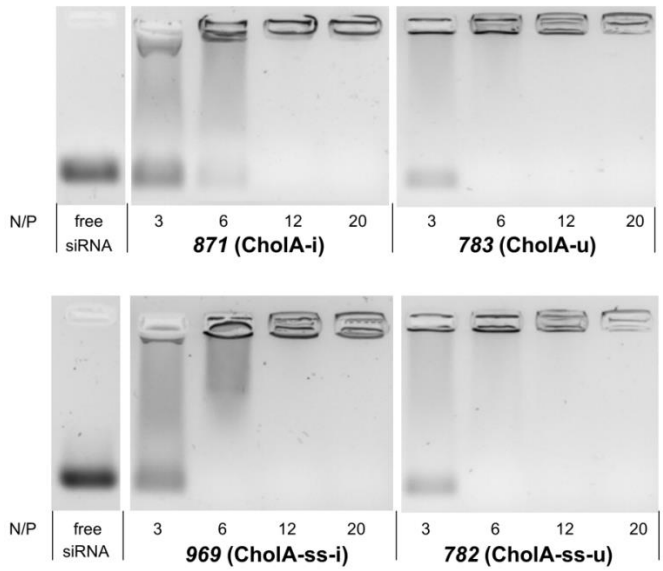

Fig. 18 siRNA binding ability of i-shape and U-shape structures analyzed with an agarose gel shift assay. The left lane shows the running distance of free siRNA in HBG that is not complexed by lipo-oligomers. Polyplexes were tested for siRNA binding ability at different N/P ratios. Top: stable structures, bottom: reducible structures. Gel shifts for U-shape structures were performed by Dr. Philipp Klein (Pharmaceutical Biotechnology, LMU).

Neither stable nor reducible polyplexes released free siRNA when exposed to 90 % full serum at 37 °C for two hours, indicating a high extracellular stability (**Fig. 19**).

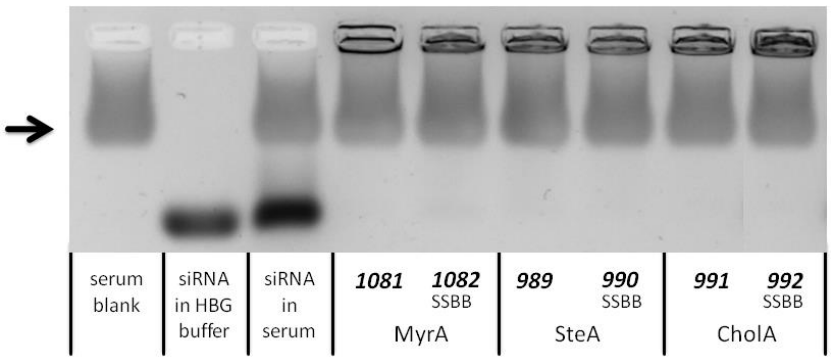

Fig. 19 Gel retardation assay of siRNA polyplexes incubated at N/P 12 for 40 min, followed by treatment with 90 % full serum for two hours at 37 °C. The black arrow points at a band that is caused by serum (see serum blank in band one). Running distance of free siRNA in HBG buffer and in 90 % serum are shown in band two and three. Serum gel shifts were performed by Dr. Philipp Klein (Pharmaceutical Biotechnology, LMU).

In contrast, treatment of polyplexes with the physiological reducing agent GSH at 37 °C resulted in a dose-dependent loss of siRNA binding efficacy for the reducible but not the stable oligomers (**Fig. 20**, **Fig. 21**). Due to the particular position of the ssbb unit, reductive cleavage leads to the release of the lipid as the most important stabilization motif, thus keeping only a weak binding ability of the remaining cationic backbone.[64] This destabilization of polyplexes is expected to provide better accessibility of siRNA at intracellular GSH concentrations (~10 mM).

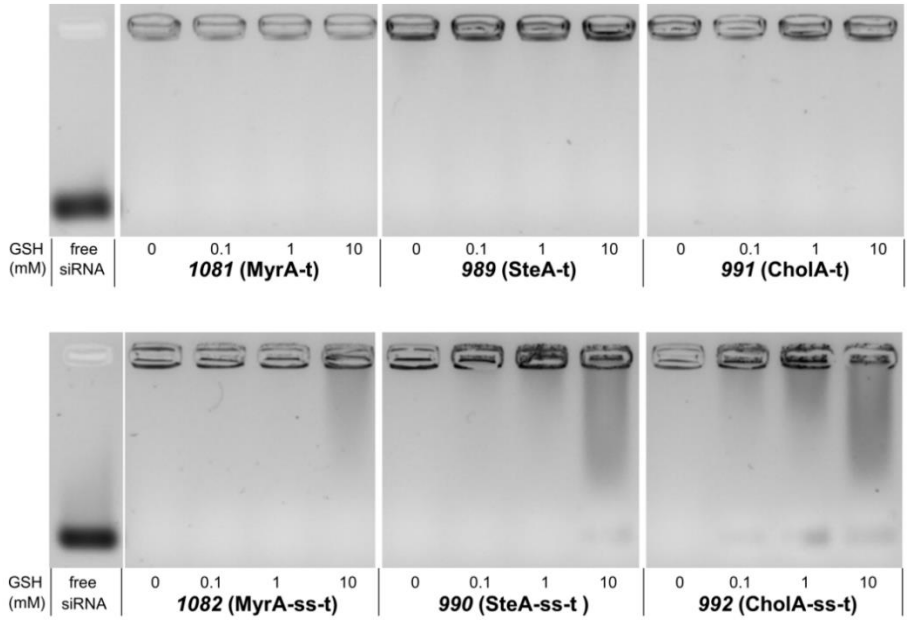

Fig. 20 siRNA binding ability of T-shape structures under reducing conditions analyzed with an agarose gel shift assay. The left lane shows the running distance of free siRNA in HBG that is not complexed by lipo-oligomers. Lipopolyplexes were formed at N/P 20 followed by 90 min treatment at 37 °C with different concentrations of GSH in HEPES buffer pH 7.4. Top: stable structures, bottom: reducible structures.

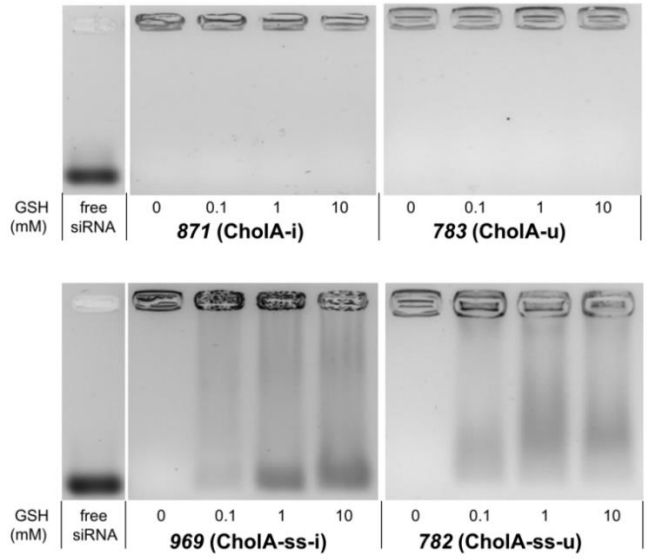

Fig. 21 siRNA binding ability of i-shape and U-shape structures under reducing conditions analyzed with an agarose gel shift assay. The left lane shows the running distance of free siRNA in HBG that is not complexed by lipo-oligomers. Lipopolyplexes were formed at N/P 20 followed by 90 min treatment at 37 °C with different concentrations of GSH in HEPES buffer pH 7.4. Top: stable structures, bottom: reducible structures. Gel shifts for U-shape structures were performed by Dr. Philipp Klein (Pharmaceutical Biotechnology, LMU).

The particle sizes of siRNA lipopolyplexes were measured by dynamic light scattering (DLS). All T-shape polyplexes showed uniform sizes between 105 - 138 nm z-average (**Table 14**).

Table 14 Particle size (Z-average) and zeta potential of siRNA polyplexes determined with a DLS zetasizer. Measurements for t- and U-shape structures were performed by Dr. Philipp Klein (Pharmaceutical Biotechnology, LMU).

Oligomer	N/P	z-average [nm]	Mean PDI	Mean Zeta Potential [mV]
1081 (MyrA-t)	12	105.0 ± 1.8	0.15 ± 0	27.0 ± 0.8
1082 (MyrA-ss-t)	12	107.7 ± 0.5	0.14 ± 0.02	28.6 ± 0.8
989 (SteA-t)	12	125.3 ± 1.0	0.12 ± 0.01	29.3 ± 1.6
990 (SteA-ss-t)	12	137.9 ± 1.6	0.13 ± 0.01	26.8 ± 0.9
991 (CholA-t)	12	131.7 ± 0.5	0.13 ± 0	29.4 ± 4.2
992 (CholA-ss-t)	12	128.3 ± 0.5	0.13 ± 0.01	30.9 ± 0.7
871 (CholA-i)	12	275.0 ± 7.2	0.24 ± 0.01	23.4 ± 0.7
969 (CholA-ss-i)	12	237.8 ± 4.2	0.20 ± 0.01	25.2 ± 0.3
783 (CholA-u)	12	122.7 ± 2.0	0.26 ± 0.02	31.5 ± 0.7
782 (CholA-ss-u)	12	181.2 ± 4.7	0.27 ± 0.01	29.1 ± 3.3

The sizes of i-shape and U-shape polyplexes showed higher polydispersity. All formulations revealed a positive zeta potential of around 23 – 32 mV due to an excess of cationic oligomer (**Table 14**). T-shape oligomers were found as well-suited for the evaluation of structure-activity relationships, since all of them formed polyplexes with reliable sizes and low polydispersity.

3.2.4 siRNA transfection efficiency

Gene silencing experiments were performed in Neuro2A neuroblastoma cells stably expressing an eGFP-Luciferase fusion protein (**Fig. 22**). Silencing by siGFP (light bars) can be quantified by a standard luciferase assay. In all cases, gene silencing was more effective for the bioreducible T-shape oligomers (**Fig. 22B**) as compared to their stable analogs (**Fig. 22A**). A reduced luciferase expression in control experiments using siCtrl (dark bars) is caused by unspecific cytotoxic effects and not by a specific knockdown of the eGFPLuc gene. Thus, from evaluating the luciferase levels of the siCtrl polyplexes, an enhanced biocompatibility of the reducible structures (**Fig. 22B**) can be concluded.

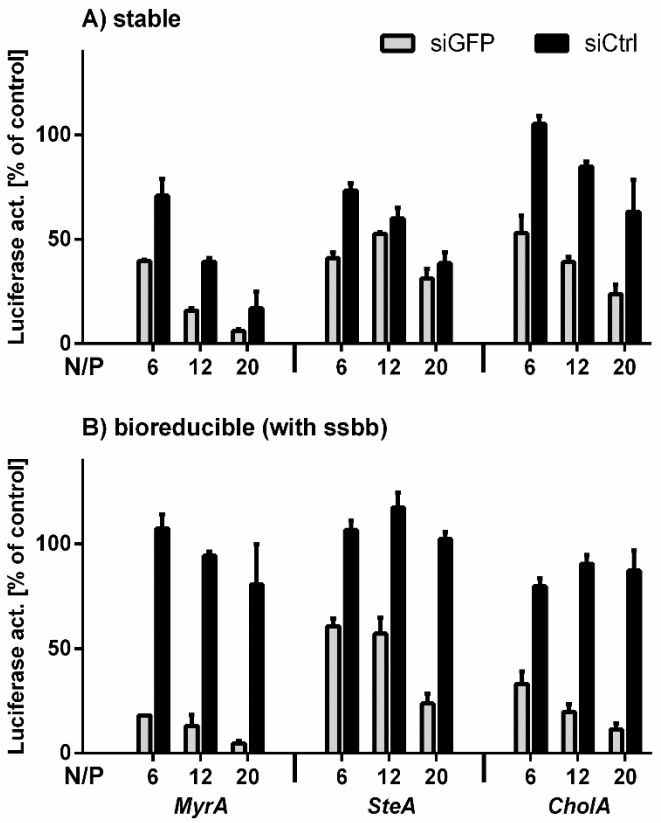

Fig. 22 Gene silencing of T-shape oligomers in neuroblastoma cells. Lipopolyplexes with 500 ng / 37 pmol eGFP-targeted siRNA (siGFP) / well respectively control siRNA (siCtrl) at N/P 6, 12 and 20 were tested for eGFPLuc gene silencing in Neuro2A-eGFPLuc cells. A) Lipopolyplexes made of stable structures ***1081***, ***989*** and ***991*** B) Lipopolyplexes made of bioreducible structures ***1082***, ***990*** and ***992***. The luciferase activity of siRNA-treated cells is presented related to buffer-treated cells. HBG-treated cells were set to 100 %. Data are presented as mean value (± SD) out of triplicates**.** Dose-dependent gene silencing transfections are shown in **Fig. 24** and **Fig. 25**. Transfections were performed by Dr. Dian-Jang Lee (Pharmaceutical Biotechnology, LMU).

Similar findings, an enhanced gene silencing and especially the reduction of cytotoxicity, were also made for bioreducible i-shape and U-shape lipo-oligomers (**Fig. 23**).

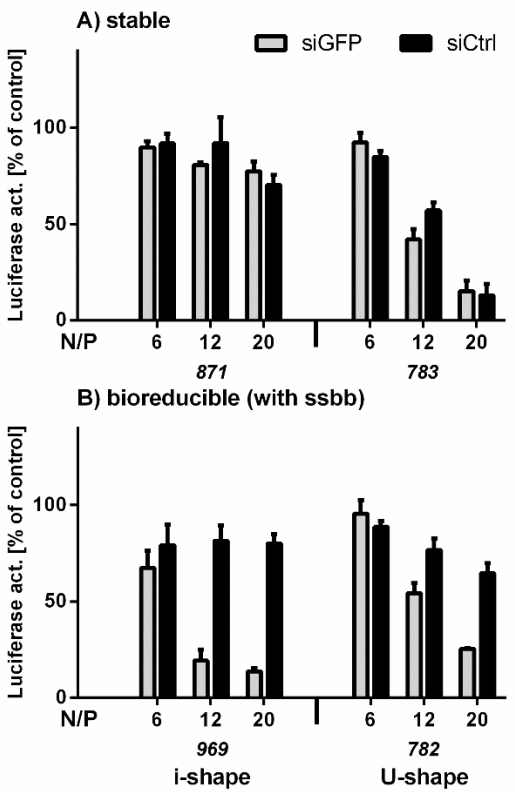

Fig. 23 Gene silencing of i-shape and U-shape oligomers in neuroblastoma cells. Lipopolyplexes with 500 ng / 37 pmol eGFP-targeted siRNA (siGFP) / well respectively control siRNA (siCtrl) at N/P 6, 12 and 20 were tested for eGFPLuc gene silencing in Neuro2A/eGFPLuc cells. A) Lipopolyplexes made of stable structures ***871*** and ***783*** B) Lipopolyplexes made of bioreducible structures ***969*** and ***782***. The luciferase activity of siRNA-treated cells is presented related to buffer-treated cells. HBG-treated cells were set to 100 %. Data are presented as mean value (± SD) out of triplicates**.** Transfections for i-shapes were performed by Dr. Dian-Jang Lee, transfections for u-shapes were performed by Dr. Katharina Müller (Pharmaceutical Biotechnology, LMU).

Based on the starting formulation of 37 pmol siRNA (370 nM) with 1.44 nmol oligomer (N/P 12), the dose of siRNA was reduced either at a constant N/P 12 (**Fig. 24**) or a constant dose of 1.44 nmol oligomer (**Fig. 25**). In the latter case, significant gene silencing was still observed for reducible MyrA polyplexes at 1.2 pmol / 12 nM siRNA.

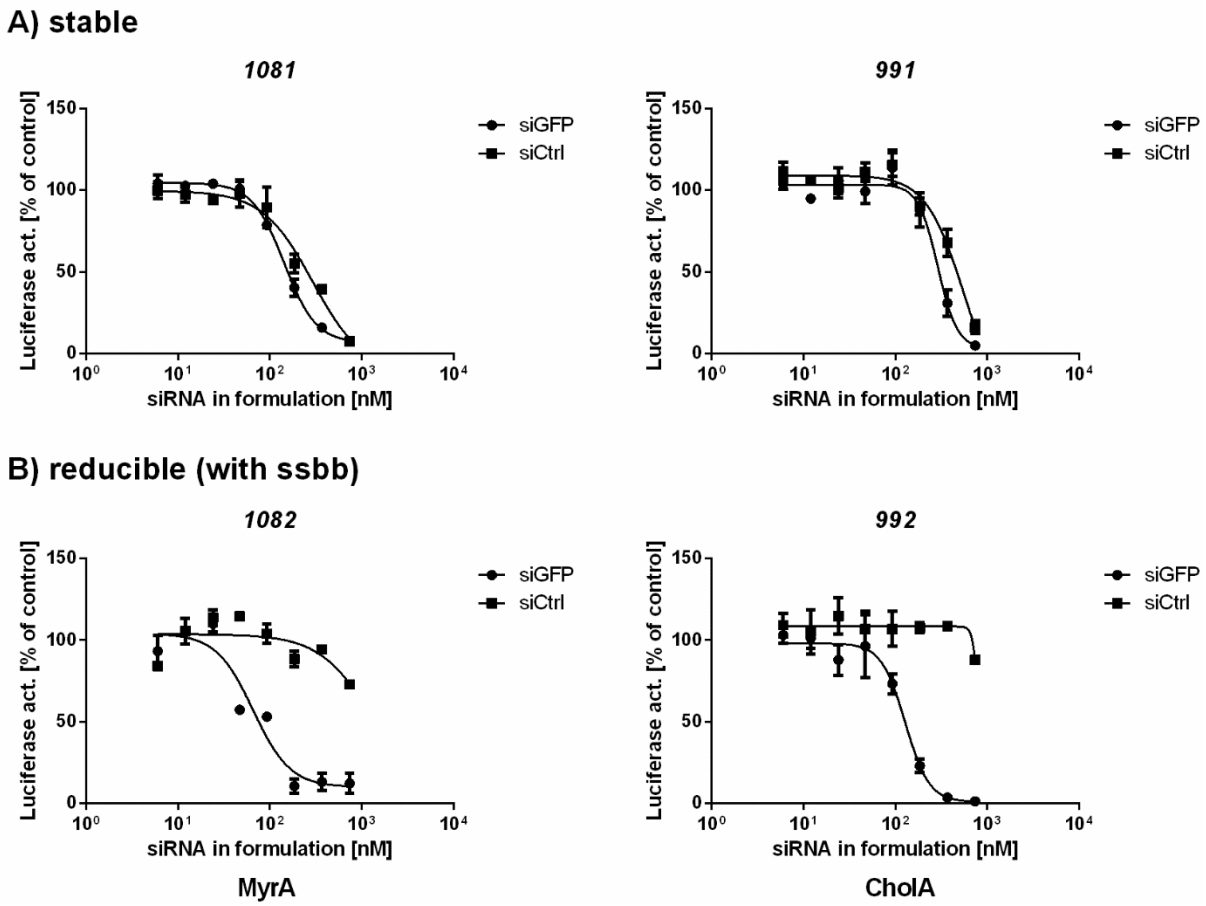

Fig. 24 Dose-dependent gene silencing of T-shape oligomers at N/P 12 in neuroblastoma cells. Lipopolyplexes with eGFP-targeted siRNA (siGFP) respectively control siRNA (siCtrl) were examined for eGFPLuc gene silencing in Neuro2A/eGFPLuc cells. The oligomer amount was adjusted for each formulation to keep it constant at N/P 12. Formulations including siRNA from 6, 12, 27, 47, 93, 185, 370 up to 740 nM were tested. A) Lipopolyplexes made of stable structures ***1081*** and ***991*** B) Lipopolyplexes made of bioreducible structures ***1082*** and ***992***. The luciferase activity of siRNA-treated cells is presented related to buffer-treated cells. HBG-treated cells were set to 100 %. Data are presented as mean value (± SD) out of triplicates. Transfections were performed by Dr. Dian-Jang Lee (Pharmaceutical Biotechnology, LMU).

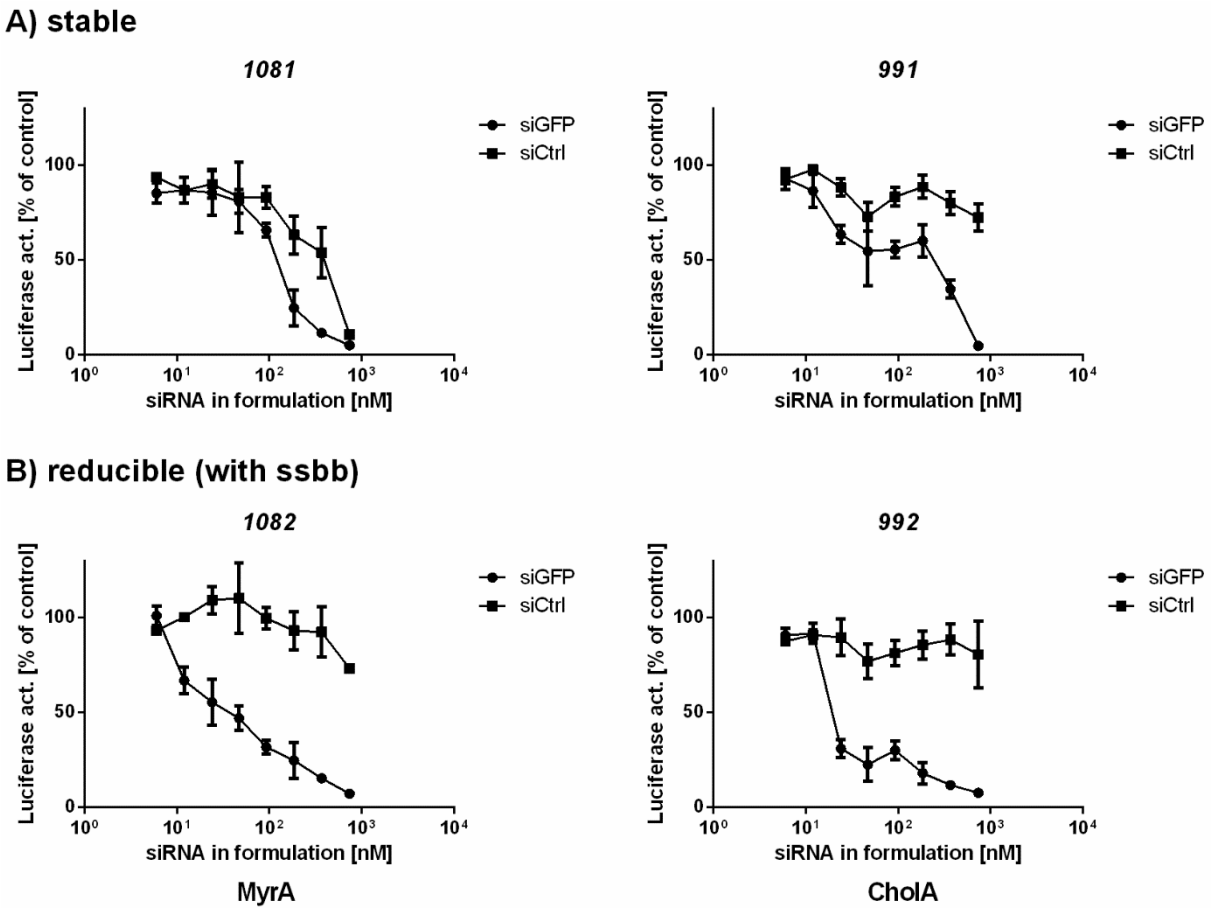

Fig. 25 Dose-dependent gene silencing of T-shape oligomers in neuroblastoma cells. Lipopolyplexes with eGFP-targeted siRNA (siGFP) respectively control siRNA (siCtrl) at constant oligomer amount of 1.44 nmol (N/P 12 at 500 ng siRNA) were examined for eGFPLuc gene silencing in Neuro2A/eGFPLuc cells. Formulations including siRNA from 6, 12, 27, 47, 93, 185, 370 up to 740 nM were tested. A) Lipopolyplexes made of stable structures ***1081*** and ***991*** B) Lipopolyplexes made of bioreducible structures ***1082*** and ***992***. The luciferase activity of siRNA-treated cells is presented related to buffer-treated cells. HBG-treated cells were set to 100 %. Data are presented as mean value (± SD) out of triplicates. Transfections were performed by Dr. Dian-Jang Lee (Pharmaceutical Biotechnology, LMU).

The beneficial effects of reducible polyplexes are also confirmed in DU145/eGFPLuc prostate cancer cells (**Fig. 26**).

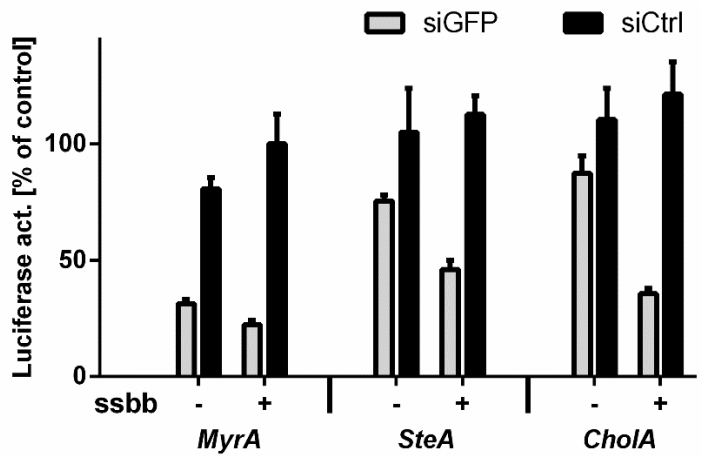

Fig. 26 Gene silencing of T-shape oligomers in prostate cancer cells. Lipopolyplexes with 500 ng eGFP-targeted siRNA (siGFP) respectively control siRNA (siCtrl) at N/P 12 were tested for eGFPLuc gene silencing in DU145/eGFPLuc cells. Lipopolyplexes made of stable structures (***1081***, ***989*** and ***991***) and bioreducible structures (***1082***, ***990*** and ***992***) are shown. The luciferase activity of siRNA treated cells is presented related to buffer-treated cells. HBG-treated cells were set to 100 %. Data are presented as mean value (± SD) out of triplicates. Transfections were performed by Dr. Dian-Jang Lee (Pharmaceutical Biotechnology, LMU).

Gene silencing experiments were performed in HeLa-derived KB/eGFPLuc cells and revealed a negative influence of the bioreducible building block. While the stable structures merdiated gene silencing, the efficiency for biodegradable structures was significantly decreased (**Fig. 27**). Obviously not all cell lines profit from a bioreducible character of the nucleic acid carrier, which could be explained by premature disulfide cleavage occurring at the extracellular cell surface. High extracellular disulfide cleavage was previously reported for HeLa cells and could potentially also account for KB cells.[191] When focusing on the comparison of the three different fatty acids, SteA and CholA lipo-oligomers (no or only moderate silencing for the stable versions) strongly benefited from the incorporation of the ssbb with regard to gene silencing in Neuro2A and DU145 cell lines. In contrast, the stable MyrA lipo-oligomer displayed gene silencing activity combined with significant cytotoxicity (**Fig. 22A**); here the reducible ssbb unit eliminated the cytotoxicity without reducing the gene silencing activity (**Fig. 22B**).

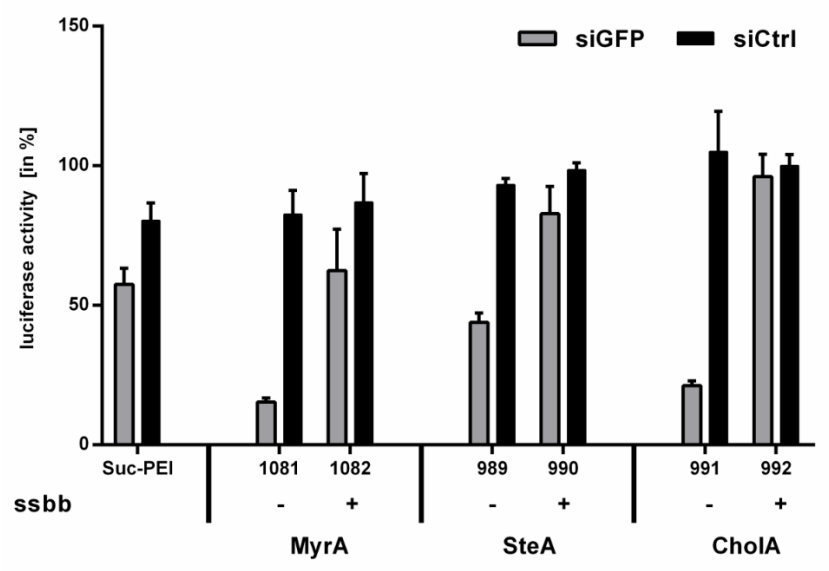

Fig. 27 Gene silencing of T-shape oligomers in KB cells**.** Lipopolyplexes with 500 ng/37 pmol eGFP-targeted siRNA (siGFP) per well respectively control siRNA (siCtrl) at N/P 12 were tested for eGFPLuc gene silencing in KB-eGFPLuc cells. Lipopolyplexes made of stable structures ***1081***, ***989*** and ***991*** (- ssbb) and lipopolyplexes made of bioreducible structures ***1082***, ***990*** and ***992*** (+ ssbb) were tested. The luciferase activity of siRNA-treated cells is presented related to buffer-treated cells. HBG-treated cells were set to 100 %. Data are presented as mean value (± SD) out of triplicates. Transfections were performed by Dr. Dian-Jang Lee (Pharmaceutical Biotechnology, LMU).

The findings for non-reducible lipo-oligomers are consistent with our earlier observations[192], where SteA derivatives showed poor gene silencing activity and MyrA derivatives exhibited not only gene silencing activity but cytotoxicity. For non-reducible structures, the unsaturated C18 fatty acids oleic acid and linoleic acid were the optimum lipid units with regard to transfection efficacy and cell tolerability.[43, 44, 64] Still, due to the higher stability during synthesis and storage, in the current work saturated fatty acids were the preferred option for integration into solid phase synthesized lipo-oligomers.

Nevertheless, incorporation of the bioreducible linker into oleic acid containing oligomers was also found to further enhance transfection efficacy and cell tolerability (**Fig. 28**).

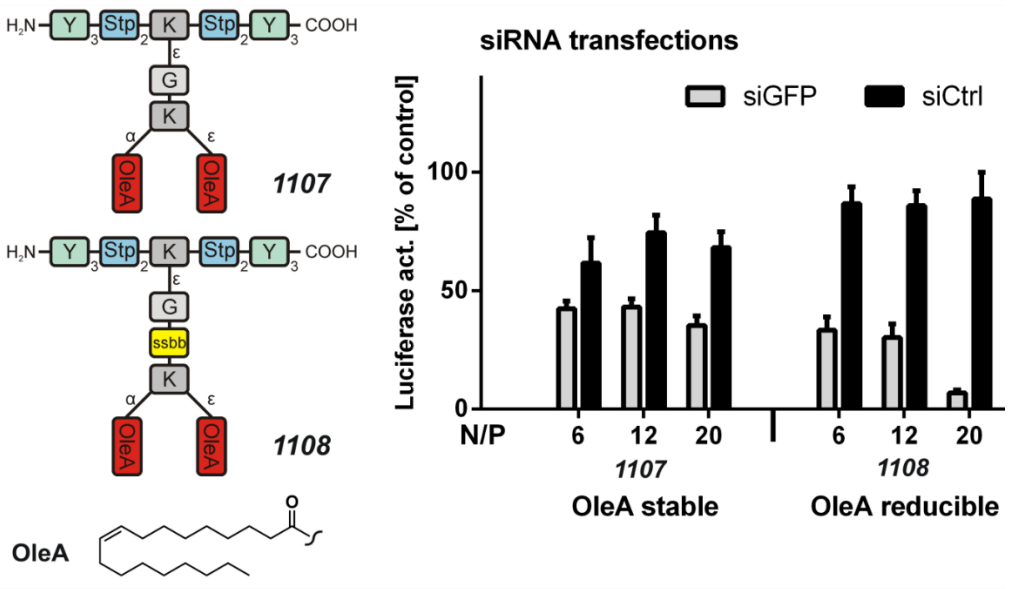

Fig. 28 Gene silencing of oleic acid containing T-shape oligomers in neuroblastoma cells. Lipopolyplexes with 500 ng / 37 pmol eGFP-targeted siRNA (siGFP) / well respectively control siRNA (siCtrl) at N/P 6, 12 and 20 were tested for eGFPLuc gene silencing in Neuro2A/eGFPLuc cells. The luciferase activity of siRNA-treated cells is presented related to buffer-treated cells. HBG-treated cells were set to 100 %. Data are presented as mean value (± SD) out of triplicates**.** Transfections were performed by Dr. Dian-Jang Lee (Pharmaceutical Biotechnology, LMU).

The different fatty acids may influence the extent of hydrophobic stabilization of siRNA polyplexes, but do also strongly affect the lytic properties of the lipo-oligomers, both in the stable and reducible setting. At endosomal pH, the cationic parts receive increased cationization, which in combination with the hydrophobic domain facilitates endosomal membrane destabilization and escape into the cytosol. An erythrocyte leakage assay compared the different fatty acid versions of stable (**Fig. 29A**) and the ssbb containing reducible (**Fig. 29B**) lipo-oligomers. MyrA structures displayed a far higher leakage activity (highest at pH 5.5) than the SteA structures, whereas oligomers with the bulky CholA did not display lytic effects.

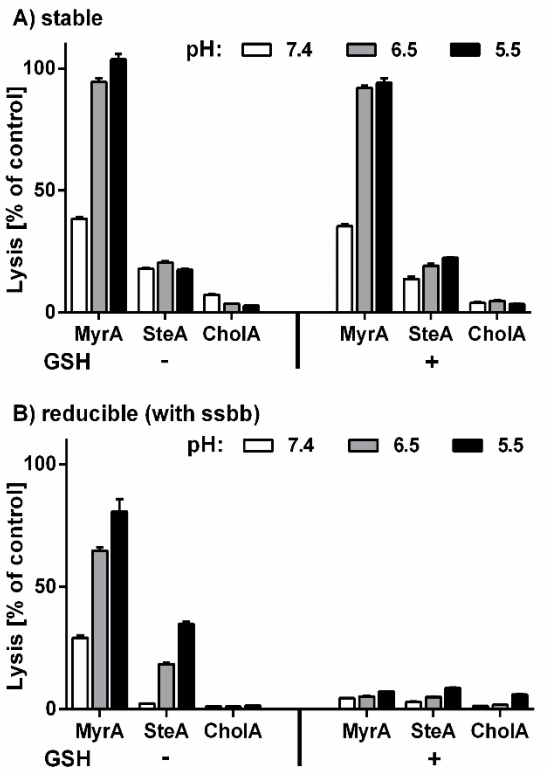

Fig. 29 Erythrocyte leakage of oligomers at different pH and under reducing conditions. A) Stable lipo-oligomers ***1081***, ***989*** and ***991***. B) bioreducible lipo-oligomers ***1082***, ***990*** and ***992***. The final concentration of oligomers was 7.5 µM. GSH treated lipo-oligomers were incubated with 10 mM GSH in PBS adjusted to pH 7.4 at 37 °C for 90 min (right-hand side). PBS-treated erythrocytes were set to 0 %. Triton X served as positive control and was set to 100 %. Data are presented as mean value (± SD) out of quadruplicates.

This finding is in agreement with literature, showing that cationic dimyristyl lipids strongly promote membrane fusion events. Deviations of hydrophobic volume and hydrophilic-lipophilic ratio from an optimum hampered membrane interactions.[168] Treatment with GSH did not affect the stable analogs but extinguished the lytic activity of the reducible lipo-oligomers, consistent with their lower cytotoxicity. This observation can be attributed to the integration of the ssbb as a linker between the cationic and the lipophilic part, as reductive cleavage results in an uncharged fatty acid structure and an oligocationic part with significantly reduced amphiphilic character. Both compounds alone were not able to lyse membranes anymore.

3.3 Precise Enzymatic Cleavage Sites for Improved Bioactivity of siRNA Lipo-Polyplexes

This chapter has been adapted from:

Reinhard, S.,* Wang, Y., Dengler, S., Wagner, E. (2018) Precise Enzymatic Cleavage Sites for Improved Bioactivity of siRNA Lipo-Polyplexes, Bioconjug Chem 29(11) (2018) 3649-3657

* Corresponding author

Although polycations fulfill several extracellular and intracellular delivery requirements, the therapeutic window between transfer efficiency and cytotoxicity is usually narrow. Nondegradable polymers like the potent and commonly used transfection polymer polyethylenimine (PEI) show significant toxicity in a time-and concentration-dependent manner with a two-stage mechanism: phase 1 short-term toxicity results from compromised plasma membrane integrity, while phase 2 long-term (> 24 h) toxicity is caused by intracellular mechanisms after internalization of the polyplexes.[193, 194] PEI-induced damage of lysosomal and mitochondrial membranes is a potential cause for late-phase cell death. The disintegration of mitochondrial membranes leads to the release of pro-apoptotic cytochrome c and an energy crisis due to ATP-leakage, while perturbation of lysosomal membranes contributes to cellular stress through possible release of lysosomal cathepsins.[193-200]

The degradation of cationic polymers in low molecular weight subunits reduces both acute toxicity and negative long-term effects, which might occur after repeated administration.[32, 201-203] Biodegradable cationic polymers can be designed by introduction of ester bonds,[204, 205] disulfides,[201, 206, 207] ketals,[208] imines,[209] polyglutamic acid amides, and other degradable amide bonds.[210, 211]

Release of siRNAs from endosomes into the cytosol occurs at low rates (1−2 %) for lipid nanoparticles.[212, 213] This implies that large amounts of cationic carriers accumulate in lysosomes, which represent the terminal organelles on the endocytic pathway[196, 214] unless dumped by emergency exocytosis.[215] Specific degradation of nucleic acid carriers by endolysosomal enzymes therefore appears as an attractive strategy to destroy abundant carrier molecules while ensuring high extracellular stability. Lysosomes mediate the degradation of extracellular particles from

endocytosis and of intracellular components from autophagy with more than 60 different types of hydrolytic enzymes.[216] Endolysosomal cysteine proteases like cathepsin B are involved in protein degradation and turnover in cells.[217, 218] Cathepsin B, together with cathepsin L and D, is one of the most abundant lysosomal proteases with concentrations as high as 1 mM and ubiquitous expression.[217] Cathepsin B has both endo- and exopeptidase activity, which was utilized for enzyme-triggered, intracellular drug delivery[219-221] as well as for nucleic acid delivery with degradable peptide-HPMA copolymers. Polyplexes formed with biodegradable copolymers showed similar transfection efficiency but less cytotoxicity compared to nondegradable structures.[222]

In this chapter, we evaluated the cathepsin B-triggered cleavage of oligoaminoamides based on the synthetic solid-phase compatible building block succinoyl-tetraethylene-pentamine (Stp), which contains the pH-responsive diaminoethylene motif of the transfection polymer PEI, and different peptide linkers placed between two Stp units. A library of myristic acid- and Stp-containing sequence-defined lipo-oligomers with tailored biodegradability was synthesized by introducing either short cleavable L-arginine dipeptides, noncleavable D-arginine dipeptide linkers, or varieties of both. Endolysosomal degradation was simulated by incubation with cathepsin B at pH 5.5, and the fragments were identified by MALDI-TOF mass spectrometry. The influence of tailored intracellular cleavability on cell tolerability and transfection efficiency was studied in Huh7-eGFPLuc and DU145-eGFPLuc cells.

3.3.1 Degradability of test oligomers by cathepsin B

For solid-phase assisted synthesis of sequence-defined oligomers, natural and artificial amino acids, synthetic building blocks, and fatty acids can be used. While linear peptide sequences of natural L-amino acids usually are readily cleavable by proteases, the degradability might be hampered when oligoamide structures contain artificial building blocks or are synthesized in branched configurations. Repeating units of the synthetic building block Stp provide oligoaminoamides with both nucleic acid binding and endosomal buffering capacity and therefore can be substantial parts of nucleic acid carriers. A library of test structures was synthesized to study the cathepsin B-triggered degradation of Stp-containing oligomers (**Fig. 30**).

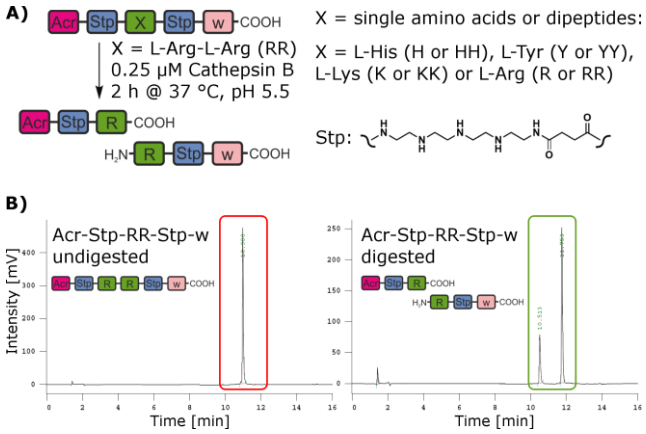

Fig. 30 Enzymatic degradation of test structures. A) Single L-amino acid or dipeptide linkers are placed at position X between two amidebound units of the synthetic building block Stp. Left: Cathepsin triggered degradation of a test structure containing a L-Arg-L-Arg linker (Acr-Stp-**RR**-Stp-w). B) HPLC-Chromatogram of Acr-Stp-**RR**-Stp-w before (left) and after (right) incubation with cathepsin B.

The test oligomers consist of two Stp units connected by one or two of the natural L-amino acids lysine, arginine, histidine, or tyrosine, which have been used in our published nucleic acid carriers.[223] Lysine and arginine bind and complex nucleic acids, histidine provides endosomal buffer capacity, and tyrosines are involved in aromatic polyplex stabilization. The test structures were equipped with acridine (Acr) at the N-terminus and D-tryptophane (w) at the C-terminus to facilitate the detection of fragments by HPLC-DAD. The degradability of the test oligomers was evaluated by incubation with cathepsin B at endolysosomal pH 5.5. After 2 h of incubation at 37 °C, the percentage of cleaved material was determined by HPLC (**Table 15**). The test structure containing two amide-bound Stp units without any natural L-amino acid linkers was not degradable by cathepsin B. This enzyme resistance is the most relevant information for carriers based on Stp block oligomers and is consistent with findings that length of Stp oligomers correlates with cytotoxicity.[40] No cleavage was also found for test oligomers containing one or two histidines or one tyrosine. A low fraction of degraded material was detected when two tyrosines (8.6 %) or one lysine (16 %) were placed between the Stp units. Arginine was the preferred substrate of the enzyme with cleavage rates of 47 % with one and 100 % with two L-arginines.

Table 15 Cathepsin-triggered degradation of test structures

Test structure[a] N→C	Degradation fragments[b]	Peptide degradation [%][c]
Acr-Stp-Stp-w	-	0
Acr-Stp-**H**-Stp-w	-	0
Acr-Stp-**HH**-Stp-w	-	0
Acr-Stp-**Y**-Stp-w	-	0
Acr-Stp-**YY**-Stp-w	Acr-Stp-**Y** + **Y**-Stp-w	8.6
Acr-Stp-**K**-Stp-w	Acr-Stp-**K** + Stp-w	16
Acr-Stp-**KK**-Stp-w	Acr-Stp-**K** + **K**-Stp-w	100
Acr-Stp-**R**-Stp-w	Acr-Stp-**R** + Stp-w	47
Acr-Stp-**RR**-Stp-w	Acr-Stp-**R** + **R**-Stp-w	100

[a]Test structures contain no linker (Acr-Stp-Stp-w) or L-His (**H** or **HH**), L-Tyr (**Y** or **YY**), L-Lys (**K** or **KK**), or L-Arg (**R** or **RR**) single amino acid or dipeptide linkers. [b]Identified by MALDI-TOF mass spectrometry after HPLC. [c]Determined by HPLC.

3.3.2 T-Shaped lipo-oligomers with designed enzymatic degradability

Based on the results of the cathepsin-triggered degradation of test oligomers, a library of Stp- and arginine-containing T-shaped lipo-oligomers with precisely introduced cleavage sites was synthesized (**Fig. 31A**, **Table 16**).

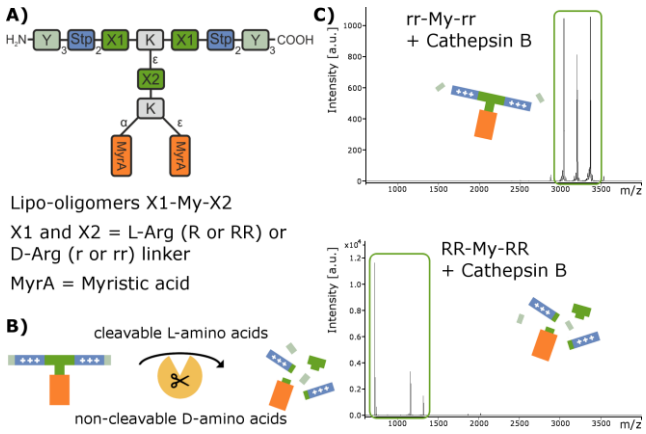

Fig. 31 A) Scheme of lipo-oligomers ***X1-My-X2*** with cleavable single amino acid or dipeptide L-arginine sequences (R or RR) or noncleavable D-arginine linkers (r or rr) at sites X1 and X2. My is used as the abbreviation for T-shaped lipo-oligomers containing a dimyristic acid domain. An overview of all structures and the linkers can be found in **Table 16**. Y: L-tyrosine, K: L-lysine. B) Enzymatic degradation only occurs when L-amino acids are incorporated. C) MALDI mass spectra of rr-My-rr (top) containing only D-Arg linkers and RR-My-RR (bottom) containing only L-Arg linkers after digestion.

Table 16 Lipo-oligomers as shown in Figure 31 with cleavable L-arginine sequences, non-cleavable D-arginine linkers or varieties of both.

Lipo-oligomers ***X1-My-X2***	X1	X2
My	-	-
My-RR	-	L-Arg-L-Arg
RR-My	L-Arg-L-Arg	-
RR-My-RR	L-Arg-L-Arg	L-Arg-L-Arg
RR-My-rr	L-Arg-L-Arg	D-Arg-D-Arg
rr-My-RR	D-Arg-D-Arg	L-Arg-L-Arg
rr-My-rr	D-Arg-D-Arg	D-Arg-D-Arg
My-R	-	L-Arg
My-r	-	D-Arg
R-My	L-Arg	-
R-My-R	L-Arg	L-Arg
R-My-r	L-Arg	D-Arg
r-My	D-Arg	-
r-My-R	D-Arg	L-Arg
r-My-r	D-Arg	D-Arg

Arginine was preferred over lysine as a single L-Arg linker between two amide-bound Stp units in the test oligomers and showed significantly higher degradability compared to the L-Lys linker. However, the linkage via the L-Lys dipeptide showed complete cleavage in the test structure and could potentially also be integrated in lipo-oligomers as a motif for efficient enzymatic degradation. Biodegradability was tailored by placing either cleavable L-arginine or noncleavable D-arginine dipeptides or varieties of both linkers between a lipophilic dimyristic acid (MyrA) domain and a Stp-containing cationic siRNA-binding unit. The later domain contains also two tyrosine tripeptides, which flank the Stp-units at the C- and N-terminus and are incorporated to enhance polyplex stabilization.[64] The lipo-oligomers were incubated with cathepsin B to simulate endolysosomal degradation. Fragments of cathepsin B-triggered cleavage were identified by MALDI-TOF mass spectrometry. Fragments resulting from cleavage between two L-arginines both at sites X1 and X2 were found (**Fig. 31B** and **Fig. 31C**, and see the Analytical Data in section **6.4.4**, **Table 22**). When no arginines (My) or D-arginine dipeptides were incorporated instead of L-Arg-L-Arg, no cleavage was

detectable at sites X1 and X2. In all cases, cleavage of up to five of six tyrosines was detectable.

3.3.3 Lytic activity of bioresponsive lipo-oligomers

Amphiphilic lipo-oligomers containing cationizable, bioresponsive Stp units together with hydrophobic moieties usually display a pH-responsive membranolytic activity. This was confirmed in an erythrocyte leakage assay at three pH values covering the range from early to late endosomal/lysosomal conditions. The lytic activities of all lipo-oligomers were highest at the lowest pH 5.5 (**Fig. 32A**).

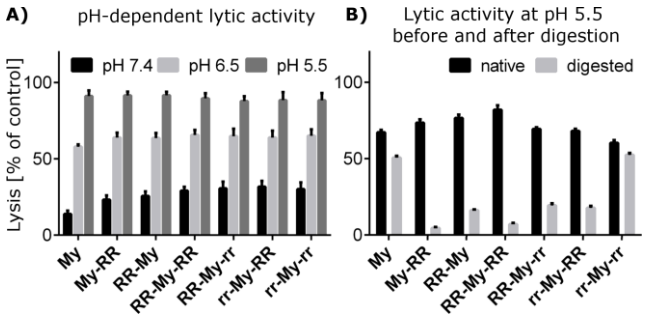

Fig. 32 Erythrocyte leakage of lipo-oligomers A) at different pH conditions at 5 mM concentration and B) at endolysosomal pH 5.5 after incubation with cathepsin B-containing buffer (digested) or buffer only (native) at 2.5 mM concentration.

Although the lytic activities at pH 7.4 were low compared to the endosomal/lysosomal conditions, an increasing erythrocyte lysis was observed for structures with more arginines (14 % for My without arginines and ~30 % for structures with six arginines). This indicates that the incorporation of arginines can potentially impact short-term toxicity resulting from plasma membrane disruption. Bioresponsive behavior with low lytic potential at neutral pH and increasing lysis at lower pH values is highly desirable and necessary for efficient endosomal escape. However, as nucleic acid carriers accumulate in lysosomes, highly lytic structures might trigger toxicity by intracellular mechanisms. The incorporation of degradable L-arginine dipeptides as linkers between the oligocationic and lipophilic moieties should result in reduced amphiphilic character of the lipo-oligomers after cleavage, thereby reducing cytotoxicity caused by lysosome and organelle damage. Reduced lytic activity of biodegraded structures was verified in an erythrocyte leakage assay at pH 5.5 before and after incubation with cathepsin B. For this assay, the concentration of the lipo-oligomers was reduced to 2.5 mM to avoid

a saturation of the assay, as the lytic activities of all lipo-oligomers at 5 mM concentration were close to 100 % at pH 5.5. All lipo-oligomers showed >50 % lysis in native form (**Fig. 32B**). Structures containing at least one L-Arg dipeptide sequence either at site X1 or X2 displayed significantly reduced lytic activity after degradation, while the nondegradable structures ***My*** and ***rr-My-rr*** largely retained their lytic potential after incubation with cathepsin B. Similar, but less pronounced, effects were found for lipo-oligomers containing only single L-arginines as cleavage sites, in agreement with a reduced degradability of such structures (**Fig. 33**, **Table 16**).

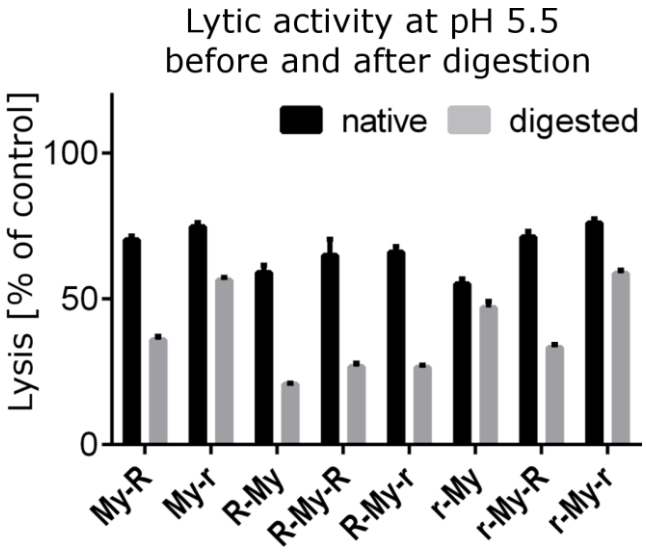

Fig. 33 Erythrocyte leakage of lipo-oligomers containing only single L- or D-arginines at endo/lysosomal pH 5.5 before and after incubation with cathepsin B.

Lipo-oligomers containing cleavable L-arginine linkers with reduced lytic activities at endolysosomal pH conditions after internalization and degradation could potentially cause less intracellular membrane damage and thereby display higher cell tolerability.

3.3.4 Improved cell tolerability without hampering gene silencing efficiency

The influence of improved endolysosomal degradability on cell tolerability and transfection efficiency was studied in human hepatoma Huh7/eGFPLuc and human prostate carcinoma DU145/eGFPLuc cells. Lipo-polyplexes were formed by mixing lipo-oligomers with siRNA at a constant N/P value, which depicts the ratio of protonatable amines (N) of the oligomers to phosphates (P) of the siRNA. The N/P value does not present charge ratios, as only a fraction of the protonatable amines of

Stp are protonated at physiological pH. Biophysical characterization showed no significant differences in size, zeta potential, or siRNA binding (**Fig. 34**, **Table 17**).

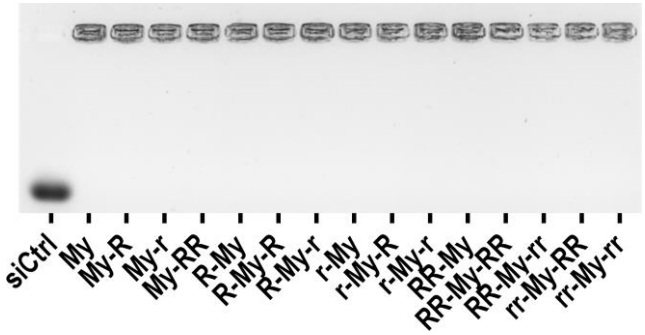

Fig. 34 Agarose gel shift siRNA binding assay with lipo-polyplexes at N/P 20. All lipo-oligomers show full siRNA binding.

Table 17 Particle size (z-average), polydispersity index (PDI) and zeta potential of siRNA lipo-polyplexes at N/P 20 determined with a DLS zetasizer.

Lipo-oligomer	z-average [nm]	Mean PDI	Mean zeta potential [mV]
My	85.3 ± 0.9	0.18 ± 0.01	26.9 ± 1.4
My-R	74.9 ± 0.9	0.18 ± 0.02	25.9 ± 0.2
My-r	70.9 ± 1.2	0.22 ± 0.01	28.2 ± 2.3
My-RR	68.0 ± 0.8	0.17 ± 0.01	26.7 ± 0.7
R-My	69.5 ± 0.9	0,19 ± 0.00	25.8 ± 3.5
R-My-R	67.7 ± 0.9	0.17 ± 0.02	27.7 ± 1.3
R-My-r	67.8 ± 0.7	0.19 ± 0.01	26.5 ± 1.6
r-My	70.1 ± 0.7	0.15 ± 0.01	29.3 ± 1.0
r-My-R	71.7 ± 0.1	0.16 ± 0.01	27.3 ± 0.7
r-My-r	61.9 ± 0.7	0.19 ± 0.01	26.8 ± 1.5
RR-My	63.4 ± 0.6	0.20 ± 0.01	27.1 ± 1.0
RR-My-RR	61.1 ± 0.8	0.23 ± 0.01	27.4 ± 1.0
RR-My-rr	71.8 ± 1.3	0.26 ± 0.04	25.0 ± 1.1
rr-My-RR	63.7 ± 0.2	0.22 ± 0.01	28.0 ± 0.3
rr-My-rr	64.9 ± 0.3	0.18 ± 0.00	26.3 ± 2.9

In previous work, lipo-oligomers containing the saturated C14 short chain myristic acid were found to display not only efficient gene silencing but also high lytic activity and cytotoxicity.[43, 44, 174] This renders MyrA-containing oligomers as good model structures to study the effect of lysosomal detoxification. However, phase 1 short-term toxicity resulting from plasma membrane damage might still occur and veil any effects of improved intracellular degradability on phase 2 long-term toxicity. For this reason, incubation times on cells were kept short (4 h), and the read-out of cytotoxicity and

gene silencing assays were measured after further 44 h long-term incubation in fresh media. Metabolic cell activities compared to buffer-treated cells, as an indicator for cell viability, were measured via MTT assays. Buffer-treated cells were set to 100 %. For MTT assays, only lipo-oligomers without siRNA were added to the cells. Biodegradable structures containing L-arginine dipeptides either at site X1 or X2 showed excellent cell tolerability on Huh7 cells compared to the highly toxic nondegradable ***My*** and ***rr-My-rr*** oligomers (**Fig. 35A**).

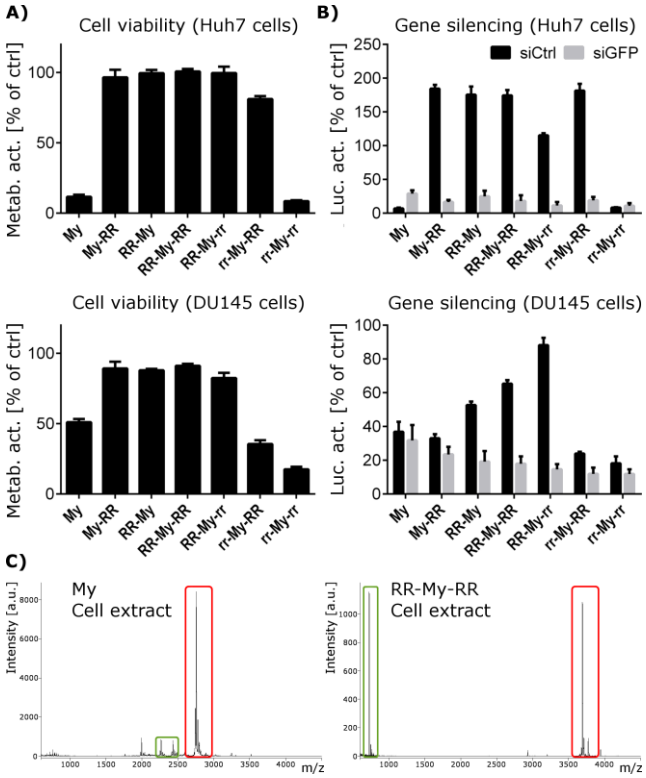

Fig. 35 A) Metabolic activity indicating cell viability of human hepatoma Huh7-eGFPLuc (top) and human prostate carcinoma DU145-eGFPLuc cells (bottom) compared to buffer-treated cells determined by MTT assay after incubation with lipo-oligomers with tailored biodegradability. Lipo-oligomer solutions were used in the same concentrations as in gene silencing experiments but without the addition of siRNA. B) Gene silencing of lipo-polyplexes (N/P 20) formed by mixing of lipo-oligomers and eGFP-targeted siRNA (siGFP) or control siRNA (siCtrl) compared to buffer-treated cells. C) MALDI mass spectra of cell extracts after transfection with My (left) or highly degradable RR-My-RR (right) after transfection showing both undigested lipo-oligomers (red) and fragments of endolysosomal degradation (green). Transfections and cell viability assays were performed by Dr. Yanfang Wang (Pharmaceutical Biotechnology, LMU).

Improved cell tolerability of degradable structures was also found in DU145 cells; the nondegradable oligomers did not display as strong toxicity as in HUH7 cells. These

results are in good agreement with the reduced lytic potential of enzyme-degraded carriers (**Fig. 32B**), indicating that lysosomal cleavage enhanced cell tolerability. Gene silencing experiments were performed in cells stably expressing an eGFP-Luciferase fusion protein. Gene silencing by siGFP (light bars), resulting in decreased luciferase activity, is quantified by a standard luciferase assay. In the absence of unspecific effects, cells treated with analogous control siCtrl lipo-polyplexes (black bars) should maintain luciferase activity close to 100 % (buffer-treated cells); reduced levels of luciferase activity in siCtrl treated cells are an indicator of cytotoxicity. Cells were transfected at N/P 20, as this ratio was found to enable efficient gene silencing. Improved knockdown of the eGFP-Luciferase gene in siGFP-treated cells would not be expected for biodegradable oligomers, as reduced lytic activity after enzymatic cleavage might even hamper the escape of the nucleic acid cargo into the cytosol. Notably, all siGFP lipo-polyplexes show similar levels of eGFP-Luciferase expression in both Huh7- and DU145 cells, indicating that transfection efficiency is not reduced by the introduction of enzymatic cleavage sites (**Fig. 35B**). Luciferase activities in Huh7 cells treated with ***My*** and ***rr-My-rr*** siCtrl-polyplexes are significantly reduced compared to buffer-treated cells. The unspecific reduction of gene expression for nondegradable structures is in agreement with the reduced cell viability detected in the MTT assay. Interestingly, siCtrl-polyplexes formed with structures containing at least one L-arginine dipeptide linker showed luciferase activities well above 100 %, which has previously been observed for nontoxic transfections of Huh7/eGFPLuc transgenic cells (unpublished data). In this cell line, the eGFP-luciferase fusion gene is stably expressed under control of a CMV promoter. The transcription of transgenes from the CMV promoter can be up-regulated by a variety of mild stresses by activation of MAP protein kinases.[224] The transfection of siRNA with cationic lipo-oligomers could potentially result in stress-activation of transgene expression. However, the improved biocompatibility of degradable lipo-oligomers is supported by the results from the MTT assay, which showed metabolic cell activities similar to buffer-treated cells. The positioning of the cleavable linker did not significantly influence MTT and gene silencing assays in Huh7 cells. For DU145 cells, only lipo-oligomers containing cleavable L-arginines at site X1 (***RR-My***, ***RR-My-RR***, and ***RR-My-rr***) showed significantly reduced toxicity and higher luciferase expression of siCtrl treated compared to siGFP treated cells. This indicates that not only the introduction of cleavage sites but also their precise positioning might affect cell tolerability. Lipo-

oligomers with only single L-arginines as cleavage sites at position X1 also showed improved cell viabilities in MTT and gene silencing assays in both cell lines compared to nondegradable structures or structures with degradable linkers only at site X2 (**Fig. 36**).

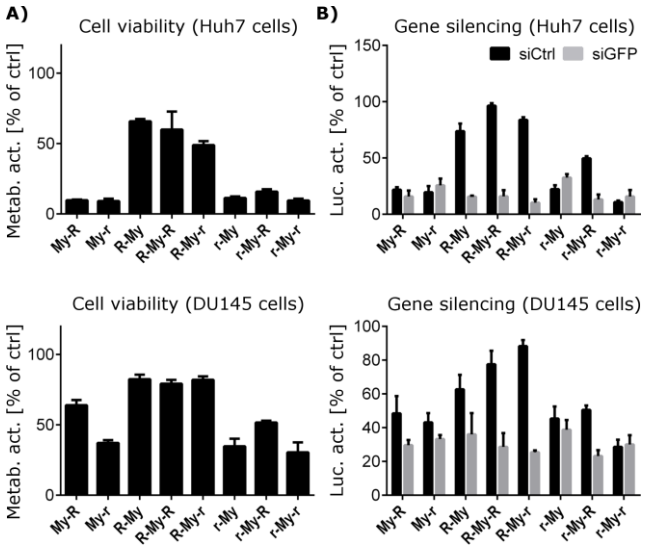

Fig. 36 A) Metabolic activity indicating cell viability of human hepatoma Huh7- (top) and human prostate carcinoma DU145-eGFPLuc cells (bottom) determined by MTT assay after incubation with lipo-oligomers containing only single L- or D-arginines. B) Gene silencing of lipo-polyplexes at N/P 20 formed by mixing of lipo-oligomers and eGFP-targeted siRNA (siGFP) or control siRNA (siCtrl). Transfections and cell viability assays were performed by Dr. Yanfang Wang (Pharmaceutical Biotechnology, LMU).

Integration of cleavage sites at position X1 within the more hydrophilic part of the lipo-oligomers seems preferable for these structures, possibly due to better accessibility for endolysosomal proteases and therefore more efficient degradation; cleavage site X2 is positioned at the side chain of a branching central lysine followed by a hydrophobic diacyl domain. In Huh7 cells, dipeptide linkers showed a superior effect on cell tolerability compared to single L-arginine linkers. Incorporation of cleavage sites at position X2 was only beneficial for dipeptides. At site X1, metabolic activities were ranging from 49−66 % for single L-Arg linkers, while structures with dipeptide motifs showed similar cell viability as buffer-treated control cells. This is in accordance with a more efficient cathepsin-triggered degradation of test oligomers with dipeptide linkers. Cell viability assays in Huh7 cells were also performed with lipo-polyplexes formed by mixing of lipo-oligomers with siGFP and siCtrl, as polyplexes could potentially be less toxic than carriers in isolation. In this cell line, siRNA lipo-polyplexes showed similar results compared to MTT assays with only lipo-oligomers (**Fig. 37**).

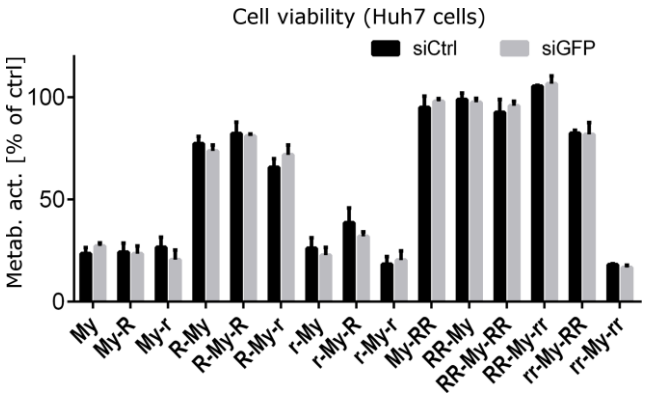

Fig. 37 Metabolic activity indicating cell viability of human hepatoma Huh7/eGFPLuc cells determined by MTT assay after incubation with polyplexes at N/P 20 formed by mixing of lipo-oligomers and eGFP-targeted siRNA (siGFP) or control siRNA (siCtrl). Cell viability assays were performed by Dr. Yanfang Wang (Pharmaceutical Biotechnology, LMU).

3.3.5 Oligomer cleavage detected in cell transfections

Fragments of degradation were identified from lysates of cells transfected with lipo-polyplexes in agreement with cathepsin B incubation assays, indicating that endolysosomal degradation takes place after cellular internalization (**Fig. 35C**, and see the Analytical Data in section 6.4.4, **Table 22**). In contrast to degradation assays with cathepsin B, significant amounts of nondegraded material were found in cell lysates, which can be attributed to noninternalized material at the cell surface, intact lipo-oligomers that were released into the cytosol or nondegraded structures in the lysosomes. Cathepsin B-triggered degradation of lipo-oligomers was studied after addition of siRNA to examine the influence of electrostatic interaction with nucleic acids on the degradability of the carrier. At N/P 1, no degradation of lipo-oligomers was detectable, indicating that the binding of nucleic acid phosphates to L-arginine side chains prevents enzymatic cleavage. When lipo-oligomers were added in excess (N/P 20), efficient cleavage similar to the degradation of lipo-oligomers without siRNA was found (see the Analytical Data in section **6.4.4**, **Table 22**).

3.4 Delivery of siRNA and Proteins into Glioma and Brain

The increasing prevalence of diseases affecting the central nervous system (CNS) urgently demands the development of biologic drugs like proteins, antibodies, peptides or nucleic acids capable of crossing the blood-brain barrier (BBB).[225, 226] Efficient delivery of therapeutics into the brain is restricted by the BBB, which is formed by endothelial cells together with astrocytes, pericytes, and the basal lamina at the plasma membrane of the capillary of brain parenchyma.[227] Microvessels in the brain are only 40 µm apart, which allows for complete and almost instantaneous distribution throughout the entire CNS once a therapeutic substance or formulation is able to cross the BBB.[228] As large molecule drugs or nanoparticles lack the requirements for free diffusion into the brain (molecular weight < 400 Da, < 8 hydrogen bonds), such therapeutics need to be designed to exploit carrier-mediated transport (CMT) or receptor-mediated transport (RMT) systems or need to undergo adsorptive-mediated transcytosis (AMT).[229, 230] Sequence-defined oligoaminoamides have been used for receptor-targeted delivery of siRNA[146] and pDNA[231] to glioma *in vivo*. For siRNA delivery, a non-targeted lipo-oligomer was mixed with a PEGylated oligomer containing an Angiopep-2 ligand targeting the LRP-1 receptor, which is overexpressed both on the surface of the brain capillary endothelial cells (BCECs) and glioma cells.[146] A similar cascade-targeting strategy was used for the delivery of therapeutic pDNA. Here, a non-targeted three-arm histidine oligomer was mixed with a PEGylated oligomer containing the IL-6 receptor targeting heptapeptide I_6P_7. IL-6 receptor expression was detected on the BBB and in various brain tumors such as glioblastoma. Targeted delivery of pDNA encoding inhibitor of growth 4 (pING4) significantly prolonged the survival time of orthotopic U87 glioma-bearing mice.[231] The proangiogenic receptor APLNR and its cognate ligand apelin play a central role in controlling glioblastoma vascularization.[232] Therefore, peptide sequences derived from the endogenous apelin ligand such as apelin-13 or the mutant APLNR ligand apelin-F13A could not only be used to inhibit glioblastoma angiogenesis but also for glioma-targeted delivery of nucleic acids and proteins.

Notably, in late stages of glioma development, the BBB is impaired by formation of fenestrations, altered thickness of the basal lamina and tight junction disruption.[233] Delivery into the brain with an unimpaired BBB however is a major obstacle in the treatment of neural diseases. RMT using endogenous BBB receptor transporters such

as the transferrin receptor (TfR) was described to enable the re-engineering of biologic drugs that cross the BBB.[228] However, modification of siRNA lipo-ploxyplexes with transferrin or an anti-murine TfR antibody failed to show enhanced uptake into the brain *in vivo*, probably due to insufficient stability and disassembly of the polyplexes.[113] Several studies show BBB crossing and brain delivery of drug- or protein-loaded poly-lactide-co-glycolide (PLGA) nanoparticles after conjugation with the glycosylated heptapeptide g7, which is derived from the opioid peptide MMP-2200.[234-237] These nanoparticles are hypothesized to use membrane-membrane interactions triggering endocytosis and macropinocytosis-like processes due to the helical conformation of the g7 peptide.[238] Click-chemistry is an elegant approach to functionalize polyplexes formed with azide-bearing oligoaminoamides and nucleic acids by post-modification with DBCO-containing shielding and targeting agents. Bivalent bis-DBCO agents potentially allow for crosslinking of two lipo-oligomers and thereby can increase polyplex stability *in vivo*.[239] In this chapter, we evaluate cellular uptake in brain endothelial and neuroblastoma cells and gene silencing efficiency of siRNA lipo-polyplexes after post-modification with a g7-containing bis-DBCO-PEG_{24} agent or non-targeted control structures.

3.4.1 Apelin receptor targeted delivery of GFP into glioma cells

The ability of apelin-derived peptide ligands to improve the uptake of proteins in glioma cells via APLNR targeting was studied *in vitro*. Four equivalents of apelin-13, the mutant APLNR ligand apelin-F13A and a scrambled apelin-13scr, all containing a PEG_{24} spacer and a cysteine at the N-terminus, were linked to eGFP (enhanced green fluorescent protein) via SPDP (succinimidyl 3-(2-pyridyldithio)propionate) linkers. Apelin-modified eGFP variants were administered to GBM14 cells. Both apelin-13 and apelin-F13A linked eGFP were internalised by the cells, while eGFP modified with the negative control apelin-13scr was not (**Fig. 38A**). The specificity of APLNR-mediated protein uptake was confirmed by performing a dose escalation competition assay with unlabelled peptide, showing that uptake of both peptide-modified eGFP variants was blocked by its unmodified peptide counterparts (**Fig. 38B**).

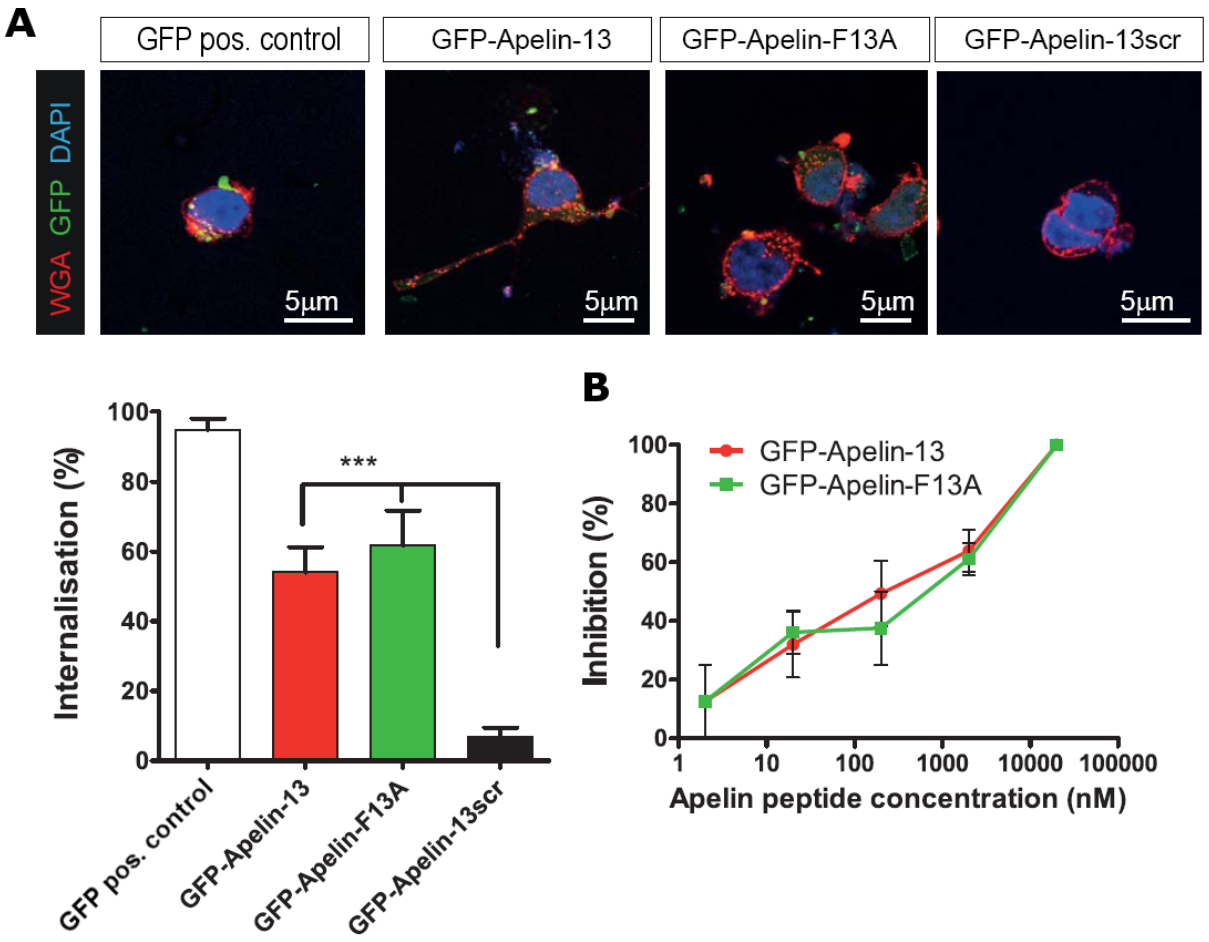

Fig. 38 Specific internalization of apelin-modified eGFP by GBM14 cells. A) The eGFP signal in confocal images of cells treated with 1 µM eGFP-peptide was compared to nuclear (DAPI) and membrane staining (wheath germ agglutinin; WGA). Internalization of eGFP-peptide conjugates was assessed by counting the percentage of cells with GFP-positive vesicles in four independent experiments. GFP-apelin-13 and GFP-apelin-F13A were taken up specifically by more than 50 % of the cells while scrambled apelin-13scr was not. GFP pos. control (GFP-linked cationic lipo-oligomer ***728*** as unspecific positive control) was taken up by all cells. B) Dose-response curve of the inhibition of eGFP internalization. GBM14 cells were pre-treated with escalating amounts of unlabeled apelin-13 or apelin-F13A peptide for 30 min before GFP-linked apelin-13 or apelin-F13A (200 nM) were applied, respectively. Inhibition of internalization by increasing concentrations (2, 20, 200, 2000 and 20000 nM) demonstrates the specificity of GFP-Apelin peptide internalization. GFP-Scale bar, 15 mm; Student's t-test, *** $p \leq 0.005$. The uptake assays were performed by Giorgia Mastrella in the group of Prof. Rainer Glaß and Dr. Roland Kälin (Department of Neurosurgery, University Hospital of Munich (LMU).

Similar studies were performed with apelin-modified siRNA polyplexes. The azide-containing biodegradable t-shape oligomer ***1073*** (N→C: K(N_3)-Y_3-Stp_2-K-ε[G-ssbb-K-α,ε(CholA)$_2$]Stp_2-Y_3)^{240} was modified with each 1 eq DBCO-PEG_{24}-apelin-13, -apelin-F13A or –apelin-13scr. The uptake in GBM14 cells was not increased by APLNR ligand

modification (data not shown). This finding could be explained by high unspecific uptake of polyplexes compared to the low uptake of unmodified eGFP.

3.4.2 Design of lipo-oligomers and targeting and shielding agents for click chemistry

Azide-bearing T-shaped lipo-oligomers with two (***1198***) or four (***1215***) Stp units at each side of the cationic backbone were synthesized to enable post-modification of siRNA lipo-polyplexes with DBCO-containing shielding and targeting structures by click chemistry (**Fig. 39**).

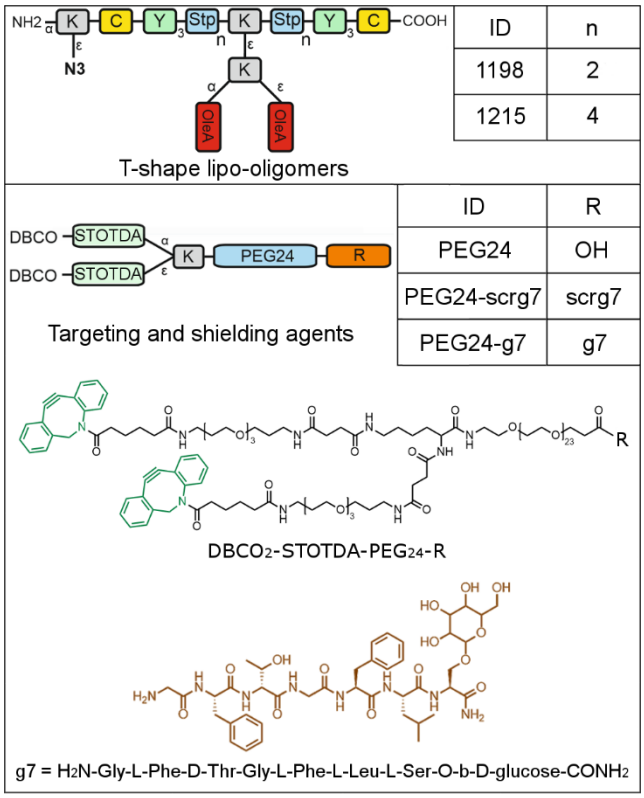

Fig. 39 Brain-targeted sequence-defined oligomers with T-shape topology. Top: schematic overview of the structures with different modifications (Y: tyrosine, K: lysine, C: cystein, Stp: succinoyl-tetraethylene-pentamine, OleA: oleic acid). The structures contain an azide function for modification with DBCO-bearing shielding and targeting agents and two (***1198***) or four (***1215***) Stp units at each side of the cationic backbone. Oligomer ***1215*** was synthesized by Jie Lou (Pharmaceutical Biotechnology, LMU). IDs are unique database identification numbers. Bottom: Targeting and shielding agents with bis-DBCO moieties for click chemistry, a PEG_{24} unit for polyplex shielding and g7 (H_2N-Gly-L-Phe-D-Thr-Gly-L-Phe-L-Leu-L-Ser(O-β-D-Glucose)-$CONH_2$) as ligand or scrg7 (H_2N-Gly-Leu-Phe-Phe-Gly-Ser(O-β-D-Glucose)-D-Thr-$CONH_2$) as scrambled control sequence.

Both lipo-oligomers contain cysteines and tyrosine trimers for enhanced polyplex stabilization and a dioleic acid domain for enhanced lipid membrane interaction.[43, 64] The shielding agents contain two DBCO moieties (bis-DBCO) which potentially enables crosslinking of two lipo-oligomers on the surface of polyplexes. Two succinylated PEG_3-spacer (STOTDA) were placed before a PEG_{24} shielding domain. The glycosylated heptapeptide g7 was introduced as ligand to improve the uptake in brain endothelial cells. Non-targeted control structures contain either no ligand (PEG_{24}) or a scrambled sequence of g7 (PEG_{24}-scrg7).

3.4.3 Biophysical characterization of lipo-polyplexes with and without post-modification

Particle sizes, polydispersity indices and zeta potentials of siRNA lipo-polyplexes with or without post-modification were measured by dynamic light scattering (DLS). All polyplexes showed uniform sizes between 139 - 159 nm z-average (**Table 18**).

Table 18 Particle size (z-average), polydispersity index (PDI) and zeta potential of siRNA lipo-polyplexes at N/P 20 determined with a DLS zetasizer.

Formulation	z-average [nm]	Mean PDI	Mean zeta potential [mV]
1198	146.0 ± 1.5	0.19 ± 0.01	34.0 ± 1.2
1198 + PEG_{24}	159.0 ± 3.7	0.20 ± 0.02	8.6 ± 0.6
1198 + PEG_{24}-scrg7	150.4 ± 4.5	0.18 ± 0.03	9.1 ± 0.2
1198 + PEG_{24}-g7	156.2 ± 2.3	0.19 ± 0.02	5.2 ± 1.0
1215	138.8 ± 1.9	0.14 ± 0.01	40.2 ± 2.5
1215 + PEG_{24}	138.0 ± 2.5	0.18 ± 0.01	18.2 ± 2.2
1215 + PEG_{24}-scrg7	142.6 ± 1.4	0.19 ± 0.01	19.7 ± 1.0
1215 + PEG_{24}-g7	147.6 ± 3.1	0.21 ± 0.02	13.0 ± 2.1

The zeta potentials of ***1198*** formulations (34 mV unshielded, 5.2 – 8.6 mV after post-modification) are significantly lower compared to ***1215*** polyplexes (40 mV unshielded, 13 – 20 mV after post-modification), probably due the higher charge density of ***1215*** with 8 Stp units per oligomer compared to only 4 Stps of ***1198***. Shielding of polyplexes was more efficient for ***1198*** formulations, as PEGylation reduced the zeta potential of the unshielded polyplexes to 15 - 27 % compared to 32 – 49 % for ***1215***. The binding ability of the lipo-oligomers to siRNA was determined by measuring the electrophoretic mobility of siRNA in a 2.5 % agarose gel. All formulations showed full siRNA binding in HBG buffer at N/P 12 (**Fig. 40** top).

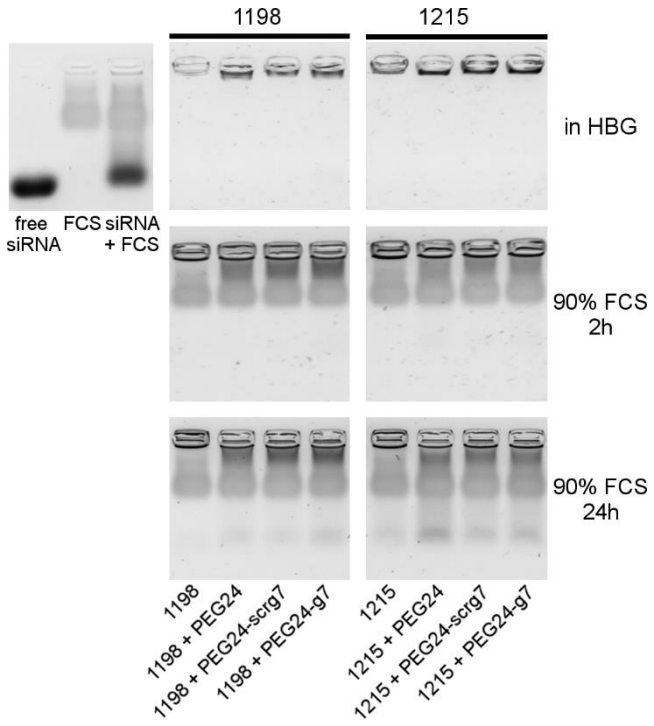

Fig. 40 Agarose gel shift assays of lipo-polyplexes before and after modification with targeting and shielding agents. Lipo-polyplexes were formed at N/P 12 and subsequently modified with bis-DBCO agents for 4h. Polyplexes were analysed either in HBG or after treatment at 37 °C with 90 % serum (FCS).

Polyplexes were exposed to 90 % full serum at 37 °C for two and 24 hours (**Fig. 40** bottom). Incubation with serum at body temperature can be indicative for polyplex stability in the blood stream. All formulations fully retained the siRNA after two hours of incubation. After 24 hours, small amounts of siRNA were released from polyplexes with ***1198*** after post-modification, but not from the unmodified polyplexes. For ***1215*** formulations, the post-modified polyplexes released slightly more siRNA than the ***1198*** formulations and also the unmodified ***1215*** polyplexes released small amounts of siRNA after 24 h. This indicates a minor benefit in stability of ***1198*** probably due to a more favorable ratio of positively charged Stp units to stabilizing motifs compared to ***1215***.

3.4.4 Cellular uptake in brain endothelial and neuroblastoma cells and gene silencing efficiency

All formulations were tested for cellular internalization in bEnd.3 mouse brain endothelial cells and Neuro2A mouse neuroblastoma cells (**Fig. 41A**).

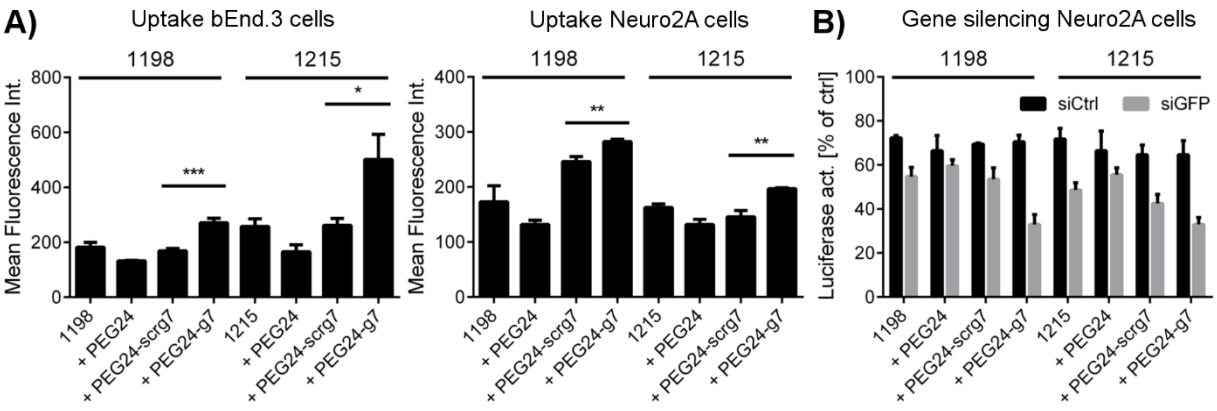

Fig. 41 A) Mean fluorescence intensity (MFI) data for cellular internalization of Cy5-labeled siRNA formulations (left: bEnd.3 cells; right: Neuro2A cells) with or without modification with targeting and shielding agents determined by flow cytometry. B) Gene silencing of formulations with eGFP-targeted siRNA (siGFP) or control siRNA (siCtrl) in Neuro2A/eGFPLuc cells. Uptake assays and transfections were performed by Jasmin Kuhn (Pharmaceutical Biotechnology, LMU).

The uptake in brain endothelial cells, which form the inner layer of the brain capillary wall, is a crucial first hurdle for efficient delivery into the brain. Polyplexes formed with Cy5-labeled siRNA with or without post-modification with targeting and shielding agents were incubated for 45 min on cells. After washing with heparin to remove non-internalized polyplexes, the mean fluorescence intensity (MFI) was determined by flow cytometry. As expected, polyplexes shielded with PEG_{24} showed reduced cellular uptake compared to unshielded polyplexes. The uptake of g7-targeted lipo-polyplexes in bEnd.3 was increased by 60 % for ***1198*** polyplexes and 90 % for ***1215*** polyplexes compared to PEG_{24}-scrg7 modified control formulations and was also higher than for unshielded polyplexes. A similar, but less pronounced effect was found in Neuro2A cells with an increase in MFI of 15 % for ***1198*** and 35 % for ***1215*** formulations with PEG_{24}-g7 compared to PEG_{24}-scrg7. Gene silencing experiments were performed in Neuro2A/eGFPLuc reporter cells. All formulations showed low gene silencing efficiency with a slight reduction in gene expression for formulations with the g7 ligand compared to non-targeted controls. Altogether, the g7 ligand showed a positive but moderate effect on cellular uptake in both bEnd.3 and Neuro2A cells and transfection efficiency in Neuro2A cells. Cellular uptake and gene silencing efficiency were similar for ***1198*** and ***1215***, indicating no clear benefit for any of the two lipo-oligomers.

4 Discussion

4.1 Optimized Solid-Phase-Assisted Synthesis of Oleic Acid Containing siRNA Nanocarriers

Incorporation of fatty acids in cationic nucleic acid carriers provides both polyplex stabilization by hydrophobic interactions and enhanced membrane interactions for efficient cellular uptake and endosomal release.[37, 43] The *cis*-unsaturated fatty acid oleic acid (C18:1 *cis*) has been incorporated in well-known cationic lipids[162] and sequence-defined lipo-oligomers[43, 44] and promotes membrane lipid disorders by interacting with anionic phospholipids.[164] The incorporation of unsaturated fatty acids in sequence-defined oligomers via solid-phase assisted synthesis however bears the risk of producing side products caused by addition of TFA to the double bonds during cleavage. Standard peptide synthesis protocols recommend high amounts of TFA (50 – 95 %) and incubation times of 30 – 60 min at room temperature for complete cleavage of acid-labile protecting groups like O*t*Bu, *t*Bu, Trt and Boc.[185] For the synthesis of lipo-oligomers containing both unsaturated fatty acids and amino acids with protected side chains, the cleavage protocol has to be as mild as possible to minimize side products by TFA-addition while ensuring complete cleavage of protecting groups. Test peptides with oleic acid and natural and artificial amino acids, which have been used in our published nucleic acid carriers, were synthesized. Cleavage assays were performed at various temperatures and incubation times, and the influence of alkene scavangers and precooling of the resin and cleavage cocktails was studied. The reaction kinetics of the addition of TFA to OleA at 4 °C and 22 °C were determined. Although TFA adds at a higher rate to alkenes at 22 °C, the amount of side products was lower after the cleavage time which was sufficient to deprotect all amino acid side chains. Precooling of resin and cleavage cocktail siginificantly reduced the formation of TFA adducts, as exothermic cleavage of protecting groups and the product from the resin increases the temperature of the cleavage solution after addition. The addition of 4 % alkene scavengers had no influence on the formation of side products, presumably because of the huge excess of 90 % TFA. An optimized cleavage protocol, comprising precooling of the cleavage cocktail and the resin and 20 min incubation time at 22 °C, was used to synthesize a library of lipo-oligomers containing cysteines, tyrosines, lysines and the synthetic building block Stp together

with either oleic acid (***OleA-t***) or chemically stable stearic acid (***SteA-t***) and 8-nonanamidooctanoic acid (***NonOcA-t***) moieties. Low amounts of side products were removed by HPLC purification of the crude product and high yields of the purified products were achieved. TFA esters resulting from addition of TFA to alkenes are hydrolyzed under neutral or basic aqueous conditions and form hydroxylated hydrocarbons. This side reaction was forced by long-time treatment with TFA followed by TFA-ester hydrolysis, generating a mono-hydroxylated hydrocarbon chain (***OH-SteA-t***). Comparing the siRNA delivery characteristics of the oleic acid containing lipo-oligomer ***OleA-t*** to structures with modified hydrophobic moieties (***OH-SteA-t*** and ***NonOcA-t***) revealed differences in membrane-lytic potentials. A shift toward enhanced lytic activity at pH 7.4 was observed for ***OH-SteA-t*** and ***NonOcA-t***, while ***OleA-t*** displayed a highly desirable pH-dependency of membrane lysis toward endosomal acidic pH. These findings can explain the significant cytotoxicity of ***OH-SteA-t*** and ***NonOcA-t*** as compared with nontoxic ***OleA-t***. The choice of the cell line influences the finding, as DU145 cells seemed to be more sensitive to changes in lytic potential than Neuro2A cells. Thus, ***OH-SteA-t*** as side product of ***OleA-t*** synthesis might negatively affect the properties of the resulting lipo-polyplexes. In conclusion, ***OleA-t*** showed particularly favorable pH dependency of endosomolytic activity, efficient gene silencing and excellent cell tolerability compared to its counterparts. TFA-mediated cleavage of the oligomer and subsequent purification has to be critically controlled in order to retain the unsaturated hydrocarbon chain character and ensure high yields of the synthesis. Notably, the cleavage protocol was optimized for the synthesis of structures containic both oleic acid and amino acids with Trt (Cys, His), Boc (Trp, Lys, Stp), O*t*Bu (Glu) and *t*Bu (Tyr) protecting groups. TFA concentrations in the cleavage cocktails might be lowered and thus result in even less side products if unsaturated fatty acids are incorporated in structures with amino acids containing protecting groups which are cleavable under mild conditions (such as Fmoc-Lys(Mtt)-OH instead of Fmoc-Lys(Boc)-OH[185]). Some protecting groups of amino acid side chains, such as Mtr, Pmc or Pbf of the arginine guanidino group, might however require harsher conditions[185] compared to the optimized cleavage protocol in this chapter, resulting in more side products.

4.2 Precise Redox-Sensitive Cleavage Sites for Improved Bioactivity of siRNA Lipopolyplexes

In the first chapter, lipo-oligomers were found to display slight variations in pH-specific lytic profiles dependant on the incorporated hydrophobic moieties in agreement with previous work.[43, 44] Besides membrane destabilization mediated by membrane interactions at low endolysosomal pH, the hydrophobic domains in cationic lipo-oligomers offer polyplex stabilization in the extracellular space. Although high stability of siRNA polyplexes is desirable for *in vivo* circulation and cellular uptake, intracellular disassembly promotes cytosolic release and subsequent incorporation of siRNA in the RNA-induced silencing complex. To improve cytosolic disassembly of lipo-polyplexes, bioreducible sequence-defined lipo-oligomers were synthesized by solid-phase assisted synthesis by incorporating the disulfide building block Fmoc-succinoyl-cystamine between a lipophilic diacyl (bis-myristyl, bis-stearyl or bis-cholestanyl) domain and an ionizable oligocationic siRNA binding unit.

The applicability of the disulfide building block for solid-phase assisted synthesis and cleavability under physiologic conditions was evaluated for test structure ***740***. As disulfides are degradable in presence of hydroxyl anions[241], 1-Hydroxybenzotriazole hydrate was not used for coupling reactions of the ssbb and all subsequent reactions. The ssbb was shown to be stable during standard Fmoc-based solid-phase assisted synthesis and could be disassembled in presence of cytosolic gluathione concentrations.

The redox-triggered disassembly of lipo-polyplexes could also be demonstrated for lipo-oligomers containing the ssbb by performing agarose gel shifts assays under reducing conditions. While bioreducible structures showed a release of siRNA at intracellular concentrations of 1 – 10 mM glutathione, the stable analogs did not show any siRNA release in presence of increasing amounts of GSH. Major differences in membrane lytic activity could be observed for the different hydrophobic diacyl moieties. While myristic acid, in accordance with literature[168], showed high lytic activity especially at late endosomal pH, cholanic acid and stearic acid showed only moderate lytic activity. The pH sensitivity of the cationic lipo-oligomers can be explained by increasing protonation of the ionizable cationic backbone that is used for nucleic acid binding.

The lytic activity of biodegradable oligomers could be abolished after incubation with glutathione at intracellular concentrations (10 mM). Glutathione-triggered degradation of the lipo-oligomers should on the one hand reduce lytic activity of the lipo-oligomers in the cytosol after endosomal release and on the other hand improve the accessibility of siRNA for facilitated incorporation into the RISC. Consistent with both hypotheses, the reducible siRNA polyplexes show lower cytotoxicity and higher gene silencing efficacy in Neuro2A and DU145 cells compared to their stable analogs.

Suprisingly, a negative influence of the bioreducible building block on gene silencing activity was found for HeLa-derived KB cells. As high extracellular disulfide cleavage was previously reported for HeLa cells[191], disulfide cleavage occurring at the extracellular cell surface might be an explanation for this finding.

In sum, bioreducible siRNA carriers offer increased gene silencing efficiency in certain cell lines by combining extracellular polyplex stability, high lytic activity under endosomal conditions and cytosolic degradability leading to cleavage products with low cytotoxicity and improved siRNA release from the disassembled polyplexes. Nevertheless, for cell lines with exceptional extracellular redox environments, the redox-sensitivity of carriers can also be a disadvantage.

4.3 Precise Enzymatic Cleavage Sites for Improved Bioactivity of siRNA Lipo-Polyplexes

In the previous chapter, a new class of redox-sensitive lipo-oligomers was successfully established for siRNA delivery. Biodegradable sequence-defined oligomers were generated by introducing a disulfide-containing building block between a lipophilic diacyl domain and an ionizable oligocationic siRNA-binding unit. Degradable siRNA polyplexes showed higher gene silencing efficiency and lower cytotoxicity than their stable analogs. Premature disulfide cleavage of carriers by cell surface oxidoreductases may however present a significant obstacle depending on tissue and cell types.[71] Moreover, glutathione-triggered cleavage is initiated after cytosolic release and therefore effects only a small fraction of cytosolic carriers, as endosomal escape is a major bottleneck for delivery. Degradation of lipo-oligomers by endolysosomal enzymes therefore appears as an attractive strategy to destroy abundant potentially toxic carrier molecules while ensuring high extracellular stability. The resistance to

degradation by the lysosomal protease cathepsin B of a test structure containing two amide-bound Stp units without any natural L-amino acid linkers is consistent with findings that length of Stp oligomers correlates with cytotoxicity.[40] This may present a problem for the cell metabolism, as the majority of transfection material is known to initially accumulate in the lysosomal compartment and needs to be dumped from cells[215] before serious organelle damage. Therefore, one or two of the natural L-amino acids lysine, arginine, histidine, or tyrosine, which have been used in our published nucleic acid carriers[223], were incorporated in a library of test structures between two Stp units to identify sequences which are readily cleavable. Arginine showed the highest enzymatic degradabiliy of all tested amino acids and test structures containing dipeptides were cleaved faster compared to single L-amino acid linkers. Biodegradability of lipo-oligomeric nucleic acid carriers was tailored by precise integration of L-Arg dipeptides or single L-arginines as enzymatic cleavage sites. Similar degradation fragments were found after incubation of lipo-oligomers with the endolysosomal protease cathepsin B as in cell lysates after transfection. Introducing short cleavable L-Arg dipeptide linkers significantly improved cell tolerability after transfection without hampering gene silencing efficiency. Reduced lytic activities of degraded lipo-oligomers at endolysosomal pH conditions after internalization can be hypothesized as an underlying mechanism for the decreased toxicity. Our data indicate that the cleavage sites should preferably be integrated in the hydrophilic parts of carriers.

Introducing enzymatically cleavable amino acid linkers however could lead to rapid degradation of the carrier by blood proteases and thus may limit the *in vivo* stability of polyplexes or the excess of free lipo-oligomers. Further optimization could target the development and integration of more cathepsin-specific cleavage sites, such as the Phe-Lys-Phe-Leu (FKFL) motif, which was integrated in cathepsin-degradable peptide-HPMA copolymers and showed intact polymers even after serum incubation for 4 hours.[89, 222] The choice of the amino acid linkers may also alter the properties of the nucleic acid carrier. Linkers containing several arginines or lysines will participate in nucleic acid binding and could potentially promote lytic acitivities and short term toxicity resulting from compromised plasma membrane integrity at neutral pH.

4.4 Delivery of siRNA and Proteins into Glioma and the Brain

Modification of eGFP with the apelin-derived peptide ligands apelin-13 and apelin-F13A was shown to improve the uptake in glioma cells via specific APLNR targeting. Although apelin-modification of proteins could be a promising strategy to trigger uptake into glioma via APLNR interaction, an additional endosomal escape mechanism might be needed for efficient cytosolic or nuclear delivery. Endosomal escape of proteins could potentially be improved by dual modification with both apelin peptides and endosomolytic peptides. Although apelin and APLNR were found to be dramatically upregulated in in glioblastoma-associated microvascular proliferations, apelin was undetectable in the healthy brain and APLNR mRNA expression was very low in normal brain vessels.[242] This renders APLNR targeting as promising strategy for glioma models, but not for enhanced delivery of therapeutics into the brain through a healthy BBB. Apelin-modification of polyplexes could facilitate nucleic acid delivery into glioma, but failed to show an effect in preliminary studies, probably due to high unspecific uptake of unmodified polyplexes.

Formulation of nucleic acids with cationic lipo-oligomers provides both polyplex stability and pH-specific lytic activity for endosomal escape. Unshielded cationic lipo-polyplexes however can interact unspecifically with serum proteins or off-target tissues *in vivo*.[113, 243] Shielding agents can be equipped with ligands to improve tissue specificity. Transferrin and an anti-TfR antibody were used for transferrin receptor targeting, but did not show enhanced uptake into the brain, possibly due to a destabilizing effect of such large protein ligands.[113] Small peptide ligands such as I_6P_7 and angiopep-2 present an alternative to larger protein ligands and were used for successful delivery of nucleic acids into glioma *in vivo*.[146, 231] The work in this chapter was carried out within the COMPACT (Collaboration on the Optimization of Macromolecular Pharmaceutical Access to Cellular Targets) consortium where several preselected peptide ligands were screened at LMU Munich and collaborating institutions for uptake and transcytosis in brain endothelial cells and BBB models. Screening of the peptide ligands RVG (targeting the alpha-7 nicotinic receptor)[244], EPRNEEK (targeting the laminin receptor)[245], I_6P_7 (targeting the interleukin 6 receptor)[246] and g7 (reported to undergo adsorption-mediated endocytosis)[238] revealed a positive ligand effect in healthy BBB models only in case of g7 (data not shown for other ligands).

Post-modification of polyplexes formed by mixing of azide-bearing oligomers and siRNA with bis-DBCO-containing shielding and targeting agents by bio-orthogonal click chemistry is an elegant approach to avoid side reactions and to potentially increase polyplex stability by crosslinking of oligomers.[239] Azide-bearing T-shaped lipo-oligomers ***1198*** and ***1215*** were synthesized and polyplexes were post-modified with shielding agents containing a bis-DBCO moiety and either a g7 ligand for enhanced brain uptake or non-targeted controls. While polyplex sizes were in a similar range after post-modification, a significant reduction of zeta-potentials after modification down to 15 - 27 % for ***1198*** and 32 – 49 % for ***1215*** compared to unmodified polyplexes was detected, which should reduce unspecific interactions of the polyplexes. Higher shielding efficiency for ***1198*** might be beneficial compared to ***1215***, which has a higher charge density with 8 instead of 4 Stp units per oligomer. Modification of lipo-polyplexes with hydrophilic shielding agents, especially with higher equivalents containing longer PEG chains, bears the risk of polyplex destabilization.[239] Notably, electrophoretic mobility assays evaluating the binding ability of lipo-oligomers to siRNA revealed no destabilization of polyplexes after post-modification in HBG buffer and after two hours of incubation in 90 % FCS at 37 °C. Only after 24 h of incubation in serum a minor destabilizing effect of the shielding and targeting agents could be observed, indicating that these formulations could be suitable for application *in vivo*. Polyplexes containing lipo-oligomer ***1198*** released less siRNA than ***1215*** polyplexes, giving hint to a potential benefit in long-term extracellular stability of ***1198***. Higher stability of ***1198*** compared to ***1215*** oligomers could be attributed to the ratio of positively charged Stp units to stabilizing motifs, which is lower for ***1198*** and potentially beneficial for polyplex stability.

Brain capillary endothelial cells form a restrictive layer and prevent the majority of therapeutics from entering brain parenchyma. As tight junctions between adjacent BCECs prevent paracellular diffusion, cellular uptake in these cells a crucial first step in BBB crossing and brain delivery.[229] Polyplexes modified with PEG_{24}-g7, a shielding agent containing the opioid-derived g7 ligand, show enhanced uptake in mouse brain endothelial cells compared to unshielded polyplexes and polyplexes modified with shielding agents without ligand (PEG_{24}) or with a scambled control ligand (PEG_{24}-scrg7). The effect of g7-targeting could be observed for both ***1198*** and ***1215*** polyplexes, but was rather moderate with a less than 2-fold increase in mean fluorescence. An even less pronounced effect of g7-modification on cellular

internalization was found in Neuro2A neuroblastoma cells. Gene silencing efficiency in Neuro2A/eGFPLuc reporter cells was low for all tested formulations, but a moderate increase in gene knockdown was found for g7-modified polyplexes for both ***1198*** and ***1215*** and could be attributed to the slightly enhanced cellular uptake in this cell line. Giovanni Tosi, who repeatedly reported BBB crossing and brain delivery of g7-modified PLGA nanoparticles with various loadings *in vivo*, was consulted within the COMPACT consortium to discuss the data generated with the g7 ligand. His group extensively studied cell-specific uptake, distribution and neuronal cell-to-cell transport *in vitro* and *in vivo*. Tosi pointed out the limited predictive value of *in vitro* assays in case of g7-modified nanoparticles and strongly encouraged *in vivo* biodistribution assays. Although g7-targeted PLGA nanoparticles showed efficient uptake in mouse brain after i.v. injection, they lack an endosomal escape mechanism and therefore have only been used for the delivery of hydrophobic drugs or lysosomal enzymes for the treatment of lysosomal storage disorders.[234, 235, 237] Targeted siRNA lipo-polyplexes could provide enhanced endosomal escape efficiency and therefor potentially enable cytosolic delivery of RNAi therapeutics. However, it remains unclear if g7-modified lipo-polyplexes would exploit uptake and distribution mechanisms similar to negatively charged PLGA nanoparticles. Further testing in cellular BBB models or *in vivo* biodistribution studies are essential to evaluate if this delivery system is able to cross the BBB, as uptake in endothelial cells is only a first critical step of the brain delivery process. Azide-bearing lipo-oligomers are a highly versatile delivery platform which can be equipped with any DBCO-functionalized ligands. Further optimization could include ligands such as the protease-resistant TfR-targeting retro enantio peptide THRre[247, 248], cyclic MiniAp-4[249] or properly configured glucose in combination with rapid glycaemic increase after fasting.[250]

5 Summary

The transfer of therapeutic genes and oligonucleotides offers great opportunities for the treatment of severe diseases including genetic disorders and cancer.[251, 252] Efficient and safe delivery of nucleic acids is a major challenge. Stable nucleic acid complexation, low unspecific interactions with blood components and non-target cells, specific cellular uptake, endosomal escape and intracellular cargo release at the target site are critical parameters of the delivery process which can be addressed by formulation with multifunctional, bioresponsive, sequence-defined nucleic acid carriers. Solid-phase assisted synthesis enables modular assembly using natural amino acids, synthetic building blocks and other moieties such as fatty acids.

In this thesis, the synthesis of oleic acid containing lipo-oligomers was optimized with a new cleavage protocol, and biodegradable moieties were precisely integrated with a disulfide building block or enzymatic cleavage sites. Further, lipo-polyplexes and proteins were modified with targeting and shielding domains to enhance uptake in glioma and brain endothelial cells.

In the first part, the kinetics of TFA addition to oleic acid, which occurs as a side reaction during the oligomer cleavage, were studied with test oligomers and an optimized cleavage protocol was developed to minimize side products. Lipo-oligomers with intact oleic acid were synthesized in high yields (> 60 %) by precooling of both resin and cleavage cocktail, reduction of cleavage time and subsequent HPLC purification. Structures containing oleic acid showed particularly favorable pH dependency of endosomolytic activity, efficient gene silencing and excellent cell tolerability compared to its counterparts containing chemically stable or hydroxylated hydrocarbon chains.

In the second and third part, we presented biodegradable lipo-oligomers as siRNA carriers. Bioreducible carriers were synthesized by precise introduction of a disulfide bond between the cationic backbone and the hydrophobic domain via a Fmoc-protected cystamine building block, which is compatible with solid-phase assisted synthesis. Bioreducible carriers combined extracellular polyplex stability with siRNA release under cytosolic conditions and a high lytic activity under endosomal conditions with low cytotoxicity. However, their applicability must be evaluated for each cell line,

as reductive environments may differ and may result in premature extracellular disulfide cleavage.

In the third part, it was found that Stp-based oligoaminoamides are resistant toward enzymatic degradation by the lysosomal enzyme cathepsin B, which may present a problem for the cell metabolism. Biodegradability was tailored by precise integration of enzymatic cleavage sites such as L-Arg dipeptides. Cleavage sites should preferably be integrated into the hydrophilic parts of carriers. Introducing short cleavable L-Arg dipeptide linkers significantly improved cell tolerability after transfection without hampering gene silencing efficiency. Reduced lytic activities of degraded lipo-oligomers at endolysosomal pH conditions after internalization can be hypothesized as an underlying mechanism for the decreased toxicity. Evaluation of different cleavage motifs may enable further optimization regarding faster degradability by lysosomal enzymes or reduced cleavability by extracellular blood proteases, which could result in a loss of stability *in vivo*.

In the fourth part, modification of eGFP with the apelin-derived peptide ligands apelin-13 and apelin-F13A resulted in improved uptake in glioma cells via specific APLNR targeting. Still, an additional endosomal escape mechanism might be needed for efficient cytosolic or nuclear delivery. Modification of polyplexes with apelin-derived ligands could be a promising strategy to facilitate nucleic acid delivery into glioma, but not into the brain with a healthy BBB, as the expression of APLNR is low in normal brain vessels. Various peptide and protein ligands were tested for enhanced uptake in brain endothelial cells, where only the glycosylated heptapeptide g7 showed a slight increase of siRNA internalization by up to 90 %.

6 Appendix

6.1 Abbreviations

AMT	Adsorptive-mediated transcytosis
APLNR	Apelin receptor
BBB	Blood-brain barrier
BCECs	Brain capillary endothelial cells
BECF	Brain extracellular fluid
Boc	*tert*-Butoxycarbonyl protecting group
BODIPY	Boron-dipyrromethene
bPEI	Branched polyethylenimine
CholA	5β-Cholanic acid
CMT	Carrier-mediated transport
CNS	Central nervous system
DBCO	Dibenzocyclooctyne group
DCM	Dichloromethane
DCVC	Dry column vacuum chromatography
DIPEA	*N,N*-Diisopropylethylamine
DLS	Dynamic light scattering
DMEM	Dulbecco's modified Eagle's medium
DMF	*N,N*-Dimethylformamide
DNA	Desoxyribonucleic acid
EDTA	Ethylendiaminetetraacetic acid
EG5	Eglin 5
EGFP	Enhanced green fluorescent protein
FA	Folic acid
FCS	Fetal calf serum
Fmoc	Fluorenylmethoxycarbonyl protecting group
FolA	Folic acid
GFP	Green fluorescent protein
GNPs	Gold nanoparticles
GSH	Glutathione

HBG	Hepes-buffered glucose
HBTU	2-(1H-benzotriazole-1-yl)-1,1,3,3-tetramethyluronium hexafluorophosphate
HEPES	*N*-(2-hydroxethyl) piperazine-N‘-(2-ethansulfonic acid)
HMW	High molecular weight
HOBt	1-Hydroxybenzotriazole
IL-6	Interleukin 6
INF7	An endosomolytic influenza virus derived peptide
DHFR	Dihydrofolate reductase
Dde	4,4-Dimethyl-2,6-dioxocyclohexylidene)ethyl protecting group
LPEI	Linear polyethylenimine
LRP-1	Low Density Lipoprotein Receptor-Related Protein 1
MALDI-TOF	Matrix-assisted laser desorption/ionization – Time of flight
mM	Millimolar
mRNA	Messenger RNA
MTBE	Methyl *tert*-butyl ether
MTT	3-(4,5-dimethylthiazol-2-yl)-2,5-diphenyltetrazolium bromide
MTX	Methotrexate
mV	Millivolt
MyrA	Myristic acid
N/P	Nitrogen to phosphates ratio
NHS	*N*-Hydroxysuccinimide
nm	Nanometer
NMP	*N*-Methyl-2-pyrrolidone
NMR	Nuclear magnetic resonance
OleA	Oleic acid
PDI	Polydispersity index
pDNA	Plasmid DNA
PEG	Polyethylene glycol
pKa	$-\log_{10} K_a$ (acid dissociation constant)
PLGA	Poly-lactide-co-glycolide
PyBOP	Benzotriazol-1-yloxy-tripyrrolidinophosphonium hexafluorophosphate
RISC	RNA-induced silencing complex
RLU	Relative light units

RMT	Receptor-mediated transport
RNA	Ribonucleic acid
RP-HPLC	Reversed-phase high-performance liquid chromatography
RT	Room temperature
SEC	Size-exclusion chromatography
siRNA	Small interfering RNA
SPDP	Succinimidyl 3-(2-pyridyldithio)propionate
Sph	Succinoyl-pentaethylene hexamine
SPS	Solid-phase synthesis
SteA	Stearic acid
Stp	Succinoyl-tetraethylene pentamine
TBE	Tris-boric acid-EDTA buffer
TEPA	Tetraethylene pentamine
TFA	Trifluoroacetic acid
TfR	Transferrin receptor
THF	Tetrahydrofuran
TIS	Triisopropylsilane

6.2 Summary of SPS Derived Oligomers

Table 19 Summary of SPS derived oligomers

Oligomer ID	Topology	Sequence (C→N)	Proton. Amines	Chapter
454	T-Shape	C-Y_3-Stp_2-K-ε[K-α,ε($OleA)_2$]αStp_2-Y_3-C	*13*	*3.1*
782	U-shape	K-αK-α,ε[Stp3-ssbb-($CholA)_2$]$_2$	19	3.2
783	U-shape	K-αK-α,ε[Stp3-($CholA)_2$]$_2$	19	3.2
871	i-Shape	Stp_4-H_6-K-α,ε(CholA)	12	3.2
969	i-Shape	Stp_4-H_6-ssbb-K-α,ε($CholA)_2$	12	3.2
989	T-Shape	Y_3-Stp_2-K-ε[G-K-α,ε($SteA)_2$]αStp_2-Y_3	13	3.2
990	T-Shape	Y_3-Stp_2-K-ε[G-ssbb-K-α,ε($SteA)_2$]αStp_2-Y_3	13	3.2
991	T-Shape	Y_3-Stp_2-K-ε[G-K-α,ε($CholA)_2$]αStp_2-Y_3	13	3.2
992	T-Shape	Y_3-Stp_2-K-ε[G-ssbb-K-α,ε($CholA)_2$]αStp_2-Y_3	13	3.2
1072	T-Shape	C-Y_3-Stp_2-K-ε[K-α,ε($SteA)_2$]αStp_2-Y_3-C	*13*	*3.1*

1081	T-Shape	Y_3-Stp_2-K-ε[G-K-α,ε(MyrA)$_2$]αStp_2-Y_3	13	3.2
1082	T-Shape	Y_3-Stp_2-K-ε[G-ssbb-K-α,ε(MyrA)$_2$]αStp_2-Y_3	13	3.2
1104	T-Shape	C-Y_3-Stp_2-K-ε[K-α,ε(OcANonA)$_2$]αStp_2-Y_3-C	*13*	*3.1*
1105	T-Shape	C-Y_3-Stp_2-K-ε[K-α,ε(OH-SteA)$_2$]αStp_2-Y_3-C	*13*	*3.1*
1107	T-Shape	Y_3-Stp_2-K-ε[G-K-α,ε(OleA)$_2$]αStp_2-Y_3	13	3.2
1108	T-Shape	Y_3-Stp_2-K-ε[G-ssbb-K-α,ε(OleA)$_2$]αStp_2-Y_3	13	3.2
1165	T-Shape	C-Y_3-Stp_2-K-ε[K-α,ε(LinA)$_2$]αStp_2-Y_3-C	*13*	*3.1*
1166	T-Shape	C-Y_3-Stp_2-K-ε[K-α,ε(OH-C(18:1))$_2$]αStp_2-Y_3-C	*13*	*3.1*
1198	T-Shape	C-Y_3-Stp_2-K-ε[K-α,ε(OleA)$_2$]αStp_2-Y_3-C-K(N_3)	13	3.4
1215	T-Shape	C-Y_3-Stp_4-K-ε[K-α,ε(OleA)$_2$]αStp_4-Y_3-C-K(N_3)	13	3.4
1286	T-Shape	Y_3-Stp_2-K-ε[K-α,ε(MyrA)$_2$]Stp_2-Y_3	13	*3.3*
1287	T-Shape	Y_3-Stp_2-K-ε[R-K-α,ε(MyrA)$_2$]Stp_2-Y_3	*14*	*3.3*
1288	T-Shape	Y_3-Stp_2-K-ε[r-K-α,ε(MyrA)$_2$]Stp_2-Y_3	*14*	*3.3*
1289	T-Shape	Y_3-Stp_2-K-ε[RR-K-α,ε(MyrA)$_2$]Stp_2-Y_3	*15*	*3.3*
1291	T-Shape	Y_3-Stp_2-R-K-R-ε[K-α,ε(MyrA)$_2$]Stp_2-Y_3	*15*	*3.3*
1292	T-Shape	Y_3-Stp_2-R-K-R-ε[R-K-α,ε(MyrA)$_2$]Stp_2-Y_3	*16*	*3.3*
1293	T-Shape	Y_3-Stp_2-R-K-R-ε[r-K-α,ε(MyrA)$_2$]Stp_2-Y_3	*16*	*3.3*
1294	T-Shape	Y_3-Stp_2-r-K-r-ε[K-α,ε(MyrA)$_2$]Stp_2-Y_3	*15*	*3.3*
1295	T-Shape	Y_3-Stp_2-r-K-r-ε[R-K-α,ε(MyrA)$_2$]Stp_2-Y_3	*16*	*3.3*
1296	T-Shape	Y_3-Stp_2-r-K-r-ε[r-K-α,ε(MyrA)$_2$]Stp_2-Y_3	*16*	*3.3*
1297	T-Shape	Y_3-Stp_2-RR-K-RR-ε[K-α,ε(MyrA)$_2$]Stp_2-Y_3	*17*	*3.3*
1298	T-Shape	Y_3-Stp_2-RR-K-RR-ε[RR-K-α,ε(MyrA)$_2$]Stp_2-Y_3	*19*	*3.3*
1299	T-Shape	Y_3-Stp_2-RR-K-RR-ε[rr-K-α,ε(MyrA)$_2$]Stp_2-Y_3	*19*	*3.3*
1301	T-Shape	Y_3-Stp_2-rr-K-rr-ε[RR-K-α,ε(MyrA)$_2$]Stp_2-Y_3	*19*	*3.3*
1302	T-Shape	Y_3-Stp_2-rr-K-rr-ε[rr-K-α,ε(MyrA)$_2$]Stp_2-Y_3	*19*	*3.3*

6.3 Summary of SPS Derived Shielding Agents

Table 20 Summary of SPS derived shielding agents

ID	Name	Sequence (N→C)	Chapter
1307	$(DBCO\text{-}STOTDA)_2$-K-PEG_{24}-COOH	$(DBCO\text{-}STOTDA)_2$-K-PEG_{24}-COOH	3.4
1308	$(DBCO\text{-}STOTDA)_2$-K-PEG_{24}-g7	$(DBCO\text{-}STOTDA)_2$-K-PEG_{24}-Gly-FtGFLL-L-Ser(O-β-D-Glucose)-$CONH_2$	3.4
1309	$(DBCO\text{-}STOTDA)_2$-K-PEG_{24}-scrg7	$(DBCO\text{-}STOTDA)_2$-K-PEG_{24}-GLFFG-Ser(O-β-D-Glucose)t-$CONH_2$	3.4
1310	C-PEG_{24}-apelin-13	C-PEG_{24}-QRPRLSHKGPMPF	3.4
1311	C-PEG_{24}-apelin-F13A	C-PEG_{24}- QRPRLSHKGPMPA	3.4
1312	C-PEG_{24}-apelin-13scr	C-PEG_{24}- HGFPRPQMPRLSK	3.4

6.4 Analytical Data

6.4.1 ^{1}H NMR spectrum of disulfide-linker building block(ssbb)

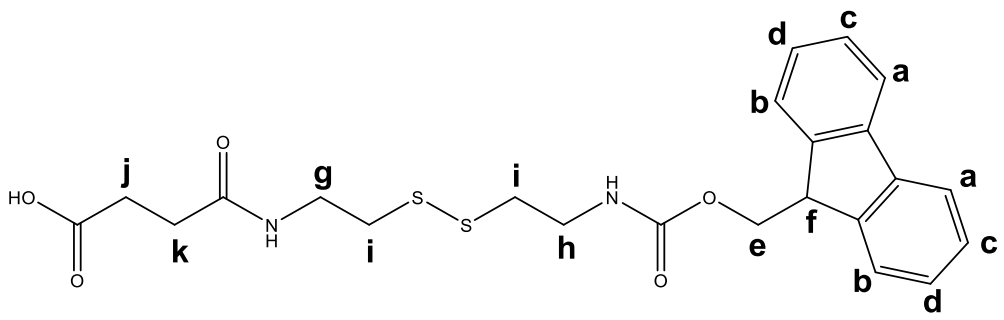

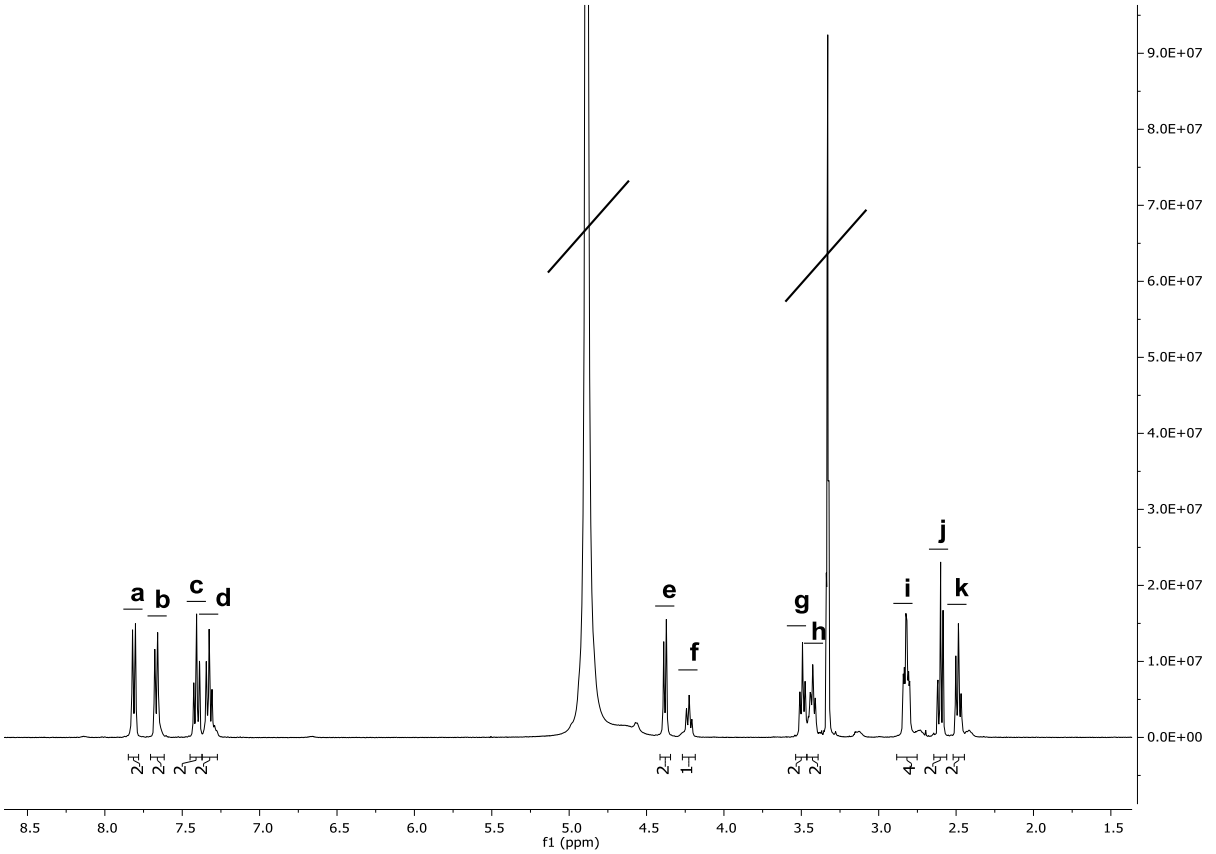

1-(9H-fluoren-9-yl)-3,12-dioxo-2-oxa-7,8-dithia-4,11-diazapentadecan-15-oic acid (ssbb) **^{1}H NMR (500 MHz, Methanol-d4)** δ (ppm) 7.81 (d, J = 7.5 Hz, H*a*, 2H), 7.67 (d, J = 7.4 Hz, H*b*, 2H), 7.41 (t, J = 7.4 Hz, H*c*, 2H), 7.33 (t, J = 7.4 Hz, H*d*, 2H), 4.38 (d, J = 6.9 Hz, H*e*, 2H), 4.22 (t, J = 6.8 Hz, H*f*, 1H), 3.49 (t, J = 6.7 Hz, H*g*, 2H), 3.43 (t, J = 6.7 Hz, H*h*, 2H), 2.76-2.87 (m, H*i*, 4H), 2.60 (t, J = 6.6 Hz, H*j*, 2H), 2.48 (t, J = 6.8 Hz, H*k*, 2H).

6.4.2 ^{1}H NMR spectra of oligomers

OleA-t

Sequence (C→N): C-Y_3-Stp_2-K-ε[K-α,ε$(OleA)_2$]αStp_2-Y_3-C

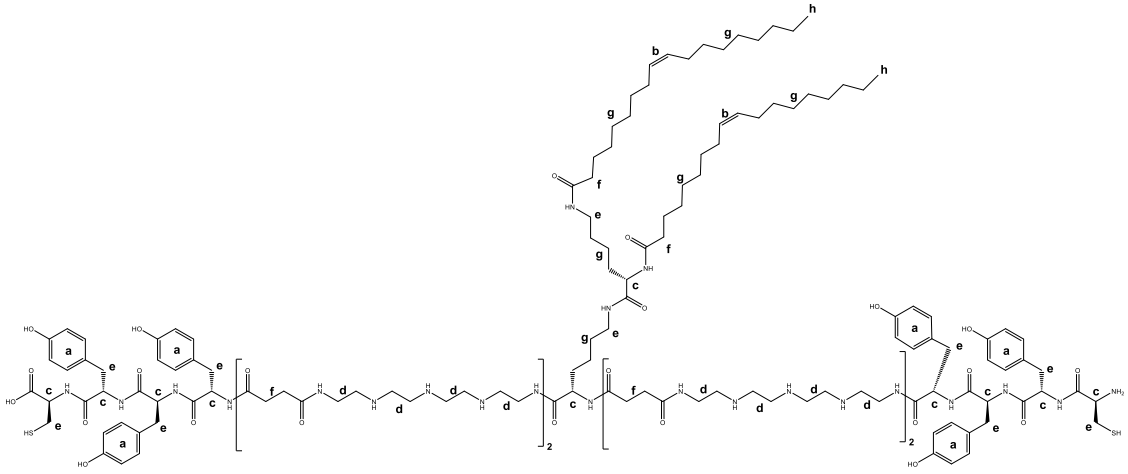

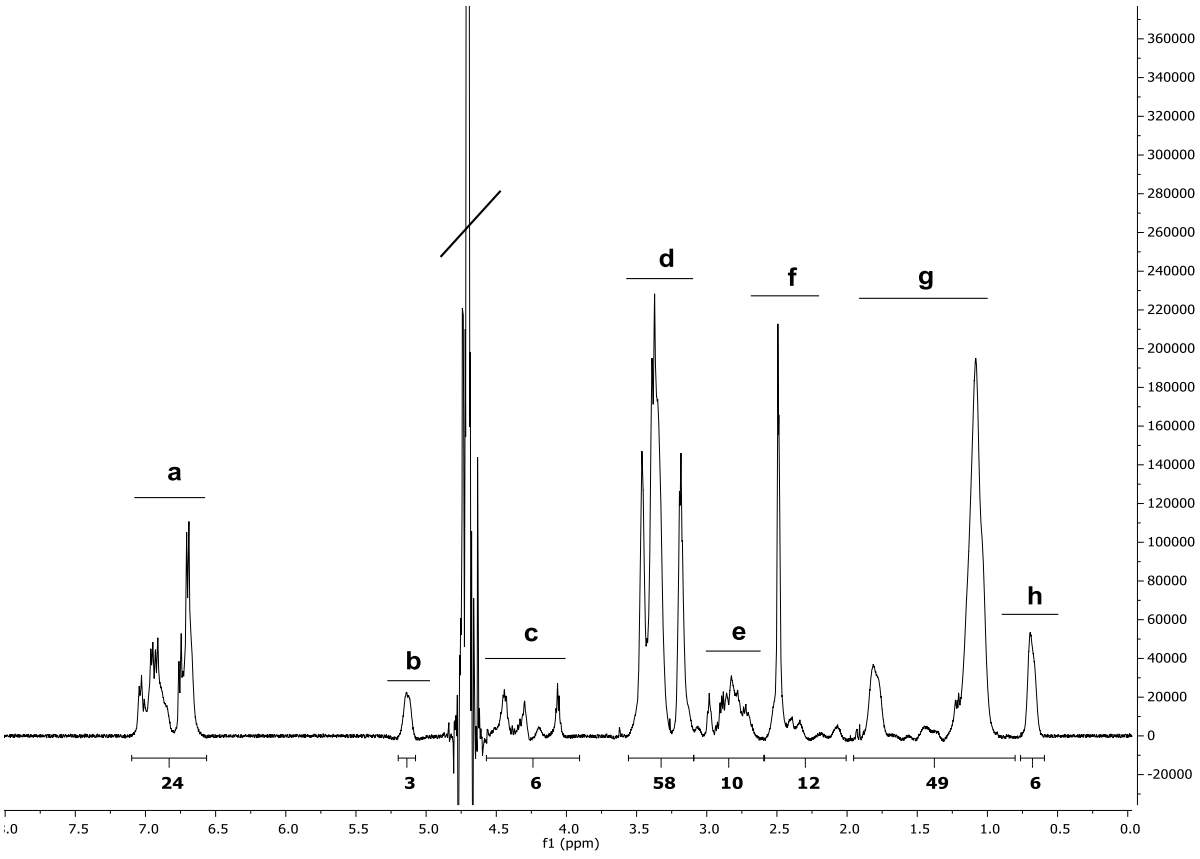

^{1}H NMR (500 MHz, Deuterium oxide) δ (ppm) = 0.65-0.85 (s, 6 H, -CH_3 oleic acid), 0.85-1.95 (m, 64 H, βγδH lysine, -CH_2- oleic acid), 2.0 -2.65 (m, 20 H, -CO-CH_2-CH_2-CO- Stp, -CO-CH_2- oleic acid), 2.65-3.1 (m, 20 H, εH lysine, tyrosine, cysteine), 3.1-3.6 (m, 64 H, -CH_2- Tp), 3.85-4.55 (m, 10 H, αH amino acids), 5.05-5.20 (s, 4 H, -CH=CH oleic acid), 6.55-7.10 (m, 24 H, -CH- tyrosine).

OH-SteA-t:

Sequence (C→N): C-Y_3-Stp_2-K-ε[K-α,ε$(OH\text{-}SteA)_2$]αStp_2-Y_3-C

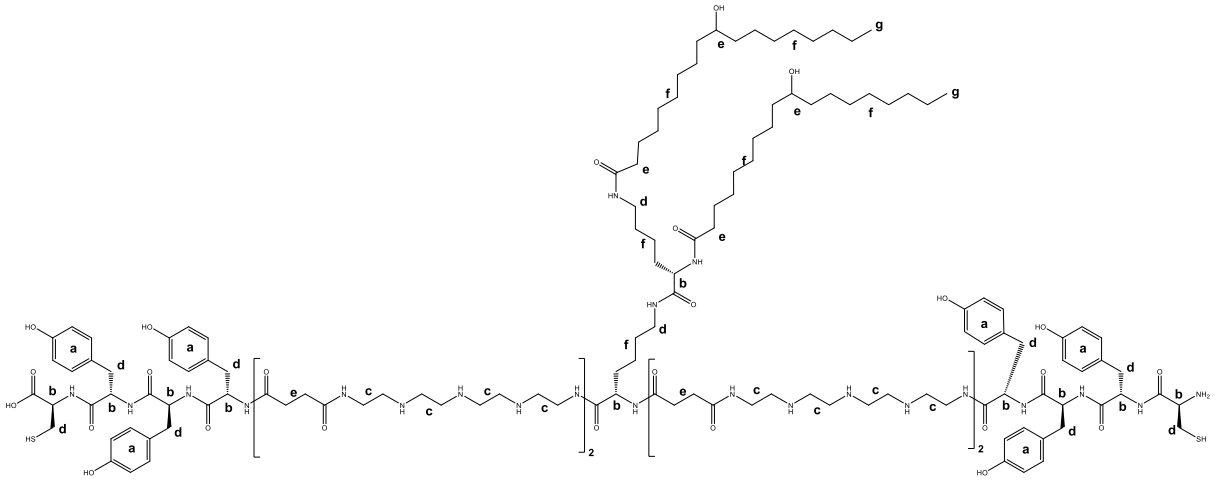

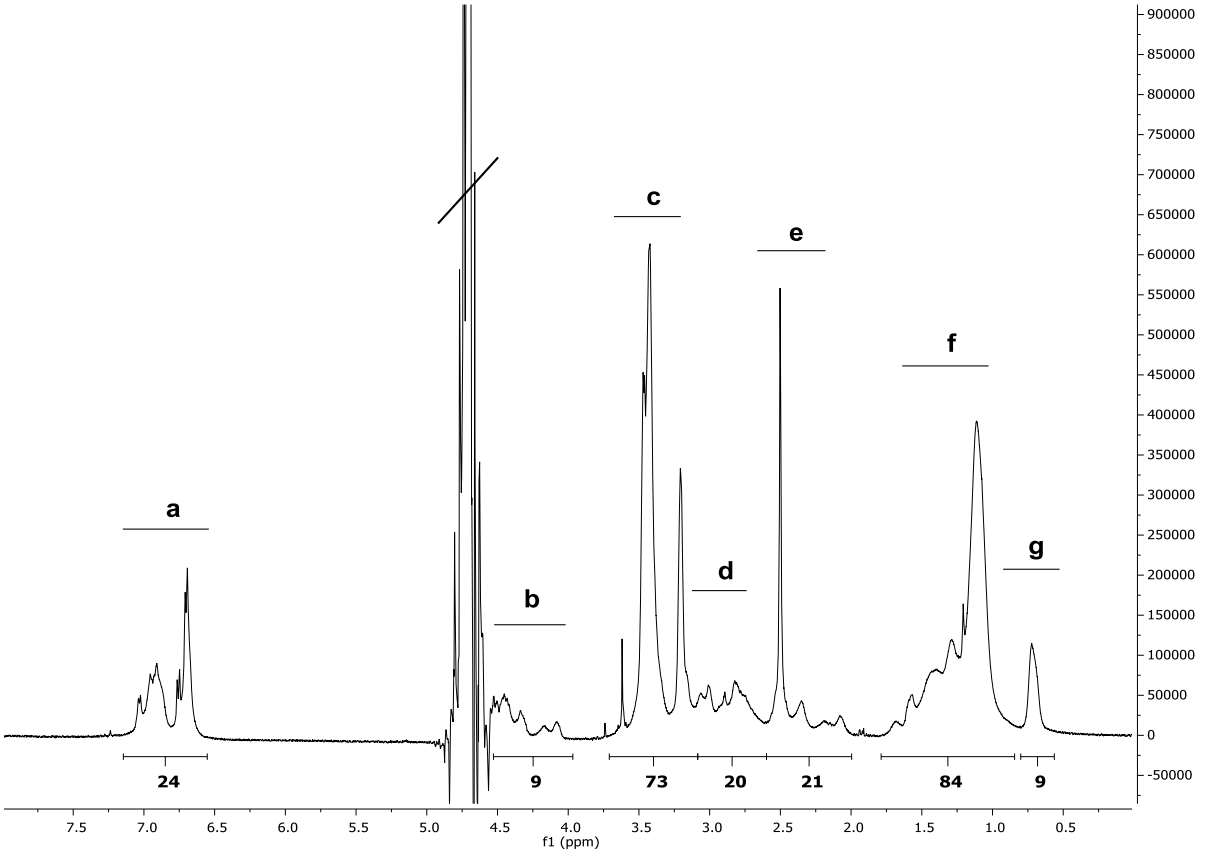

^{1}H NMR (500 MHz, Deuterium oxide) δ (ppm) = 0.60-0.80 (s, 6 H, -CH_3 hydroxystearic acid), 0.80-1.35 (m, 68 H, βγδH lysine, -CH_2- hydroxystearic acid), 2.3-2.65 (m, 22 H, -CO-CH_2-CH_2-CO- Stp, -CO-CH_2- hydroxystearic acid, =CH-OH hydroxystearic acid), 2.65-3.1 (m, 20 H, εH lysine, tyrosine, cysteine), 3.1-3.6 (m, 64 H, -CH_2- Tp), 3.90-4.55 (m, 10 H, αH amino acids), 6.55-7.10 (m, 24 H, -CH- tyrosine).

SteA-t:

Sequence (C→N): C-Y_3-Stp_2-K-ε[K-α,ε$(SteA)_2$]αStp_2-Y_3-C

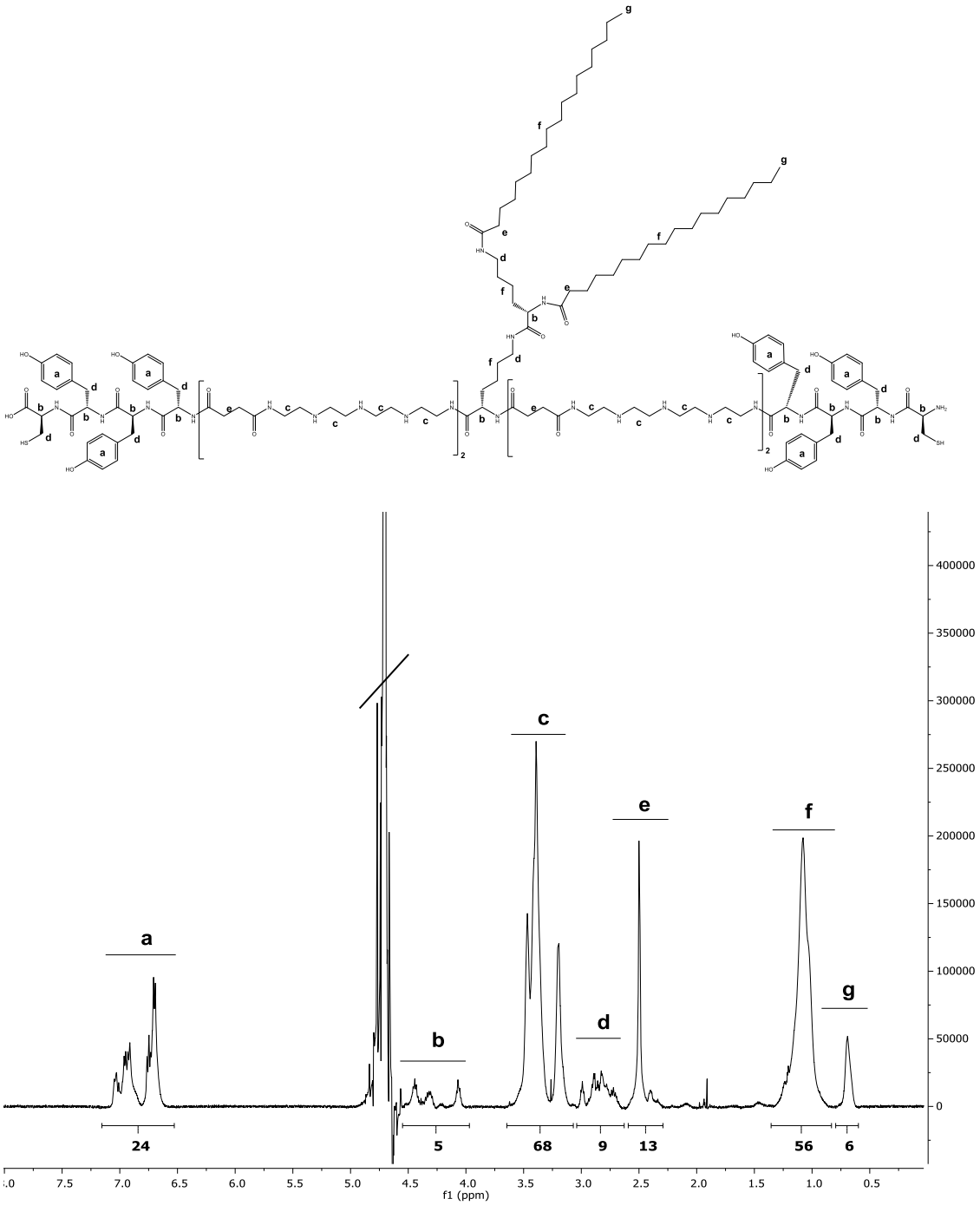

^{1}H NMR (500 MHz, Deuterium oxide) δ (ppm) = 0.60-0.80 (s, 6 H, -CH_3 stearic acid), 0.80-1.35 (m, 72 H, βγδH lysine, -CH_2- stearic acid), 2.3-2.65 (m, 20 H, -CO-CH_2-CH_2-CO- Stp, -CO-CH_2- stearic acid), 2.65-3.1 (m, 20 H, εH lysine, tyrosine, cysteine), 3.1-3.6 (m, 64 H, -CH2- Tp), 3.90-4.55 (m, 10 H, αH amino acids), 6.55-7.10 (m, 24 H, -CH- tyrosine).

***NonOcA-t*:**

Sequence (C→N): C-Y_3-Stp_2-K-ε[K-α,ε$(OcANonA)_2$]αStp_2-Y_3-C

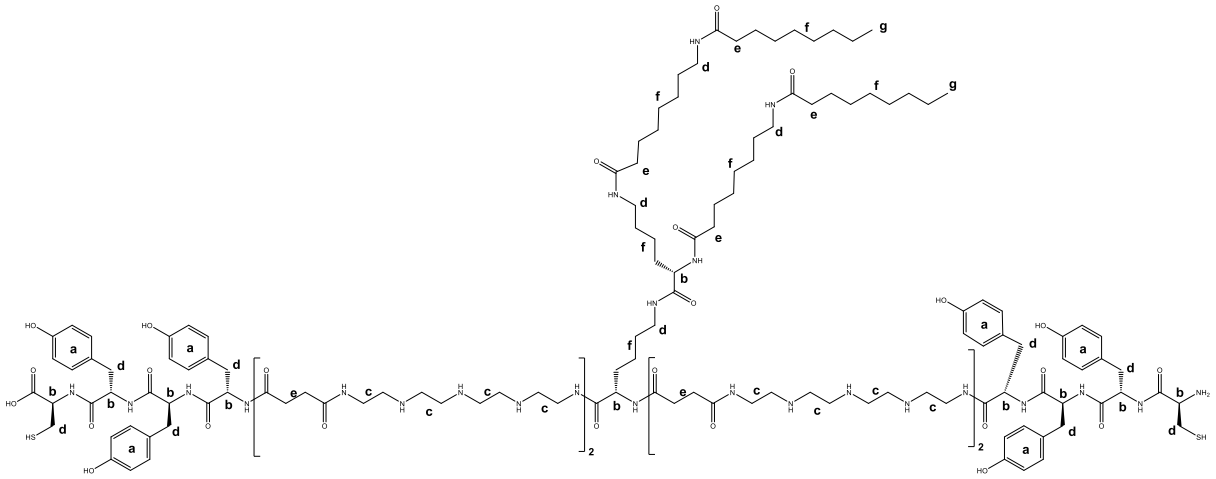

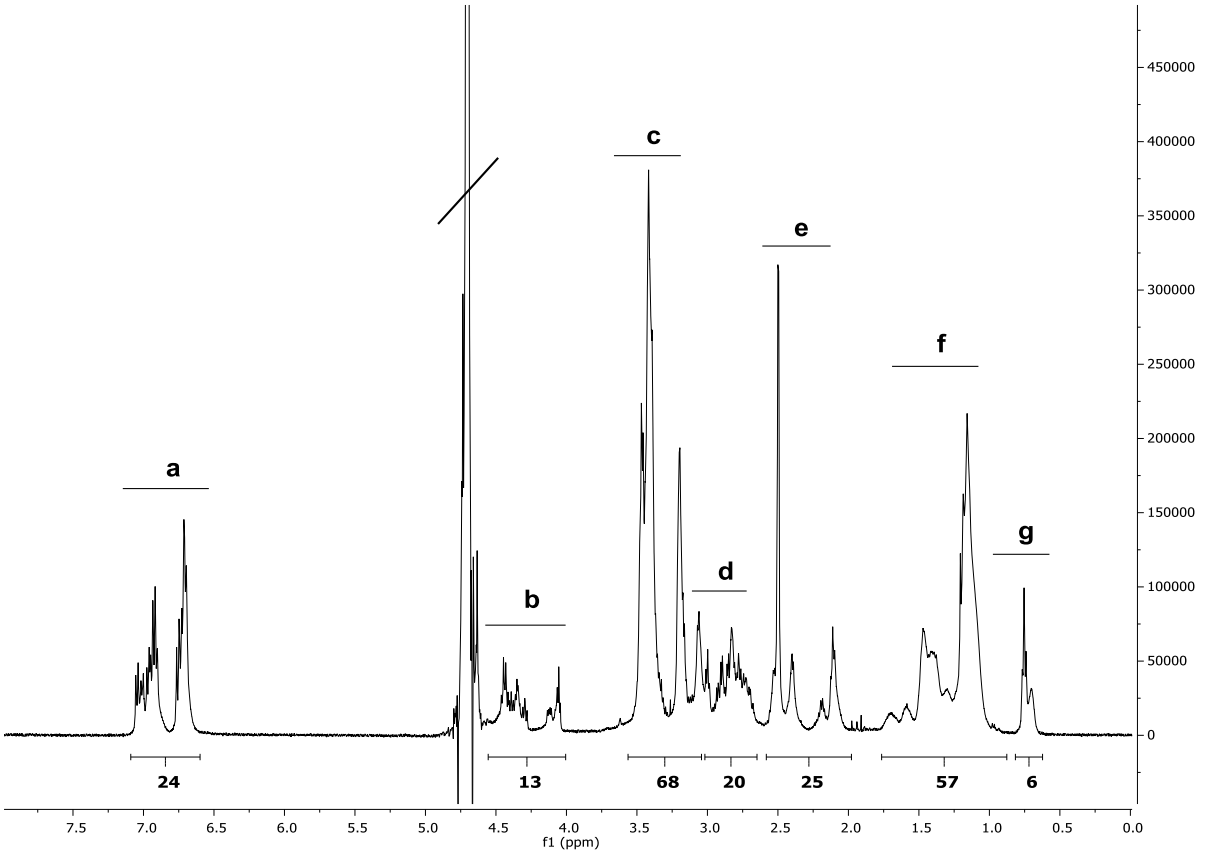

^{1}H NMR (500 MHz, Deuterium oxide) δ (ppm) = 0.60-0.80 (s, 6 H, -CH_3 nonanoic acid), 0.85-1.75 (m, 56 H, βγδH lysine, -CH_2- octanoic acid, nonanoic acid), 2.0-2.65 (m, 24 H, -CO-CH_2-CH_2-CO- Stp, -CO-CH_2- octanoic acid, nonanoic acid), 2.65-3.1 (m, 20 H, εH lysine, tyrosine, cysteine), 3.1-3.6 (m, 64 H, -CH_2- Tp), 4.00-4.55 (m, 10 H, αH amino acids), 6.55-7.10 (m, 24 H, -CH- tyrosine).

LinA-t

Sequence (C→N): C-Y_3-Stp_2-K-ε[K-α,ε$(LinA)_2$]αStp_2-Y_3-C

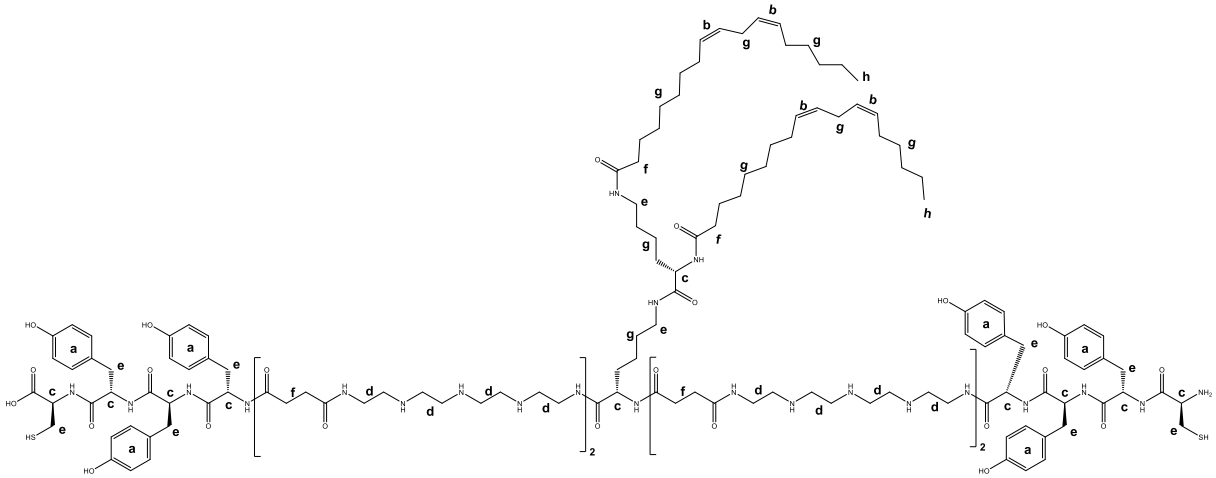

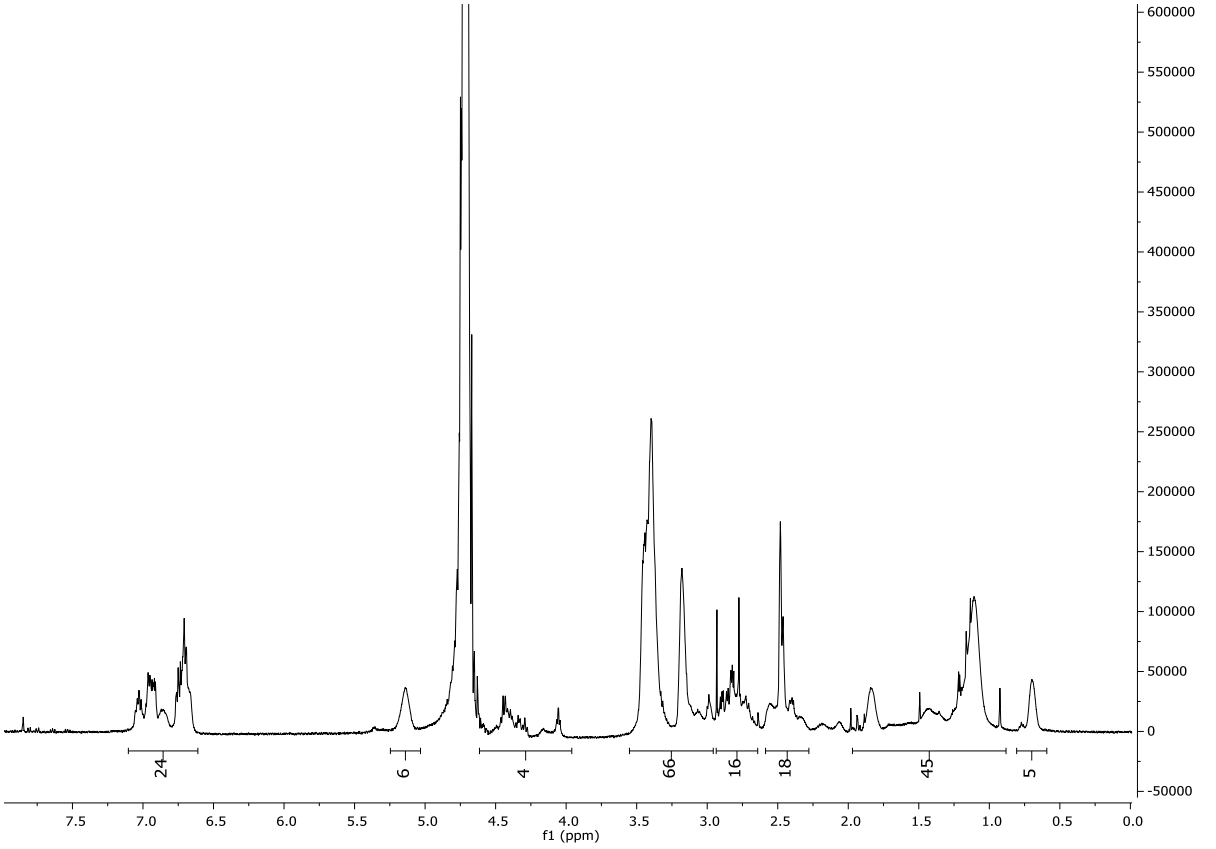

^{1}H NMR (500 MHz, Deuterium oxide) δ (ppm) = 0.60-0.80 (s, 6 H, -CH_3 linoleic acid), 0.90-2.00 (m, 56 H, βγδH lysine, -CH_2- linoleic acid), 2.30 -2.60 (m, 20 H, -CO-CH_2-CH_2-CO- Stp, -CO-CH_2- oleic acid), 2.65-2.95 (m, 20 H, εH lysine, tyrosine, cysteine), 2.95-3.55 (m, 64 H, -CH_2- Tp), 3.95-4.60 (m, 10 H, αH amino acids), 5.05-5.25 (s, 8 H, -CH=CH linoleic acid), 6.60-7.10 (m, 24 H, -CH- tyrosine).

***OH-C(C18:1)-t* (side product of LinA-t synthesis)**

Sequence (C→N): C-Y_3-Stp_2-K-ε[K-α,ε(OH-C(18:1))$_2$]αStp_2-Y_3-C

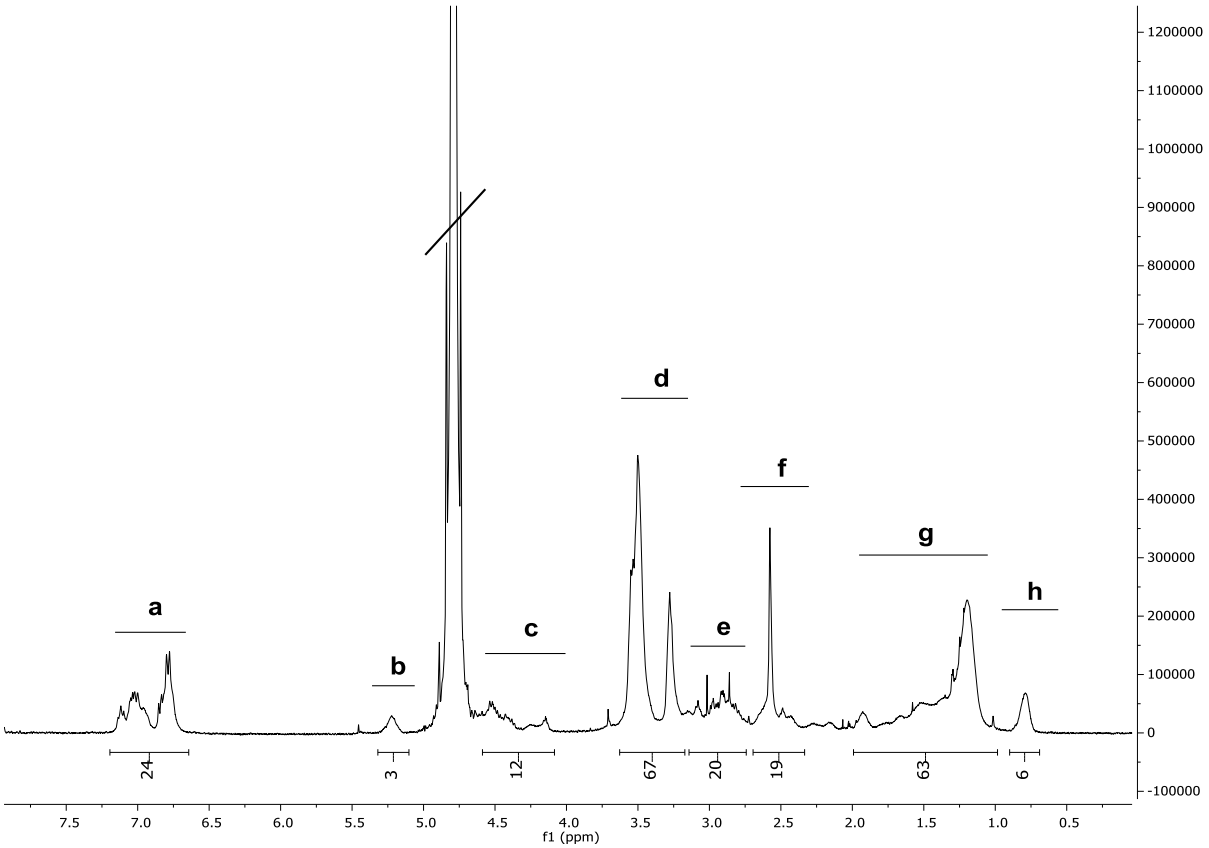

^{1}H NMR (500 MHz, Deuterium oxide) δ (ppm) = 0.70-0.90 (s, 6 H, -CH_3 hydroxyoctadecenoic acid), 1.00-2.00 (m, 60 H, βγδH lysine, -CH_2- hydroxyoctadecenoic acid), 2.35-2.70 (m, 22 H, -CO-CH_2-CH_2-CO- Stp, -CO-CH_2- hydroxyoctadecenoic acid, =CH-OH hydroxyoctadecenoic acid), 2.75-3.15 (m, 20 H, εH lysine, tyrosine, cysteine), 3.20-3.60 (m, 64 H, -CH_2- Tp), 4.10-4.60 (m, 10 H, αH amino acids), 5.10-5.30 (s, 4 H, -CH=CH hydroxyoctadecenoic acid), 6.65-7.20 (m, 24 H, -CH- tyrosine).

***740* (test structure)**

Sequence (C→N): W-Stp2-ssbb-L3-W

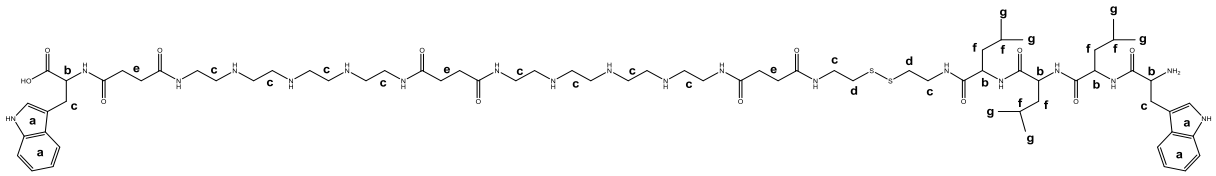

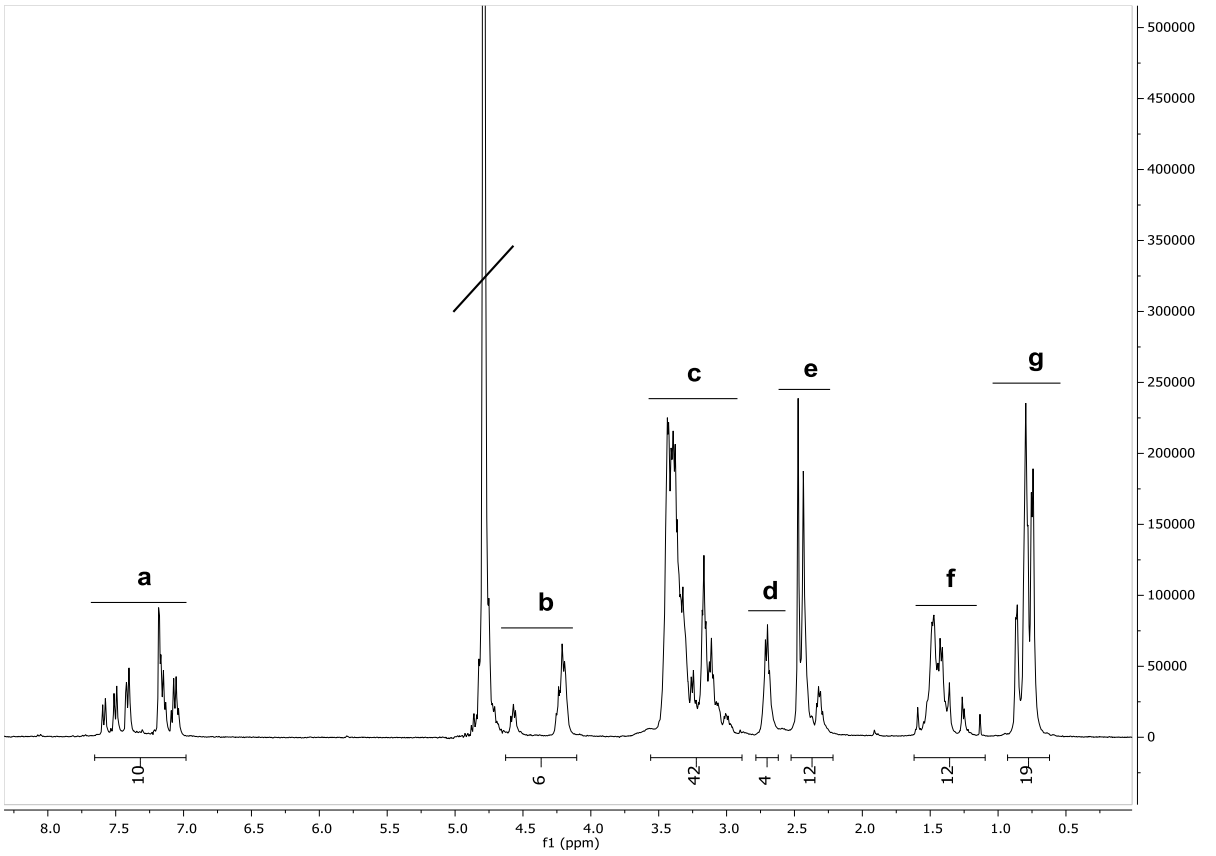

^{1}H NMR (500 MHz, Deuterium oxide) δ (ppm) = 0.60-0.95 (m, 18 H, δH leucine), 1.10-1.60 (m, 12 H, βγH leucine), 2.20-2.50 (m, 12 H, -CO-CH2-CH2-CO- Stp and ssbb), 2.60-2.80 (m, 4 H, -CH2-SS-CH2-), 2.90-3.55 (m, 40 H, -CH2- Tp and ssbb, εH tryptophane), 4.10-4.60 (m, 5 H, αH tryptophanes and leucines), 7.00-7.65 (m, 10 H, aromatic H tryptophane).

782

Sequence (C→N): K-αK-α,ε[Stp$_3$-ssbb-(CholA)$_2$]$_2$

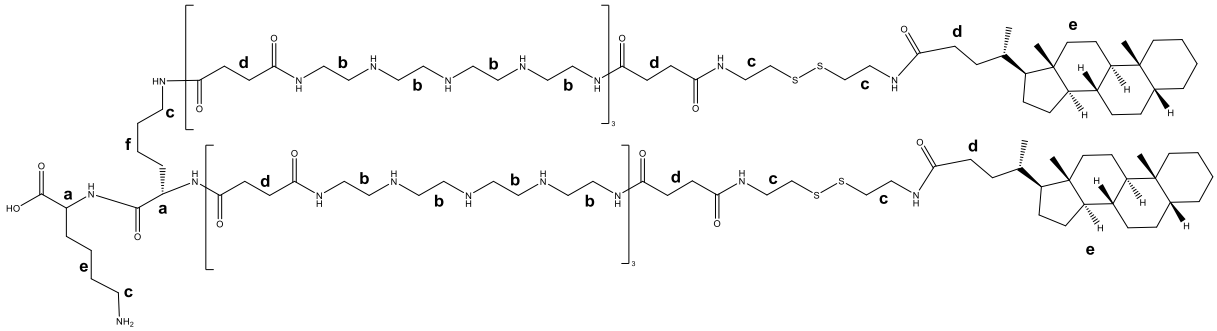

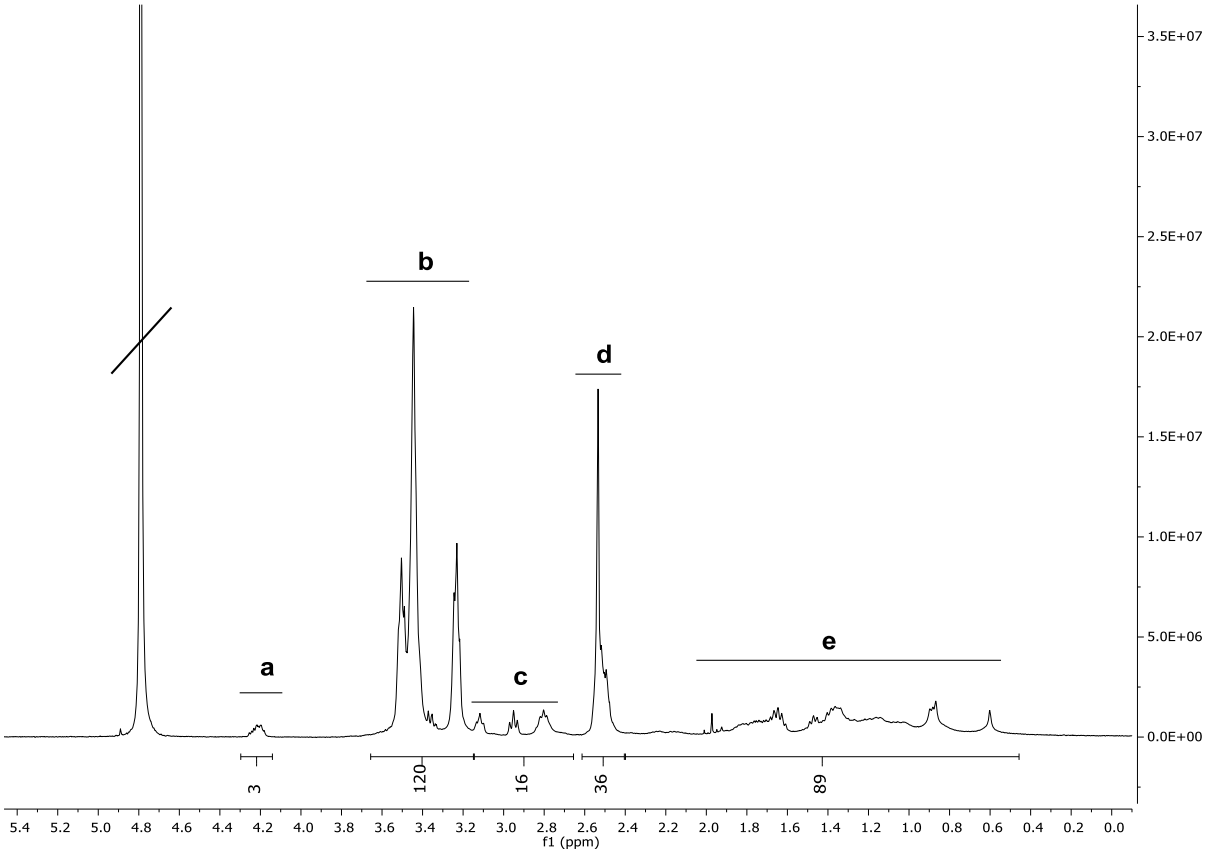

^{1}H NMR (500 MHz, Deuterium oxide) δ (ppm) = 0.45-2.40 m, 88 H, βγδH lysine, cholanic acid), 2.40-2.60 (m, 36 H, -CO-CH2-CH2-CO- Stp and ssbb, -CO-CH2-cholanic acid), 2.65-3.15 (m, 12 H, εH lysine, -CH2- ssbb), 3.15-3.65 (m, 96 H, -CH2-Tp), 4.15-4.30 (m, 2 H, αH lysines).

783

Sequence (C→N): K-αK-α,ε[Stp_3-$(CholA)_2$]$_2$

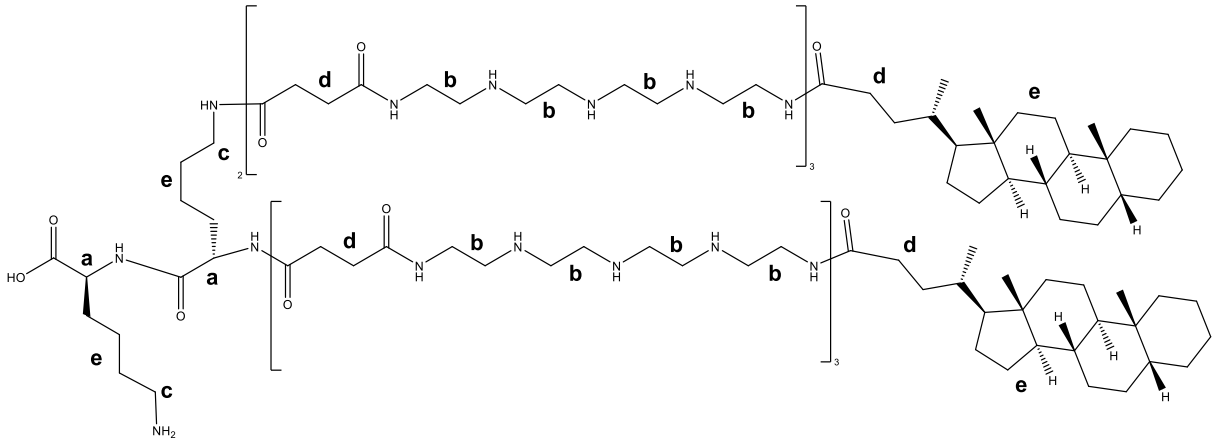

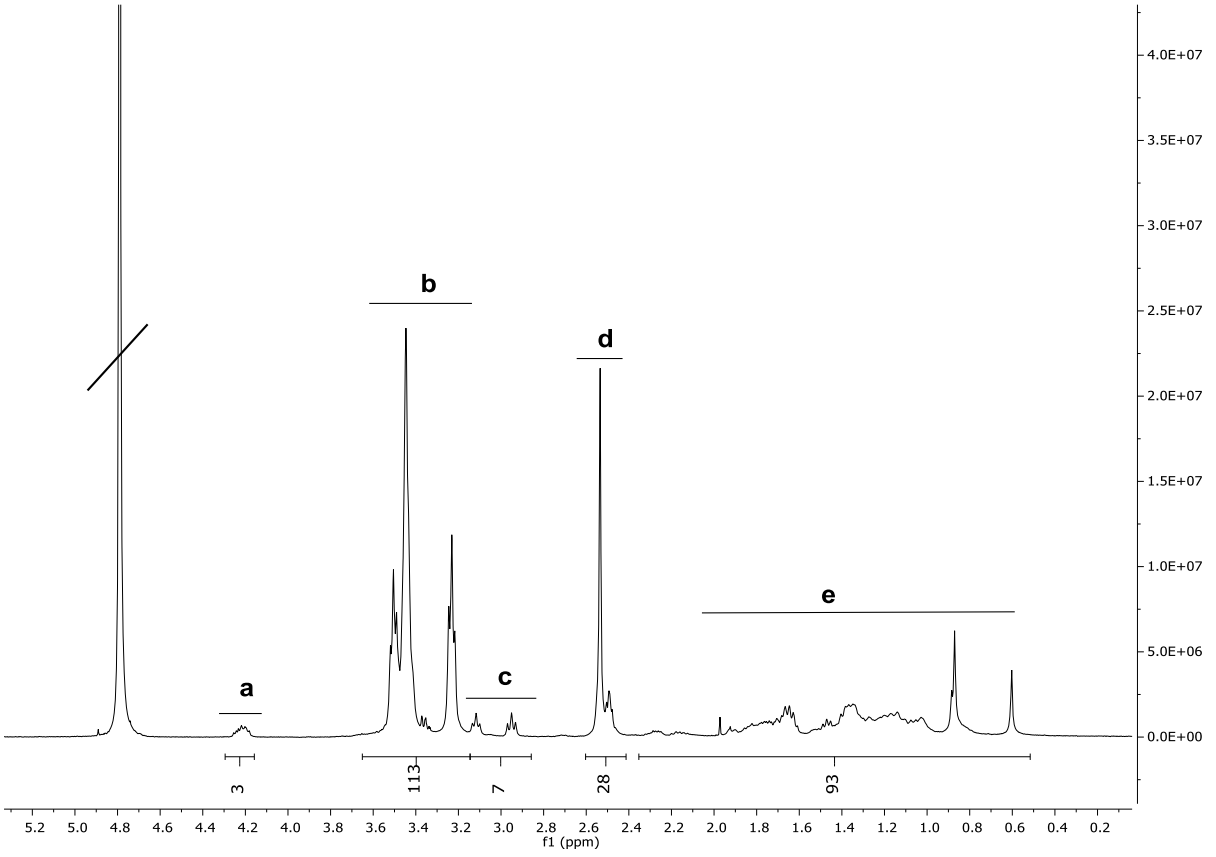

^{1}H NMR (500 MHz, Deuterium oxide) δ (ppm) = 0.50-2.35 m, 88 H, βγδH lysine, cholanic acid), 2.40-2.60 (m, 28 H, -CO-CH_2-CH_2-CO- Stp, -CO-CH_2- cholanic acid), 2.85-3.15 (m, 4 H, εH lysine), 3.15-3.65 (m, 96 H, -CH_2- Tp), 4.15-4.30 (m, 2 H, αH lysines).

871

Sequence (C→N): Stp_4-H_6-K-α,ε$(CholA)_2$

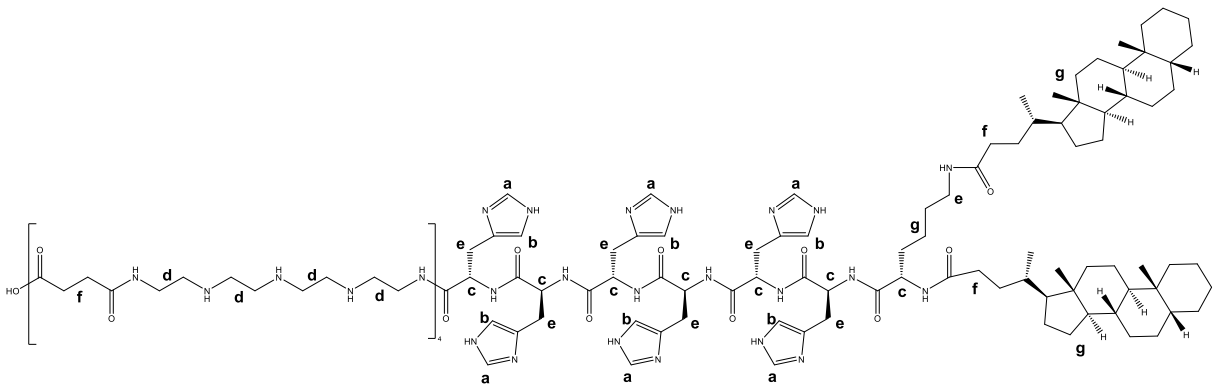

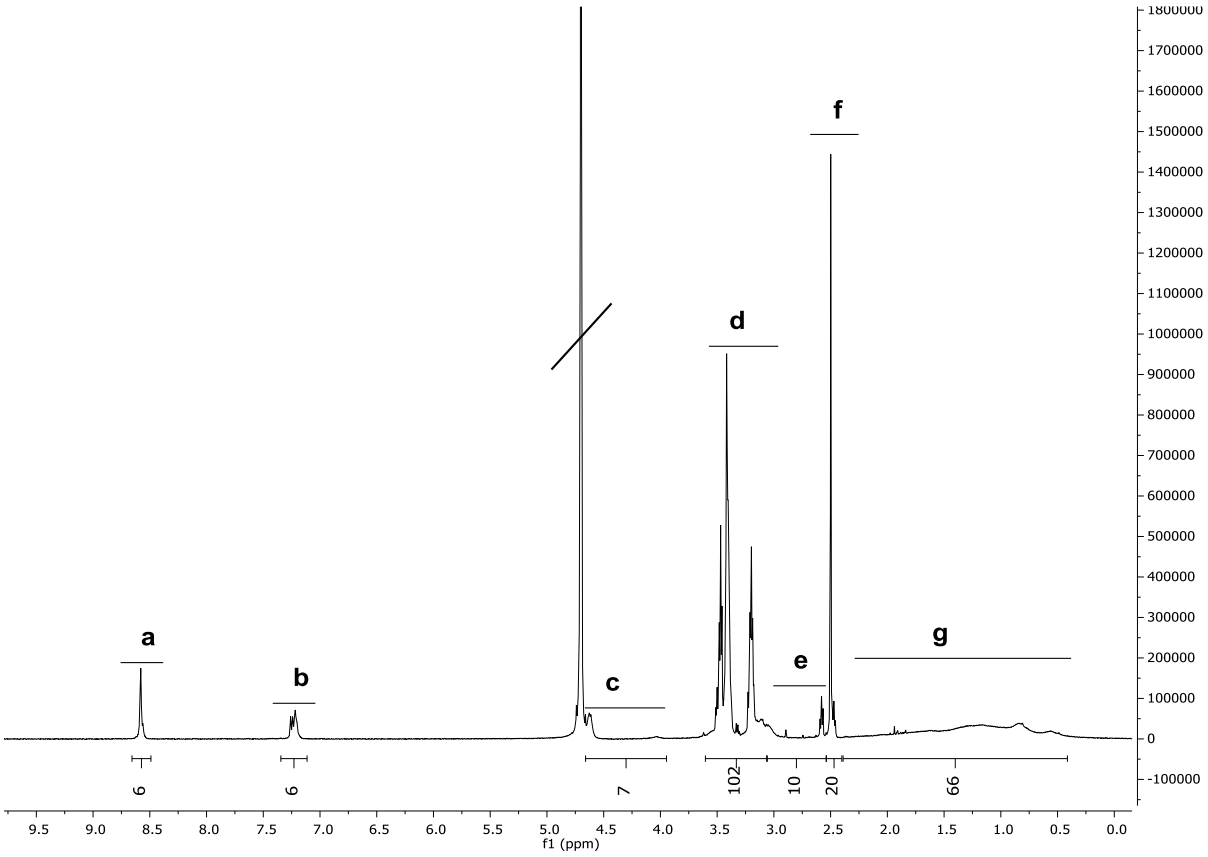

^{1}H NMR (500 MHz, Deuterium oxide) δ (ppm) = 0.40-2.30 m, 82 H, βγδH lysine, cholanic acid), 2.40-2.55 (m, 20 H, -CO-CH2-CH2-CO- Stp, -CO-CH2- cholanic acid), 2.55-3.05 (m, 14 H, εH lysine and histidine), 3.05-3.60 (m, 64 H, -CH2- Tp), 3.95-4.65 (m, 7 H, αH lysines and histidines), 7.10-7.35 (d, 6 H, aromatic H histidine), 8.5-8.65 (m, 6 H, aromatic H histidine).

969

Sequence (C→N): Stp4-H6-ssbb-K-α,ε(CholA)2

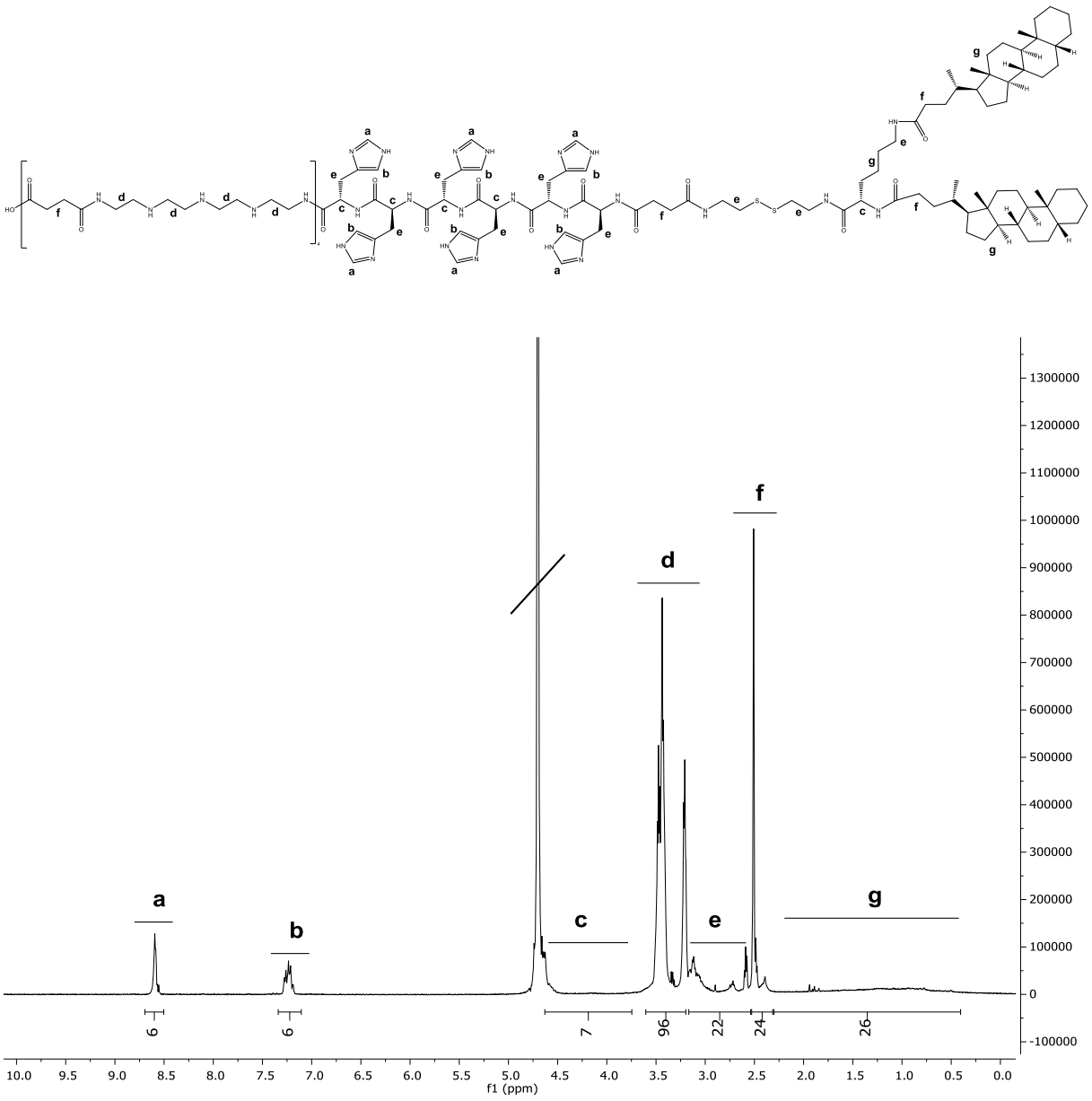

^{1}H NMR (500 MHz, Deuterium oxide) δ (ppm) = 0.40-2.30 m, 82 H, βγδH lysine, cholanic acid), 2.30-2.55 (m, 24 H, -CO-CH2-CH2-CO- Stp and ssbb, -CO-CH2- cholanic acid), 2.55-3.15 (m, 22 H, εH lysine and histidine, -CH2- ssbb), 3.15-3.65 (m, 64 H, -CH2- Tp), 3.75-4.65 (m, 7 H, αH lysines and histidines), 7.10-7.35 (d, 6 H, aromatic H histidine), 8.50-8.70 (m, 6 H, aromatic H histidine).

989

Sequence (C→N): Y_3-Stp_2-K-ε[G-K-α,ε$(SteA)_2$]αStp_2-Y_3

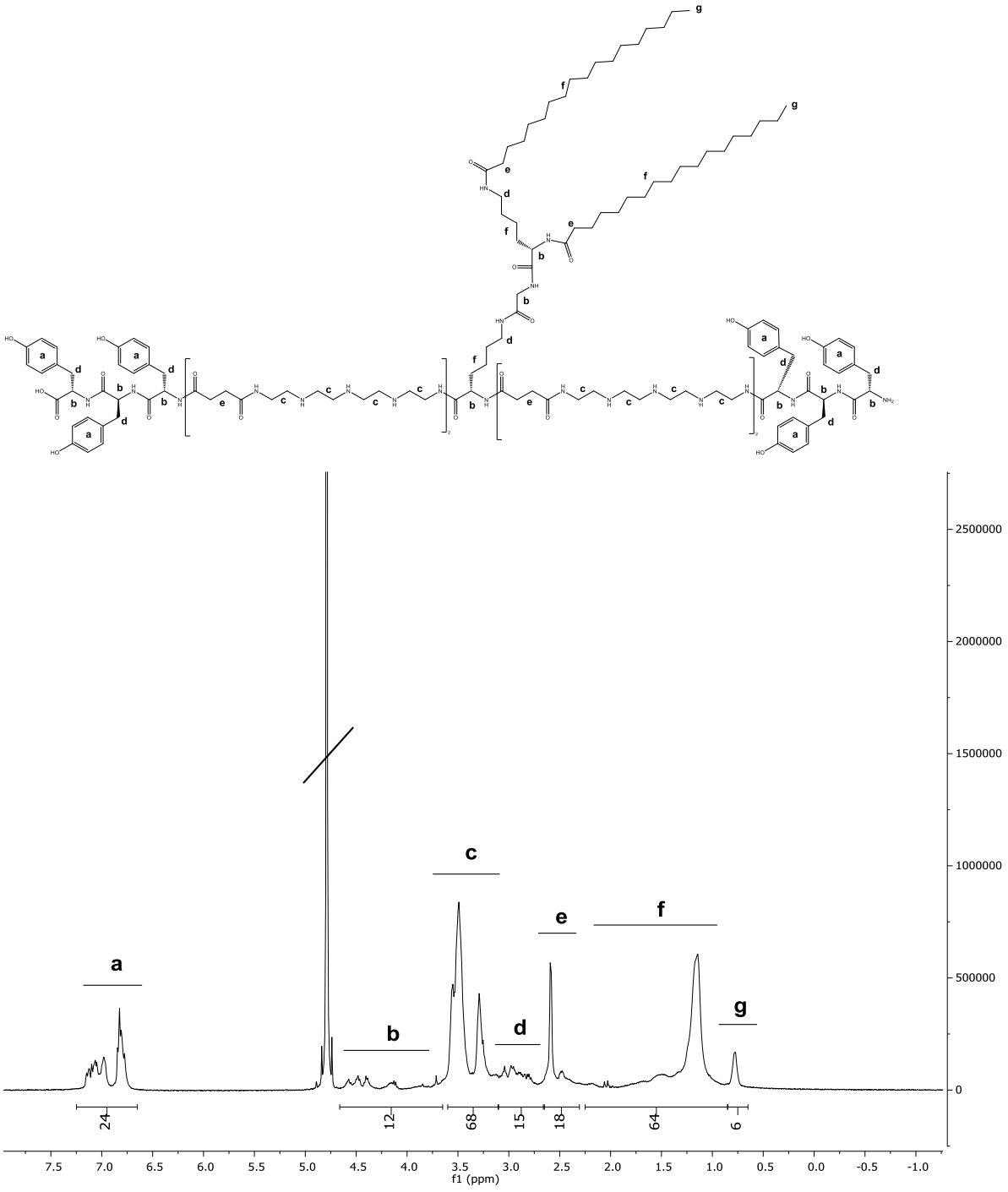

^{1}H NMR (500 MHz, Deuterium oxide) δ (ppm) = 0.65-0.85 (s, 6 H, -CH3 stearic acid), 0.85-2.25 (m, 76 H, βγδH lysine, -CH2- stearic acid), 2.3-2.65 (m, 20 H, -CO-CH2-CH2-CO- Stp, -CO-CH2- stearic acid), 2.65-3.1 (m, 16 H, εH lysine and tyrosine), 3.1-3.6 (m, 64 H, -CH2- Tp), 3.65-4.65 (m, 10 H, αH amino acids), 6.65-7.25 (m, 24 H, -CH- tyrosine).

***990*:** Sequence (C→N): Y_3-Stp_2-K-ε[G-ssbb-K-α,ε$(SteA)_2$]αStp_2-Y_3

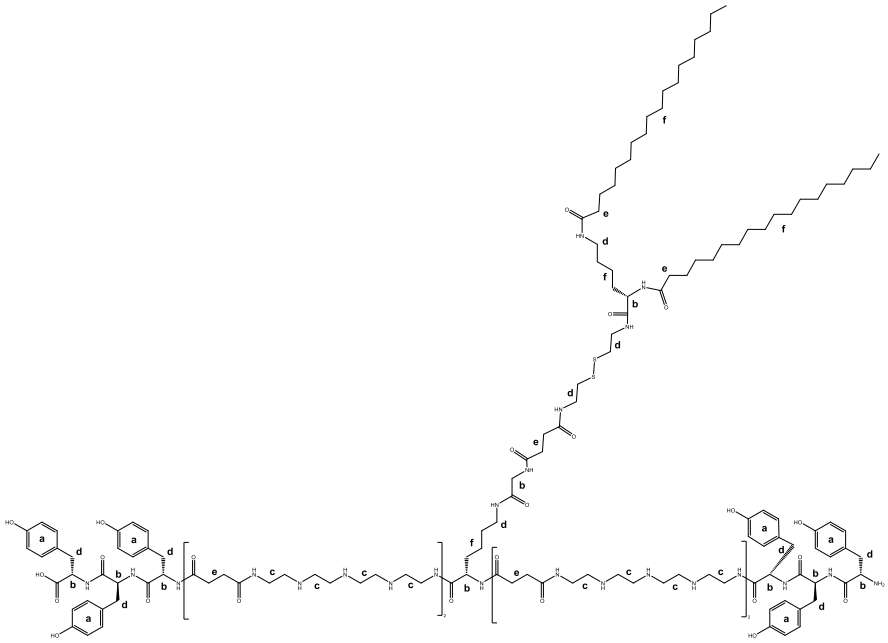

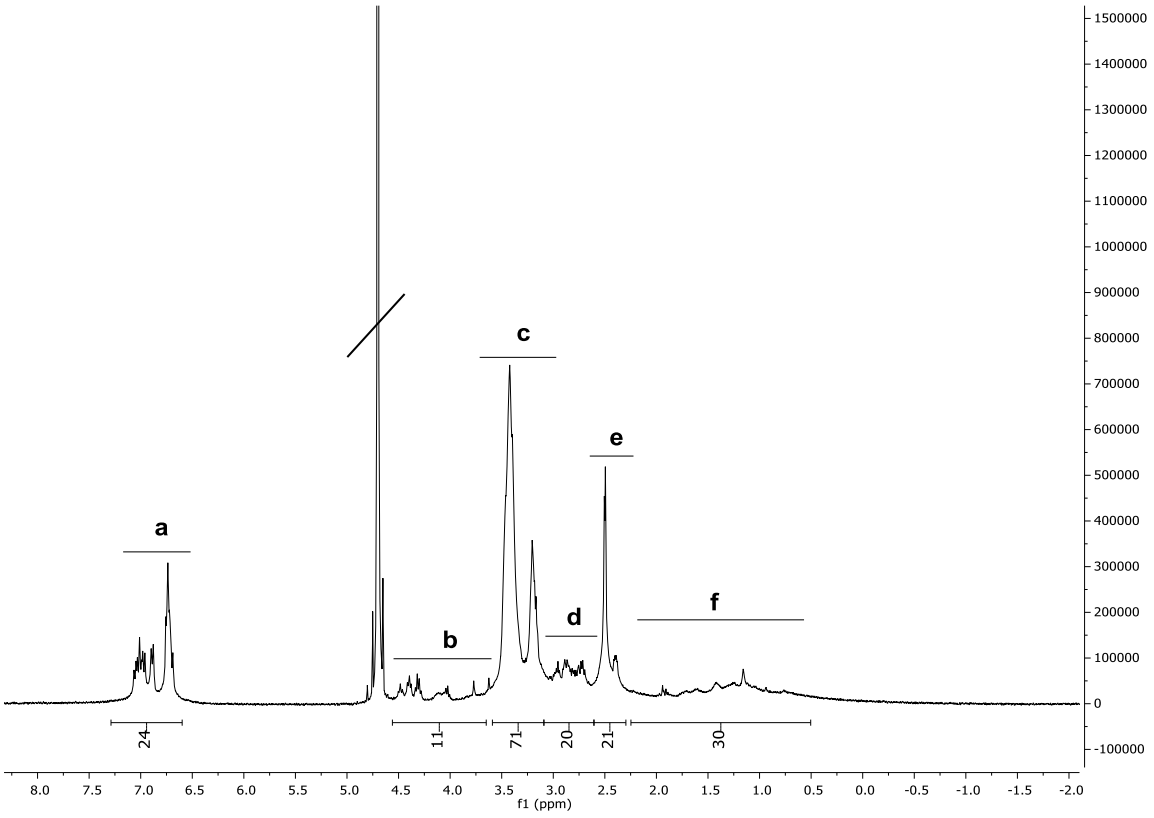

^{1}H NMR (500 MHz, Deuterium oxide) δ (ppm) = 0.50-2.25 (m, 82 H, βγδH lysine, -CH2- and -CH3 stearic acid), 2.3-2.6 (m, 24 H, -CO-CH2-CH2-CO- Stp and ssbb, -CO-CH2- stearic acid), 2.6-3.1 (m, 24 H, εH lysine and tyrosine, -CH2- ssbb), 3.1-3.6 (m, 64 H, -CH2- Tp), 3.65-4.55 (m, 10 H, αH amino acids), 6.6-7.3 (m, 24 H, -CH- tyrosine).

991: Sequence (C→N): Y_3-Stp_2-K-ε[G-K-α,ε$(CholA)_2$]αStp_2-Y_3

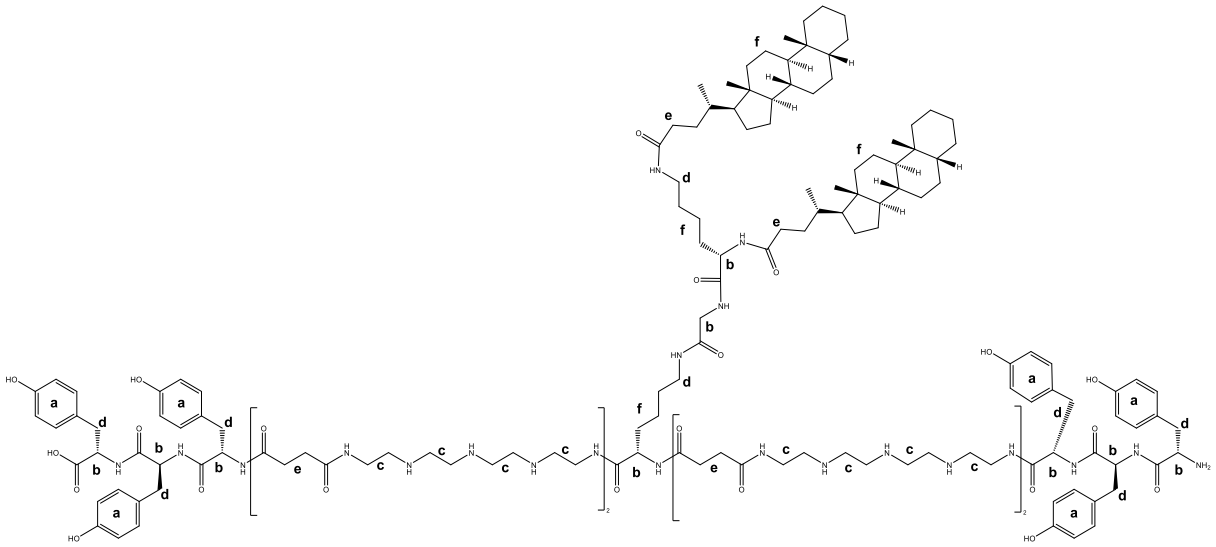

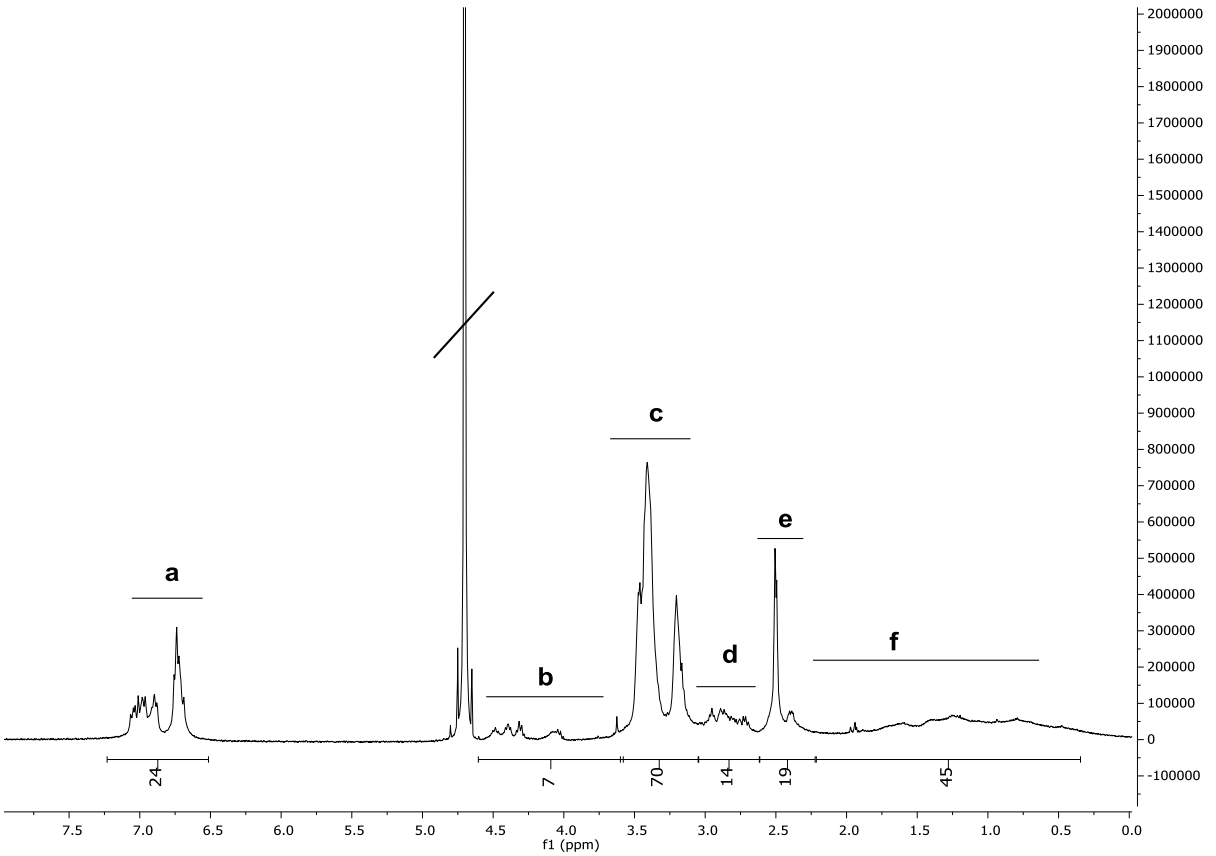

^{1}H NMR (500 MHz, Deuterium oxide) δ (ppm) = 0.35-2.20 (m, 88 H, βγδH lysine, cholanic acid), 2.2-2.6 (m, 20 H, -CO-CH2-CH2-CO- Stp, -CO-CH2- cholanic acid), 2.6-3.05 (m, 16 H, εH lysine and tyrosine), 3.05-3.60 (m, 64 H, -CH2- Tp), 3.60-4.60 (m, 10 H, αH amino acids), 6.50-7.25 (m, 24 H, -CH- tyrosine).

***992*:** Sequence (C→N): Y_3-Stp_2-K-ε[G-ssbb-K-α,ε$(CholA)_2$]αStp_2-Y_3

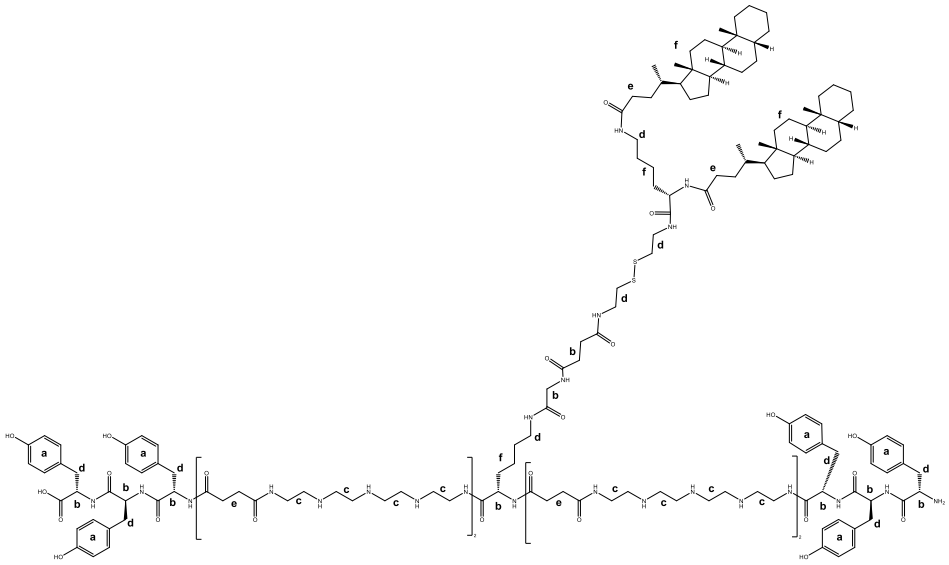

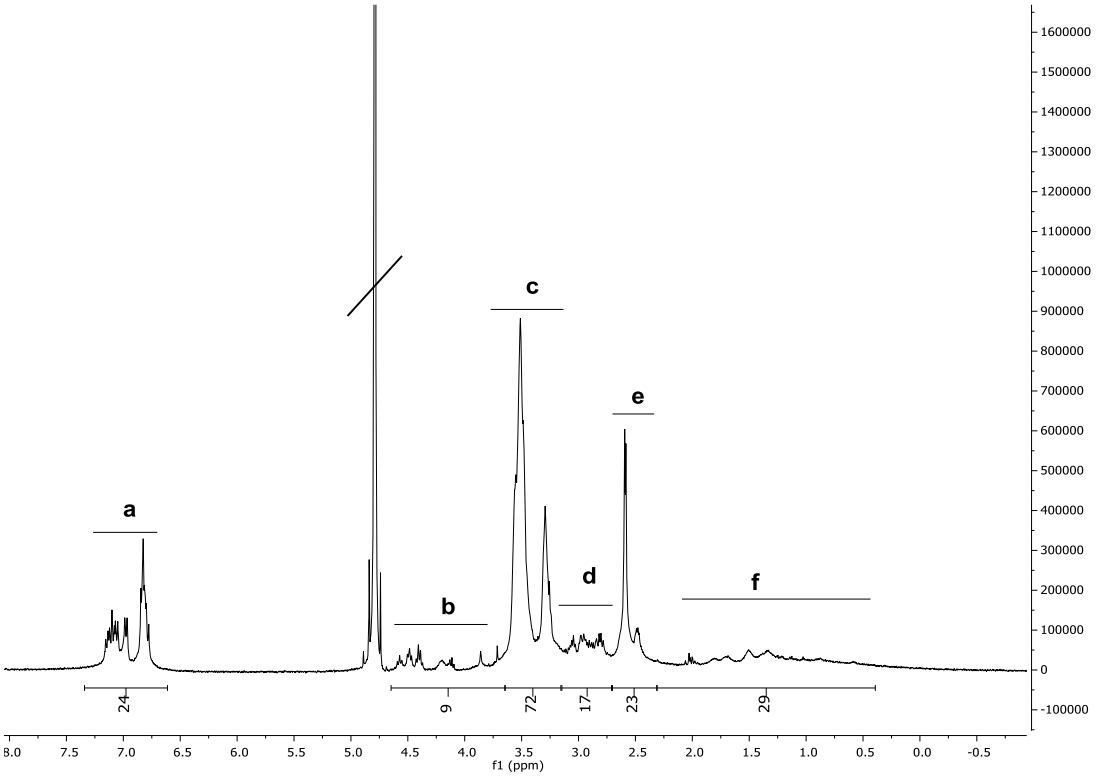

^{1}H NMR (500 MHz, Deuterium oxide) δ (ppm) = 0.40-2.30 (m, 88 H, βγδH lysine, cholanic acid), 2.3-2.7 (m, 24 H, -CO-CH2-CH2-CO- Stp and ssbb, -CO-CH2- cholanic acid), 2.70-3.15 (m, 24 H, εH lysine and tyrosine, -CH2- ssbb), 3.15-3.80 (m, 64 H, -CH2- Tp), 3.65-4.65 (m, 10 H, αH amino acids), 6.60-7.35 (m, 24 H, -CH- tyrosine).

1081

Sequence (C→N): Y_3-Stp_2-K-ε[G-K-α,ε$(MyrA)_2$]αStp_2-Y_3

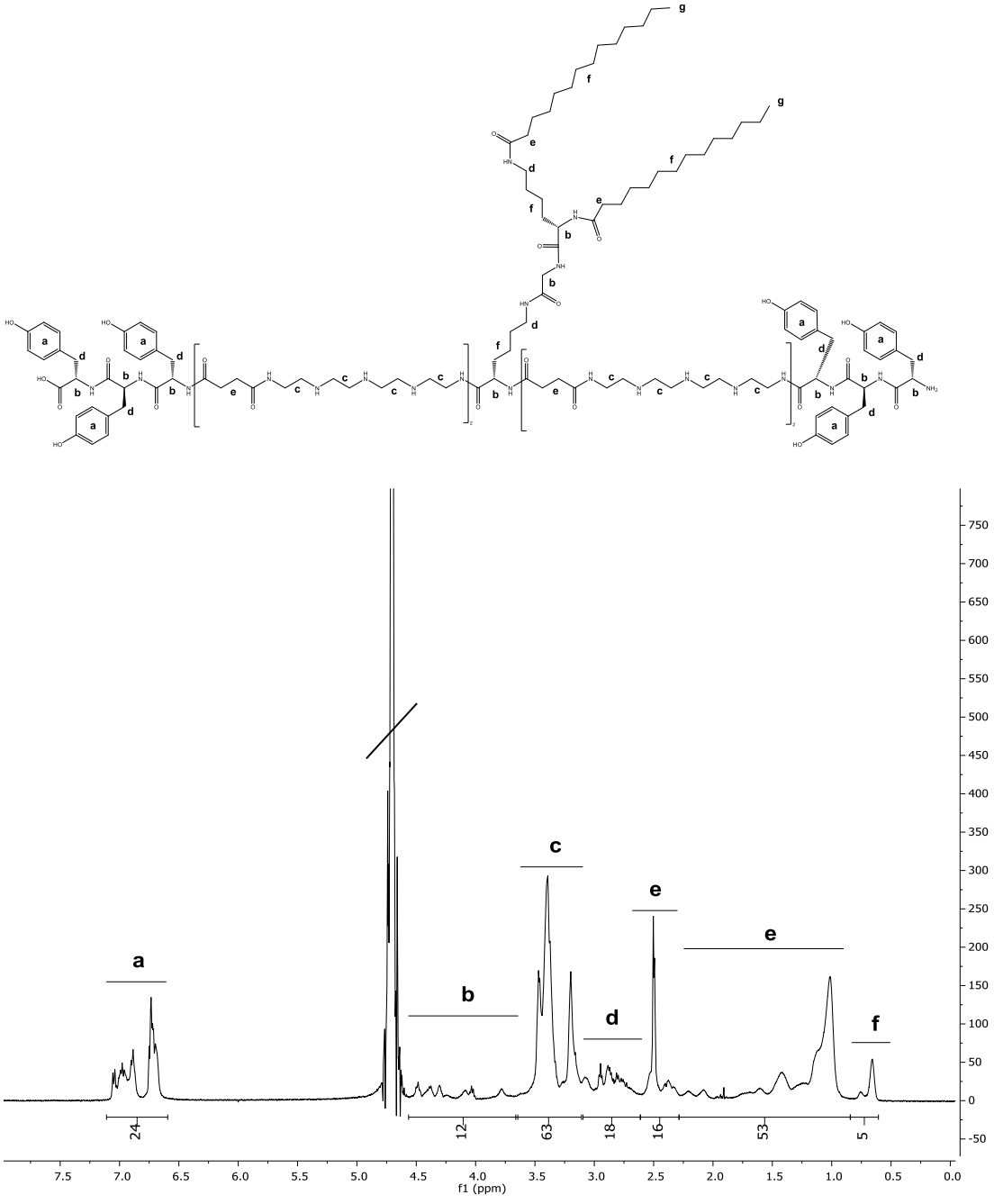

^{1}H NMR (500 MHz, Deuterium oxide) δ (ppm) = 0.60-0.85 (s, 6 H, -CH3 myristic acid), 0.85-2.30 (m, 56 H, βγδH lysine, myristic acid), 2.3-2.6 (m, 20 H, -CO-CH2-CH2-CO-Stp, -CO-CH2- myristic acid), 2.6-3.10 (m, 16 H, εH lysine and tyrosine), 3.10-3.65 (m, 64 H, -CH2- Tp), 3.65-4.55 (m, 10 H, αH amino acids), 6.60-7.10 (m, 24 H, -CH-tyrosine).

1082

Sequence (C→N): Y_3-Stp_2-K-ε[G-ssbb-K-α,ε$(MyrA)_2$]αStp_2-Y_3

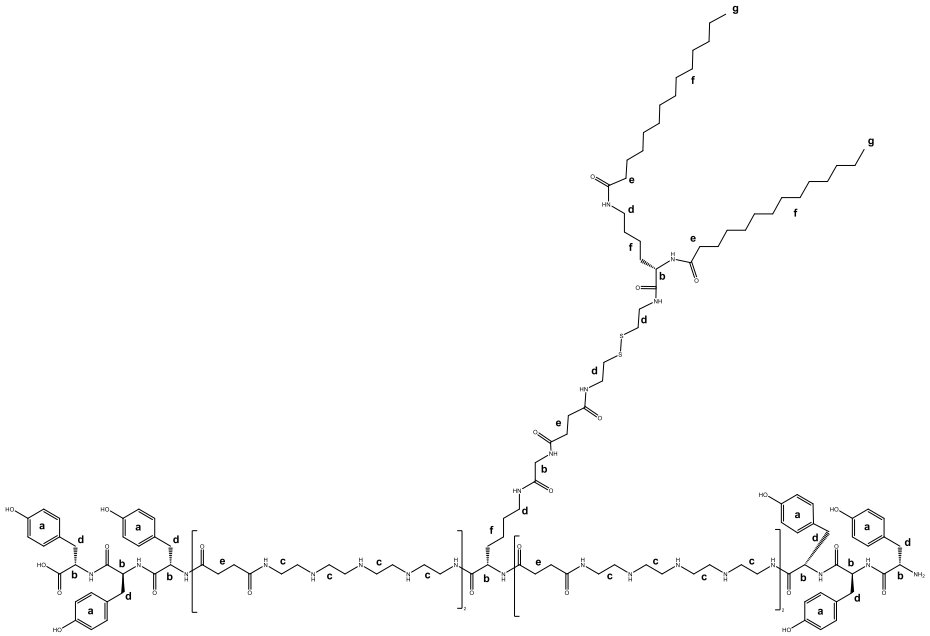

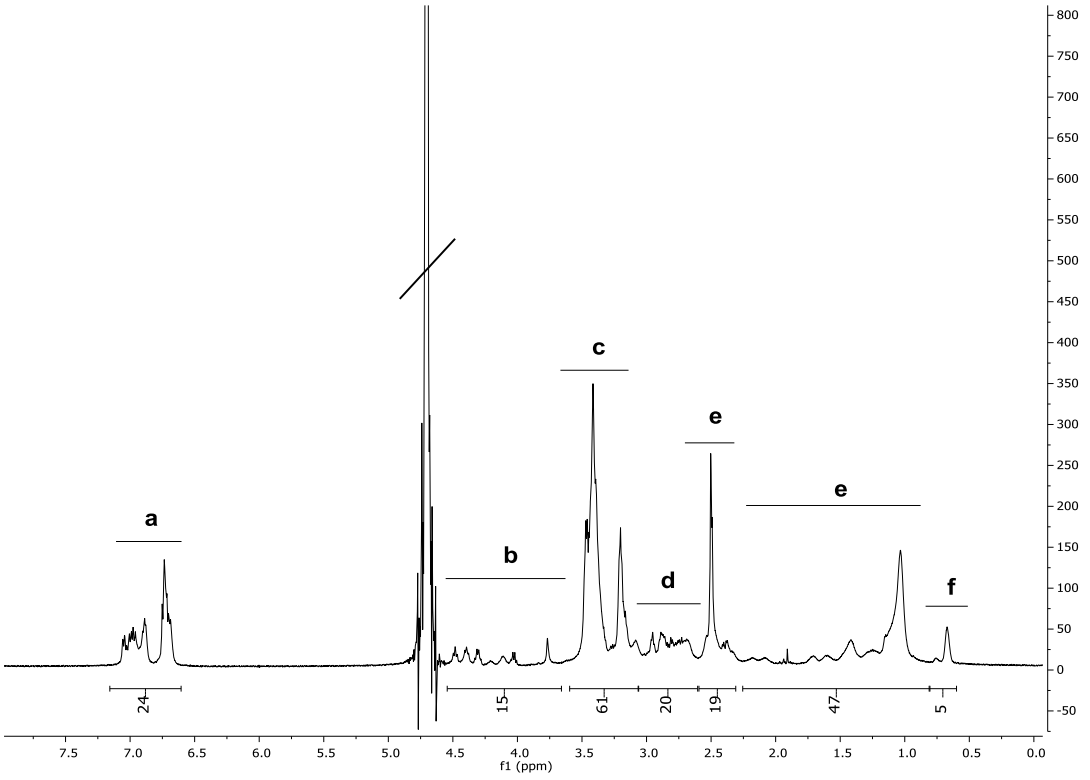

^{1}H NMR (500 MHz, Deuterium oxide) δ (ppm) = 0.60-0.80 (s, 6 H, -CH3 myristic acid), 0.80-2.25 (m, 56 H, βγδH lysine, myristic acid), 2.3-2.6 (m, 24 H, -CO-CH2-CH2-CO- Stp and ssbb, -CO-CH2- myristic acid), 2.60-3.05 (m, 24 H, εH lysine and tyrosine, -CH2- ssbb), 3.05-3.60 (m, 64 H, -CH2- Tp), 3.65-4.55 (m, 10 H, αH amino acids), 6.60-7.15 (m, 24 H, -CH- tyrosine).

1107

Sequence (C→N): Y_3-Stp_2-K-ε[G-K-α,ε$(OleA)_2$]αStp_2-Y_3

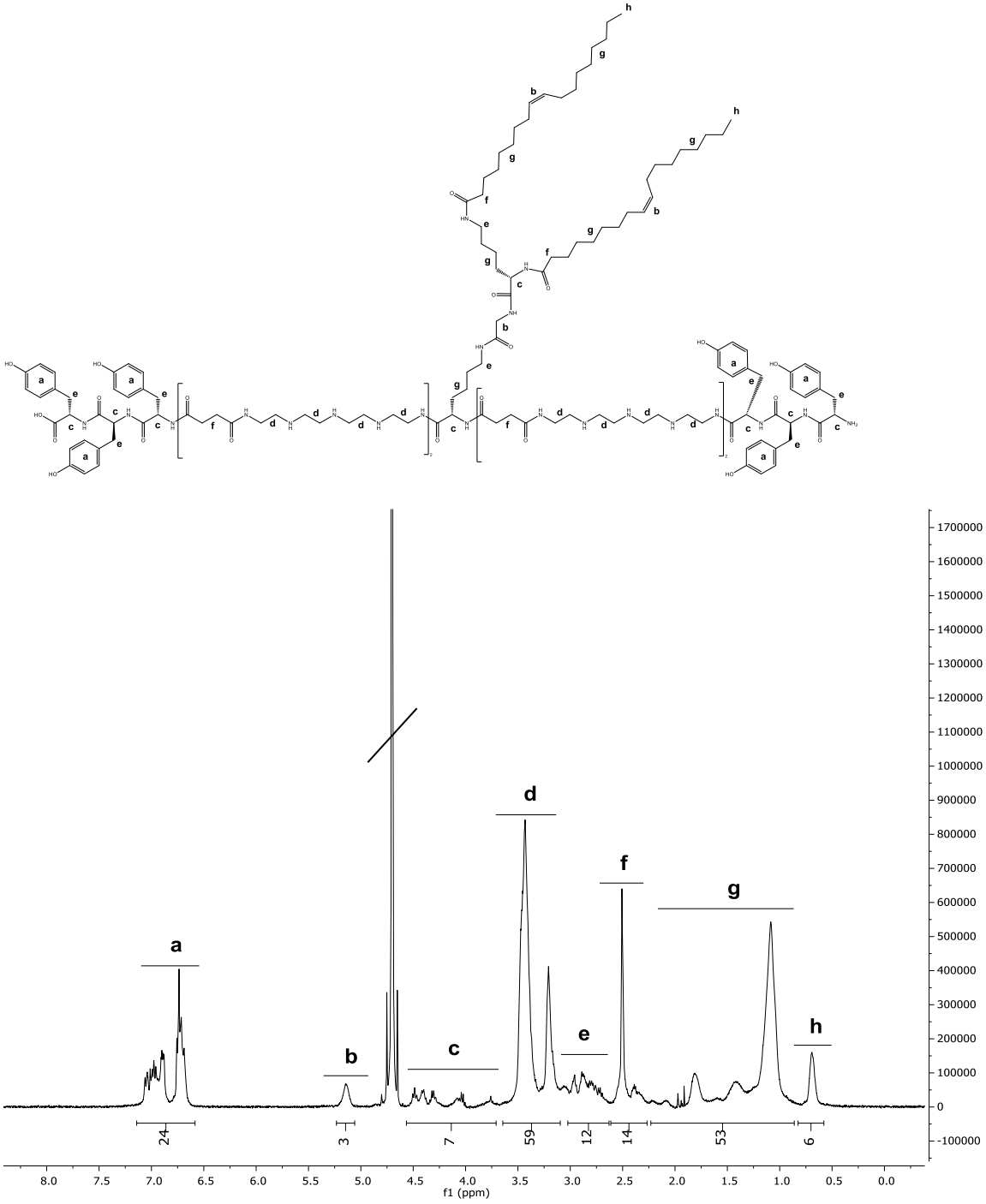

^{1}H NMR (500 MHz, Deuterium oxide) δ (ppm) = 0.60-0.85 (s, 6 H, -CH3 oleic acid), 0.85-2.25 (m, 72 H, βγδH lysine, -CH_2- oleic acid), 2.25-2.60 (m, 20 H, -CO-CH_2-CH_2-CO- Stp, -CO-CH2- oleic acid), 2.65-3.1 (m, 16 H, εH lysine and tyrosine), 3.1-3.65 (m, 64 H, -CH2- Tp), 3.70-4.55 (m, 10 H, αH amino acids), 5.05 – 5.25 (s, 4 H, -CH=CH- oleic acid), 6.60 -7.15 (m, 24 H, -CH- tyrosine).

1108

Sequence (C→N): Y_3-Stp_2-K-ε[G-ssbb-K-α,ε$(OleA)_2$]αStp_2-Y_3

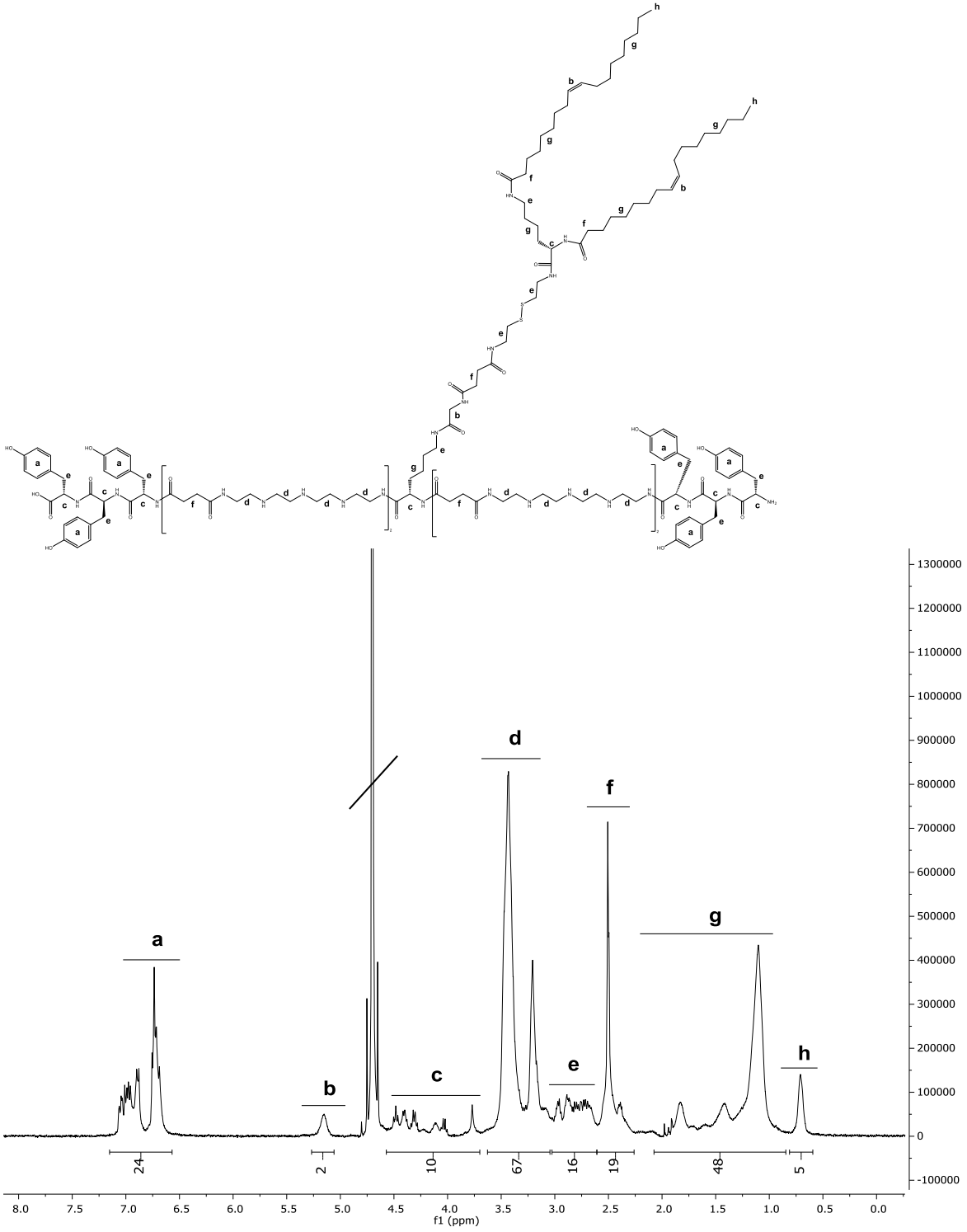

^{1}H NMR (500 MHz, Deuterium oxide) δ (ppm) = 0.60-0.80 (s, 6 H, -CH_3 oleic acid), 0.85-2.10 (m, 72 H, βγδH lysine, -CH_2- oleic acid), 2.25-2.60 (m, 22 H, -CO-CH_2-CH_2-CO- Stp, -CO-CH_2- oleic acid), 2.60-3.0 (m, 22 H, εH lysine and tyrosine), 3.05-3.65 (m, 64 H, -CH2- Tp), 3.70-4.60 (m, 10 H, αH amino acids), 5.00 – 5.25 (s, 4 H, -CH=CH- oleic acid), 6.55 -7.15 (m, 24 H, -CH- tyrosine).

My

Sequence (N→C): Y_3-Stp_2-K-ε[K-α,ε$(MyrA)_2$]Stp_2-Y_3

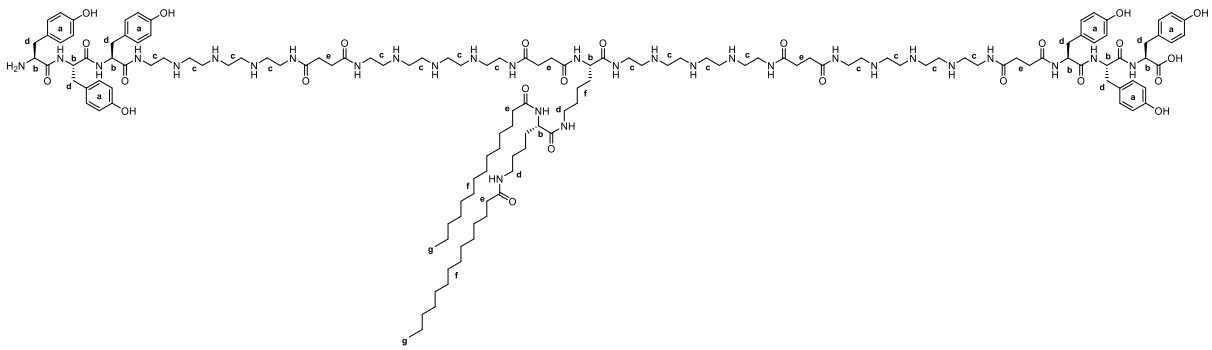

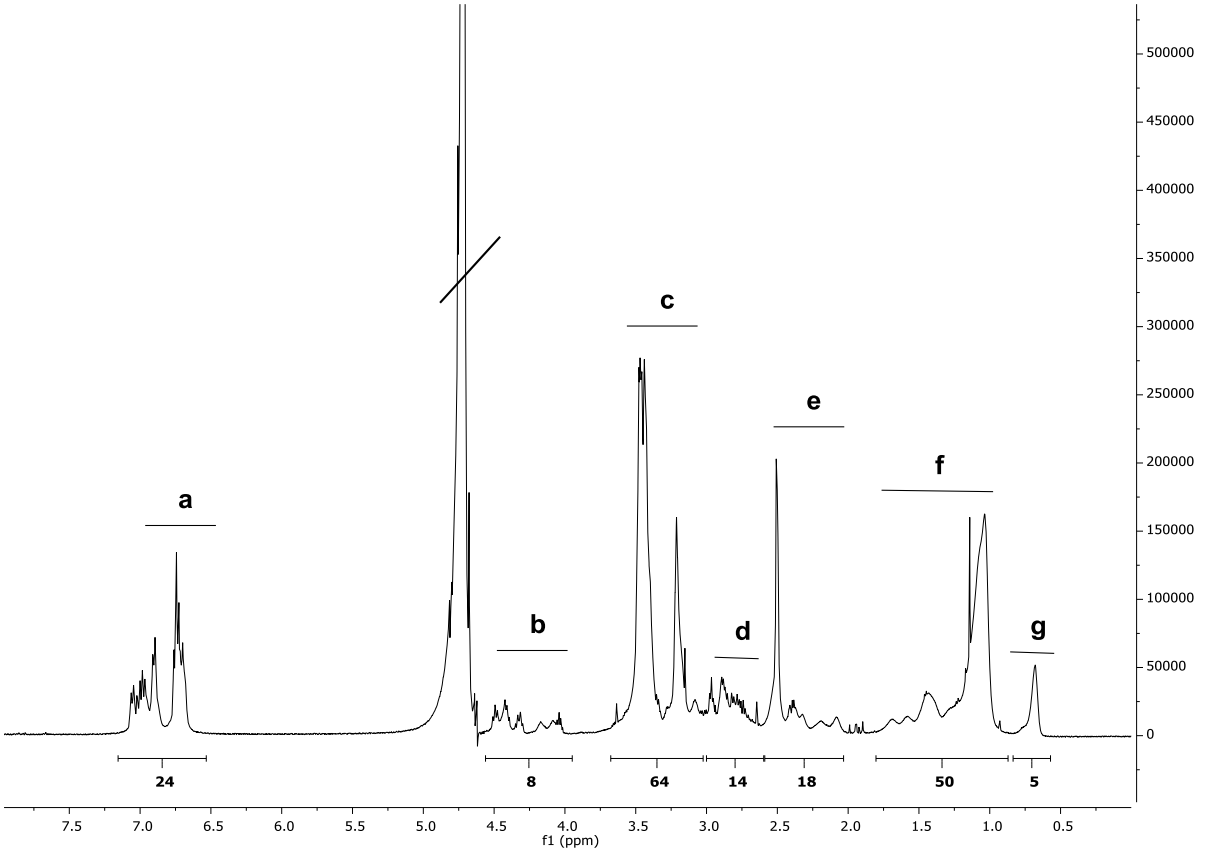

^{1}H NMR (500 MHz, Deuterium oxide) δ (ppm) = 0.57-0.84 (s, 6 H, -CH_3 myristic acid), 0.87-1.8 (m, 56 H, βγδH lysine, -CH_2- myristic acid), 2.0 -2.6 (m, 20 H, -CO-CH_2-CH_2-CO- Stp, -CO-CH_2- myristic acid), 2.6-3.0 (m, 16 H, εH lysine, βH tyrosine), 3.0-3.7 (m, 64 H, -CH_2- tepa), 3.9-4.6 (m, 8 H, αH amino acids), 6.5-7.2 (m, 24 H, -CH- tyrosine).

My-R

Sequence (N→C): Y_3-Stp_2-K-ε[R-K-α,ε(MyrA)2]Stp_2-Y_3

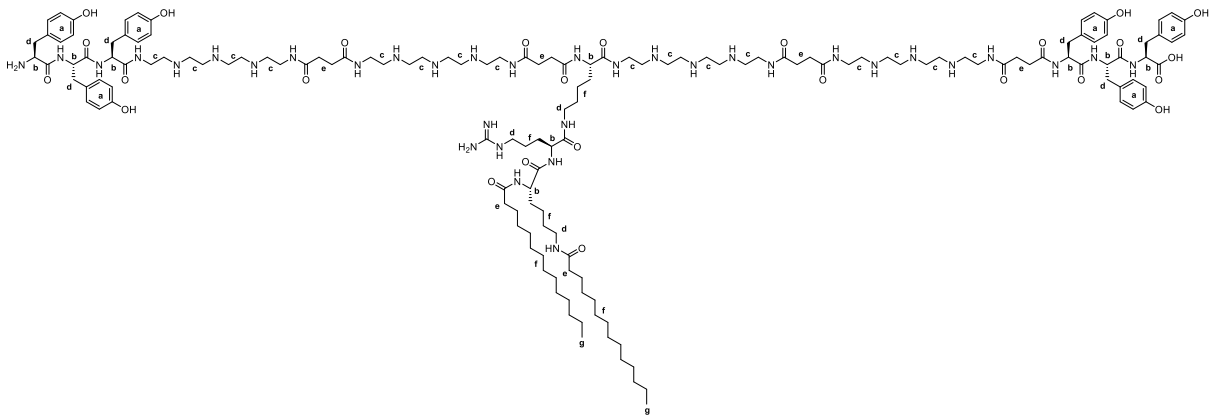

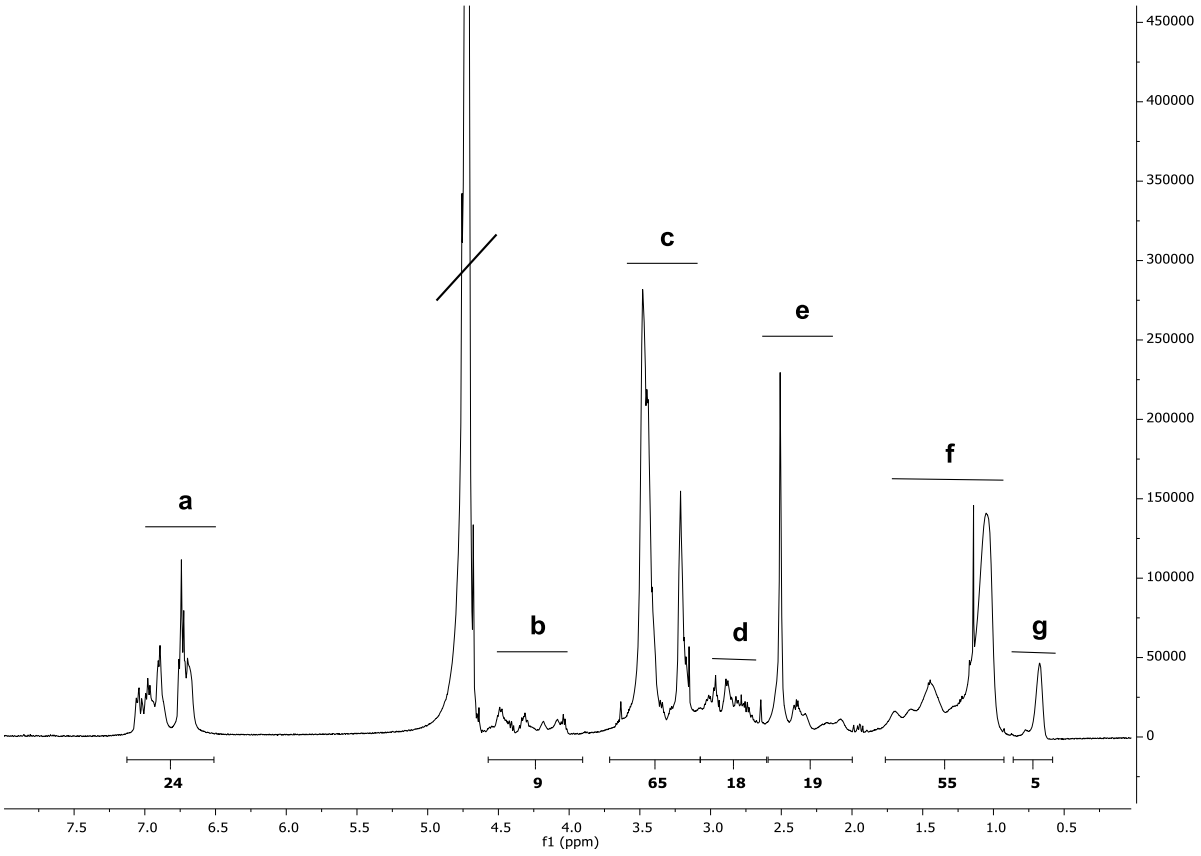

^{1}H NMR (500 MHz, Deuterium oxide) δ (ppm) = 0.58-0.86 (s, 6 H, -CH_3 myristic acid), 0.93-1.8 (m, 60 H, βγδH lysine, βγH arginine, -CH_2- myristic acid), 2.0 -2.6 (m, 20 H, -CO-CH_2-CH_2-CO- Stp, -CO-CH_2- myristic acid), 2.6-3.1 (m, 18 H, εH lysine, δH arginine, βH tyrosine), 3.1-3.7 (m, 64 H, -CH_2- tepa), 3.9-4.6 (m, 9 H, αH amino acids), 6.5-7.1 (m, 24 H, -CH- tyrosine).

My-r

Sequence (N→C): Y_3-Stp_2-K-ε[r-K-α,ε$(MyrA)_2$]Stp_2-Y_3

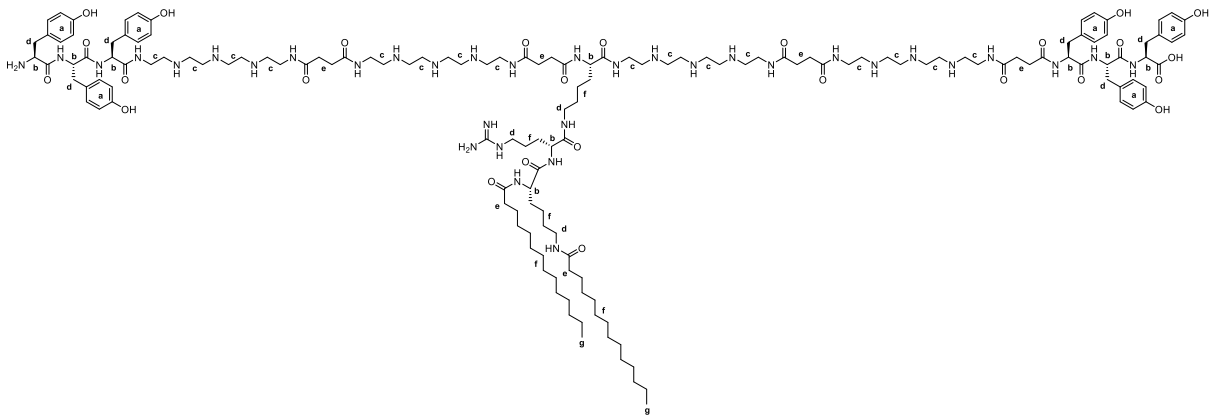

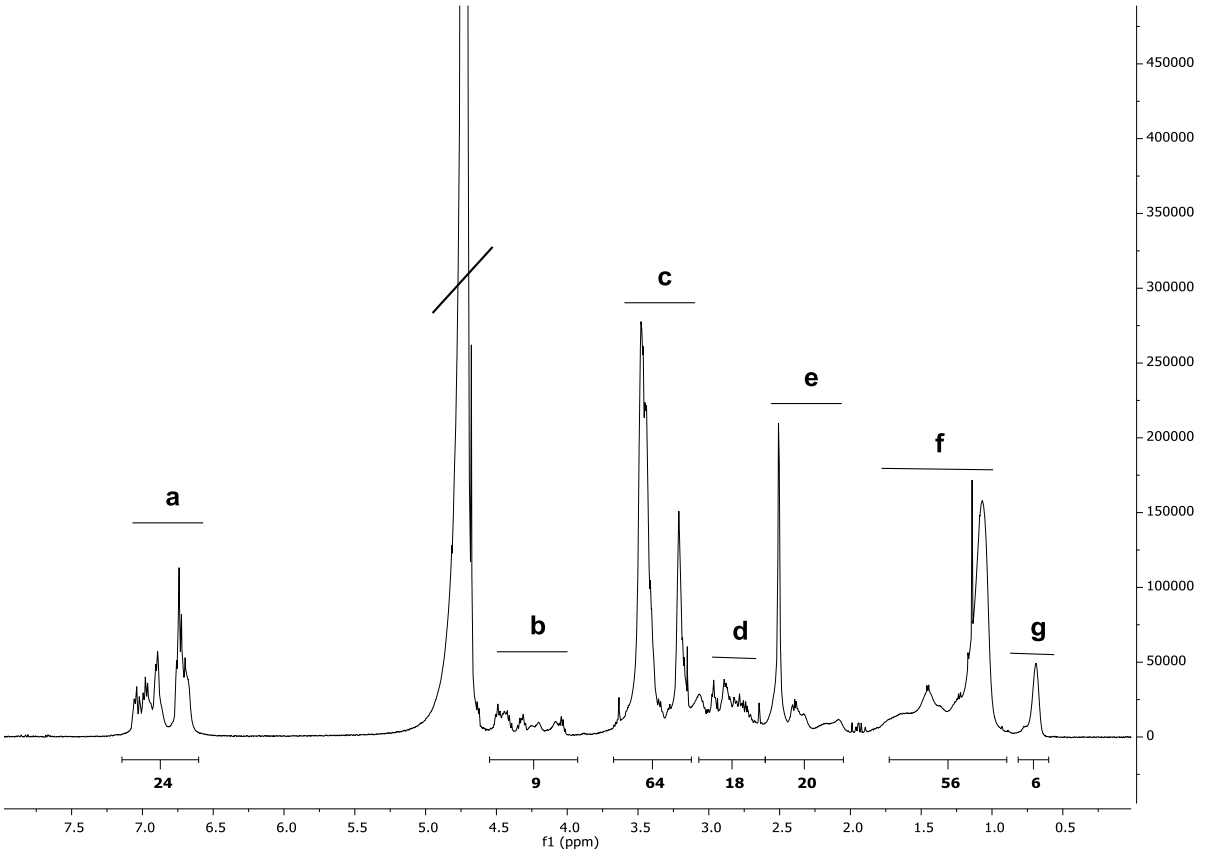

^{1}H NMR (500 MHz, Deuterium oxide) δ (ppm) = 0.60-0.82 (s, 6 H, -CH_3 myristic acid), 0.90-1.7 (m, 60 H, βγδH lysine, βγH arginine, -CH_2- myristic acid), 2.0 -2.6 (m, 20 H, -CO-CH_2-CH_2-CO- Stp, -CO-CH_2- myristic acid), 2.6-3.1 (m, 18 H, εH lysine, δH arginine, βH tyrosine), 3.1-3.7 (m, 64 H, -CH_2- tepa), 3.9-4.5 (m, 9 H, αH amino acids), 6.6-7.1 (m, 24 H, -CH- tyrosine).

My-RR

Sequence (N→C): Y_3-Stp_2-K-ε[**RR**-K-α,ε$(MyrA)_2$]Stp_2-Y_3

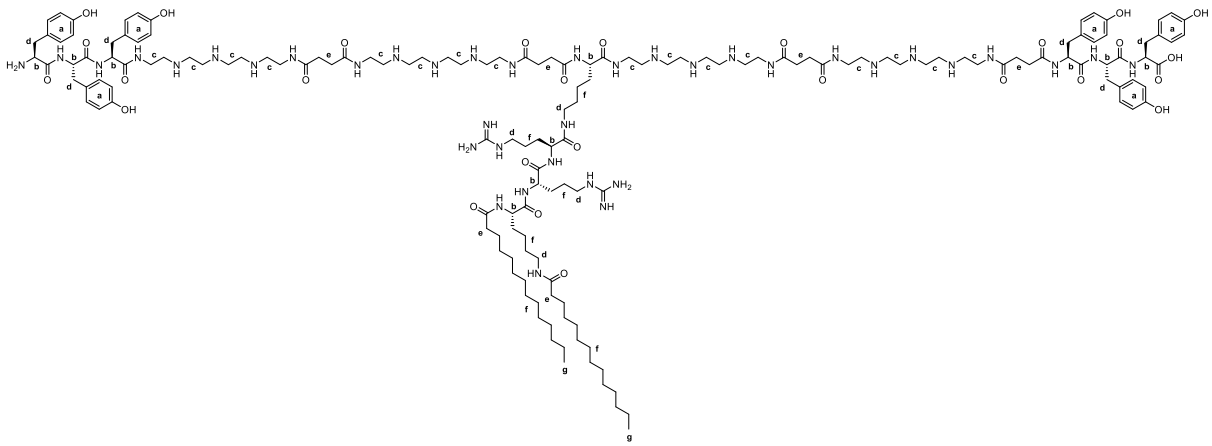

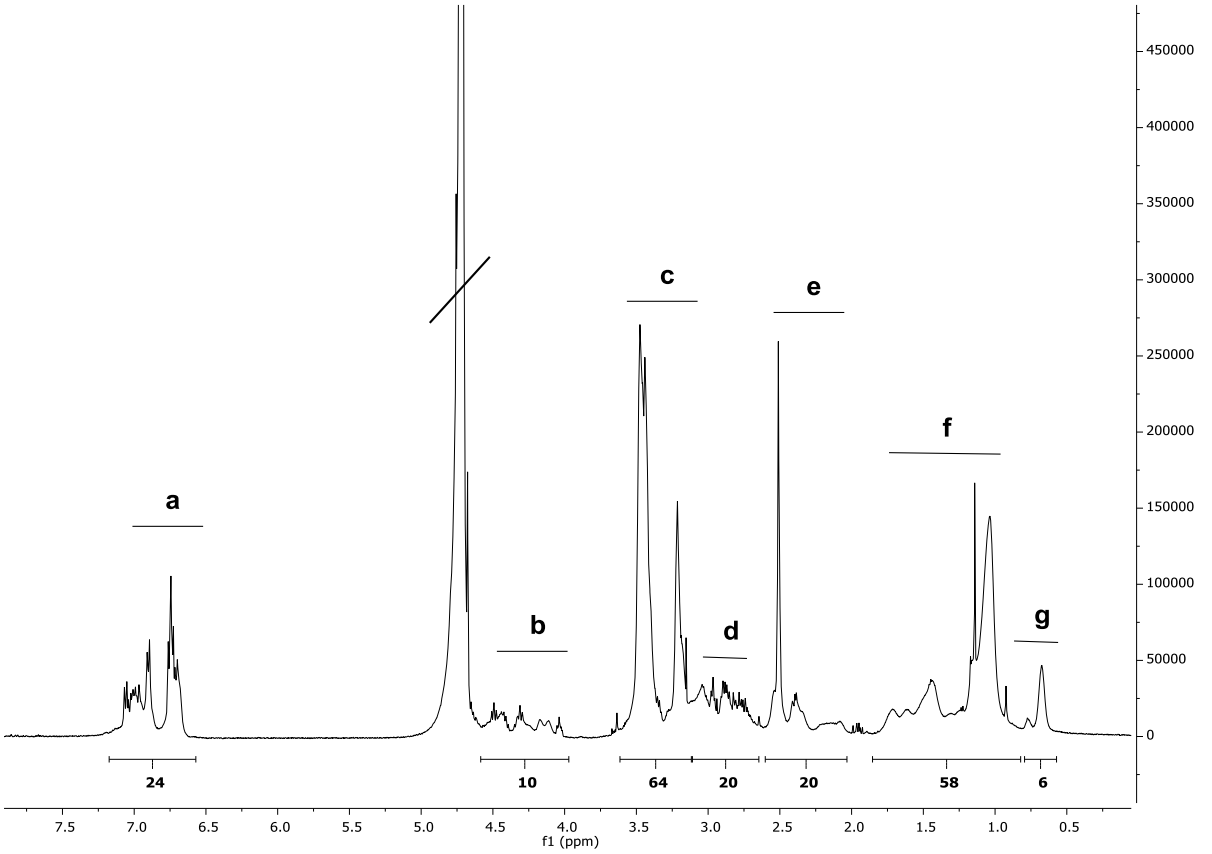

^{1}H NMR (500 MHz, Deuterium oxide) δ (ppm) = 0.57-0.79 (s, 6 H, -CH_3 myristic acid), 0.82-1.9 (m, 64 H, βγδH lysine, βγH arginine, -CH_2- myristic acid), 2.0 -2.6 (m, 20 H, -CO-CH_2-CH_2-CO- Stp, -CO-CH_2- myristic acid), 2.6-3.1 (m, 20 H, εH lysine, δH arginine, βH tyrosine), 3.1-3.6 (m, 64 H, -CH_2- tepa), 4.0-4.6 (m, 10 H, αH amino acids), 6.6-7.2 (m, 24 H, -CH- tyrosine).

R-My

Sequence (N→C): Y_3-Stp_2-**R**-K-ε[K-α,ε$(MyrA)_2$]**R**-Stp_2-Y_3

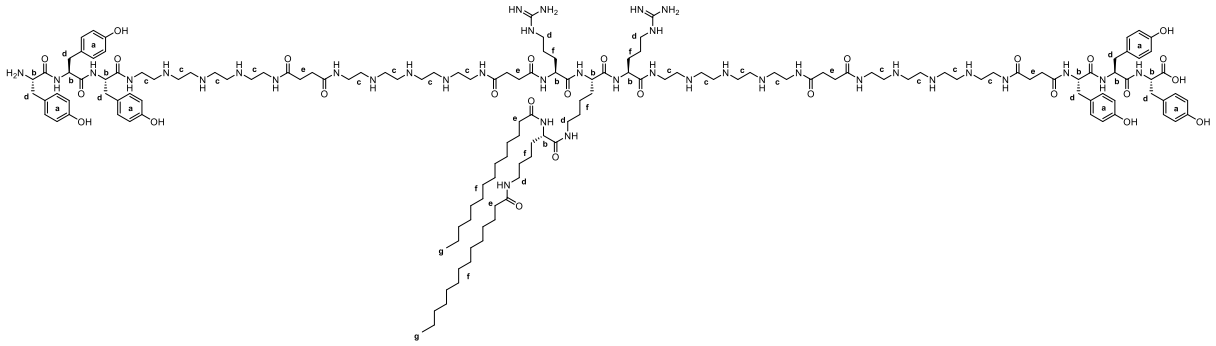

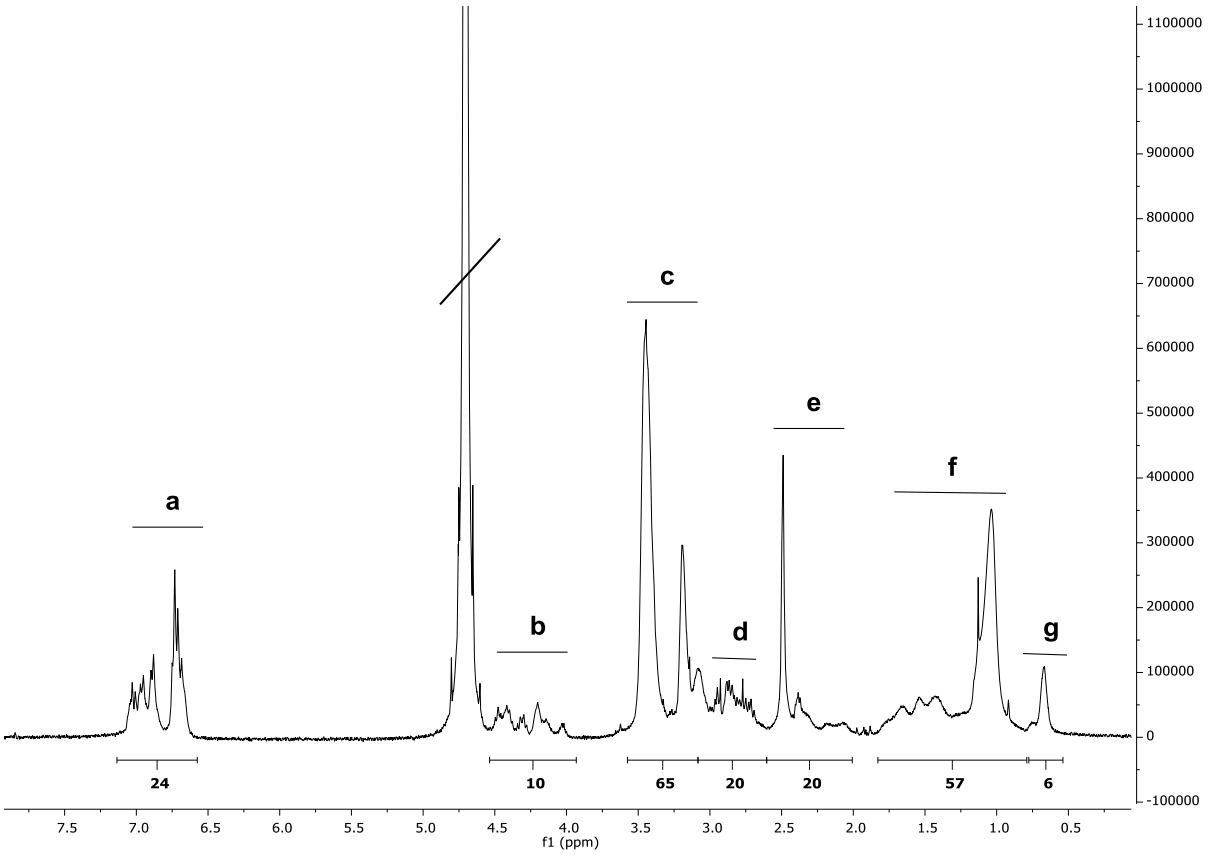

^{1}H NMR (500 MHz, Deuterium oxide) δ (ppm) = 0.54-0.78 (s, 6 H, -CH_3 myristic acid), 0.79-1.8 (m, 64 H, βγδH lysine, βγH arginine, -CH_2- myristic acid), 2.0 -2.6 (m, 20 H, -CO-CH_2-CH_2-CO- Stp, -CO-CH_2- myristic acid), 2.6-3.1 (m, 20 H, εH lysine, δH arginine, βH tyrosine), 3.1-3.6 (m, 64 H, -CH_2- tepa), 3.9-4.5 (m, 10 H, αH amino acids), 6.6-7.1 (m, 24 H, -CH- tyrosine).

R-My-R

Sequence (N→C): Y_3-Stp_2-**R**-K-ε[**R**-K-α,ε$(MyrA)_2$]**R**-Stp_2-Y_3

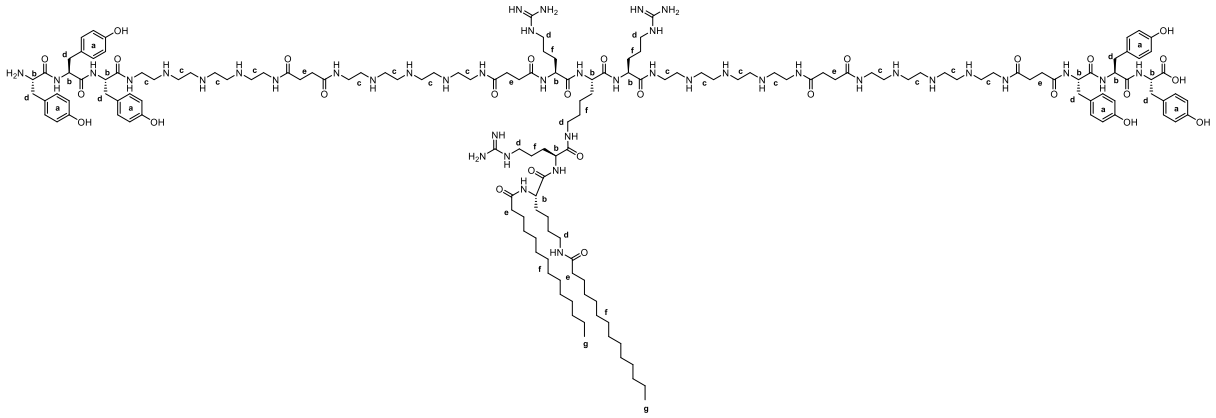

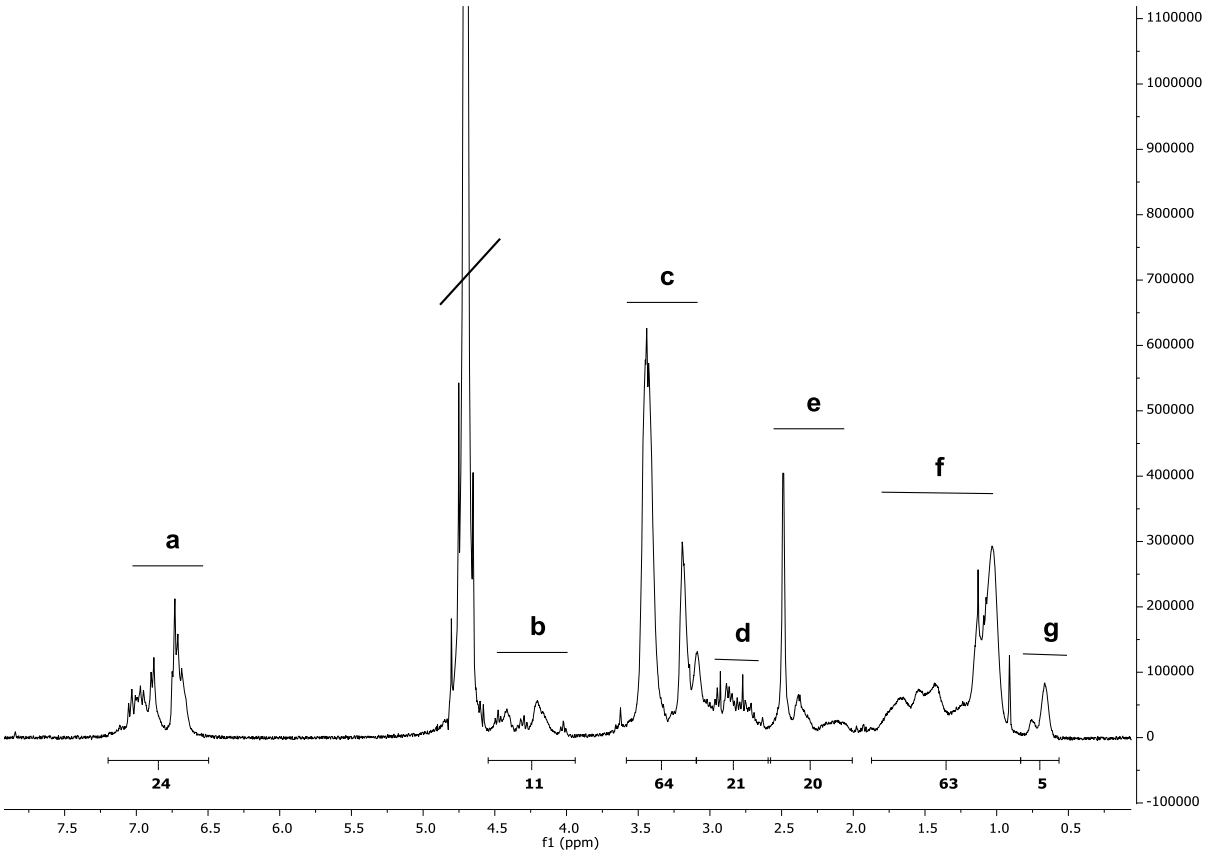

^{1}H NMR (500 MHz, Deuterium oxide) δ (ppm) = 0.57-0.83 (s, 6 H, -CH_3 myristic acid), 0.83-1.9 (m, 68 H, βγδH lysine, βγH arginine, -CH_2- myristic acid), 2.0 -2.6 (m, 20 H, -CO-CH_2-CH_2-CO- Stp, -CO-CH_2- myristic acid), 2.6-3.1 (m, 22 H, εH lysine, δH arginine, βH tyrosine), 3.1-3.6 (m, 64 H, -CH_2- tepa), 3.9-4.5 (m, 11 H, αH amino acids), 6.5-7.2 (m, 24 H, -CH- tyrosine).

R-My-r

Sequence (N→C): Y_3-Stp_2-**R**-K-ε[**r**-K-α,ε$(MyrA)_2$]**R**-Stp_2-Y_3

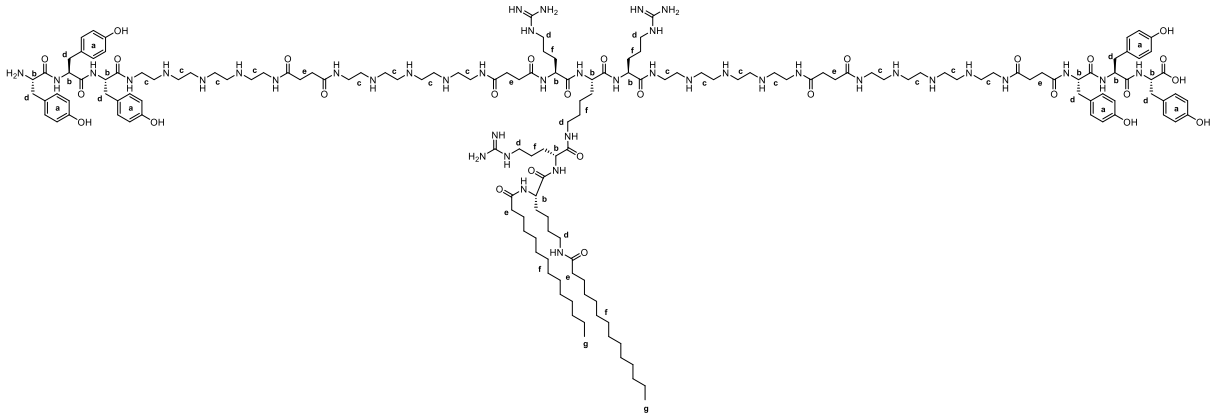

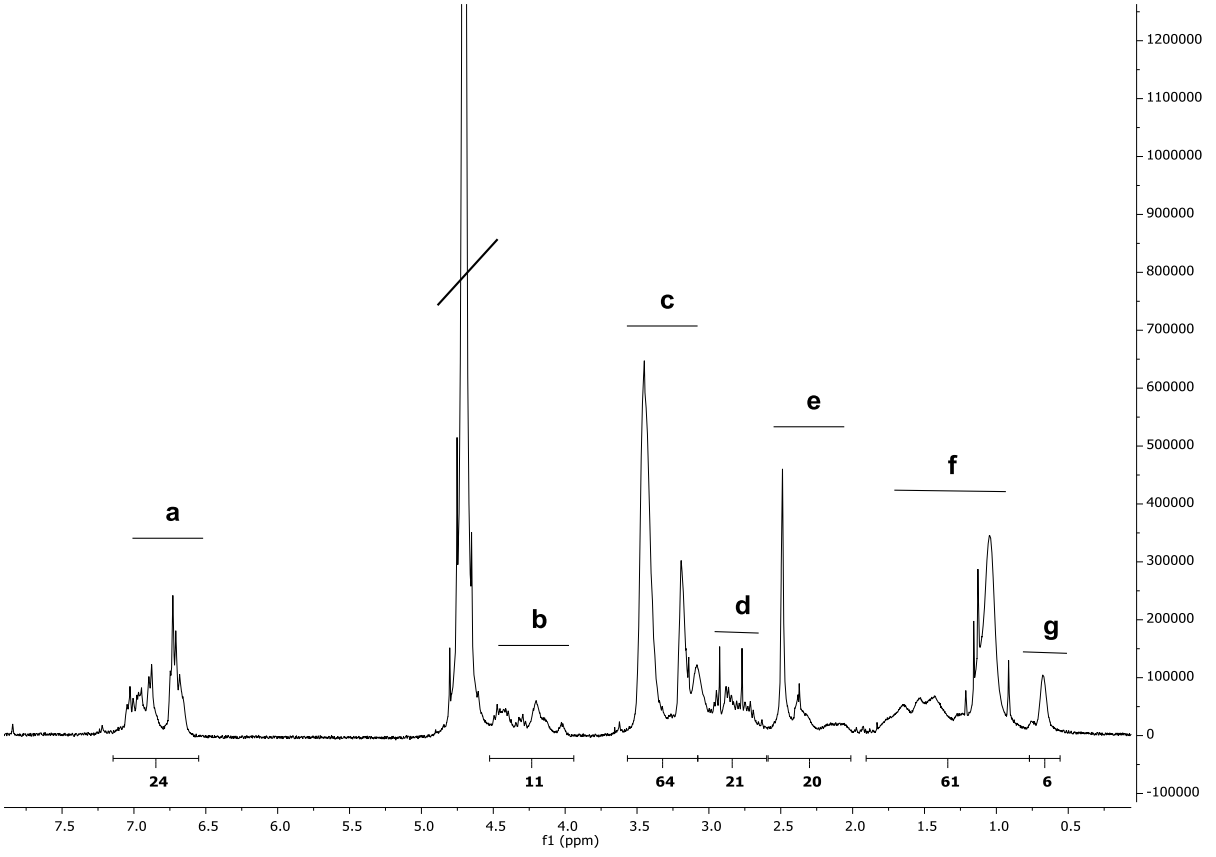

^{1}H NMR (500 MHz, Deuterium oxide) δ (ppm) = 0.56-0.72 (s, 6 H, -CH_3 myristic acid), 0.77-1.9 (m, 68 H, βγδH lysine, βγH arginine, -CH_2- myristic acid), 2.0 -2.6 (m, 20 H, -CO-CH_2-CH_2-CO- Stp, -CO-CH_2- myristic acid), 2.6-3.1 (m, 22 H, εH lysine, δH arginine, βH tyrosine), 3.1-3.6 (m, 64 H, -CH_2- tepa), 3.9-4.5 (m, 11 H, αH amino acids), 6.6-7.1 (m, 24 H, -CH- tyrosine).

r-My

Sequence (N→C): Y_3-Stp_2-**r**-K-ε[K-α,ε$(MyrA)_2$]**r**-Stp_2-Y_3

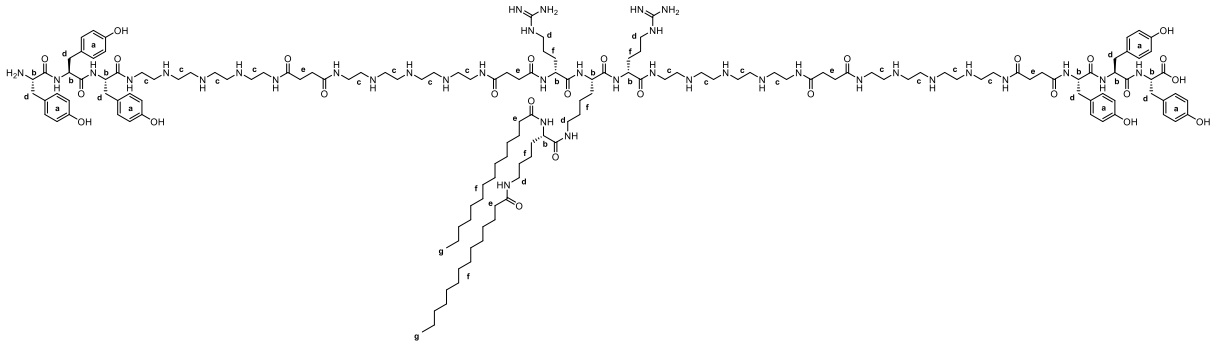

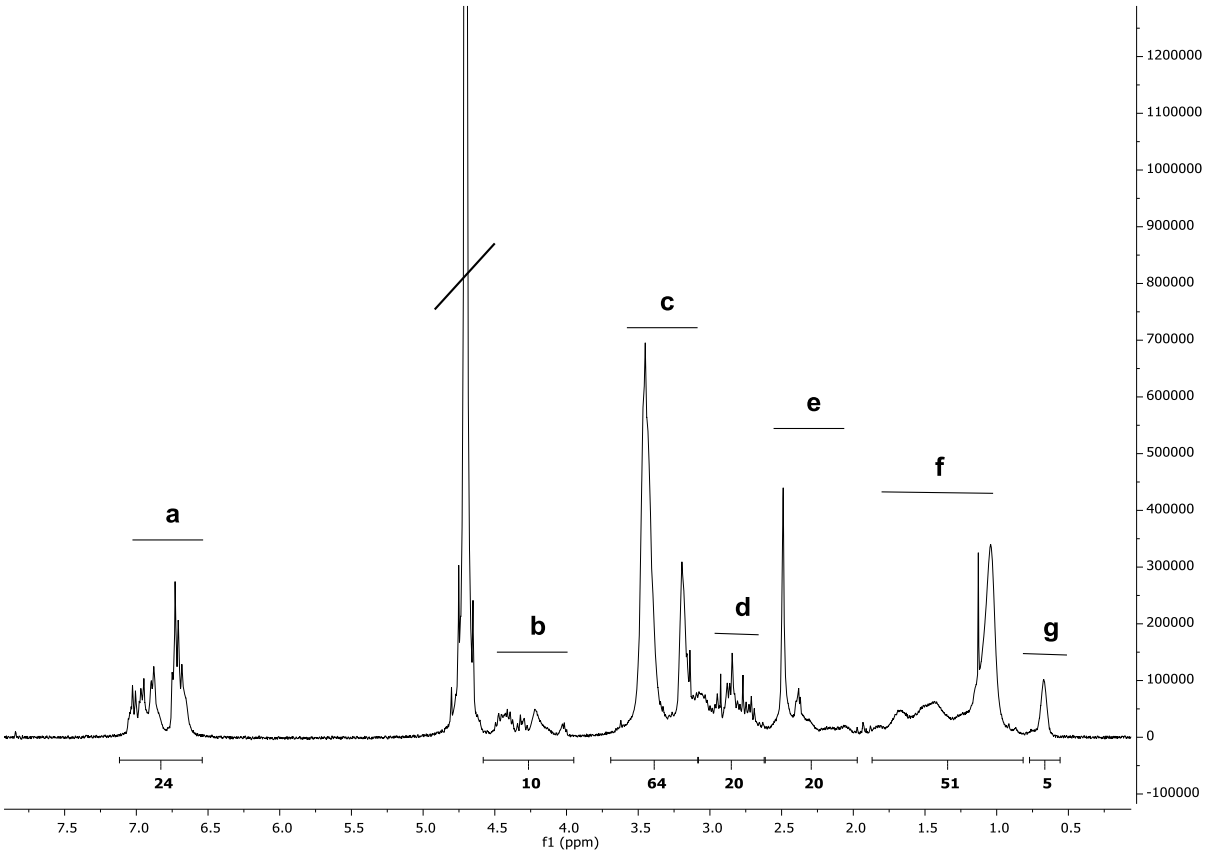

^{1}H NMR (500 MHz, Deuterium oxide) δ (ppm) = 0.56-0.77 (s, 6 H, -CH_3 myristic acid), 0.82-1.9 (m, 64 H, βγδH lysine, βγH arginine, -CH_2- myristic acid), 2.0 -2.6 (m, 20 H, -CO-CH_2-CH_2-CO- Stp, -CO-CH_2- myristic acid), 2.6-3.1 (m, 20 H, εH lysine, δH arginine, βH tyrosine), 3.1-3.7 (m, 64 H, -CH_2- tepa), 3.9-4.6 (m, 10 H, αH amino acids), 6.5-7.1 (m, 24 H, -CH- tyrosine).

r-My-R

Sequence (N→C): Y_3-Stp_2-**r**-K-ε[**R**-K-α,ε$(MyrA)_2$]**r**-Stp_2-Y_3

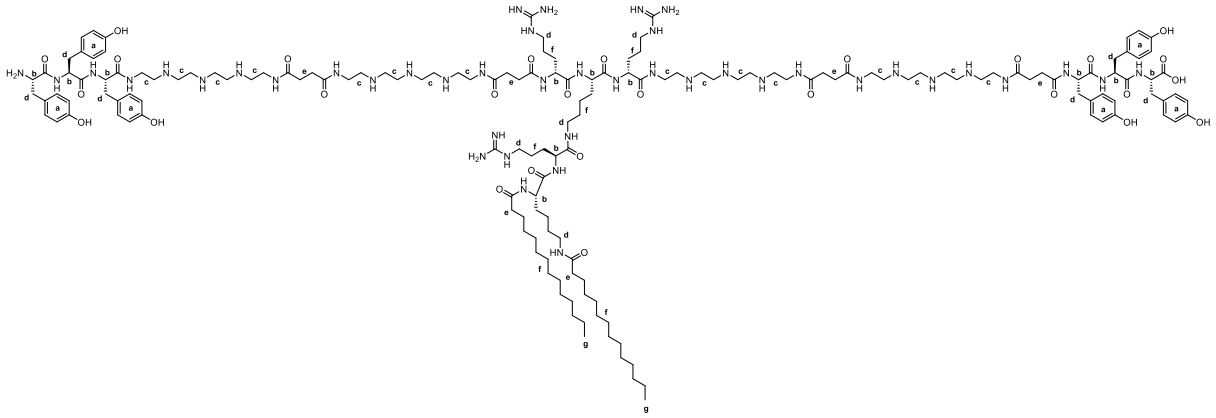

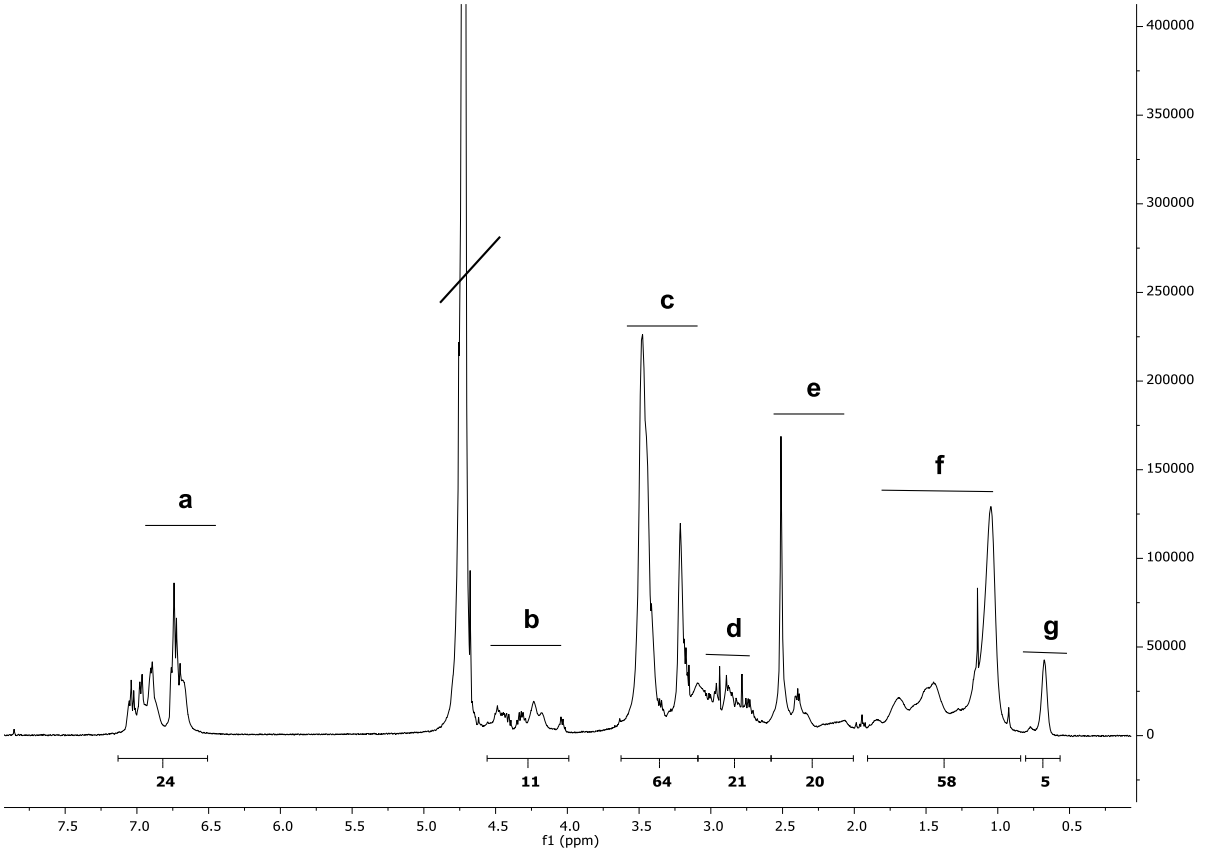

^{1}H NMR (500 MHz, Deuterium oxide) δ (ppm) = 0.57-0.81 (s, 6 H, -CH_3 myristic acid), 0.84-1.9 (m, 68 H, βγδH lysine, βγH arginine, -CH_2- myristic acid), 2.0 -2.6 (m, 20 H, -CO-CH_2-CH_2-CO- Stp, -CO-CH_2- myristic acid), 2.6-3.1 (m, 22 H, εH lysine, δH arginine, βH tyrosine), 3.1-3.6 (m, 64 H, -CH_2- tepa), 4.0-4.6 (m, 11 H, αH amino acids), 6.5-7.1 (m, 24 H, -CH- tyrosine).

r-My-r

Sequence (N→C): Y_3-Stp_2-**r**-K-ε[**r**-K-α,ε$(MyrA)_2$]**r**-Stp_2-Y_3

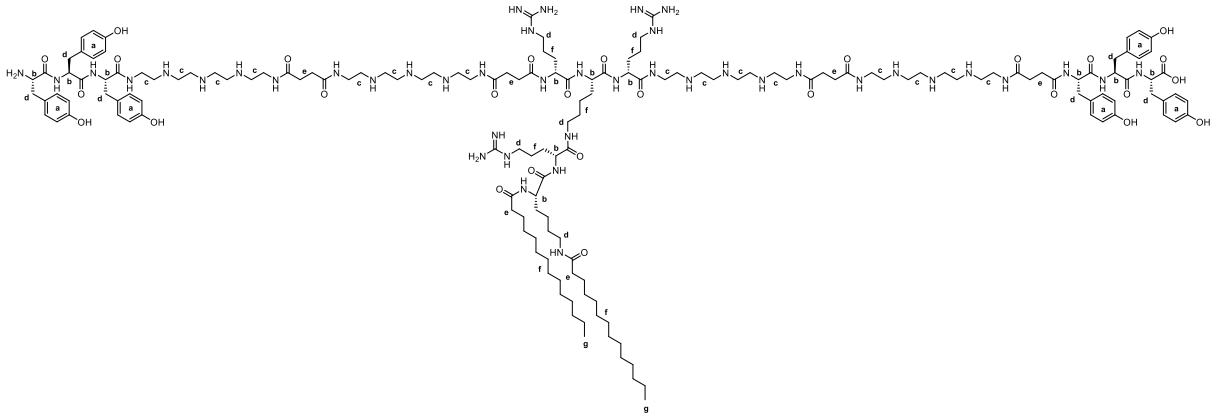

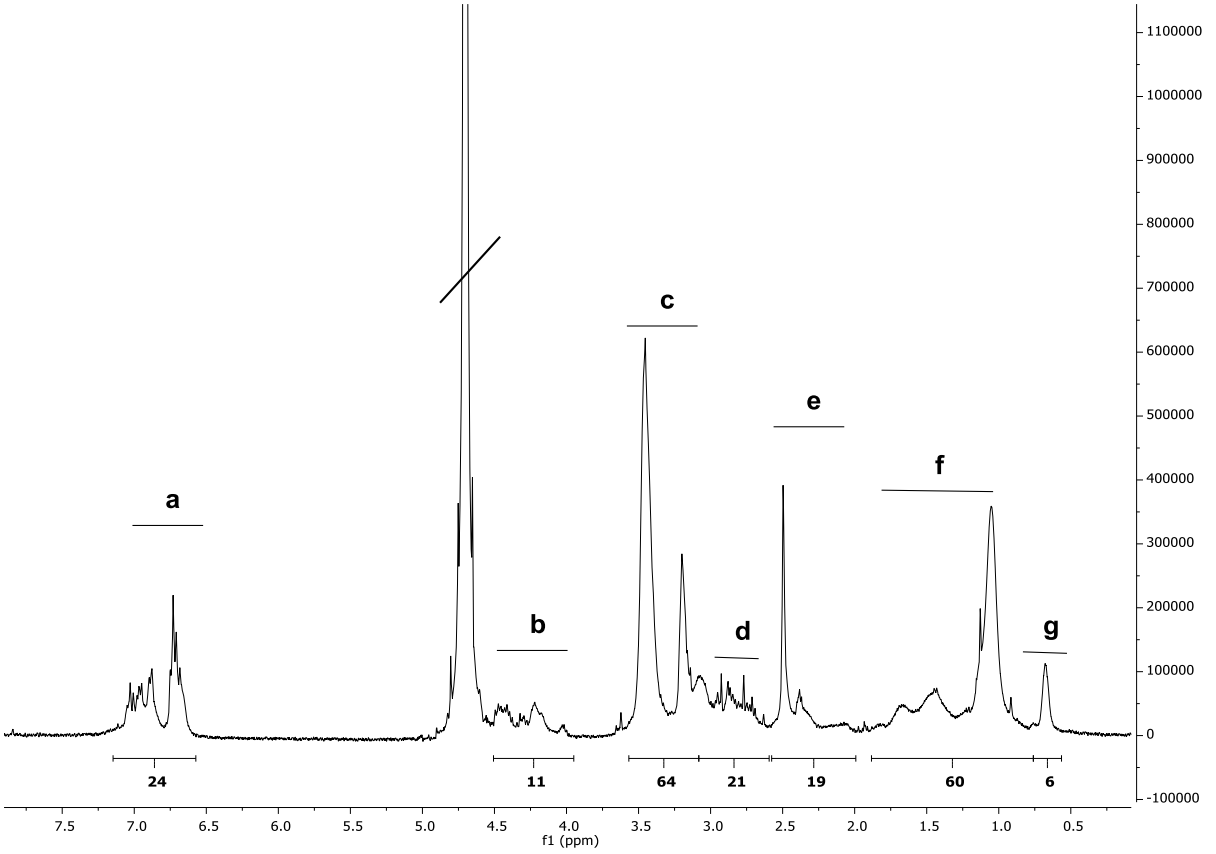

^{1}H NMR (500 MHz, Deuterium oxide) δ (ppm) = 0.57-0.76 (s, 6 H, -CH_3 myristic acid), 0.76-1.9 (m, 68 H, βγδH lysine, βγH arginine, -CH_2- myristic acid), 2.0 -2.6 (m, 20 H, -CO-CH_2-CH_2-CO- Stp, -CO-CH_2- myristic acid), 2.6-3.1 (m, 22 H, εH lysine, δH arginine, βH tyrosine), 3.1-3.6 (m, 64 H, -CH_2- tepa), 3.9-4.5 (m, 11 H, αH amino acids), 6.6-7.1 (m, 24 H, -CH- tyrosine).

RR-My

Sequence (N→C): Y_3-Stp_2-**RR**-K-ε[K-α,ε$(MyrA)_2$]**RR**-Stp_2-Y_3

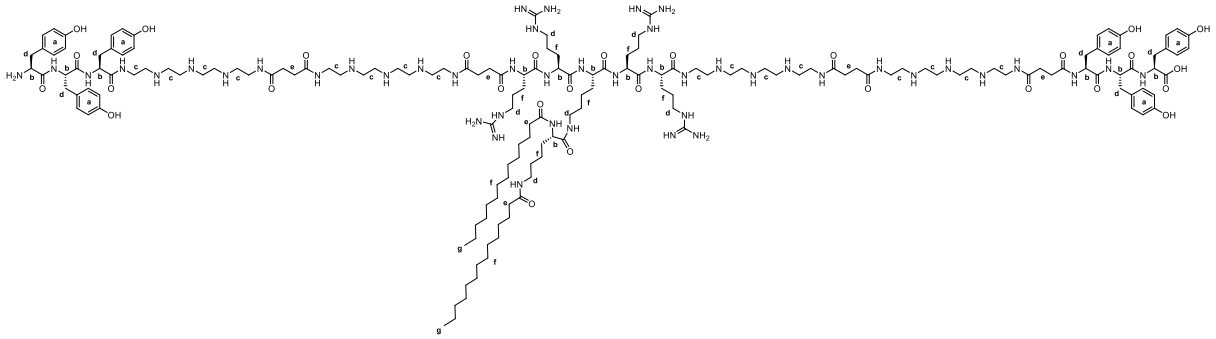

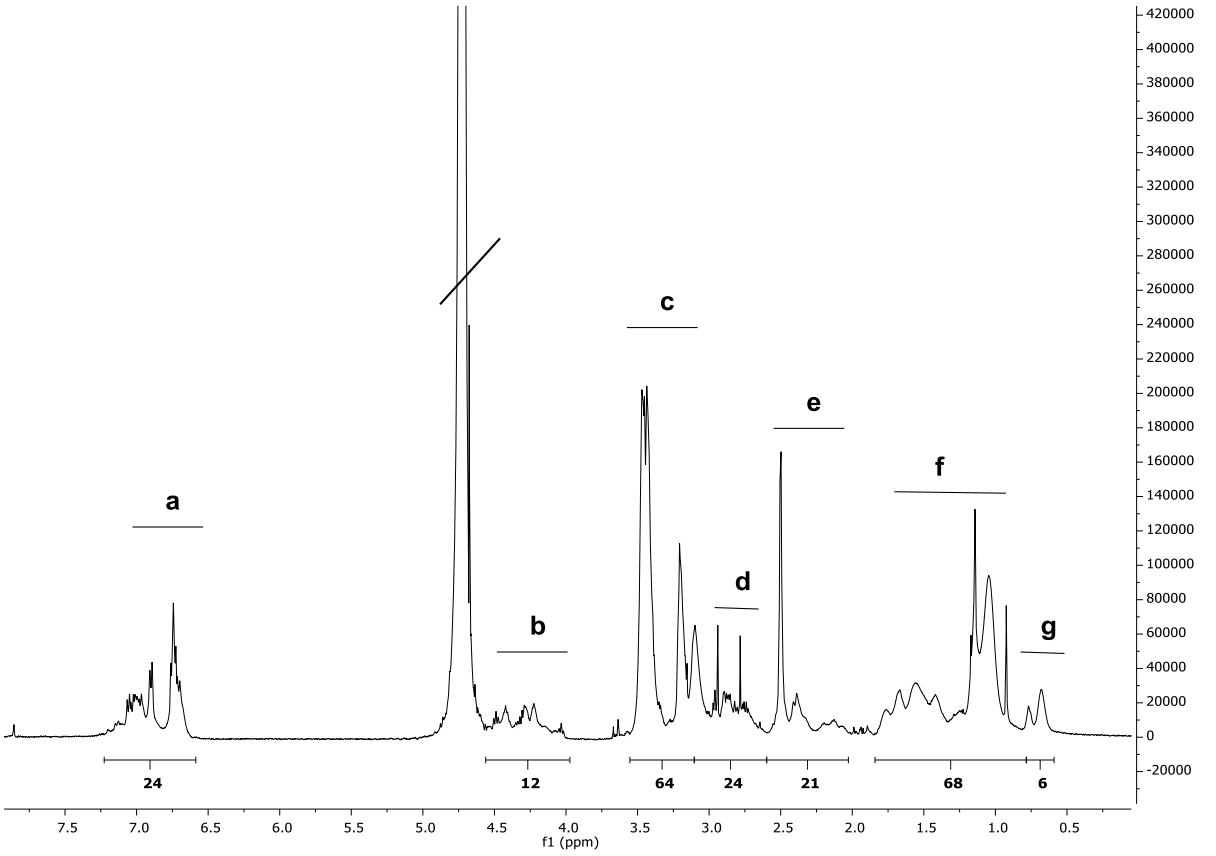

^{1}H NMR (500 MHz, Deuterium oxide) δ (ppm) = 0.59-0.78 (s, 6 H, -CH_3 myristic acid), 0.78-1.8 (m, 72 H, βγδH lysine, βγH arginine, -CH_2- myristic acid), 2.0 -2.6 (m, 20 H, -CO-CH_2-CH_2-CO- Stp, -CO-CH_2- myristic acid), 2.6-3.1 (m, 24 H, εH lysine, δH arginine, βH tyrosine), 3.1-3.6 (m, 64 H, -CH_2- tepa), 4.0-4.6 (m, 12 H, αH amino acids), 6.6-7.2 (m, 24 H, -CH- tyrosine).

RR-My-RR

Sequence (N→C): Y_3-Stp_2-**RR**-K-ε[**RR**-K-α,ε$(MyrA)_2$]**RR**-Stp_2-Y_3

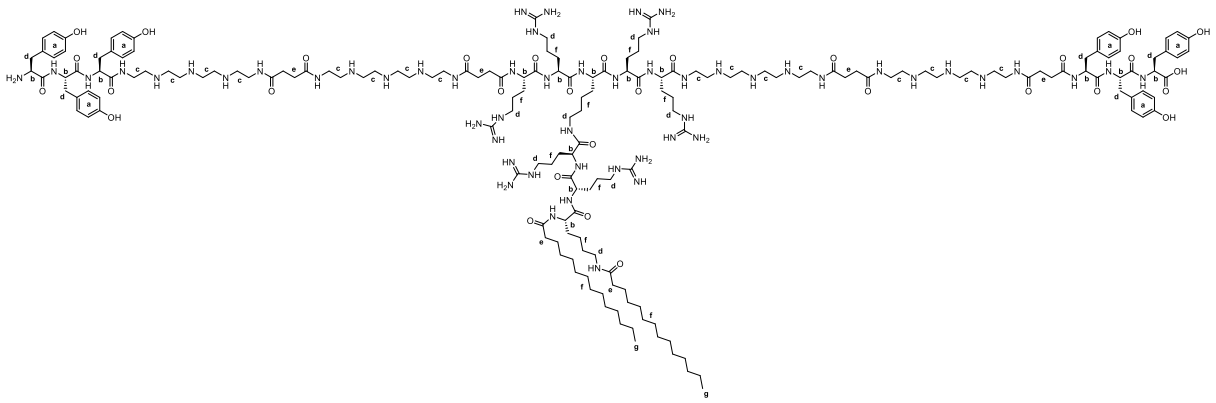

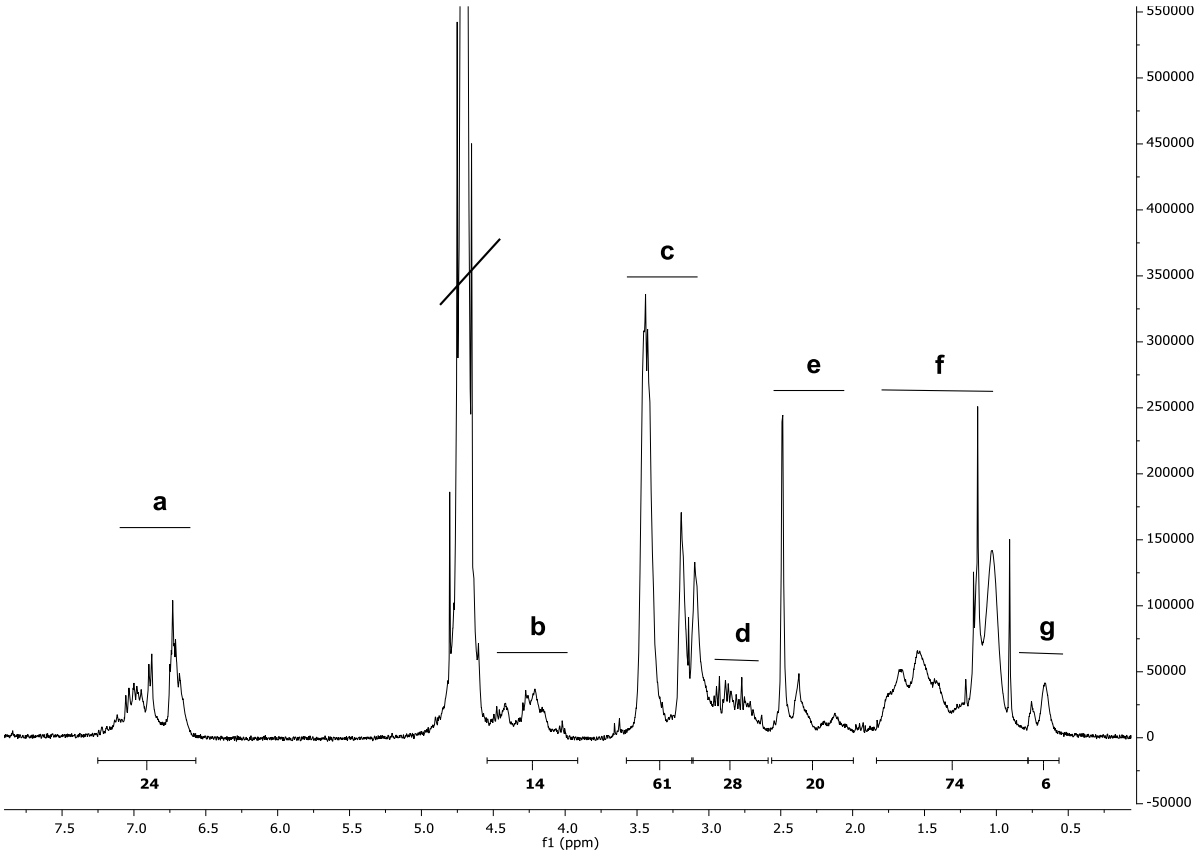

^{1}H NMR (500 MHz, Deuterium oxide) δ (ppm) = 0.56-0.78 (s, 6 H, -CH_3 myristic acid), 0.78-1.8 (m, 80 H, βγδH lysine, βγH arginine, -CH_2- myristic acid), 2.0 -2.6 (m, 20 H, -CO-CH_2-CH_2-CO- Stp, -CO-CH_2- myristic acid), 2.6-3.1 (m, 28 H, εH lysine, δH arginine, βH tyrosine), 3.1-3.6 (m, 64 H, -CH_2- tepa), 3.9-4.5 (m, 14 H, αH amino acids), 6.6-7.2 (m, 24 H, -CH- tyrosine).

RR-My-rr

Sequence (N→C): Y_3-Stp_2-**RR**-K-ε[**rr**-K-α,ε$(MyrA)_2$]**RR**-Stp_2-Y_3

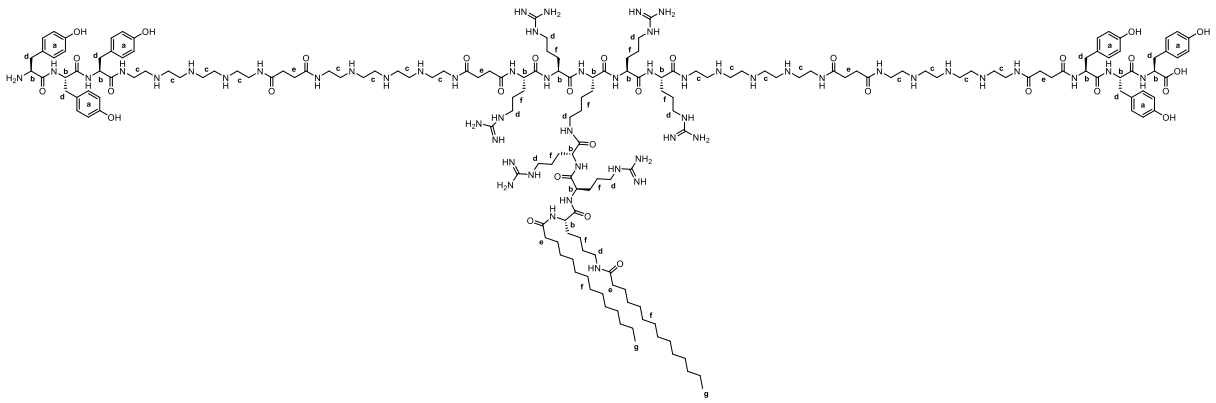

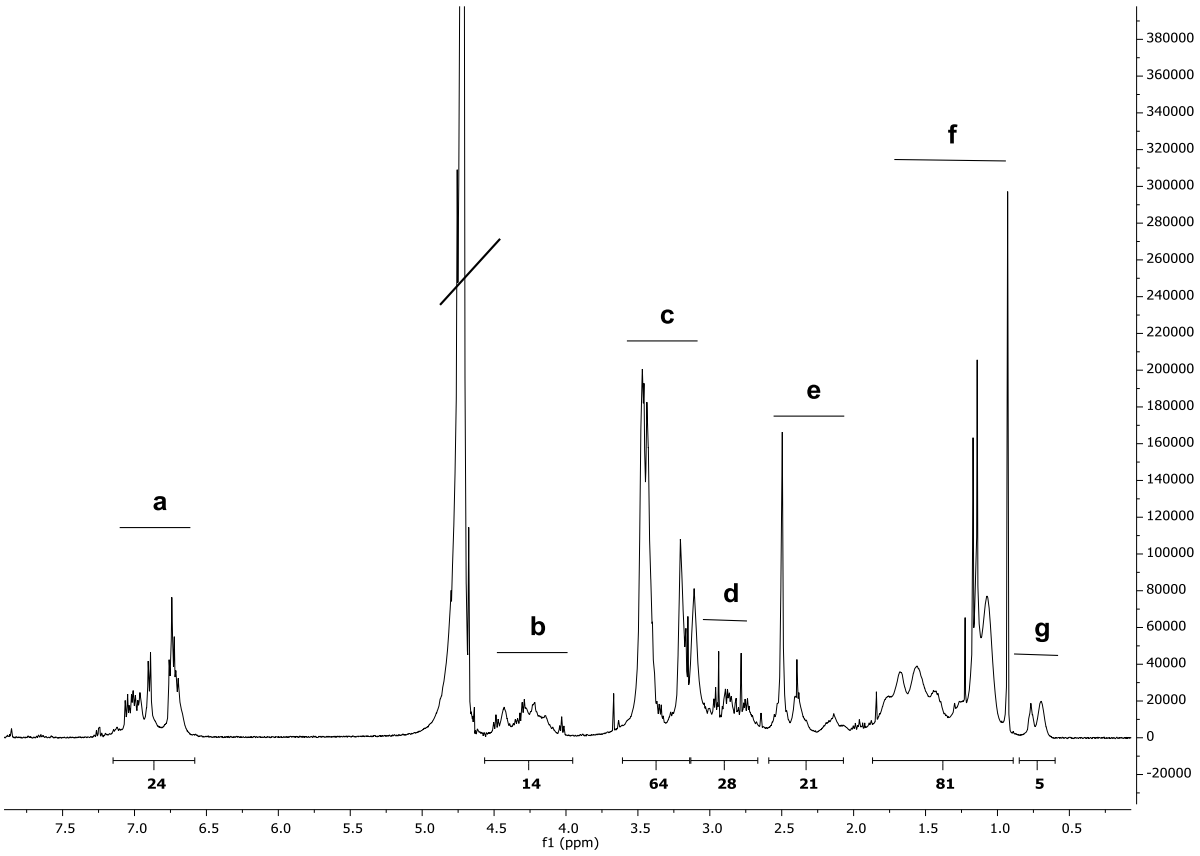

^{1}H NMR (500 MHz, Deuterium oxide) δ (ppm) = 0.60-0.85 (s, 6 H, -CH_3 myristic acid), 0.89-1.9 (m, 80 H, βγδH lysine, βγH arginine, -CH_2- myristic acid), 2.1 -2.6 (m, 20 H, -CO-CH_2-CH_2-CO- Stp, -CO-CH_2- myristic acid), 2.7-3.1 (m, 28 H, εH lysine, δH arginine, βH tyrosine), 3.1-3.6 (m, 64 H, -CH_2- tepa), 4.0-4.6 (m, 14 H, αH amino acids), 6.6-7.1 (m, 24 H, -CH- tyrosine).

rr-My-RR

Sequence (N→C): Y_3-Stp_2-**rr**-K-ε[**RR**-K-α,ε$(MyrA)_2$]**rr**-Stp_2-Y_3

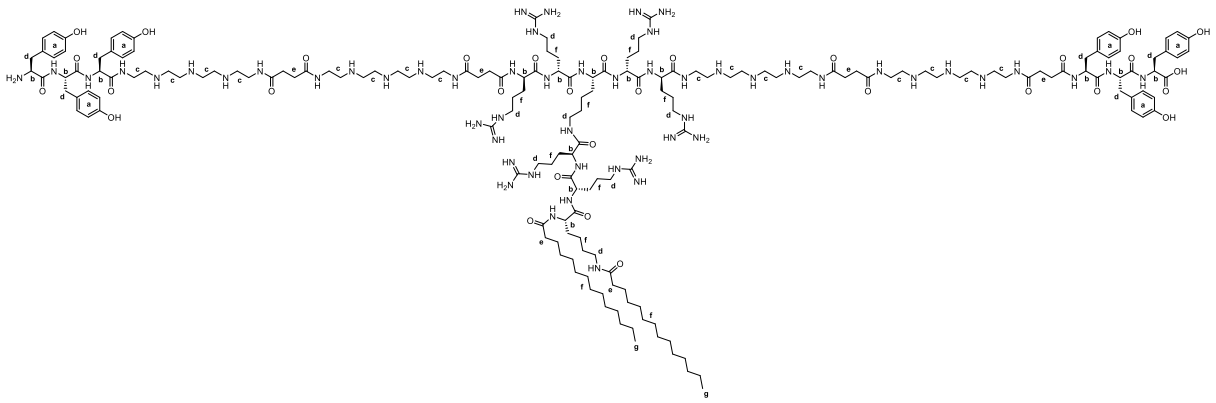

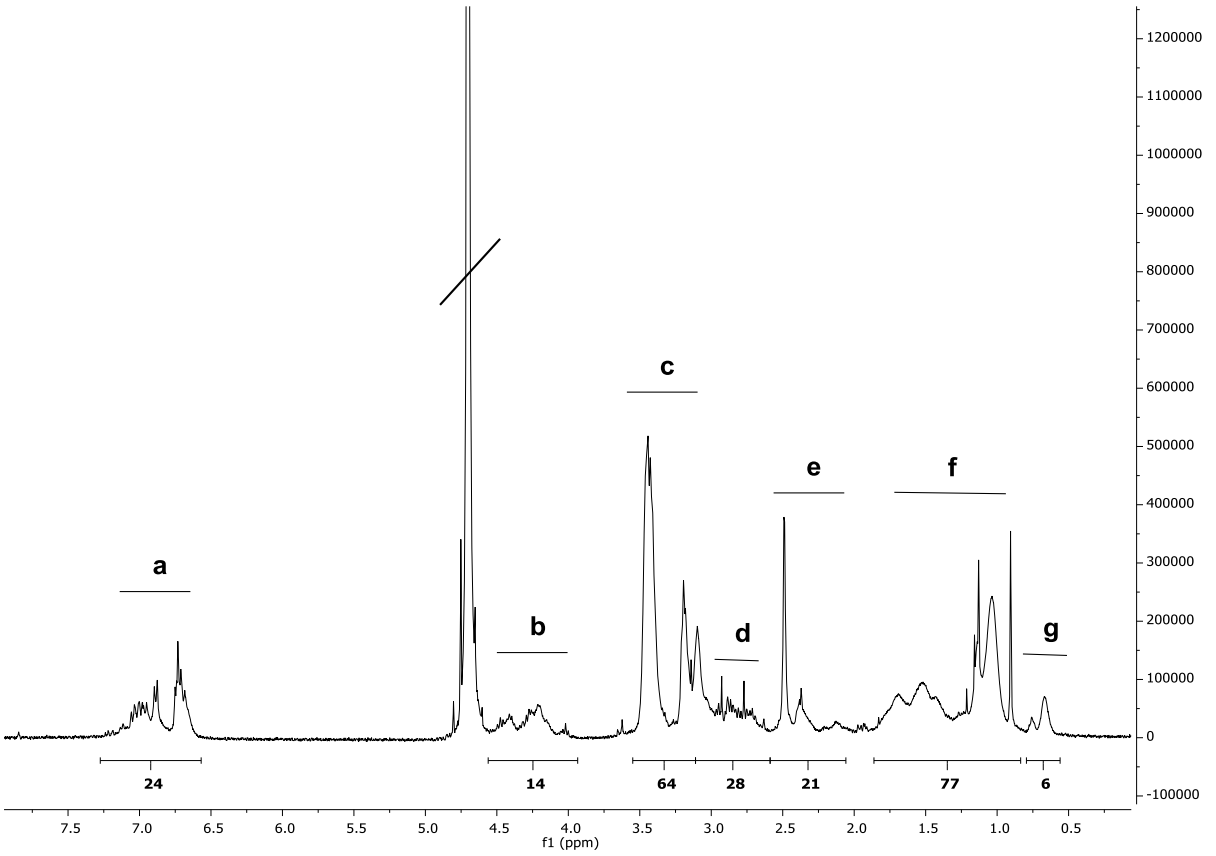

^{1}H NMR (500 MHz, Deuterium oxide) δ (ppm) = 0.56-0.80 (s, 6 H, -CH_3 myristic acid), 0.84-1.9 (m, 80 H, βγδH lysine, βγH arginine, -CH_2- myristic acid), 2.1 -2.6 (m, 20 H, -CO-CH_2-CH_2-CO- Stp, -CO-CH_2- myristic acid), 2.6-3.1 (m, 28 H, εH lysine, δH arginine, βH tyrosine), 3.1-3.5 (m, 64 H, -CH_2- tepa), 3.9-4.6 (m, 14 H, αH amino acids), 6.6-7.2 (m, 24 H, -CH- tyrosine).

rr-My-rr

Sequence (N→C): Y_3-Stp_2-**rr**-K-ε[**rr**-K-α,ε$(MyrA)_2$]**rr**-Stp_2-Y_3

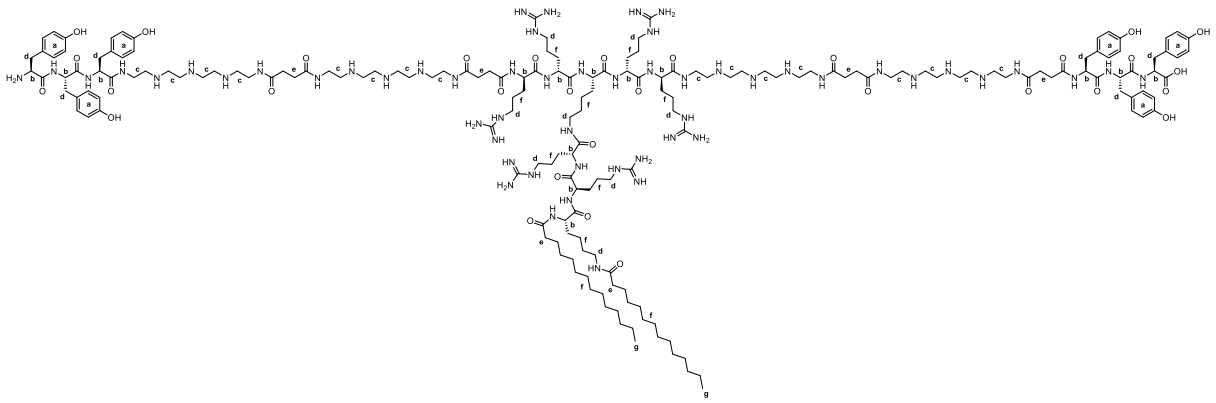

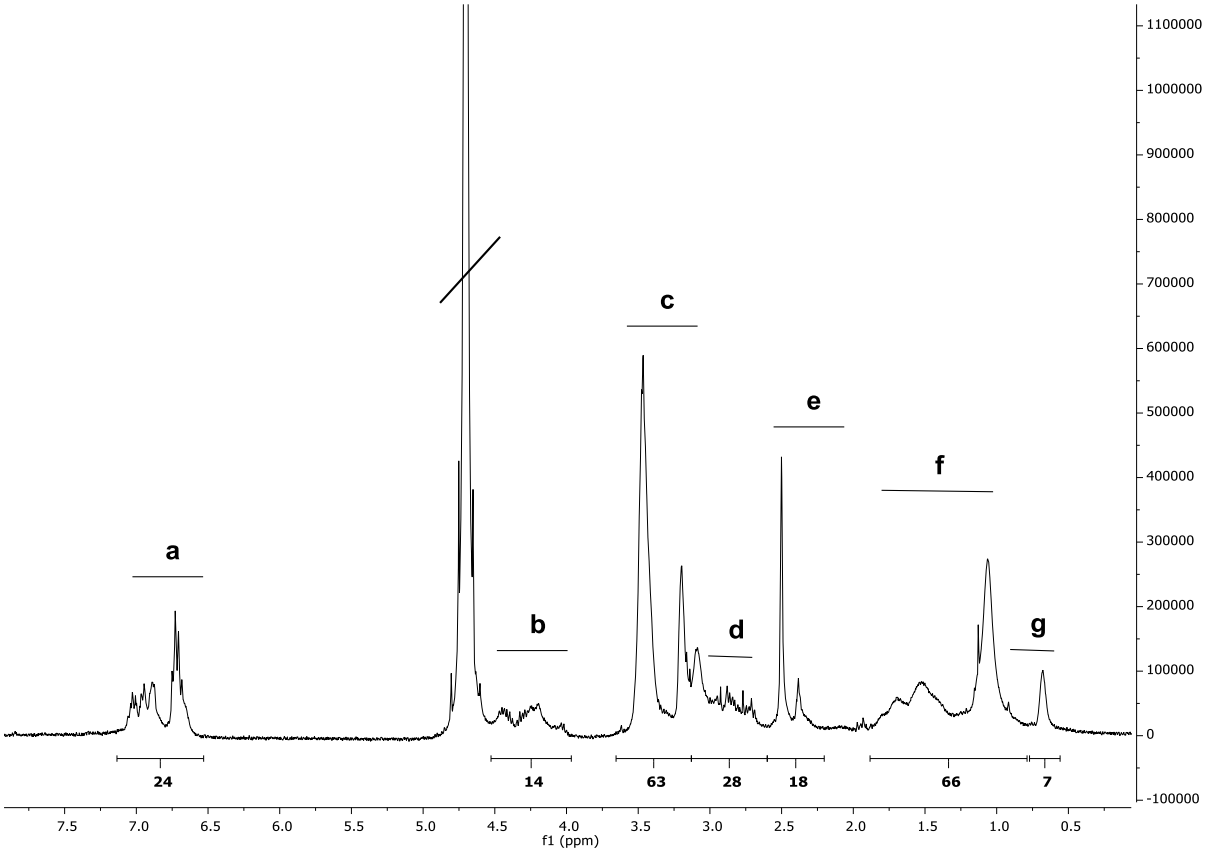

^{1}H NMR (500 MHz, Deuterium oxide) δ (ppm) = 0.56-0.77 (s, 6 H, -CH_3 myristic acid), 0.79-1.9 (m, 80 H, βγδH lysine, βγH arginine, -CH_2- myristic acid), 2.2 -2.6 (m, 20 H, -CO-CH_2-CH_2-CO- Stp, -CO-CH_2- myristic acid), 2.6-3.1 (m, 28 H, εH lysine, δH arginine, βH tyrosine), 3.1-3.7 (m, 64 H, -CH_2- tepa), 4.0-4.5 (m, 14 H, αH amino acids), 6.5-7.1 (m, 24 H, -CH- tyrosine).

6.4.3 Mass spectra of oligomers

Table 21 Summarizing table oligomers. Mass data recorded with a Bruker MALDI-TOF instrument

Oligomer	Molecular formula	$[M+H]^+$ calc.	$[M+H]^+$ found
454 (OleA-t)	$C_{156}H_{254}N_{32}O_{27}S_2$	*3070.9*	*3069.9*
1105 (OH-SteA-t)	$C_{156}H_{258}N_{32}O_{29}S_2$	*3106.9*	*3106.2*
1172 (SteA-t)	$C_{156}H_{258}N_{32}O_{27}S_2$	*3074.9*	*3074.0*
1104 (NonOcA-t)	$C_{154}H_{252}N_{34}O_{29}S_2$	*3104.9*	*3104.0*
CK_2Y_2-OleA	$C_{51}H_{81}N_7O_9S$	*966.6*	*965.1*
Stp-W-OleA	$C_{41}H_{69}N_7O_5$	*738.5*	*738.2*
CKEHEK-OleA	$C_{49}H_{84}N_{10}O_{12}S$	*1037.6*	*1036.7*
1165 (LinA-t)	$C_{156}H_{250}N_{32}O_{27}S_2$	*3066.9*	*3066.7*
1166 (OH-(C18:1)-t)	$C_{156}H_{254}N_{32}O_{29}S_2$	*3102.9*	*3102.1*
***740* (Test structure)**	$C_{72}H_{119}N_{19}O_{12}S_2$	1506.9	1506.1
782	$C_{148}H_{280}N_{38}O_{21}S_4$	3055.0	3056.1
783	$C_{132}H_{252}N_{34}O_{17}$	2587.0	2587.2
871	$C_{138}H_{232}N_{40}O_{18}$	2738.9	2739.2
969	$C_{146}H_{246}N_{42}O_{20}S_2$	2972.9	2973.2
989	$C_{152}H_{251}N_{31}O_{26}$	2927.9	2929.3
990	$C_{160}H_{265}N_{33}O_{28}S_2$	3162.0	3163.6
991	$C_{164}H_{259}N_{31}O_{26}$	3080.0	3079.0
992	$C_{172}H_{273}N_{33}O_{28}S_2$	3314.0	3314.2
1081	$C_{144}H_{235}N_{31}O_{26}$	2815.8	2813.6
1082	$C_{152}H_{249}N_{33}O_{28}S_2$	3049.9	3048.2
1107	$C_{152}H_{247}N_{31}O_{26}$	2923.9	2922.9
1108	$C_{160}H_{261}N_{33}O_{28}S_2$	3158.0	3156.3
1198	$C_{162}H_{264}N_{36}O_{28}S_2$	3229.2	3232.1
1215	$C_{210}H_{364}N_{56}O_{36}S_2$	4308.8	4305.2
Acr-Stp-Stp-w	$C_{49}H_{69}N_{13}O_7$	*952.5*	*952.5*
Acr-Stp-H-Stp-w	$C_{55}H_{76}N_{16}O_8$	*1089.6*	*1089.6*
Acr-Stp-HH-Stp-w	$C_{61}H_{83}N_{19}O_9$	*1226.7*	*1226.7*

Acr-Stp-Y-Stp-w	$C_{58}H_{78}N_{14}O_9$	*1115.6*	*1115.6*
Acr-Stp-YY-Stp-w	$C_{67}H_{87}N_{15}O_{11}$	*1278.7*	*1278.7*
Acr-Stp-K-Stp-w	$C_{55}H_{81}N_{15}O_8$	*1080.6*	*1080.6*
Acr-Stp-KK-Stp-w	$C_{61}H_{93}N_{17}O_9$	*1208.7*	*1208.7*
Acr-Stp-R-Stp-w	$C_{55}H_{81}N_{17}O_8$	*1108.7*	*1108.7*
Acr-Stp-RR-Stp-w	$C_{61}H_{93}N_{21}O_9$	*1264.8*	*1264.8*
Acr-Stp-RV-Stp-w	$C_{60}H_{90}N_{18}O_9$	*1207.7*	*1207.7*
Acr-Stp-VV-Stp-w	$C_{59}H_{87}N_{15}O_9$	*1150.7*	*1150.7*
1286 (My)	$C_{142}H_{232}N_{30}O_{25}$	*2758.8*	*2758.1*
1287 (My-R)	$C_{148}H_{244}N_{34}O_{26}$	*2914.9*	*2913.3*
1288 (My-r)	$C_{148}H_{244}N_{34}O_{26}$	*2914.9*	*2914.4*
1289 (My-RR)	$C_{154}H_{256}N_{38}O_{27}$	*3071.0*	*3070.8*
1291 (R-My)	$C_{154}H_{256}N_{38}O_{27}$	*3071.0*	*3070.8*
1292 (R-My-R)	$C_{160}H_{268}N_{42}O_{28}$	*3227.1*	*3224.9*
1293 (R-My-r)	$C_{160}H_{268}N_{42}O_{28}$	*3227.1*	*3226.2*
1294 (r-My)	$C_{154}H_{256}N_{38}O_{27}$	*3071.0*	*3070.1*
1295 (r-My-R)	$C_{160}H_{268}N_{42}O_{28}$	*3227.1*	*3227.1*
1296 (r-My-r)	$C_{160}H_{268}N_{42}O_{28}$	*3227.1*	*3226.7*
1297 (RR-My)	$C_{166}H_{280}N_{46}O_{29}$	*3383.2*	*3381.9*
1298 (RR-My-RR)	$C_{178}H_{304}N_{54}O_{31}$	*3695.4*	*3695.3*
1299 (RR-My-rr)	$C_{178}H_{304}N_{54}O_{31}$	*3695.4*	*3693.1*
1301 (rr-My-RR)	$C_{178}H_{304}N_{54}O_{31}$	*3695.4*	*3695.1*
1302 (rr-My-rr)	$C_{178}H_{304}N_{54}O_{31}$	*3695.4*	*3694.4*

6.4.4 Mass spectra of enzymatically degradable oligomers

Table 22 Summarizing table with mass data for lipo-oligomers after incubation with cathepsin B or from cell lysates. An "X" indicates that the mass was found. Mass data recorded with a Bruker MALDI-TOF instrument

My **Structure (N→C)**	**Mass [M+H]**	**Lipo-oligomer**	**Polyplex N/P 1**	**Polyplex N/P 20**	**Cell lysate**
Y_3-Stp_2-K-ε[K-α,ε$(MyrA)_2$]Stp_2-Y_3	2758.8		x		x
Y_{2-3}-Stp_2-K-ε[K-α,ε$(MyrA)_2$]Stp_2-Y_{2-3} ↓Y	2595.7	x		x	
Y_{1-3}-Stp_2-K-ε[K-α,ε$(MyrA)_2$]Stp_2-Y_{1-3} ↓Y_2	2432.7	x		x	x
Y_{1-3}-Stp_2-K-ε[K-α,ε$(MyrA)_2$]Stp_2-Y_{1-3} ↓Y_3	2269.6	x		x	x
Y_{0-1}-Stp_2-K-ε[K-α,ε$(MyrA)_2$]Stp_2-Y_{1-2} ↓Y_4	2106.5	x		x	

My-R **Structure (N→C)**	**Mass [M+H]**	**Lipo-oligomer**
Y_3-Stp_2-K-ε[**R**-K-α,ε$(MyrA)_2$]Stp_2-Y_3	2914.9	
Y_{2-3}-Stp_2-K-ε[**R**-K-α,ε$(MyrA)_2$]Stp_2-Y_{2-3} ↓Y	2751.8	x
Y_{1-3}-Stp_2-K-ε[**R**-K-α,ε$(MyrA)_2$]Stp_2-Y_{1-3} ↓Y_2	2588.8	x
Y_{1-3}-Stp_2-K-ε[**R**-K-α,ε$(MyrA)_2$]Stp_2-Y_{1-3} ↓Y_3	2425.7	x
Y_{0-1}-Stp_2-K-ε[**R**-K-α,ε$(MyrA)_2$]Stp_2-Y_{1-2} ↓Y_4	2262.6	x
R-K-α,ε$(MyrA)_2$ ↓ Y_3-Stp_2-K-Stp_2-Y_3	723.6	x

My-r **Structure (N→C)**	**Mass [M+H]**	**Lipo-oligomer**
Y_3-Stp_2-K-ε[**r**-K-α,ε$(MyrA)_2$]Stp_2-Y_3	2914.9	
Y_{2-3}-Stp_2-K-ε[**r**-K-α,ε$(MyrA)_2$]Stp_2-Y_{2-3} ↓Y	2751.8	x
Y_{1-3}-Stp_2-K-ε[**r**-K-α,ε$(MyrA)_2$]Stp_2-Y_{1-3} ↓Y_2	2588.8	x
Y_{1-3}-Stp_2-K-ε[**r**-K-α,ε$(MyrA)_2$]Stp_2-Y_{1-3} ↓Y_3	2425.7	x
Y_{1-3}-Stp_2-K-ε[**r**-K-α,ε$(MyrA)_2$]Stp_2-Y_{1-3} ↓Y_3	2262.6	x

My-RR **Structure (N→C)**	**Mass [M+H]**	**Lipo-oligomer**	**Polyplex N/P 1**	**Polyplex N/P 20**	**Cell lysate**
Y_3-Stp_2-K-ε[**RR**-K-α,ε$(MyrA)_2$]Stp_2-Y_3	3071.0		x	x	x
Y_{1-3}-Stp_2-K-ε[**RR**-K-α,ε$(MyrA)_2$]Stp_2-Y_{1-3} ↓Y_2	2744.9	x		x	
Y_{1-3}-Stp_2-K-ε[**RR**-K-α,ε$(MyrA)_2$]Stp_2-Y_{1-3} ↓Y_3	2581.8	x		x	x
Y_{0-1}-Stp_2-K-ε[**RR**-K-α,ε$(MyrA)_2$]Stp_2-Y_{1-2} ↓Y_4	2418.7	x		x	
R-K-α,ε$(MyrA)_2$ ↓ Y_3-Stp_2-K-ε[**R**]-Stp_2-Y_3	723.6	x		x	x

R-My **Structure (N→C)**	**Mass [M+H]**	**Lipo-oligomer**
Y_3-Stp_2-**R**-K-ε[K-α,ε$(MyrA)_2$]**R**-Stp_2-Y_3	3071.0	
K-ε[K-α,ε$(MyrA)_2$]**R**-Stp_2-Y_3 ↓Y_3- Stp_2-**R**	1883.3	x
K-ε[K-α,ε$(MyrA)_2$]**R**-Stp_2-Y_2 ↓Y_3- Stp_2-**R**; Y	1720.2	x
K-ε[K-α,ε$(MyrA)_2$]**R**-Stp_2-Y_1 ↓Y_3- Stp_2-**R**; Y_2	1557.2	x
K-ε[K-α,ε$(MyrA)_2$]**R** ↓Y_3- Stp_2-**R**; Stp_2-Y_3	851.7	x

R-My-R **Structure (N→C)**	**Mass [M+H]**	**Lipo-oligomer**
Y_3-Stp_2-**R**-K-ε[**R**-K-α,ε$(MyrA)_2$]**R**-Stp_2-Y_3	3227.1	
K-ε[**R**-K-α,ε$(MyrA)_2$]**R**-Stp_2-Y_3 ↓Y_3- Stp_2-**R**	2039.4	x
K-ε[**R**-K-α,ε$(MyrA)_2$]**R**-Stp_2-Y_2 ↓Y_3- Stp_2-**R**; Y	1876.3	x
K-ε[**R**-K-α,ε$(MyrA)_2$]**R**-Stp_2-Y_1 ↓Y_3- Stp_2-**R**; Y_2	1713.3	x
K-ε[**R**-K-α,ε$(MyrA)_2$]**R** ↓Y_3- Stp_2-**R**; Stp_2-Y_3	1008.5	x
Y_1- Stp_2-**R** ↓K-ε[**R**-K-α,ε$(MyrA)_2$]**R**-Stp_2-Y_3 ; Y_2	880.6	x
R-K-α,ε$(MyrA)_2$ ↓ Y_3-Stp_2-**R**-K-**R**-Stp_2-Y_3	723.6	x

R-My-r **Structure (N→C)**	**Mass [M+H]**	**Lipo-oligomer**
Y_3-Stp_2-**R**-K-ε[**r**-K-α,ε(MyrA)$_2$]**R**-Stp_2-Y_3	3227.1	
K-ε[**r**-K-α,ε(MyrA)$_2$]**R**-Stp_2-Y_3 ↓Y_3- Stp_2-**R**	2039.4	x
K-ε[**r**-K-α,ε(MyrA)$_2$]**R**-Stp_2-Y_2 ↓Y_3- Stp_2-**R**; Y	1876.3	x
K-ε[**r**-K-α,ε(MyrA)$_2$]**R**-Stp_2-Y_1 ↓Y_3- Stp_2-**R**; Y_2	1713.3	x
K-ε[**r**-K-α,ε(MyrA)$_2$]**R** ↓Y_3- Stp_2-**R**; Stp_2-Y_3	1008.5	x
r-My **Structure (N→C)**	**Mass [M+H]**	**Lipo-oligomer**
Y_3-Stp_2-**r**-K-ε[K-α,ε(MyrA)$_2$]**r**-Stp_2-Y_3	3071.0	
Y_{2-3}-Stp_2-**r**-K-ε[K-α,ε(MyrA)$_2$]**r**-Stp_2-Y_{2-3} ↓Y	2909.8	x
Y_{1-3}-Stp_2-**r**-K-ε[K-α,ε(MyrA)$_2$]**r**-Stp_2-Y_{1-3} ↓Y_2	2746.7	x
Y_{1-3}-Stp_2-**r**-K-ε[K-α,ε(MyrA)$_2$]**r**-Stp_2-Y_{1-3} ↓Y_3	2583.6	x
Y_{0-1}-Stp_2-**r**-K-ε[K-α,ε(MyrA)$_2$]**r**-Stp_2-Y_{1-2} ↓Y_4	2420.5	x
r-My-R **Structure (N→C)**	**Mass [M+H]**	**Lipo-oligomer**
Y_3-Stp_2-**r**-K-ε[**R**-K-α,ε(MyrA)$_2$]**r**-Stp_2-Y_3	3227.1	
Y_{2-3}-Stp_2-**r**-K-ε[**R**-K-α,ε(MyrA)$_2$]**r**-Stp_2-Y_{2-3} ↓Y	3064.0	x
Y_{1-3}-Stp_2-**r**-K-ε[**R**-K-α,ε(MyrA)$_2$]**r**-Stp_2-Y_{1-3} ↓Y_2	2901.0	x
Y_{1-3}-Stp_2-**r**-K-ε[**R**-K-α,ε(MyrA)$_2$]**r**-Stp_2-Y_{1-3} ↓Y_3	2737.9	x
Y_{0-1}-Stp_2-**r**-K-ε[**R**-K-α,ε(MyrA)$_2$]**r**-Stp_2-Y_{1-2} ↓Y_4	2574.8	x
R-K-α,ε(MyrA)$_2$ ↓ Y_3-Stp_2-**r**-K-**r**-Stp_2-Y_3	723.6	x

r-My-r **Structure (N→C)**	**Mass [M+H]**	**Lipo-oligomer**
Y_3-Stp_2-**r**-K-ε[**r**-K-α,ε$(MyrA)_2$]**r**-Stp_2-Y_3	3227.1	
Y_{2-3}-Stp_2-**r**-K-ε[**r**-K-α,ε$(MyrA)_2$]**r**-Stp_2-Y_{2-3} ↓Y	3064.0	x
Y_{1-3}-Stp_2-**r**-K-ε[**r**-K-α,ε$(MyrA)_2$]**r**-Stp_2-Y_{1-3} ↓Y_2	2901.0	x
Y_{1-3}-Stp_2-**r**-K-ε[**r**-K-α,ε$(MyrA)_2$]**r**-Stp_2-Y_{1-3} ↓Y_3	2737.9	x
Y_{0-1}-Stp_2-**r**-K-ε[**r**-K-α,ε$(MyrA)_2$]**r**-Stp_2-Y_{1-2} ↓Y_4	2574.8	x
Y_0-Stp_2-**r**-K-ε[**r**-K-α,ε$(MyrA)_2$]**r**-Stp_2-Y_1 ↓Y_5	2411.8	x

RR-My **Structure (N→C)**	**Mass [M+H]**	**Lipo-oligomer**	**Polyplex N/P 1**	**Polyplex N/P 20**	**Cell lysate**
Y_3-Stp_2-**RR**-K-ε[K-α,ε$(MyrA)_2$]**RR**-Stp_2-Y_3	3383.2		x		x
K-ε[K-α,ε$(MyrA)_2$]**RR**-Stp_2-Y_3 ↓Y_3- Stp_2-**RR**	2039.4	x		x	x
K-ε[K-α,ε$(MyrA)_2$]**RR**-Stp_2-Y_2 ↓Y_3- Stp_2-**RR**; Y	1875.3	x		x	
K-ε[K-α,ε$(MyrA)_2$]**RR**-Stp_2-Y_1 ↓Y_3- Stp_2-**RR**; Y_2	1713.3	x		x	
K-ε[K-α,ε$(MyrA)_2$]**RR** ↓Y_3- Stp_2-**RR**; Stp_2-Y_3	1007.8	x		x	x

RR-My-RR **Structure (N→C)**	**Mass [M+H]**	**Lipo-oligomer**	**Polyplex N/P 1**	**Polyplex N/P 20**	**Cell lysate**
Y_3-Stp_2-**RR**-K-ε[**RR**-K-α,ε$(MyrA)_2$]**RR**-Stp_2-Y_3	3695.4		x		x
K-ε[**RR**-K-α,ε$(MyrA)_2$]**RR**-Stp_2-Y_1 ↓Y_3-Stp_2-**RR**; Y_2	2025.5	x			
R-K-ε[**RR**-K-α,ε$(MyrA)_2$]**R** ↓2 x Y_3-Stp_2-**R**	1320.0	x		x	
K-ε[**RR**-K-α,ε$(MyrA)_2$]**R** ↓Y_3-Stp_2-**RR; R**-Stp_2-Y_3	1163.9	x		x	
RR-K-α,ε$(MyrA)_2$ ↓Y_3-Stp_2-**RR**-K-**RR**-Stp_2-Y_3	879.7	x		x	

R-K-α,ε(MyrA)$_2$ ↓Y$_3$-Stp$_2$-**RR**-K-ε[**R**]-**RR**-Stp$_2$-Y$_3$	723.6	x		x	x
RR-My-rr **Structure (N→C)**	**Mass [M+H]**	**Lipo-oligomer**	**Polyplex N/P 1**	**Polyplex N/P 20**	**Cell lysate**
Y$_3$-Stp$_2$-**RR**-K-ε[**rr**-K-α,ε(MyrA)$_2$]**RR**-Stp$_2$-Y$_3$	3695.4		x		x
R-K-ε[**rr**-K-α,ε(MyrA)$_2$]**R** ↓2 x Y$_3$-Stp$_2$-**R**	1320.0	x		x	x
K-ε[**rr**-K-α,ε(MyrA)$_2$]**R** ↓Y$_3$-Stp$_2$-**RR; R**-Stp$_2$-Y$_3$	1163.9	x		x	x
rr-My-RR **Structure (N→C)**	**Mass [M+H]**	**Lipo-oligomer**	**Polyplex N/P 1**	**Polyplex N/P 20**	**Cell lysate**
Y$_3$-Stp$_2$-**rr**-K-ε[**RR**-K-α,ε(MyrA)$_2$]**rr**-Stp$_2$-Y$_3$	3695.4		x		x
Y$_{1-3}$-Stp$_2$-**rr**-K-ε[**RR**-K-α,ε(MyrA)$_2$]**rr**-Stp$_2$-Y$_{1-3}$ ↓Y$_2$	3369.3	x			
Y$_{1-3}$-Stp$_2$-**rr**-K-ε[**RR**-K-α,ε(MyrA)$_2$]**rr**-Stp$_2$-Y$_{1-3}$ ↓Y$_3$	3206.2	x			
Y$_{0-1}$-Stp$_2$-**rr**-K-ε[**RR**-K-α,ε(MyrA)$_2$]**rr**-Stp$_2$-Y$_{1-2}$ ↓Y$_4$	3042.1	x			
Y$_{0-1}$-Stp$_2$-**rr**-K-[**R**]**rr**-Stp$_2$-Y$_{1-2}$ ↓Y$_4$; **R**-K-α,ε(MyrA)$_2$	2338.5	x			
RR-K-α,ε(MyrA)$_2$ ↓Y$_3$-Stp$_2$-**rr**-K-**rr**-Stp$_2$-Y$_3$	879.7	x		x	
R-K-α,ε(MyrA)$_2$ ↓Y$_3$-Stp$_2$-**rr**-K-ε[**R**]-**rr**-Stp$_2$-Y$_3$	723.6	x		x	x
rr-My-rr **Structure (N→C)**	**Mass [M+H]**	**Lipo-oligomer**	**Polyplex N/P 1**	**Polyplex N/P 20**	**Cell lysate**
Y$_3$-Stp$_2$-**rr**-K-ε[**RR**-K-α,ε(MyrA)$_2$]**rr**-Stp$_2$-Y$_3$	3695.4		x		x
Y$_{2-3}$-Stp$_2$-**rr**-K-ε[**rr**-K-α,ε(MyrA)$_2$]**rr**-Stp$_2$-Y$_{2-3}$ ↓Y$_1$	3532.3	x		x	
Y$_{1-3}$-Stp$_2$-**rr**-K-ε[**rr**-K-α,ε(MyrA)$_2$]**rr**-Stp$_2$-Y$_{1-3}$ ↓Y$_2$	3369.3	x		x	
Y$_{1-3}$-Stp$_2$-**rr**-K-ε[**rr**-K-α,ε(MyrA)$_2$]**rr**-Stp$_2$-Y$_{1-3}$ ↓Y$_3$	3206.2	x		x	x
Y$_{0-1}$-Stp$_2$-**rr**-K-ε[**rr**-K-α,ε(MyrA)$_2$]**rr**-Stp$_2$-Y$_{1-2}$ ↓Y$_4$	3042.1	x		x	

Y_0-Stp_2-**rr**-K-ε[**rr**-K-α,ε$(MyrA)_2$]**rr**-Stp_2-$Y_1 \downarrow Y_5$	2880.1	x

6.4.5 Mass spectra of shielding agents

Table 23 Summarizing table shielding agents. Mass data recorded with a Bruker MALDI-TOF instrument

Shielding agent	ID	Molecular formula	$[M+X]^+$ calc.	$[M+X]^+$ found
$(DBCO\text{-}STOTDA)_2$-K-PEG_{24}-COOH	***1307***	$C_{127}H_{201}N_9O_{41}$	2508.4	2505.9
$(DBCO\text{-}STOTDA)_2$-K-PEG_{24}-g7	***1308***	$C_{168}H_{259}N_{17}O_{54}$	3399.8 [Na]	3399.4 [Na]
$(DBCO\text{-}STOTDA)_2$-K-PEG_{24}-scrg7	***1309***	$C_{168}H_{259}N_{17}O_{54}$	3399.8 [Na]	3400.4 [Na]
C-PEG_{24}-apelin-13	***1310***	$C_{123}H_{217}N_{25}O_{42}S_2$	2779.5	2779.2
C-PEG_{24}-apelin-F13A	***1311***	$C_{117}H_{213}N_{25}O_{42}S_2$	2703.5	2702.9
C-PEG_{24}-apelin-13scr	***1312***	$C_{123}H_{217}N_{25}O_{42}S_2$	2779.5	2779.4

7 References

[1] J.D. Watson, F.H. Crick, Molecular structure of nucleic acids; a structure for deoxyribose nucleic acid, Nature 171(4356) (1953) 737-8.
[2] F. Crick, Central dogma of molecular biology, Nature 227(5258) (1970) 561-3.
[3] A. Fire, S. Xu, M.K. Montgomery, S.A. Kostas, S.E. Driver, C.C. Mello, Potent and specific genetic interference by double-stranded RNA in Caenorhabditis elegans, Nature 391(6669) (1998) 806-11.
[4] S.M. Elbashir, J. Harborth, W. Lendeckel, A. Yalcin, K. Weber, T. Tuschl, Duplexes of 21-nucleotide RNAs mediate RNA interference in cultured mammalian cells, Nature 411(6836) (2001) 494-8.
[5] M.T. McManus, B.B. Haines, C.P. Dillon, C.E. Whitehurst, L. van Parijs, J. Chen, P.A. Sharp, Small interfering RNA-mediated gene silencing in T lymphocytes, J Immunol 169(10) (2002) 5754-60.
[6] A. Turchinovich, B. Burwinkel, Distinct AGO1 and AGO2 associated miRNA profiles in human cells and blood plasma, RNA Biol 9(8) (2012) 1066-75.
[7] M.E. Davis, J.E. Zuckerman, C.H. Choi, D. Seligson, A. Tolcher, C.A. Alabi, Y. Yen, J.D. Heidel, A. Ribas, Evidence of RNAi in humans from systemically administered siRNA via targeted nanoparticles, Nature 464(7291) (2010) 1067-70.
[8] V. Brower, RNA interference advances to early-stage clinical trials, J Natl Cancer Inst 102(19) (2010) 1459-61.
[9] R. Kanasty, J.R. Dorkin, A. Vegas, D. Anderson, Delivery materials for siRNA therapeutics, Nat Mater 12(11) (2013) 967-77.
[10] E. Wagner, Polymers for siRNA delivery: inspired by viruses to be targeted, dynamic, and precise, Acc Chem Res 45(7) (2012) 1005-13.
[11] S. Boeckle, E. Wagner, Optimizing targeted gene delivery: chemical modification of viral vectors and synthesis of artificial virus vector systems, AAPS J 8(4) (2006) E731-42.
[12] E. Wagner, Converging paths of viral and non-viral vector engineering, Mol Ther 16(1) (2008) 1-2.
[13] E. Wagner, C. Plank, K. Zatloukal, M. Cotten, M.L. Birnstiel, Influenza virus hemagglutinin HA-2 N-terminal fusogenic peptides augment gene transfer by transferrin-polylysine-DNA complexes: toward a synthetic virus-like gene-transfer vehicle, Proc Natl Acad Sci U S A 89(17) (1992) 7934-8.
[14] G. Zuber, E. Dauty, M. Nothisen, P. Belguise, J.P. Behr, Towards synthetic viruses, Adv Drug Deliv Rev 52(3) (2001) 245-53.
[15] Y.L. Chiu, T.M. Rana, siRNA function in RNAi: a chemical modification analysis, RNA 9(9) (2003) 1034-48.
[16] A.D. Judge, V. Sood, J.R. Shaw, D. Fang, K. McClintock, I. MacLachlan, Sequence-dependent stimulation of the mammalian innate immune response by synthetic siRNA, Nat Biotechnol 23(4) (2005) 457-62.
[17] D.V. Morrissey, J.A. Lockridge, L. Shaw, K. Blanchard, K. Jensen, W. Breen, K. Hartsough, L. Machemer, S. Radka, V. Jadhav, N. Vaish, S. Zinnen, C. Vargeese, K. Bowman, C.S. Shaffer, L.B. Jeffs, A. Judge, I. MacLachlan, B. Polisky, Potent and persistent in vivo anti-HBV activity of chemically modified siRNAs, Nat Biotechnol 23(8) (2005) 1002-7.
[18] A.L. Jackson, P.S. Linsley, Recognizing and avoiding siRNA off-target effects for target identification and therapeutic application, Nat Rev Drug Discov 9(1) (2010) 57-67.

[19] K.A. Whitehead, J.E. Dahlman, R.S. Langer, D.G. Anderson, Silencing or stimulation? siRNA delivery and the immune system, Annu Rev Chem Biomol Eng 2 (2011) 77-96.
[20] E. Wagner, Strategies to improve DNA polyplexes for in vivo gene transfer: will "artificial viruses" be the answer?, Pharm Res 21(1) (2004) 8-14.
[21] G.F. Walker, C. Fella, J. Pelisek, J. Fahrmeir, S. Boeckle, M. Ogris, E. Wagner, Toward synthetic viruses: endosomal pH-triggered deshielding of targeted polyplexes greatly enhances gene transfer in vitro and in vivo, Mol Ther 11(3) (2005) 418-25.
[22] S. Mehier-Humbert, R.H. Guy, Physical methods for gene transfer: improving the kinetics of gene delivery into cells, Adv Drug Deliv Rev 57(5) (2005) 733-53.
[23] M.A. Mintzer, E.E. Simanek, Nonviral vectors for gene delivery, Chem Rev 109(2) (2009) 259-302.
[24] J. Wang, Z. Lu, M.G. Wientjes, J.L. Au, Delivery of siRNA therapeutics: barriers and carriers, AAPS J 12(4) (2010) 492-503.
[25] K. Nishina, T. Unno, Y. Uno, T. Kubodera, T. Kanouchi, H. Mizusawa, T. Yokota, Efficient in vivo delivery of siRNA to the liver by conjugation of alpha-tocopherol, Mol Ther 16(4) (2008) 734-40.
[26] S. Lau, B. Graham, N. Cao, B.J. Boyd, C.W. Pouton, P.J. White, Enhanced extravasation, stability and in vivo cardiac gene silencing via in situ siRNA-albumin conjugation, Mol Pharm 9(1) (2012) 71-80.
[27] M. Sioud, A. Mobergslien, Efficient siRNA targeted delivery into cancer cells by gastrin-releasing peptides, Bioconjug Chem 23(5) (2012) 1040-9.
[28] J.K. Nair, J.L. Willoughby, A. Chan, K. Charisse, M.R. Alam, Q. Wang, M. Hoekstra, P. Kandasamy, A.V. Kel'in, S. Milstein, N. Taneja, J. O'Shea, S. Shaikh, L. Zhang, R.J. van der Sluis, M.E. Jung, A. Akinc, R. Hutabarat, S. Kuchimanchi, K. Fitzgerald, T. Zimmermann, T.J. van Berkel, M.A. Maier, K.G. Rajeev, M. Manoharan, Multivalent N-acetylgalactosamine-conjugated siRNA localizes in hepatocytes and elicits robust RNAi-mediated gene silencing, J Am Chem Soc 136(49) (2014) 16958-61.
[29] B.R. Meade, K. Gogoi, A.S. Hamil, C. Palm-Apergi, A. van den Berg, J.C. Hagopian, A.D. Springer, A. Eguchi, A.D. Kacsinta, C.F. Dowdy, A. Presente, P. Lonn, M. Kaulich, N. Yoshioka, E. Gros, X.S. Cui, S.F. Dowdy, Efficient delivery of RNAi prodrugs containing reversible charge-neutralizing phosphotriester backbone modifications, Nat Biotechnol 32(12) (2014) 1256-61.
[30] R. Parmar, J.L. Willoughby, J. Liu, D.J. Foster, B. Brigham, C.S. Theile, K. Charisse, A. Akinc, E. Guidry, Y. Pei, W. Strapps, M. Cancilla, M.G. Stanton, K.G. Rajeev, L. Sepp-Lorenzino, M. Manoharan, R. Meyers, M.A. Maier, V. Jadhav, 5'-(E)-Vinylphosphonate: A Stable Phosphate Mimic Can Improve the RNAi Activity of siRNA-GalNAc Conjugates, Chembiochem (2016).
[31] A. Vaheri, J.S. Pagano, Infectious poliovirus RNA: a sensitive method of assay, Virology 27(3) (1965) 434-6.
[32] U. Lächelt, E. Wagner, Nucleic Acid Therapeutics Using Polyplexes: A Journey of 50 Years (and Beyond), Chem Rev 115(19) (2015) 11043-78.
[33] O. Boussif, F. Lezoualc'h, M.A. Zanta, M.D. Mergny, D. Scherman, B. Demeneix, J.P. Behr, A versatile vector for gene and oligonucleotide transfer into cells in culture and in vivo: polyethylenimine, Proc Natl Acad Sci U S A 92(16) (1995) 7297-301.
[34] S.C. De Smedt, J. Demeester, W.E. Hennink, Cationic polymer based gene delivery systems, Pharm Res 17(2) (2000) 113-26.
[35] D.W. Pack, A.S. Hoffman, S. Pun, P.S. Stayton, Design and development of polymers for gene delivery, Nat Rev Drug Discov 4(7) (2005) 581-93.

[36] K. Miyata, N. Nishiyama, K. Kataoka, Rational design of smart supramolecular assemblies for gene delivery: chemical challenges in the creation of artificial viruses, Chem. Soc. Rev. 41(7) (2012) 2562-2574.
[37] S.C. Semple, A. Akinc, J. Chen, A.P. Sandhu, B.L. Mui, C.K. Cho, D.W.Y. Sah, D. Stebbing, E.J. Crosley, E. Yaworski, I.M. Hafez, J.R. Dorkin, J. Qin, K. Lam, K.G. Rajeev, K.F. Wong, L.B. Jeffs, L. Nechev, M.L. Eisenhardt, M. Jayaraman, M. Kazem, M.A. Maier, M. Srinivasulu, M.J. Weinstein, Q. Chen, R. Alvarez, S.A. Barros, S. De, S.K. Klimuk, T. Borland, V. Kosovrasti, W.L. Cantley, Y.K. Tam, M. Manoharan, M.A. Ciufolini, M.A. Tracy, A. de Fougerolles, I. MacLachlan, P.R. Cullis, T.D. Madden, M.J. Hope, Rational design of cationic lipids for siRNA delivery, Nat Biotech 28(2) (2010) 172-176.
[38] M. Mevel, T. Haudebourg, T. Colombani, P. Peuziat, L. Dallet, B. Chatin, O. Lambert, M. Berchel, T. Montier, P.A. Jaffres, P. Lehn, B. Pitard, Important role of phosphoramido linkage in imidazole-based dioleyl helper lipids for liposome stability and primary cell transfection, The journal of gene medicine 18(1-3) (2016) 3-15.
[39] Z. Kadlecova, L. Baldi, D. Hacker, F.M. Wurm, H.A. Klok, Comparative study on the in vitro cytotoxicity of linear, dendritic, and hyperbranched polylysine analogues, Biomacromolecules 13(10) (2012) 3127-37.
[40] C. Scholz, P. Kos, L. Leclercq, X. Jin, H. Cottet, E. Wagner, Correlation of Length of Linear Oligo(ethanamino) Amides with Gene Transfer and Cytotoxicity, ChemMedChem (2014).
[41] C. Scholz, P. Kos, E. Wagner, Comb-like oligoaminoethane carriers: change in topology improves pDNA delivery, Bioconjug Chem 25(2) (2014) 251-61.
[42] D. Schaffert, N. Badgujar, E. Wagner, Novel Fmoc-polyamino acids for solid-phase synthesis of defined polyamidoamines, Org Lett 13(7) (2011) 1586-9.
[43] D. Schaffert, C. Troiber, E.E. Salcher, T. Fröhlich, I. Martin, N. Badgujar, C. Dohmen, D. Edinger, R. Kläger, G. Maiwald, K. Farkasova, S. Seeber, K. Jahn-Hofmann, P. Hadwiger, E. Wagner, Solid-phase synthesis of sequence-defined T-, i-, and U-shape polymers for pDNA and siRNA delivery, Angew Chem Int Ed Engl 50(38) (2011) 8986-9.
[44] T. Fröhlich, D. Edinger, R. Kläger, C. Troiber, E. Salcher, N. Badgujar, I. Martin, D. Schaffert, A. Cengizeroglu, P. Hadwiger, H.P. Vornlocher, E. Wagner, Structure-activity relationships of siRNA carriers based on sequence-defined oligo (ethane amino) amides, J Control Release 160(3) (2012) 532-41.
[45] V.A. Bloomfield, Condensation of DNA by multivalent cations: considerations on mechanism, Biopolymers 31(13) (1991) 1471-81.
[46] E. Wagner, M. Cotten, R. Foisner, M.L. Birnstiel, Transferrin-polycation-DNA complexes: the effect of polycations on the structure of the complex and DNA delivery to cells, Proc.Natl.Acad.Sci.U.S.A 88(10) (1991) 4255-4259.
[47] V.A. Bloomfield, DNA condensation by multivalent cations, Biopolymers 44(3) (1997) 269-82.
[48] K. Osada, H. Oshima, D. Kobayashi, M. Doi, M. Enoki, Y. Yamasaki, K. Kataoka, Quantized folding of plasmid DNA condensed with block catiomer into characteristic rod structures promoting transgene efficacy, J Am Chem Soc 132(35) (2010) 12343-8.
[49] A. Dirisala, K. Osada, Q. Chen, T.A. Tockary, K. Machitani, S. Osawa, X. Liu, T. Ishii, K. Miyata, M. Oba, S. Uchida, K. Itaka, K. Kataoka, Optimized rod length of polyplex micelles for maximizing transfection efficiency and their performance in systemic gene therapy against stroma-rich pancreatic tumors, Biomaterials 35(20) (2014) 5359-68.

[50] W. Zhang, W. Rödl, D. He, M. Döblinger, U. Lächelt, E. Wagner, Combination of sequence-defined oligoaminoamides with transferrin-polycation conjugates for receptor-targeted gene delivery, The journal of gene medicine 17(8-9) (2015) 161-72.
[51] C. Dohmen, D. Edinger, T. Fröhlich, L. Schreiner, U. Lächelt, C. Troiber, J. Rädler, P. Hadwiger, H.P. Vornlocher, E. Wagner, Nanosized multifunctional polyplexes for receptor-mediated siRNA delivery, ACS Nano 6(6) (2012) 5198-208.
[52] R.S. Burke, S.H. Pun, Extracellular barriers to in Vivo PEI and PEGylated PEI polyplex-mediated gene delivery to the liver, Bioconjug Chem 19(3) (2008) 693-704.
[53] C. Scholz, E. Wagner, Therapeutic plasmid DNA versus siRNA delivery: common and different tasks for synthetic carriers, J Control Release 161(2) (2012) 554-65.
[54] E. Wagner, Biomaterials in RNAi therapeutics: quo vadis?, Biomater. Sci. 1 (2013) 804–809.
[55] S. Matsumoto, R.J. Christie, N. Nishiyama, K. Miyata, A. Ishii, M. Oba, H. Koyama, Y. Yamasaki, K. Kataoka, Environment-responsive block copolymer micelles with a disulfide cross-linked core for enhanced siRNA delivery, Biomacromolecules 10(1) (2009) 119-27.
[56] R.G. Parmar, M. Busuek, E.S. Walsh, K.R. Leander, B.J. Howell, L. Sepp-Lorenzino, E. Kemp, L.S. Crocker, A. Leone, C.J. Kochansky, B.A. Carr, R.M. Garbaccio, S.L. Colletti, W. Wang, Endosomolytic bioreducible poly(amido amine disulfide) polymer conjugates for the in vivo systemic delivery of siRNA therapeutics, Bioconjug Chem 24(4) (2013) 640-7.
[57] A. Akinc, A. Zumbuehl, M. Goldberg, E.S. Leshchiner, V. Busini, N. Hossain, S.A. Bacallado, D.N. Nguyen, J. Fuller, R. Alvarez, A. Borodovsky, T. Borland, R. Constien, A. de Fougerolles, J.R. Dorkin, K. Narayanannair Jayaprakash, M. Jayaraman, M. John, V. Koteliansky, M. Manoharan, L. Nechev, J. Qin, T. Racie, D. Raitcheva, K.G. Rajeev, D.W. Sah, J. Soutschek, I. Toudjarska, H.P. Vornlocher, T.S. Zimmermann, R. Langer, D.G. Anderson, A combinatorial library of lipid-like materials for delivery of RNAi therapeutics, Nat Biotechnol 26(5) (2008) 561-9.
[58] A. Philipp, X. Zhao, P. Tarcha, E. Wagner, A. Zintchenko, Hydrophobically modified oligoethylenimines as highly efficient transfection agents for siRNA delivery, Bioconjug Chem 20(11) (2009) 2055-61.
[59] G. Creusat, A.S. Rinaldi, E. Weiss, R. Elbaghdadi, J.S. Remy, R. Mulherkar, G. Zuber, Proton sponge trick for pH-sensitive disassembly of polyethylenimine-based siRNA delivery systems, Bioconjug Chem 21(5) (2010) 994-1002.
[60] S. Uchida, H. Kinoh, T. Ishii, A. Matsui, T.A. Tockary, K.M. Takeda, H. Uchida, K. Osada, K. Itaka, K. Kataoka, Systemic delivery of messenger RNA for the treatment of pancreatic cancer using polyplex nanomicelles with a cholesterol moiety, Biomaterials 82 (2016) 221-8.
[61] D.B. Rozema, D.L. Lewis, D.H. Wakefield, S.C. Wong, J.J. Klein, P.L. Roesch, S.L. Bertin, T.W. Reppen, Q. Chu, A.V. Blokhin, J.E. Hagstrom, J.A. Wolff, Dynamic PolyConjugates for targeted in vivo delivery of siRNA to hepatocytes, Proc Natl Acad Sci U S A 104(32) (2007) 12982-7.
[62] M. Meyer, C. Dohmen, A. Philipp, D. Kiener, G. Maiwald, C. Scheu, M. Ogris, E. Wagner, Synthesis and biological evaluation of a bioresponsive and endosomolytic siRNA-polymer conjugate, Mol Pharm 6(3) (2009) 752-62.
[63] S. Svenson, R.I. Case, R.O. Cole, J. Hwang, S.R. Kabir, D. Lazarus, P. Lim Soo, P.S. Ng, C. Peters, P. Shum, B. Sweryda-Krawiec, S. Tripathi, D. van der Poll, S. Eliasof, Tumor Selective Silencing Using an RNAi-Conjugated Polymeric Nanopharmaceutical, Mol Pharm 13(3) (2016) 737-47.

[64] C. Troiber, D. Edinger, P. Kos, L. Schreiner, R. Kläger, A. Herrmann, E. Wagner, Stabilizing effect of tyrosine trimers on pDNA and siRNA polyplexes, Biomaterials 34(5) (2013) 1624-33.
[65] L. Wightman, R. Kircheis, V. Rössler, S. Carotta, R. Ruzicka, M. Kursa, E. Wagner, Different behavior of branched and linear polyethylenimine for gene delivery in vitro and in vivo, The journal of gene medicine 3(4) (2001) 362-72.
[66] J.C. Kasper, D. Schaffert, M. Ogris, E. Wagner, W. Friess, The establishment of an up-scaled micro-mixer method allows the standardized and reproducible preparation of well-defined plasmid/LPEI polyplexes, Eur J Pharm Biopharm 77(1) (2011) 182-5.
[67] J.C. Kasper, C. Troiber, S. Kuchler, E. Wagner, W. Friess, Formulation development of lyophilized, long-term stable siRNA/oligoaminoamide polyplexes, Eur J Pharm Biopharm 85(2) (2013) 294-305.
[68] C. Troiber, J.C. Kasper, S. Milani, M. Scheible, I. Martin, F. Schaubhut, S. Kuchler, J. Rädler, F.C. Simmel, W. Friess, E. Wagner, Comparison of four different particle sizing methods for siRNA polyplex characterization, Eur J Pharm Biopharm (2012).
[69] D. He, K. Müller, A. Krhac Levacic, P. Kos, U. Lächelt, E. Wagner, Combinatorial Optimization of Sequence-Defined Oligo(ethanamino)amides for Folate Receptor-Targeted pDNA and siRNA Delivery, Bioconjug Chem 27(3) (2016) 647-59.
[70] F.Q. Schäfer, G.R. Buettner, Redox environment of the cell as viewed through the redox state of the glutathione disulfide/glutathione couple, Free Radic Biol Med 30(11) (2001) 1191-212.
[71] P.M. Klein, E. Wagner, Bioreducible polycations as shuttles for therapeutic nucleic acid and protein transfection, Antioxidants & redox signaling 21(5) (2014) 804-17.
[72] P.M. Klein, K. Müller, C. Gutmann, P. Kos, A. Krhac Levacic, D. Edinger, M. Höhn, J.C. Leroux, M.A. Gauthier, E. Wagner, Twin disulfides as opportunity for improving stability and transfection efficiency of oligoaminoethane polyplexes, J Control Release 205 (2015) 109-19.
[73] C. Wu, J.C. Leroux, M.A. Gauthier, Twin disulfides for orthogonal disulfide pairing and the directed folding of multicyclic peptides, Nat Chem 4(12) (2012) 1044-9.
[74] A.L. Bolcato-Bellemin, M.E. Bonnet, G. Creusat, P. Erbacher, J.P. Behr, Sticky overhangs enhance siRNA-mediated gene silencing, Proc Natl Acad Sci U S A 104(41) (2007) 16050-5.
[75] H. Mok, S.H. Lee, J.W. Park, T.G. Park, Multimeric small interfering ribonucleic acid for highly efficient sequence-specific gene silencing, Nat Mater 9(3) (2010) 272-8.
[76] K. Brunner, J. Harder, T. Halbach, J. Willibald, F. Spada, F. Gnerlich, K. Sparrer, A. Beil, L. Mockl, C. Brauchle, K.K. Conzelmann, T. Carell, Cell-penetrating and neurotargeting dendritic siRNA nanostructures, Angew Chem Int Ed Engl 54(6) (2015) 1946-9.
[77] H. Chang Kang, Y.H. Bae, Co-delivery of small interfering RNA and plasmid DNA using a polymeric vector incorporating endosomolytic oligomeric sulfonamide, Biomaterials 32(21) (2011) 4914-24.
[78] P. Heissig, P.M. Klein, P. Hadwiger, E. Wagner, DNA as Tunable Adaptor for siRNA Polyplex Stabilization and Functionalization, Mol Ther Nucleic Acids 5 (2016) e288.
[79] C. Dohmen, T. Fröhlich, U. Lächelt, I. Rohl, H.P. Vornlocher, P. Hadwiger, E. Wagner, Defined Folate-PEG-siRNA Conjugates for Receptor-specific Gene Silencing, Mol Ther Nucleic Acids 1 (2012) e7.
[80] E. Wagner, Effects of membrane-active agents in gene delivery, J Control Release 53(1-3) (1998) 155-8.

[81] S. Boeckle, J. Fahrmeir, W. Roedl, M. Ogris, E. Wagner, Melittin analogs with high lytic activity at endosomal pH enhance transfection with purified targeted PEI polyplexes, J Control Release 112(2) (2006) 240-8.
[82] C. Plank, K. Mechtler, F.C. Szoka, Jr., E. Wagner, Activation of the complement system by synthetic DNA complexes: a potential barrier for intravenous gene delivery, Hum Gene Ther 7(12) (1996) 1437-46.
[83] O.M. Merkel, R. Urbanics, P. Bedocs, Z. Rozsnyay, L. Rosivall, M. Toth, T. Kissel, J. Szebeni, In vitro and in vivo complement activation and related anaphylactic effects associated with polyethylenimine and polyethylenimine-graft-poly(ethylene glycol) block copolymers, Biomaterials 32(21) (2011) 4936-42.
[84] P. Chollet, M.C. Favrot, A. Hurbin, J.L. Coll, Side-effects of a systemic injection of linear polyethylenimine-DNA complexes, The journal of gene medicine 4(1) (2002) 84-91.
[85] S. Zalipsky, N. Mullah, J.A. Harding, J. Gittelman, L. Guo, S.A. DeFrees, Poly(ethylene glycol)-grafted liposomes with oligopeptide or oligosaccharide ligands appended to the termini of the polymer chains, Bioconjug Chem 8(2) (1997) 111-8.
[86] S.H. Pun, M.E. Davis, Development of a nonviral gene delivery vehicle for systemic application, Bioconjug Chem 13(3) (2002) 630-9.
[87] N.C. Bellocq, S.H. Pun, G.S. Jensen, M.E. Davis, Transferrin-containing, cyclodextrin polymer-based particles for tumor-targeted gene delivery, Bioconjug Chem 14(6) (2003) 1122-32.
[88] M.A. Wolfert, E.H. Schacht, V. Toncheva, K. Ulbrich, O. Nazarova, L.W. Seymour, Characterization of vectors for gene therapy formed by self-assembly of DNA with synthetic block co-polymers, Hum Gene Ther 7(17) (1996) 2123-33.
[89] R.N. Johnson, D.S. Chu, J. Shi, J.G. Schellinger, P.M. Carlson, S.H. Pun, HPMA-oligolysine copolymers for gene delivery: optimization of peptide length and polymer molecular weight, J Control Release 155(2) (2011) 303-11.
[90] R. Laga, R. Carlisle, M. Tangney, K. Ulbrich, L.W. Seymour, Polymer coatings for delivery of nucleic acid therapeutics, J Control Release 161(2) (2012) 537-53.
[91] M. Noga, D. Edinger, W. Rödl, E. Wagner, G. Winter, A. Besheer, Controlled shielding and deshielding of gene delivery polyplexes using hydroxyethyl starch (HES) and alpha-amylase, J Control Release 159(1) (2012) 92-103.
[92] M. Hornof, M. de la Fuente, M. Hallikainen, R.H. Tammi, A. Urtti, Low molecular weight hyaluronan shielding of DNA/PEI polyplexes facilitates CD44 receptor mediated uptake in human corneal epithelial cells, The journal of gene medicine 10(1) (2008) 70-80.
[93] F. Manzenrieder, R. Luxenhofer, M. Retzlaff, R. Jordan, M.G. Finn, Stabilization of virus-like particles with poly(2-oxazoline)s, Angew Chem Int Ed Engl 50(11) (2011) 2601-5.
[94] P. Heller, A. Birke, D. Huesmann, B. Weber, K. Fischer, A. Reske-Kunz, M. Bros, M. Barz, Introducing PeptoPlexes: polylysine-block-polysarcosine based polyplexes for transfection of HEK 293T cells, Macromol Biosci 14(10) (2014) 1380-95.
[95] K. Kunath, A. von Harpe, H. Petersen, D. Fischer, K. Voigt, T. Kissel, U. Bickel, The structure of PEG-modified poly(ethylene imines) influences biodistribution and pharmacokinetics of their complexes with NF-kappaB decoy in mice, Pharm Res 19(6) (2002) 810-7.
[96] T. Merdan, K. Kunath, H. Petersen, U. Bakowsky, K.H. Voigt, J. Kopecek, T. Kissel, PEGylation of poly(ethylene imine) affects stability of complexes with plasmid DNA under in vivo conditions in a dose-dependent manner after intravenous injection into mice, Bioconjug Chem 16(4) (2005) 785-92.

[97] H. Maeda, The enhanced permeability and retention (EPR) effect in tumor vasculature: the key role of tumor-selective macromolecular drug targeting, Adv Enzyme Regul 41 (2001) 189-207.
[98] C. Fella, G.F. Walker, M. Ogris, E. Wagner, Amine-reactive pyridylhydrazone-based PEG reagents for pH-reversible PEI polyplex shielding, Eur J Pharm Sci 34(4-5) (2008) 309-20.
[99] K.A. Mislick, J.D. Baldeschwieler, J.F. Kayyem, T.J. Meade, Transfection of folate-polylysine DNA complexes: evidence for lysosomal delivery, Bioconjug Chem 6(5) (1995) 512-5.
[100] B. Liang, M.L. He, Z.P. Xiao, Y. Li, C.Y. Chan, H.F. Kung, X.T. Shuai, Y. Peng, Synthesis and characterization of folate-PEG-grafted-hyperbranched-PEI for tumor-targeted gene delivery, Biochem Biophys Res Commun 367(4) (2008) 874-80.
[101] L. Novo, E. Mastrobattista, C.F. van Nostrum, W.E. Hennink, Targeted decationized polyplexes for cell specific gene delivery, Bioconjug Chem 25(4) (2014) 802-12.
[102] I. Martin, C. Dohmen, C. Mas-Moruno, C. Troiber, P. Kos, D. Schaffert, U. Lächelt, M. Teixido, M. Gunther, H. Kessler, E. Giralt, E. Wagner, Solid-phase-assisted synthesis of targeting peptide-PEG-oligo(ethane amino)amides for receptor-mediated gene delivery, Org Biomol Chem 10(16) (2012) 3258-68.
[103] G.Y. Wu, C.H. Wu, Receptor-mediated gene delivery and expression in vivo 738, J Biol Chem 262 (1988) 14621-14624.
[104] E. Wagner, M. Zenke, M. Cotten, H. Beug, M.L. Birnstiel, Transferrin-polycation conjugates as carriers for DNA uptake into cells, Proc.Natl.Acad.Sci.U.S.A 87(9) (1990) 3410-3414.
[105] Z.M. Ding, R.J. Cristiano, J.A. Roth, B. Takacs, M.T. Kuo, Malarial circumsporozoite protein is a novel gene delivery vehicle to primary hepatocyte cultures and cultured cells, J Biol Chem 270(8) (1995) 3667-76.
[106] M. Buschle, M. Cotten, H. Kirlappos, K. Mechtler, G. Schaffner, W. Zauner, M.L. Birnstiel, E. Wagner, Receptor-mediated gene transfer into human T lymphocytes via binding of DNA/CD3 antibody particles to the CD3 T cell receptor complex, Hum Gene Ther 6(6) (1995) 753-61.
[107] J.L. Coll, E. Wagner, V. Combaret, K. Metchler, H. Amstutz, I. Iacono-Di-Cacito, N. Simon, M.C. Favrot, In vitro targeting and specific transfection of human neuroblastoma cells by chCE7 antibody-mediated gene transfer, Gene Ther. 4(2) (1997) 156-161.
[108] N. Shahidi-Hamedani, W.T. Shier, F. Moghadam Ariaee, K. Abnous, M. Ramezani, Targeted gene delivery with noncovalent electrostatic conjugates of sgc-8c aptamer and polyethylenimine, The journal of gene medicine 15(6-7) (2013) 261-9.
[109] Y. Nie, D. Schaffert, W. Rödl, M. Ogris, E. Wagner, M. Gunther, Dual-targeted polyplexes: one step towards a synthetic virus for cancer gene therapy, J Control Release 152(1) (2011) 127-34.
[110] P. Kos, U. Lächelt, D. He, Y. Nie, Z. Gu, E. Wagner, Dual-targeted polyplexes based on sequence-defined peptide-PEG-oligoamino amides, J Pharm Sci 104(2) (2015) 464-75.
[111] J. DeRouchey, G.F. Walker, E. Wagner, J.O. Rädler, Decorated rods: a "bottom-up" self-assembly of monomolecular DNA complexes, J Phys Chem B 110(10) (2006) 4548-54.
[112] H.S. Choi, W. Liu, F. Liu, K. Nasr, P. Misra, M.G. Bawendi, J.V. Frangioni, Design considerations for tumour-targeted nanoparticles, Nat Nanotechnol 5(1) (2010) 42-7.

[113] W. Zhang, K. Müller, E. Kessel, S. Reinhard, D. He, P.M. Klein, M. Höhn, W. Rödl, S. Kempter, E. Wagner, Targeted siRNA Delivery Using a Lipo-Oligoaminoamide Nano-Core with an Influenza Peptide and Transferrin Shell, Adv Healthc Mater (2016).
[114] W. Zauner, D. Blaas, E. Kuechler, E. Wagner, Rhinovirus-mediated endosomal release of transfection complexes, J Virol 69(2) (1995) 1085-92.
[115] C. Plank, W. Zauner, E. Wagner, Application of membrane-active peptides for drug and gene delivery across cellular membranes, Adv Drug Deliv Rev 34(1) (1998) 21-35.
[116] C. Plank, B. Oberhauser, K. Mechtler, C. Koch, E. Wagner, The influence of endosome-disruptive peptides on gene transfer using synthetic virus-like gene transfer systems, J Biol Chem 269(17) (1994) 12918-24.
[117] M. Cotten, F. Langle-Rouault, H. Kirlappos, E. Wagner, K. Mechtler, M. Zenke, H. Beug, M.L. Birnstiel, Transferrin-polycation-mediated introduction of DNA into human leukemic cells: stimulation by agents that affect the survival of transfected DNA or modulate transferrin receptor levels, Proc.Natl.Acad.Sci.U.S.A 87(11) (1990) 4033-4037.
[118] P. Erbacher, A.C. Roche, M. Monsigny, P. Midoux, Putative role of chloroquine in gene transfer into a human hepatoma cell line by DNA/lactosylated polylysine complexes, Exp Cell Res 225 (1996) 186-194.
[119] J. Cheng, R. Zeidan, S. Mishra, A. Liu, S.H. Pun, R.P. Kulkarni, G.S. Jensen, N.C. Bellocq, M.E. Davis, Structure-function correlation of chloroquine and analogues as transgene expression enhancers in nonviral gene delivery, J.Med.Chem 49(22) (2006) 6522-6531.
[120] J.P. Behr, The Proton Sponge: a Trick to Enter Cells the Viruses Did Not Exploit, Chimia 51(1/2) (1997) 34-36.
[121] N.D. Sonawane, F.C. Szoka, Jr., A.S. Verkman, Chloride accumulation and swelling in endosomes enhances DNA transfer by polyamine-DNA polyplexes, J Biol Chem 278(45) (2003) 44826-31.
[122] J.D. Ziebarth, Y. Wang, Understanding the protonation behavior of linear polyethylenimine in solutions through Monte Carlo simulations, Biomacromolecules 11(1) (2010) 29-38.
[123] A.M. Funhoff, C.F. van Nostrum, G.A. Koning, N.M. Schuurmans-Nieuwenbroek, D.J. Crommelin, W.E. Hennink, Endosomal escape of polymeric gene delivery complexes is not always enhanced by polymers buffering at low pH, Biomacromolecules 5(1) (2004) 32-9.
[124] R.V. Benjaminsen, M.A. Mattebjerg, J.R. Henriksen, S.M. Moghimi, T.L. Andresen, The possible "proton sponge " effect of polyethylenimine (PEI) does not include change in lysosomal pH, Mol Ther 21(1) (2013) 149-57.
[125] P. Kos, U. Lächelt, A. Herrmann, F.M. Mickler, M. Döblinger, D. He, A. Krhac Levacic, S. Morys, C. Brauchle, E. Wagner, Histidine-rich stabilized polyplexes for cMet-directed tumor-targeted gene transfer, Nanoscale 7(12) (2015) 5350-62.
[126] U. Lächelt, P. Kos, F.M. Mickler, A. Herrmann, E.E. Salcher, W. Rödl, N. Badgujar, C. Brauchle, E. Wagner, Fine-tuning of proton sponges by precise diaminoethanes and histidines in pDNA polyplexes, Nanomedicine 10(1) (2014) 35-44.
[127] P. Midoux, M. Monsigny, Efficient gene transfer by histidylated polylysine/pDNA complexes, Bioconjug Chem 10(3) (1999) 406-11.
[128] Q. Leng, P. Scaria, J. Zhu, N. Ambulos, P. Campbell, A.J. Mixson, Highly branched HK peptides are effective carriers of siRNA, The journal of gene medicine 7(7) (2005) 977-86.

[129] X.L. Wang, S. Ramusovic, T. Nguyen, Z.R. Lu, Novel polymerizable surfactants with pH-sensitive amphiphilicity and cell membrane disruption for efficient siRNA delivery, Bioconjug Chem 18(6) (2007) 2169-77.
[130] D. Schaffert, C. Troiber, E. Wagner, New sequence-defined polyaminoamides with tailored endosomolytic properties for plasmid DNA delivery, Bioconjug Chem 23(6) (2012) 1157-65.
[131] N. Murthy, J. Campbell, N. Fausto, A.S. Hoffman, P.S. Stayton, Design and synthesis of pH-responsive polymeric carriers that target uptake and enhance the intracellular delivery of oligonucleotides, J Control Release 89(3) (2003) 365-74.
[132] K. Moller, K. Müller, H. Engelke, C. Brauchle, E. Wagner, T. Bein, Highly efficient siRNA delivery from core-shell mesoporous silica nanoparticles with multifunctional polymer caps, Nanoscale 8(7) (2016) 4007-19.
[133] D.M. Lynn, D.G. Anderson, D. Putnam, R. Langer, Accelerated discovery of synthetic transfection vectors: parallel synthesis and screening of a degradable polymer library, J Am Chem Soc 123(33) (2001) 8155-6.
[134] D.G. Anderson, D.M. Lynn, R. Langer, Semi-automated synthesis and screening of a large library of degradable cationic polymers for gene delivery, Angew Chem Int Ed Engl 42(27) (2003) 3153-8.
[135] K.T. Love, K.P. Mahon, C.G. Levins, K.A. Whitehead, W. Querbes, J.R. Dorkin, J. Qin, W. Cantley, L.L. Qin, T. Racie, M. Frank-Kamenetsky, K.N. Yip, R. Alvarez, D.W. Sah, A. de Fougerolles, K. Fitzgerald, V. Koteliansky, A. Akinc, R. Langer, D.G. Anderson, Lipid-like materials for low-dose, in vivo gene silencing, Proc Natl Acad Sci U S A 107(5) (2010) 1864-9.
[136] E. Wagner, Polymers for nucleic acid transfer-an overview, Adv Genet 88 (2014) 231-61.
[137] K.A. Whitehead, J.R. Dorkin, A.J. Vegas, P.H. Chang, O. Veiseh, J. Matthews, O.S. Fenton, Y. Zhang, K.T. Olejnik, V. Yesilyurt, D. Chen, S. Barros, B. Klebanov, T. Novobrantseva, R. Langer, D.G. Anderson, Degradable lipid nanoparticles with predictable in vivo siRNA delivery activity, Nat Commun 5 (2014) 4277.
[138] H. Cabral, Y. Matsumoto, K. Mizuno, Q. Chen, M. Murakami, M. Kimura, Y. Terada, M.R. Kano, K. Miyazono, M. Uesaka, N. Nishiyama, K. Kataoka, Accumulation of sub-100 nm polymeric micelles in poorly permeable tumours depends on size, Nat Nanotechnol 6(12) (2011) 815-23.
[139] D.J. Lee, E. Kessel, D. Edinger, D. He, P.M. Klein, L. Voith von Voithenberg, D.C. Lamb, U. Lächelt, T. Lehto, E. Wagner, Dual antitumoral potency of EG5 siRNA nanoplexes armed with cytotoxic bifunctional glutamyl-methotrexate targeting ligand, Biomaterials 77 (2016) 98-110.
[140] T.A. Garrow, A. Admon, B. Shane, Expression cloning of a human cDNA encoding folylpoly(gamma-glutamate) synthetase and determination of its primary structure, Proc Natl Acad Sci U S A 89(19) (1992) 9151-5.
[141] A.L. Jackman, D.S. Theti, D.D. Gibbs, Antifolates targeted specifically to the folate receptor, Adv Drug Deliv Rev 56(8) (2004) 1111-25.
[142] I. van Rooy, S. Cakir-Tascioglu, W.E. Hennink, G. Storm, R.M. Schiffelers, E. Mastrobattista, In vivo methods to study uptake of nanoparticles into the brain, Pharm Res 28(3) (2011) 456-71.
[143] M.W. Bradbury, The structure and function of the blood-brain barrier, Fed Proc 43(2) (1984) 186-90.
[144] N.J. Abbott, A.A. Patabendige, D.E. Dolman, S.R. Yusof, D.J. Begley, Structure and function of the blood-brain barrier, Neurobiol Dis 37(1) (2010) 13-25.

[145] M. Shilo, A. Sharon, K. Baranes, M. Motiei, J.P. Lellouche, R. Popovtzer, The effect of nanoparticle size on the probability to cross the blood-brain barrier: an in-vitro endothelial cell model, J Nanobiotechnology 13 (2015) 19.
[146] S. An, D. He, E. Wagner, C. Jiang, Peptide-like Polymers Exerting Effective Glioma-Targeted siRNA Delivery and Release for Therapeutic Application, Small 11(38) (2015) 5142-50.
[147] M. Ammirante, A. Rosati, C. Arra, A. Basile, A. Falco, M. Festa, M. Pascale, M. d'Avenia, L. Marzullo, M.A. Belisario, M. De Marco, A. Barbieri, A. Giudice, G. Chiappetta, E. Vuttariello, M. Monaco, P. Bonelli, G. Salvatore, M. Di Benedetto, S.L. Deshmane, K. Khalili, M.C. Turco, A. Leone, IKK{gamma} protein is a target of BAG3 regulatory activity in human tumor growth, Proc Natl Acad Sci U S A 107(16) (2010) 7497-502.
[148] M. Festa, L. Del Valle, K. Khalili, R. Franco, G. Scognamiglio, V. Graziano, V. De Laurenzi, M.C. Turco, A. Rosati, BAG3 protein is overexpressed in human glioblastoma and is a potential target for therapy, Am J Pathol 178(6) (2011) 2504-12.
[149] A. Zintchenko, A. Philipp, A. Dehshahri, E. Wagner, Simple Modifications of Branched PEI Lead to Highly Efficient siRNA Carriers with Low Toxicity, Bioconjugate Chemistry 19(7) (2008) 1448-1455.
[150] K. Maier, E. Wagner, Acid-Labile Traceless Click Linker for Protein Transduction, Journal of the American Chemical Society 134(24) (2012) 10169-10173.
[151] T. Fröhlich, D. Edinger, V. Russ, E. Wagner, Stabilization of polyplexes via polymer crosslinking for efficient siRNA delivery, Eur J Pharm Sci 47(5) (2012) 914-20.
[152] P. Zhang, D. He, P.M. Klein, X. Liu, R. Röder, M. Döblinger, E. Wagner, Enhanced Intracellular Protein Transduction by Sequence Defined Tetra-Oleoyl Oligoaminoamides Targeted for Cancer Therapy, Advanced Functional Materials 25(42) (2015) 6627-6636.
[153] E. Kaiser, R.L. Colescott, C.D. Bossinger, P.I. Cook, Color test for detection of free terminal amino groups in the solid-phase synthesis of peptides, Anal Biochem 34(2) (1970) 595-8.
[154] X. Zhang, M. Scalf, T.W. Berggren, M.S. Westphall, L.M. Smith, Identification of mammalian cell lines using MALDI-TOF and LC-ESI-MS/MS mass spectrometry, Journal of the American Society for Mass Spectrometry 17(4) (2006) 490-499.
[155] P. Zhang, B. Steinborn, U. Lächelt, S. Zahler, E. Wagner, Lipo-Oligomer Nanoformulations for Targeted Intracellular Protein Delivery, Biomacromolecules 18(8) (2017) 2509-2520.
[156] E.R. Lee, J. Marshall, C.S. Siegel, C. Jiang, N.S. Yew, M.R. Nichols, J.B. Nietupski, R.J. Ziegler, M.B. Lane, K.X. Wang, N.C. Wan, R.K. Scheule, D.J. Harris, A.E. Smith, S.H. Cheng, Detailed Analysis of Structures and Formulations of Cationic Lipids for Efficient Gene Transfer to the Lung, Human Gene Therapy 7(14) (1996) 1701-1717.
[157] J.B. Ma, K. Ye, D.J. Patel, Structural basis for overhang-specific small interfering RNA recognition by the PAZ domain, Nature 429(6989) (2004) 318-322.
[158] B. Martin, M. Sainlos, A. Aissaoui, N. Oudrhiri, M. Hauchecorne, J.P. Vigneron, J.M. Lehn, P. Lehn, The Design of Cationic Lipids for Gene Delivery, Current Pharmaceutical Design 11(3) (2005) 375-394.
[159] T. Le Gall, D. Loizeau, E. Picquet, N. Carmoy, J.-J. Yaouanc, L. Burel-Deschamps, P. Delépine, P. Giamarchi, P.-A. Jaffrès, P. Lehn, T. Montier, A Novel Cationic Lipophosphoramide with Diunsaturated Lipid Chains: Synthesis, Physicochemical Properties, and Transfection Activities, Journal of Medicinal Chemistry 53(4) (2010) 1496-1508.

[160] P.L. Felgner, T.R. Gadek, M. Holm, R. Roman, H.W. Chan, M. Wenz, J.P. Northrop, G.M. Ringold, M. Danielsen, Lipofection: a highly efficient, lipid-mediated DNA-transfection procedure, Proceedings of the National Academy of Sciences of the United States of America 84(21) (1987) 7413-7417.
[161] R.W. Malone, P.L. Felgner, I.M. Verma, Cationic liposome-mediated RNA transfection, Proceedings of the National Academy of Sciences of the United States of America 86(16) (1989) 6077-6081.
[162] J.-P. Behr, Gene Transfer with Synthetic Cationic Amphiphiles: Prospects for Gene Therapy, Bioconjugate Chemistry 5(5) (1994) 382-389.
[163] G.S. Harrison, Y. Wang, J. Tomczak, C. Hogan, E.J. Shpall, T.J. Curiel, P.L. Felgner, Optimization of gene transfer using cationic lipids in cell lines and primary human CD4+ and CD34+ hematopoietic cells, Biotechniques 19(5) (1995) 816-823.
[164] M.L. Shin, G. Hänsch, M.M. Mayer, Effect of agents that produce membrane disorder on lysis of erythrocytes by complement, Proceedings of the National Academy of Sciences of the United States of America 78(4) (1981) 2522-2525.
[165] S.M. Gruner, P.R. Cullis, M.J. Hope, C.P.S. Tilcock, Lipid Polymorphism:The Molecular Basis of Nonbilayer Phases, Annual Review of Biophysics and Biophysical Chemistry 14(1) (1985) 211-238.
[166] R. Koynova, L. Wang, R.C. MacDonald, An intracellular lamellar–nonlamellar phase transition rationalizes the superior performance of some cationic lipid transfection agents, Proceedings of the National Academy of Sciences 103(39) (2006) 14373-14378.
[167] B.G. Tenchov, L. Wang, R. Koynova, R.C. MacDonald, Modulation of a membrane lipid lamellar-nonlamellar phase transition by cationic lipids: a measure for transfection efficiency, Biochim Biophys Acta 1778(10) (2008) 2405-2412.
[168] R. Koynova, B. Tenchov, L. Wang, R.C. MacDonald, Hydrophobic Moiety of Cationic Lipids Strongly Modulates Their Transfection Activity, Molecular Pharmaceutics 6(3) (2009) 951-958.
[169] I. Wrobel, D. Collins, Fusion of cationic liposomes with mammalian cells occurs after endocytosis, Biochim Biophys Acta 1235(2) (1995) 296-304.
[170] I.M. Hafez, N. Maurer, P.R. Cullis, On the mechanism whereby cationic lipids promote intracellular delivery of polynucleic acids, Gene Ther 8(15) (2001) 1188-96.
[171] Y.C. Tseng, S. Mozumdar, L. Huang, Lipid-based systemic delivery of siRNA, Adv Drug Deliv Rev 61(9) (2009) 721-31.
[172] A.S. Malamas, M. Gujrati, C.M. Kummitha, R. Xu, Z.R. Lu, Design and evaluation of new pH-sensitive amphiphilic cationic lipids for siRNA delivery, J Control Release 171(3) (2013) 296-307.
[173] X.L. Wang, R. Xu, X. Wu, D. Gillespie, R. Jensen, Z.R. Lu, Targeted systemic delivery of a therapeutic siRNA with a multifunctional carrier controls tumor proliferation in mice, Mol Pharm 6(3) (2009) 738-46.
[174] P.M. Klein, S. Reinhard, D.-J. Lee, K. Müller, D. Ponader, L. Hartmann, E. Wagner, Precise redox-sensitive cleavage sites for improved bioactivity of siRNA lipopolyplexes, Nanoscale 8(42) (2016) 18098-18104.
[175] Q. Jiang, D. Yue, Y. Nie, X. Xu, Y. He, S. Zhang, E. Wagner, Z. Gu, Specially-Made Lipid-Based Assemblies for Improving Transmembrane Gene Delivery: Comparison of Basic Amino Acid Residue Rich Periphery, Molecular Pharmaceutics 13(6) (2016) 1809-1821.
[176] P.E. Peterson, G. Allen, Solvents of Low Nucleophilicity. II. Addition of Trifluoroacetic Acid to Alkenes and Cycloalkenes, The Journal of Organic Chemistry 27(5) (1962) 1505-1509.

[177] P.E. Peterson, Solvents of Low Nucleophilicity. I. Reactions of Hexyl Tosylates and Hexenes in Trifluoroacetic Acid and Other Acids1, Journal of the American Chemical Society 82(22) (1960) 5834-5837.
[178] P.E. Peterson, C. Casey, E.V.P. Tao, A. Agtarap, G. Thompson, Solvents of Low Nucleophilicity. VI. The Effects of Remote Substitutents in the Addition of Trifluoroacetic Acid to Aliphatic, Cyclic, and Bicyclic Alkenes, Journal of the American Chemical Society 87(22) (1965) 5163-5169.
[179] P.E. Peterson, E.V.P. Tao, Solvents of Low Nucleophilicity. IV. Addition of Acetic, Formic, and Trifluoroacetic Acid to Branched Alkenes, The Journal of Organic Chemistry 29(8) (1964) 2322-2325.
[180] P.E. Peterson, G. Allen, Solvents of Low Nucleophilicity. III. The Effect of Remote Substituents in the Addition of Trifluoroacetic Acid to Substituted Alkenes, Journal of the American Chemical Society 85(22) (1963) 3608-3613.
[181] G.A. Latrèmouille, A.M. Eastham, Kinetics of the addition of acids to olefins with and without boron fluoride catalysis, Canadian Journal of Chemistry 45(1) (1967) 11-16.
[182] D. Weisleder, M. Friedman, Addition of halogenated acetic acids to vinyl ketones. Nuclear magnetic resonance study of the kinetics, The Journal of Organic Chemistry 33(9) (1968) 3542-3543.
[183] R.M.G. Roberts, Kinetics and mechanism of addition of acids to olefins. Part 2. Addition of trifluoroacetic acid to (+)-(R)-limonene in weakly polar media, Journal of the Chemical Society, Perkin Transactions 2 (12) (1976) 1374-1379.
[184] J.E. Nordlander, J.E. Haky, J.P. Landino, Mechanism of addition of neat trifluoroacetic acid to protoadamantene, Journal of the American Chemical Society 102(25) (1980) 7487-7493.
[185] W. Chan, P. White, Fmoc Solid Phase Peptide Synthesis - A Practical Approach, The Practical Approach Series (2000).
[186] K.L. Kozielski, S.Y. Tzeng, J.J. Green, A bioreducible linear poly(β-amino ester) for siRNA delivery, Chemical Communications 49(46) (2013) 5319-5321.
[187] H. Wei, L.R. Volpatti, D.L. Sellers, D.O. Maris, I.W. Andrews, A.S. Hemphill, L.W. Chan, D.S. Chu, P.J. Horner, S.H. Pun, Dual responsive, stabilized nanoparticles for efficient in vivo plasmid delivery, Angew Chem Int Ed Engl 52(20) (2013) 5377-81.
[188] J. Hoon Jeong, L.V. Christensen, J.W. Yockman, Z. Zhong, J.F.J. Engbersen, W. Jong Kim, J. Feijen, S. Wan Kim, Reducible poly(amido ethylenimine) directed to enhance RNA interference, Biomaterials 28(10) (2007) 1912-1917.
[189] L. Hartmann, S. Häfele, R. Peschka-Süss, M. Antonietti, H.G. Börner, Sequence Positioning of Disulfide Linkages to Program the Degradation of Monodisperse Poly(amidoamines), Macromolecules 40(22) (2007) 7771-7776.
[190] S. Wieczorek, S. Vigne, T. Masini, D. Ponader, L. Hartmann, A.K.H. Hirsch, H.G. Börner, Combinatorial Screening for Specific Drug Solubilizers with Switchable Release Profiles, Macromolecular Bioscience 15(1) (2015) 82-89.
[191] L. Brülisauer, N. Kathriner, M. Prenrecaj, M.A. Gauthier, J.-C. Leroux, Tracking the Bioreduction of Disulfide-Containing Cationic Dendrimers, Angewandte Chemie International Edition 51(50) (2012) 12454-12458.
[192] M.A. Wolfert, L.W. Seymour, Atomic force microscopic analysis of the influence of the molecular weight of poly(L)lysine on the size of polyelectrolyte complexes formed with DNA, Gene Ther 3(3) (1996) 269-73.
[193] A. Hall, U. Lächelt, J. Bartek, E. Wagner, S.M. Moghimi, Polyplex Evolution: Understanding Biology, Optimizing Performance, Mol Ther 25(7) (2017) 1476-1490.

[194] S.M. Moghimi, P. Symonds, J.C. Murray, A.C. Hunter, G. Debska, A. Szewczyk, A two-stage poly(ethylenimine)-mediated cytotoxicity: implications for gene transfer/therapy, Mol Ther 11(6) (2005) 990-5.
[195] A.R. Klemm, D. Young, J.B. Lloyd, Effects of polyethyleneimine on endocytosis and lysosome stability, Biochemical pharmacology 56(1) (1998) 41-6.
[196] T. Bieber, W. Meissner, S. Kostin, A. Niemann, H.P. Elsasser, Intracellular route and transcriptional competence of polyethylenimine-DNA complexes, J Control Release 82(2-3) (2002) 441-54.
[197] G. Droga-Mazovec, L. Bojic, A. Petelin, S. Ivanova, R. Romih, U. Repnik, G.S. Salvesen, V. Stoka, V. Turk, B. Turk, Cysteine cathepsins trigger caspase-dependent cell death through cleavage of bid and antiapoptotic Bcl-2 homologues, J Biol Chem 283(27) (2008) 19140-50.
[198] G. Grandinetti, A.E. Smith, T.M. Reineke, Membrane and nuclear permeabilization by polymeric pDNA vehicles: efficient method for gene delivery or mechanism of cytotoxicity?, Mol Pharm 9(3) (2012) 523-38.
[199] G. Grandinetti, N.P. Ingle, T.M. Reineke, Interaction of poly(ethylenimine)-DNA polyplexes with mitochondria: implications for a mechanism of cytotoxicity, Molecular pharmaceutics 8(5) (2011) 1709-1719.
[200] A. Hall, A.K. Larsen, L. Parhamifar, K.D. Meyle, L.P. Wu, S.M. Moghimi, High resolution respirometry analysis of polyethylenimine-mediated mitochondrial energy crisis and cellular stress: Mitochondrial proton leak and inhibition of the electron transport system, Biochim Biophys Acta 1827(10) (2013) 1213-25.
[201] H. Yu, V. Russ, E. Wagner, Influence of the molecular weight of bioreducible oligoethylenimine conjugates on the polyplex transfection properties, Aaps j 11(3) (2009) 445-55.
[202] K. Itaka, K. Kataoka, Recent development of nonviral gene delivery systems with virus-like structures and mechanisms, Eur J Pharm Biopharm 71(3) (2009) 475-83.
[203] T.I. Kim, S.W. Kim, Bioreducible polymers for gene delivery, Reactive & functional polymers 71(3) (2011) 344-349.
[204] M.L. Forrest, J.T. Koerber, D.W. Pack, A Degradable Polyethylenimine Derivative with Low Toxicity for Highly Efficient Gene Delivery, Bioconjugate Chemistry 14(5) (2003) 934-940.
[205] J. Kloeckner, E. Wagner, M. Ogris, Degradable gene carriers based on oligomerized polyamines, Eur J Pharm Sci 29(5) (2006) 414-25.
[206] M.A. Gosselin, W. Guo, R.J. Lee, Efficient Gene Transfer Using Reversibly Cross-Linked Low Molecular Weight Polyethylenimine, Bioconjugate Chemistry 12(6) (2001) 989-994.
[207] M. Breunig, U. Lungwitz, R. Liebl, A. Goepferich, Breaking up the correlation between efficacy and toxicity for nonviral gene delivery, Proceedings of the National Academy of Sciences of the United States of America 104(36) (2007) 14454-14459.
[208] V. Knorr, M. Ogris, E. Wagner, An acid sensitive ketal-based polyethylene glycol-oligoethylenimine copolymer mediates improved transfection efficiency at reduced toxicity, Pharmaceutical research 25(12) (2008) 2937-2945.
[209] Y.H. Kim, J.H. Park, M. Lee, Y.H. Kim, T.G. Park, S.W. Kim, Polyethylenimine with acid-labile linkages as a biodegradable gene carrier, J Control Release 103(1) (2005) 209-19.
[210] J. Kloeckner, S. Bruzzano, M. Ogris, E. Wagner, Gene Carriers Based on Hexanediol Diacrylate Linked Oligoethylenimine: Effect of Chemical Structure of Polymer on Biological Properties, Bioconjugate Chemistry 17(5) (2006) 1339-1345.

[211] L. Chen, H. Tian, J. Chen, X. Chen, Y. Huang, X. Jing, Multi-armed poly(L-glutamic acid)-graft-oligoethylenimine copolymers as efficient nonviral gene delivery vectors, The journal of gene medicine 12(1) (2010) 64-76.
[212] J. Gilleron, W. Querbes, A. Zeigerer, A. Borodovsky, G. Marsico, U. Schubert, K. Manygoats, S. Seifert, C. Andree, M. Stöter, H. Epstein-Barash, L. Zhang, V. Koteliansky, K. Fitzgerald, E. Fava, M. Bickle, Y. Kalaidzidis, A. Akinc, M. Maier, M. Zerial, Image-based analysis of lipid nanoparticle–mediated siRNA delivery, intracellular trafficking and endosomal escape, Nature Biotechnology 31 (2013) 638.
[213] A. Wittrup, A. Ai, X. Liu, P. Hamar, R. Trifonova, K. Charisse, M. Manoharan, T. Kirchhausen, J. Lieberman, Visualizing lipid-formulated siRNA release from endosomes and target gene knockdown, Nat Biotechnol 33(8) (2015) 870-6.
[214] J.A. Mindell, Lysosomal acidification mechanisms, Annual review of physiology 74 (2012) 69-86.
[215] G. Sahay, W. Querbes, C. Alabi, A. Eltoukhy, S. Sarkar, C. Zurenko, E. Karagiannis, K. Love, D. Chen, R. Zoncu, Y. Buganim, A. Schroeder, R. Langer, D.G. Anderson, Efficiency of siRNA delivery by lipid nanoparticles is limited by endocytic recycling, Nature Biotechnology 31 (2013) 653.
[216] H. Xu, D. Ren, Lysosomal physiology, Annual review of physiology 77 (2015) 57-80.
[217] B. Turk, D. Turk, V. Turk, Lysosomal cysteine proteases: more than scavengers, Biochim Biophys Acta 1477(1-2) (2000) 98-111.
[218] D.V. Schaffer, N.A. Fidelman, N. Dan, D.A. Lauffenburger, Vector unpacking as a potential barrier for receptor-mediated polyplex gene delivery, Biotechnology and bioengineering 67(5) (2000) 598-606.
[219] J. Kopecek, P. Kopeckova, T. Minko, Z. Lu, HPMA copolymer-anticancer drug conjugates: design, activity, and mechanism of action, Eur J Pharm Biopharm 50(1) (2000) 61-81.
[220] M.S. Sutherland, R.J. Sanderson, K.A. Gordon, J. Andreyka, C.G. Cerveny, C. Yu, T.S. Lewis, D.L. Meyer, R.F. Zabinski, S.O. Doronina, P.D. Senter, C.L. Law, A.F. Wahl, Lysosomal trafficking and cysteine protease metabolism confer target-specific cytotoxicity by peptide-linked anti-CD30-auristatin conjugates, J Biol Chem 281(15) (2006) 10540-7.
[221] K. Ulbrich, V. Subr, J. Strohalm, D. Plocova, M. Jelinkova, B. Rihova, Polymeric drugs based on conjugates of synthetic and natural macromolecules. I. Synthesis and physico-chemical characterisation, J Control Release 64(1-3) (2000) 63-79.
[222] D.S. Chu, R.N. Johnson, S.H. Pun, Cathepsin B-sensitive polymers for compartment-specific degradation and nucleic acid release, J Control Release 157(3) (2012) 445-54.
[223] S. Reinhard, E. Wagner, How to Tackle the Challenge of siRNA Delivery with Sequence-Defined Oligoamino Amides, Macromol Biosci 17(1) (2017).
[224] W. Bruening, B. Giasson, W. Mushynski, H.D. Durham, Activation of stress-activated MAP protein kinases up-regulates expression of transgenes driven by the cytomegalovirus immediate/early promoter, Nucleic Acids Research 26(2) (1998) 486-489.
[225] H. Peluffo, U. Unzueta, M.L. Negro-Demontel, Z. Xu, E. Vaquez, N. Ferrer-Miralles, A. Villaverde, BBB-targeting, protein-based nanomedicines for drug and nucleic acid delivery to the CNS, Biotechnol Adv 33(2) (2015) 277-87.
[226] J.Y. Tan, D.L. Sellers, B. Pham, S.H. Pun, P.J. Horner, Non-Viral Nucleic Acid Delivery Strategies to the Central Nervous System, Front Mol Neurosci 9 (2016) 108.
[227] W.M. Pardridge, CSF, blood-brain barrier, and brain drug delivery, Expert Opin Drug Deliv 13(7) (2016) 963-75.

[228] W.M. Pardridge, Targeted delivery of protein and gene medicines through the blood-brain barrier, Clin Pharmacol Ther 97(4) (2015) 347-61.
[229] W.M. Pardridge, Drug transport across the blood-brain barrier, J Cereb Blood Flow Metab 32(11) (2012) 1959-72.
[230] F. Herve, N. Ghinea, J.M. Scherrmann, CNS delivery via adsorptive transcytosis, AAPS J 10(3) (2008) 455-72.
[231] S. Wang, S. Reinhard, C. Li, M. Qian, H. Jiang, Y. Du, U. Lächelt, W. Lu, E. Wagner, R. Huang, Antitumoral Cascade-Targeting Ligand for IL-6 Receptor-Mediated Gene Delivery to Glioma, Mol Ther 25(7) (2017) 1556-1566.
[232] R.E. Kalin, M.P. Kretz, A.M. Meyer, A. Kispert, F.L. Heppner, A.W. Brandli, Paracrine and autocrine mechanisms of apelin signaling govern embryonic and tumor angiogenesis, Developmental biology 305(2) (2007) 599-614.
[233] L.G. Dubois, L. Campanati, C. Righy, I. D'Andrea-Meira, T.C. Spohr, I. Porto-Carreiro, C.M. Pereira, J. Balca-Silva, S.A. Kahn, M.F. DosSantos, A. Oliveira Mde, A. Ximenes-da-Silva, M.C. Lopes, E. Faveret, E.L. Gasparetto, V. Moura-Neto, Gliomas and the vascular fragility of the blood brain barrier, Front Cell Neurosci 8 (2014) 418.
[234] R. Barbara, D. Belletti, F. Pederzoli, M. Masoni, J. Keller, A. Ballestrazzi, M.A. Vandelli, G. Tosi, A.M. Grabrucker, Novel Curcumin loaded nanoparticles engineered for Blood-Brain Barrier crossing and able to disrupt Abeta aggregates, Int J Pharm 526(1-2) (2017) 413-424.
[235] M. Salvalaio, L. Rigon, D. Belletti, F. D'Avanzo, F. Pederzoli, B. Ruozi, O. Marin, M.A. Vandelli, F. Forni, M. Scarpa, R. Tomanin, G. Tosi, Targeted Polymeric Nanoparticles for Brain Delivery of High Molecular Weight Molecules in Lysosomal Storage Disorders, PLoS One 11(5) (2016) e0156452.
[236] R. Chhabra, B. Ruozi, A. Vilella, D. Belletti, K. Mangus, S. Pfaender, T. Sarowar, T.M. Boeckers, M. Zoli, F. Forni, M.A. Vandelli, G. Tosi, A.M. Grabrucker, Application of Polymeric Nanoparticles for CNS Targeted Zinc Delivery In Vivo, CNS Neurol Disord Drug Targets 14(8) (2015) 1041-53.
[237] G. Tosi, L. Costantino, F. Rivasi, B. Ruozi, E. Leo, A.V. Vergoni, R. Tacchi, A. Bertolini, M.A. Vandelli, F. Forni, Targeting the central nervous system: in vivo experiments with peptide-derivatized nanoparticles loaded with Loperamide and Rhodamine-123, J Control Release 122(1) (2007) 1-9.
[238] G. Tosi, R.A. Fano, L. Bondioli, L. Badiali, R. Benassi, F. Rivasi, B. Ruozi, F. Forni, M.A. Vandelli, Investigation on mechanisms of glycopeptide nanoparticles for drug delivery across the blood-brain barrier, Nanomedicine (Lond) 6(3) (2011) 423-36.
[239] P.M. Klein, S. Kern, D.J. Lee, J. Schmaus, M. Höhn, J. Gorges, U. Kazmaier, E. Wagner, Folate receptor-directed orthogonal click-functionalization of siRNA lipopolyplexes for tumor cell killing in vivo, Biomaterials 178 (2018) 630-642.
[240] P. Klein, K. Klinker, W. Zhang, S. Kern, E. Kessel, E. Wagner, M. Barz, Efficient Shielding of Polyplexes Using Heterotelechelic Polysarcosines, Polymers 10(6) (2018) 689.
[241] M.V. Trivedi, J.S. Laurence, T.J. Siahaan, The role of thiols and disulfides on protein stability, Current protein & peptide science 10(6) (2009) 614-625.
[242] G. Mastrella, M. Hou, M. Li, V.M. Stoecklein, N. Zdouc, M.N.M. Volmar, H. Miletic, S. Reinhard, C.C. Herold-Mende, S. Kleber, K. Eisenhut, G. Gargiulo, M. Synowitz, A.L. Vescovi, P.N. Harter, J.M. Penninger, E. Wagner, M. Mittelbronn, R. Bjerkvig, D. Hambardzumyan, U. Schüller, J.-C. Tonn, J. Radke, R. Glass, R.E. Kälin, Targeting APLN/APLNR improves anti-angiogenic efficiency and blunts pro-invasive side effects of VEGFA/VEGFR2-blockade in glioblastoma, Cancer Research (2019) canres.0881.2018.

[243] B. Shi, E. Keough, A. Matter, K. Leander, S. Young, E. Carlini, A.B. Sachs, W. Tao, M. Abrams, B. Howell, L. Sepp-Lorenzino, Biodistribution of small interfering RNA at the organ and cellular levels after lipid nanoparticle-mediated delivery, J Histochem Cytochem 59(8) (2011) 727-40.
[244] S. Son, D.W. Hwang, K. Singha, J.H. Jeong, T.G. Park, D.S. Lee, W.J. Kim, RVG peptide tethered bioreducible polyethylenimine for gene delivery to brain, J Control Release 155(1) (2011) 18-25.
[245] Y. Liu, X. He, Y. Kuang, S. An, C. Wang, Y. Guo, H. Ma, J. Lou, C. Jiang, A bacteria deriving peptide modified dendrigraft poly-l-lysines (DGL) self-assembling nanoplatform for targeted gene delivery, Mol Pharm 11(10) (2014) 3330-41.
[246] A. Sturzu, S. Heckl, Magnetic resonance imaging of human glioma cells by means of an interleukin-6 receptor-targeted contrast agent, Chemical biology & drug design 75(4) (2010) 369-74.
[247] R. Prades, B. Oller-Salvia, S.M. Schwarzmaier, J. Selva, M. Moros, M. Balbi, V. Grazu, J.M. de La Fuente, G. Egea, N. Plesnila, M. Teixido, E. Giralt, Applying the retro-enantio approach to obtain a peptide capable of overcoming the blood-brain barrier, Angew Chem Int Ed Engl 54(13) (2015) 3967-72.
[248] C. Díaz-Perlas, B. Oller-Salvia, M. Sánchez-Navarro, M. Teixidó, E. Giralt, Branched BBB-shuttle peptides: chemoselective modification of proteins to enhance blood–brain barrier transport, Chemical Science 9(44) (2018) 8409-8415.
[249] B. Oller-Salvia, M. Sanchez-Navarro, S. Ciudad, M. Guiu, P. Arranz-Gibert, C. Garcia, R.R. Gomis, R. Cecchelli, J. Garcia, E. Giralt, M. Teixido, MiniAp-4: A Venom-Inspired Peptidomimetic for Brain Delivery, Angew Chem Int Ed Engl 55(2) (2016) 572-5.
[250] Y. Anraku, H. Kuwahara, Y. Fukusato, A. Mizoguchi, T. Ishii, K. Nitta, Y. Matsumoto, K. Toh, K. Miyata, S. Uchida, K. Nishina, K. Osada, K. Itaka, N. Nishiyama, H. Mizusawa, T. Yamasoba, T. Yokota, K. Kataoka, Glycaemic control boosts glucosylated nanocarrier crossing the BBB into the brain, Nat Commun 8(1) (2017) 1001.
[251] C.A. Stein, D. Castanotto, FDA-Approved Oligonucleotide Therapies in 2017, Mol Ther 25(5) (2017) 1069-1075.
[252] S.L. Ginn, A.K. Amaya, I.E. Alexander, M. Edelstein, M.R. Abedi, Gene therapy clinical trials worldwide to 2017: An update, The journal of gene medicine 20(5) (2018) e3015.

8 Publications

Original articles

Giorgia Mastrella, Mengzhuo Hou, Min Li, Veit Stöcklein, Nina Zdouc, Marie N. M. Volmar, Hrvoje Miletic, **Sören Reinhard**, Christel Herold-Mende, Susanne Kleber, Katharina Eisenhut, Gaetano Gargiulo, Michael Synowitz, Angelo L. Vescovi, Patrick Harter, Josef M. Penninger, Ernst Wagner, Michel Mittelbronn, Rolf Bjerkvig, Dolores Hambardzumyan, Ulrich Schüller, Jörg-Christian Tonn, Josefine Radke, Rainer Glass, Roland E. Kälin, APLN/APLNR-targeting improves anti-angiogenic efficiency and blunts pro-invasive side effects of VEGFA/VEGFR2-blockade in glioblastoma, *Cancer Research*, (2019) canres.0881.2018

S. Reinhard,* Y. Wang, S. Dengler, E. Wagner, Precise Enzymatic Cleavage Sites for Improved Bioactivity of siRNA Lipo-Polyplexes, *Bioconjug Chem* 29(11) (2018) 3649-3657
(*indicates corresponding authorship)

S. Reinhard, W. Zhang, E. Wagner, Optimized Solid-Phase-Assisted Synthesis of Oleic Acid Containing siRNA Nanocarriers, *ChemMedChem* 12(17) (2017) 1464-1470

S. Wang, **S. Reinhard**, C. Li, M. Qian, H. Jiang, Y. Du, U. Lächelt, W. Lu, E. Wagner, R. Huang, Antitumoral Cascade-Targeting Ligand for IL-6 Receptor-Mediated Gene Delivery to Glioma, *Mol Ther* 25(7) (2017) 1556-1566

A. Nino-Pariente, A. Arminan, **S. Reinhard**, C. Scholz, P. Kos, E. Wagner, M.J. Vicent, Design of Poly-l-Glutamate-Based Complexes for pDNA Delivery, *Macromol Biosci* 17(10) (2017)

P.M. Klein*, **S. Reinhard***, D.-J. Lee, K. Müller, D. Ponader, L. Hartmann, E. Wagner, Precise redox-sensitive cleavage sites for improved bioactivity of siRNA lipopolyplexes, *Nanoscale* 8(42) (2016) 18098-18104
(*indicates equal contributions)

W. Zhang, K. Müller, E. Kessel, **S. Reinhard**, D. He, P.M. Klein, M. Höhn, W. Rödl, S. Kempter, E. Wagner, Targeted siRNA Delivery Using a Lipo-Oligoaminoamide Nanocore with an Influenza Peptide and Transferrin Shell, *Adv Healthc Mater* 5(12) (2016) 1493-504

L. Leclercq, **S. Reinhard**, J. Chamieh, M. Döblinger, E. Wagner, H. Cottet, Fast Characterization of Polyplexes by Taylor Dispersion Analysis, Macromolecules 48(19) (2015) 7216-7221

Reviews and book chapters

S. Reinhard, E. Wagner, Sequence-defined cationic lipo-oligomers containing unsaturated fatty acids for transfection, *Methods in Molecular Biology*, estimated Print Publication Date: Feb-2019

S. Reinhard, E. Wagner, How to Tackle the Challenge of siRNA Delivery with Sequence-Defined Oligoamino Amides, *Macromol Biosci* 17(1) (2017)

9 Acknowledgments

At the end of my PhD thesis, it is my pleasure to look back on a great time and express my gratitude to many people who have supported me in the lab and in my private life.

First of all, I thank Professor Ernst Wagner for giving me the opportunity to work on my PhD thesis in his research group. I am very grateful for the continuous support, guidance and confidence that he has shown me. I was always given the freedom to realize my own ideas and projects and I learned a lot under his supervision.

I want to thank my external collaboration partners Prof. Laura Hartmann and Dr. Daniela Ponader from the Heinrich-Heine-University Düsseldorf, Prof. Hervé Cottet and Dr. Laurent Leclercq from the University of Montpellier, Dr. María Vicent and Dr. Amaya Niño-Pariente from the CIPF Valencia, Prof. Rongqin Huang and Shanshan Wang from Fudan University, Prof. Rainer Glaß, Dr. Roland Kälin and Dr. Giorgia Mastrella from the LMU Munich University Hospital and all members of the COMPACT consortium.

I thank Wei, Yanfang, Katharina, DJ, Ana and Jasmin K. for testing my formulations in cell culture.

Thank you Philipp, Uli and Stephan for teaching me synthesis and assays during my first weeks in the lab, lots of brainstorming and fruitful discussions.

Many thanks to DJ, Eva and Sunny Kernchen for carrying out *in vivo* animal experiments.

Thank you Dodo for making nanosized objects visible.

Many thanks to Wolfgang, Martina, Miriam, Ursula, Anna, Markus and Olga who kept everything running smoothly in the lab.

I thank all current and former members of the Wagner research group for an amazing time in Munich. I enjoyed the great atmosphere in the lab, made new friends and spent joyful times during ski trips, BBQs, Wiesn, dinners, sports (Bojan!), PhD-, Fasching-, Christmas- and birthday parties. The infernal DJ Duo Sören b2b IsyTrue will never be forgotten.

I thank my family for their continuous encouragement, trust and support during all periods of my life.

Thank you, Jasmin, for enriching many years of my life, your love, dedicated support and the encouragement during my PhD, although it meant having a long-distance relationship for over four years.